The oncogenic role of the lysine-specific demethylase KDM1A in chronic lymphocytic leukemia

Inaugural Dissertation

zur
Erlangung des Doktorgrades
Dr. nat. med.

der Medizinischen Fakultät
und
der Mathematisch-Naturwissenschaftlichen Fakultät
der Universität zu Köln

vorgelegt von

Qu Jiang

aus SiChuan, VR China

Hundt Druck GmbH, Köln

2022

Betreuer/in: Priv.-Doz. Dr. med. Marco Herling

Referent/in: Prof. Dr. Dr. Michal-Ruth Schweiger
                                Prof. Dr. Jan Riemer

Datum der mündlichen Prüfung: 25.10.2022

Acknowledgments

I would like to thank everyone that made this thesis possible. I'm very grateful to the whole team of the Laboratory for Lymphocyte Signaling and Oncoproteome for guiding, encouraging, and supporting me from the beginning to the end of this project. Thank you for the friendly and pleasant working atmosphere that means a lot to me. I greatly appreciate the valuable and unforgettable experience in Germany.

I would like to
- Prof. Dr. Micheal Hallek for the possibility to perform my project in the Department I of Internal Medicine at the University Hospital of Cologne.
- thank PD Dr. med. Marco Herling for giving me the opportunity to conduct this project in his group. Marco, thank you for your guidance, support, and inspiration. It was a pleasure to work with you.
- express my special gratitude to Dr. Elena Vasyutina, who, although no longer with us, was a dedicated mentor with a creative mind and who continues to inspire by her example and commitment. Many thanks to her for her supervision, inspiration, and support. She was there for me whenever I had questions or problems. Her assistance and dedicated involvement in the project made it possible for me to continue and accomplish this work.
- extend my sincere thanks to Johanna Stachelscheid for her great support and valuable suggestions. It has always been very pleasant and helpful to discuss with her. Johanna, thank you so much. I have enjoyed a lot working with you over the last years. It is one of the best memories that I will cherish forever.
- thank Jana von Jan and Linus Wahnschaffe for their help and support in the last years and during writing the thesis. Working with you has been a fantastic experience.
- thank the Herling group: Dr. Christoph Aszyk, Dr. Sabine Pützer, Dr. Sebastian Oberbeck, Dr. Alexandra Schrader, Petra Meyer, Francien Grotenhuijs, Till Braun, Annika Dechow, Dennis Jungherz, Moritz Otte, Yayi Peng, Dr. Natali Pflug, and Dr. Tony Müller for their help, friendship, and discussions. I have had a really great time with you.

I also want to thank:
- Prof. Dr. Dr. Michal-Ruth Schweiger and Prof. Dr. Jan Riemer for being my tutors and supervisors. Thank you for the valuable input at all the tutor meetings.
- Prof. Dr. Margarete Odenthal for the great help and valuable input in the last few years.
- all collaborators that provided help in this project: Prof. Dr. Stephan Stilgenbauer, Prof. Dr. Kojo Elenitoba-Johnson, Prof. Dr. Dr. Michal-Ruth Schweiger, Prof. Dr. Peter Nürnberg, Dr. Yue Zhao, CCG, microscope facility of CMMC, and proteomics facility of CECAD.
- colleagues from other groups: Dr. Zhefang Wang, Jie Wang, Dr. Anastasia Nikiforov, Dr. Lisa Rusyn, Dr. Zhiyuan Shi, and Shuaifeng Yan for their help.

My deepest gratitude goes to:

- my husband Longfei Ma, for his love, patience, understanding, unfailing support, and continuous encouragement throughout my years of study and through the process of writing this thesis. Without you, it would be very tough to get through the painful moments. Thank you so much.

- my parents, my parents-in-law, and my sister for their love, support, and understanding in my life, that I can take the way I wanted to go. This accomplishment would not have been possible without them.

- the supervisor of my master thesis, Prof. Dr. Hongbin Zhang, for his help, support, and encouragement. You are a supervisor, a father, and a friend. I would not be here today without your support.

- all my friends for their support and encouragement.

Qu Jiang, 2022

Abstract and Zusammenfassung

Abstract

Chronic lymphocytic leukemia (CLL) is the most prevalent leukemia in adults in the Western world. Despite the advances in the identification of various genomic and molecular alterations and the management of treatment for CLL, it remains an incurable disease. Epigenetic alterations are considered to centrally shape the transcriptional signatures that drive disease evolution and underlie the biological and clinical subsets in CLL. However, characterizations of epigenetic regulators, particularly histone-modifying enzymes, are very rudimentary in CLL.

Aberrant expression of the T-cell leukemia/lymphoma 1A (*TCL1A*) proto-oncogene is a hallmark of CLL and high TCL1A levels are associated with aggressive disease features. As a well-accepted disease model, *Eµ-TCL1A* transgenic (tg) mice produce B-cell proliferations that closely resemble human CLL. In the context of the yet-evolving molecular concept of the 14kDa TCL1A protein, it was shown that TCL1A interacts with the DNA methyltransferase 3A (DNMT3A), thereby reducing its enzymatic activity and contributing to epigenetic reprogramming in CLL. Fittingly, induced mono- or bi-allelic losses of *Dnmt3a* result in murine CLL. Nevertheless, the functional network around TCL1A, particularly with epigenetics, is incomplete and as a causal oncogene in CLL, a better molecular understanding would help in improving disease concepts and treatment rationales in this still incurable neoplasm.

Here, we identify the epigenetic modifier, lysine-specific demethylase KDM1A as a novel interaction partner of the TCL1A protein in B cells. This demethylase has been implicated in many cancer entities and its overexpression has been linked to poor prognoses. Currently, KDM1A inhibitors are being investigated for cancer therapy in clinal trials. In this context, we proposed that KDM1A is involved in CLL pathogenesis by altering its epigenetic landscape. Therefore, we set out to address: (1) how does TCL1A affect KDM1A's function/activity? (2) what are the biological outcomes of increased KDM1A levels in CLL? (3) which KDM1A-mediated pathways contribute to the biology of CLL?

To address these central questions, we have analyzed the subcellular localization of TCL1A and KDM1A as well as their interacting complex. TCL1A interacted with KDM1A in the nucleus. Interestingly, their protein interaction increased the histone demethylase activity of KDM1A in B cells. TCL1A also affected histone posttranslational modifications (PTMs). Furthermore, we could show that KDM1A is overexpressed in CLL B cells as compared to healthy B cells. By analyzing the gene expression profiling (GEP) data of patients included in the CLL8 trial, we demonstrated that higher *KDM1A* expression levels and the associated gene signatures correlate with adverse clinical characteristics and unfavorable clinical outcomes, e.g., higher white blood cell (WBC) counts, higher serum thymidine kinase levels, a higher rate of *TP53*

mutations/deletions, and shorter progression-free survival (PFS). In addition, enrichment of different pathways involved in tumor progression was also associated with *KDM1A* expression levels.

Next, we took advantage of the doxycycline (Dox)-inducible *Kdm1a* knockdown mouse model and the *TCL1A*-tg *Eμ-TCL1A* mice to achieve a whole-organismal *Kdm1a* knockdown in murine CLL. The genetic *Kdm1a* depletion in *Eμ-TCL1A* mice reduced the leukemic burden in peripheral blood, spleen, and bone marrow. This was accompanied by upregulation of p53 and pro-apoptotic pathways identified by RNA-sequencing analysis. The analysis of differentially expressed genes (DEGs) upon *Kdm1a* knockdown suggested that *Kdm1a* acts as a transcriptional repressor in murine CLL. This might be due to enrichment of regulatory elements of upregulated genes with H3K4 methylation upon the *Kdm1a* knockdown, which leads to activation these genes. Thus, we performed chromatin immunoprecipitation sequencing (ChIP-seq) experiments, which demonstrated an increase in H3K4me3 marks in *Kdm1a* knockdown leukemic cells. Moreover, KDM1A expression in the components of the microenvironment had an impact on their support for CLL progression. The loss of *KDM1A* in monocytic cells and stromal cells led to impaired support of CLL cell proliferation and survival in vitro. Notably, *Kdm1a* knockdown in *Eμ-TCL1A* prolonged the overall survival (OS) of leukemic animals. In vitro, KDM1A inhibition by the pharmacologic compound C12 induced apoptosis and increased H3K4/9 target methylation levels in leukemic B cells.

Overall, in completion of all aims, we established a relevant pathogenic role for KDM1A in CLL, as a pro-oncogenic molecule in CLL cells and in components of their microenvironment. Our data further provide a rationale for therapeutic KDM1A inhibition in CLL.
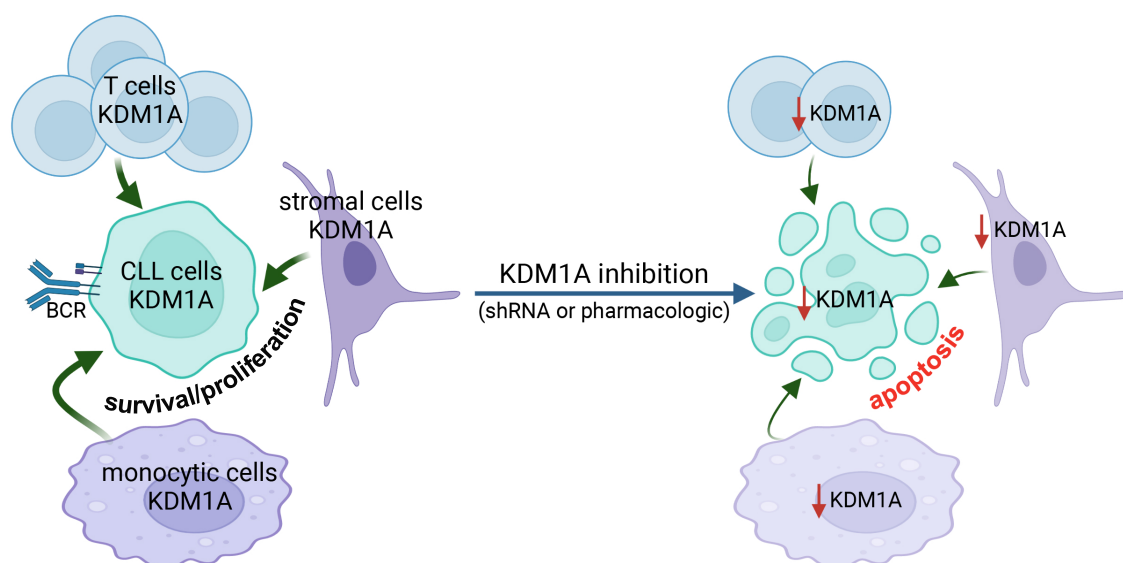
Zusammenfassung

Die chronische lymphatische Leukämie (CLL) ist die häufigste Leukämie bei Erwachsenen in der westlichen Welt. Trotz Fortschritte bei der Identifizierung verschiedener genomischer und weiterer molekularer Veränderungen und bei der Behandlung der CLL, ist diese Krankheit nach wie vor unheilbar. Es wird davon ausgegangen, dass epigenetische Veränderungen die Transkriptionssignaturen, welche die Krankheitsentwicklung vorantreiben und den biologischen sowie klinischen Untergruppen der CLL zugrunde liegen, entscheidend beeinflussen. Die Charakterisierung epigenetischer Regulatoren, insbesondere von Histon-modifizierenden Enzymen, ist bei der CLL bisher jedoch sehr rudimentär.

Eine abnorme Expression des T-cell leukemia/lymphoma 1A (*TCL1A*) Proto-Onkogens ist ein weiteres zentrales Kennzeichen der CLL. Hohe TCL1A Level sind mit aggressiven Krankheits-merkmalen assoziiert. Als anerkanntes Tumormodell der CLL erzeugt humanes TCL1A in *Eµ-TCL1A* transgenen (tg) Mäusen reife B-Zell Neoplasien, die der menschlichen CLL sehr ähnlich ist. Im Rahmen des sich entwickelnden molekularen Konzepts des 14kDa TCL1A Pro-teins wurde gezeigt, dass es mit der DNA-Methyltransferase 3A (DNMT3A) interagiert und dadurch deren enzymatische Aktivität verringert und zur epigenetischen Umprogrammierung der CLL beiträgt. Passend dazu führt der induzierte mono- oder bi-allelische Verlust von *Dnmt3a* zu CLL bei Mäusen. Dennoch ist das funktionelle Netzwerk um TCL1A, insbesondere in Bezug auf dessen Einfluss auf die epigenetische Landschaft, unvollständig. Jedoch würde ein besseres molekulares Verständnis dieses Onkogens der CLL dazu beitragen, Krank-heitskonzepte und Behandlungsrationalen dieser weiterhin inkurablen Neoplasie weiter zu verbessern.

In dieser Arbeit identifizierten wir den epigenetischen Modulator namens lysin-spezifische De-methylase KDM1A, als einen neuen Interaktionspartner des TCL1A Proteins in B-Zellen. Diese Demethylase wurde bei vielen Krebsarten nachgewiesen, und ihre Überexpression wurde mit einer jeweils schlechten Prognose in Verbindung gebracht. Derzeit werden KDM1A-Inhibitoren für die Therapie verschiedener Krebsarten in klinischen Studien untersucht. In diesem Zusammenhang postulierten wir, dass KDM1A an der Pathogenese der CLL beteiligt ist, indem es die epigenetische Landschaft verändert. Deshalb haben wir uns mit folgenden Fragen beschäftigt: (1) Wie beeinflusst TCL1A die Funktion/Aktivität von KDM1A? (2) Was sind die biologischen Konsequenzen erhöhter KDM1A-Konzentrationen in der CLL? (3) Wel-che KDM1A-vermittelten Signalwege tragen zur Pathogenese der CLL bei?

Um diese zentralen Fragen zu beantworten, haben wir zunächst die subzelluläre Lokalisierung von TCL1A und KDM1A sowie deren interagierende Proteinkomplexe analysiert. TCL1A in-teragierte mit KDM1A im Zellkern. Interessanterweise erhöhte diese Proteininteraktion die

Histondemethylase-Aktivität von KDM1A in B-Zellen. TCL1A beeinflusste zudem posttranslationale Histon-Modifikationen (PTMs). Außerdem konnten wir zeigen, dass KDM1A in CLL-B-Zellen im Vergleich zu gesunden B-Zellen überexprimiert ist. Durch die Analyse von Genexpressionsprofilen (GEP) von Patientenproben aus der prospektiven CLL8-Studie konnten wir eine Korrelation zwischen einer erhöhten *KDM1A*-Expression, welche mit bestimmten Gensignaturen assoziiert ist, und prognostisch ungünstigen klinischen Merkmalen und Verläufen nachweisen, z. B. mit einer höheren Leukämiezellzahl im Blut, höheren Thymidinkinase-Serumspiegeln, einer höheren Rate an *TP53*-Mutationen/Deletionen und einem kürzeren progressionsfreien Überleben. Darüber hinaus wurde das vermehrte Vorkommen verschiedener an der Tumorprogression beteiligter Signalwege mit dem *KDM1A*-Expressionsniveau in Verbindung gebracht.

Als Nächstes nutzten wir ein Doxycyclin (Dox)-induzierbares Kdm1a-Knockdown-Mausmodell und *TCL1A*-tg *Eµ-TCL1A*-Mäuse. Die Kombination beider Modelle erlaubte es, einen *Kdm1a*-Knockdown im gesamten Organismus bei muriner CLL zu erreichen. Die genetische *Kdm1a*-Depletion in *Eµ-TCL1A*-Mäusen reduzierte die leukämische Last im peripheren Blut, in der Milz und im Knochenmark. Dies ging in RNA-Sequenzieranalysen mit einer Hochregulierung von p53 sowie pro-apoptotischer Signalwege einher. Die Analyse der differentiell exprimierten Gene (DEGs) nach *Kdm1a*-Knockdown deutet darauf hin, dass Kdm1a bei der murinen CLL als transkriptioneller Repressor wirkt. Dies könnte auf eine Anreicherung regulatorischer Elemente von hochregulierten Genen mit H3K4-Methylierung zurückzuführen sein, was zu deren Aktivierung nach Kdm1a-Knockdown führt. Daher führten wir Experimente der Chromatin-Immunpräzipitations-Sequenzierung (ChIP-seq) durch. Diese zeigten eine Zunahme der H3K4me3-Markierungen in leukämischen *Kdm1a*-Knockdown Zellen. Darüber hinaus hat die Expression von KDM1A in Komponenten des Mikromilieus einen Einfluss auf deren Unterstützung der CLL Progression. Der Verlust von KDM1A in monozytären und Stromazellen führte zu einer beeinträchtigten Unterstützung der CLL-Proliferation und des Überlebens der Tumorzellen. Insbesondere verlängerte der Knockdown von *Kdm1a* in *Eµ-TCL1A* das Überleben leukämischer Tiere. In vitro induzierte die Hemmung von KDM1A durch den Wirkstoff C12 Apoptose und erhöhte die Methylierungslevel von H3K4/9-Zielsequenzen in B-Zelllinien und CLL-Patientenproben.

Insgesamt konnten wir eine relevante pathogenetische Rolle von KDM1A bei CLL als pro-onkogenes Molekül in CLL-Zellen und ihrem Mikromilieu nachweisen. Zudem liefern unsere Daten eine Rationale für die therapeutische Hemmung von KDM1A in der CLL, zumindest als synergistischer Partner in Kombinationsstrategien.

List of Abbreviations

°C	Degree celsius
5′-hmC	5′-hydroxymethylcytosine
5′-mC	5′-methylcytosine
5′-UmC	5′-unmethylcytosine
AGO2	Argonaute RISC catalytic component 2
AKT	Protein kinase B
allo-HSCT	Allogeneic hematopoietic stem cell transplantation
AML	Acute myeloid leukemia
AOL	Amine oxidase-like
AP-1	Activator protein 1
APRIL	A proliferation-inducing ligand
APS	Ammonium persulfate
AR	Androgen receptor
ATM	Ataxia telangiectasia mutated
B-ALL	B-cell acute lymphoblastic leukemia
BAFF	B-cell activating factor
BC-ALL	B-cell childhood acute lymphoblastic leukemia
BCL-2	B-cell lymphoma-2
BCR	B-cell receptor
BET	Bromodomain and Extra-Terminal motif
BLK	Tyrosine-protein kinase BLK
BM	Bone marrow
BMSC	Bone marrow stromal cell
bp	Base pair
BR	Bendamustine with rituximab
BSA	Bovine serum albumin
BSC	Best supportive care
BTK	Bruton's tyrosine kinase
CAK	Complex aberrant karyotype
CAR-T	Genetically modified T cells with chimeric antigen receptor
CCND1	Cyclin D1
CCND3	Cyclin D3
CD	Cluster of differentiation
cDNA	Complementary DNA
CHD2	Chromodomain-helicase-DNA-binding protein 2
ChIP	Chromatin immunoprecipitation
CHK6	Cell division protein kinase 6
CIRS	Comorbidity illness rating scale
CLL	Chronic lymphocytic leukemia
CNA	Copy number alteration
CoREST	Corepressor transcription repressor complex
CpG	Cytosine-guanine dinucleotides
CRCs	Core regulatory circuits
CRNDE	Colorectal neoplasia differentially expressed
CTLA-4	T-lymphocyte associated antigen-4

Ctrl.	Control
CXCR4	CXC motif chemokine receptor 4
Cy	Cyanine
DAPK1	Death-associated protein kinase 1
DDR	DNA damage response
del	Deletion
DICOM	Digital imaging and communications in medicine
DMEM	Dulbecco's modified eagle medium
DMSO	Dimethyl sulfoxide
DNA	Deoxyribonucleic acid
DNMT	DNA (cytosine-5)-methyltransferase
dNTP	Deoxynucleoside triphosphate
Dox	Doxycycline
DPBS	Dulbecco's phosphate-buffered saline
ds	Double-stranded
DSMZ	Deutsche Sammlung von Mikroorganismen und Zellkulturen
DUSP22	Dual specificity phosphatase 22
E. coli	Escherichia coli
e.g.	*Exempli gratia*
EBF1	Early B-cell factor 1
ECL	Enhanced chemiluminescence
EDTA	Ethylenediaminetetraacetic acid
EMT	Epithelial to mesenchymal transition
ER	Estrogen receptor
ESC	Embryonic stem cell
et al.	*Et alii*
EZH2	Enhancer of zeste homolog 2
FACS	Fluorescence activated cell sorting
FAD	Flavin adenine dinucleotide
FBS	Fetal bovine serum
FBXW7	F-box and WD repeat-containing protein 7
FCR	Fludarabine, cyclophosphamide and rituximab
FDG	Fluorescein di-V-galactoside
FISH	Fluorescence in situ hybridization
FOX	Forkhead box
FOXO3	Forkhead box protein O3
g	Gram or force
GC	Germinal center
GEP	Gene expression profiling
GSEA	Gene set enrichment analysis
h	Hour(s)
H3K27ac	Acetylated histone 3 on lysine 27
H3K4me1/me2	Mono- and di-methyl histone H3 lysine 4
H3K4me3	Tri-methyl histone H3 lysine 4
HD	Healthy donor
HDAC	Histone deacetylase
HEPES	4-(2-Hydroxyethyl)piperazine-1-ethanesulfonic acid

HIF-1α	Hypoxia-inducible factor 1-alpha
HRP	Horseradish peroxidase
HSC	Hematopoietic stem cell
HSP90	Heat shock protein 90
IF	Immunofluorescent
Ig	Immunoglobulin
IGF1R	Insulin-like growth factor 1 receptor
IGHV	Immunoglobulin heavy chain variable genes
IKKb	Iκb-kinase β
IL	Interleukin
Iono	Ionomycin
IP	Immunoprecipitation
IP3	Inositol 1,4,5-triphosphate;
ITAMs	Immunoreceptor tyrosine-based activation motifs
Itg2l	Integrin beta 2-like
JMJD6	Jumonji domain-containing 6 protein
kb	Kilobase
KD	Knockdown
kDa	Kilodalton
KDM1A / LSD1	Lysine-specific demethylase 1A
KDM4	Histone lysine demethylase subfamily 4
KEGG	Kyoto Encyclopedia of Genes and Genomes
Ki-67	Marker of proliferation Ki-67
Klf	Kruppel-like factor
L	Liter
LB	Lysogeny broth
LEF	Lymphoid enhancer-binding factor
M	Molar
M	Mutated
mA	Milliampere
MACS	Magnetic-activated cell sorting
MBL	Monoclonal B cell lymphocytosis
MDSC	Myeloid-derived suppressor cells
min	Minute(s)
miR	Micro RNA
mL	Milliliter
MLL	Mixed-lineage leukemia
mM	Millimolar
MRI	Magnetic resonance imaging
mRNA	Messenger RNA
MS	Mass spectrometry
MTCP1	Mature T-cell proliferation 1
MYC	Oncogene carried by the Avian virus, myelocytomatosis
MYD88	Myeloid differentiation primary response 88
na	Not available
NBRE	Nerve growth factor-responsive element
NC	Nitrocellulose

NDR	Nucleosome-depleted region
NF-κB	Nuclear factor kappa-light-chain-enhancer of activated B cells
NFAT	Nuclear factor of activated T cells
NFATC1	Nuclear factor of activated T cells, cytoplasmic 1
ng	Nanogram
NK	Natural killer
NLC	Nurse-like cell
nm	Nanometer
NOTCH	Neurogenic locus notch homolog protein
NOTCH1	Notch homolog 1, translocation-associated
NR4A1	Nuclear receptor subfamily 4 group A member 1
NSG	Next-generation sequencing
NuRD	Nucleosome Remodeling and Deacetylase
Oct3/4	Octamer-binding transcription factor 4
OD	Optical density
OS	Overall survival
P value	Probability value
p53	Protein 53
PARP	Poly (adp-ribose) -polymerase 1
PAX5	Paired box protein Pax-5
PB	Peripheral blood
PBS	Phosphate buffered saline
PBST	Phosphate buffered saline with Tween
PCR	Polymerase chain reaction
PD	Progressive disease
PD-1	Programmed cell death protein 1
PD-L1	Programmed cell death 1 ligand 1
PETG	Phenylethyl β-D-thiogalactopyranoside
PFA	Paraformaldehyde
PFS	Progression-free survival
pH	Potentium hydrogenium
PI3K	Phosphatidylinositol 3-kinase
PKCα	Protein kinase C alpha
PKCβ	Protein kinase C beta
PLCγ	Phospholipase C gamma
PMA	Phorbol-12-myristate-13-acetate
Pou5f1	POU class 5 homeobox 1
PR	Partial remission;
PRC2	Polycomb repressive complex 2
PS	Phosphatidylserine
PTM	Post-transcriptional modification
qRT-PCR	Quantitative real-time PCR
Rapgef3	Rap guanine nucleotide exchange factor 3
RB1	Retinoblastoma protein
RBC	Red blood cells
RFU	Relative fluorescence unit
RNA	Ribonucleic acid

ROI	Region of interest
rpm	Rounds per minute
RPMI	Roswell park memorial institute
RT	Room temperature
RT	Reverse transcription
RT-PCR	Reverse transcription PCR
s	Second
SCLC	Small cell lung cancer
SD	Stable disease
SDS	Sodium dodecyl sulfate
SDS PAGE	Sodium dodecyl sulfate polyacrylamide gel electrophoresis
seq	Sequencing
Ser	Serine
SETD2	SET domain containing 2
SF3B1	Splicing factor 3B subunit 1
shRNA	Small hairpin RNA
Sox2	SRY-box transcription factor 2
SP1	Specificity protein 1
SRC	Proto-oncogene tyrosine-protein kinase Src
STAT3	Signal transducer and activator of transcription 3
SWIRM	Swi3p/rsc8p/moira
SYC	Spleen tyrosine kinase
SYK	Spleen associated tyrosine kinase
T-PLL	T-prolymphocytic leukemia
TAE	Tris-acetate-EDTA
TCF	T-cell factor
TCF4	Transcription factor 4
TCL1A	T-cell leukemia/lymphoma 1A
TCL1B	T-cell leukemia/lymphoma 1B
TCR	T-cell receptor
TEMED	Tetramethylethylenediamine
TERT	Telomerase reverse transcriptase
TF	Transcription factor
tg	Transgenic
TLX	Tailless-like
TNBC	Triple-negative breast cancer
TP53	Tumor suppressor protein 53
TP63	Tumor protein 63
Tri12	Trisomy 12
TSS	Transcription start sites
TWIST2	Twist family transcription factor 2
U	Unmutated
US	United states
USP28	Ubiquitin-specific peptidase 28
V	Volt
Vs.	Versus
WBC	White blood cell

WHO	World Health organization
Wnt	Wingless-related integration site
WT	Wild type
XPO1	Exportin 1
ZAP70	Zeta-chain-associated protein kinase 70
ZIP	Zero interaction potency
ZNF217	Zinc Finger Protein 217
µg	Microgram
µL	Microliter
µM	Micromolar
µm	Micrometer

Table of contents

1 Introduction

1.1 Chronic lymphocytic leukemia

According to the global cancer data from the world health organization (WHO), 19.3 million new cases and 10 million deaths of cancer have been estimated in 2020.[1] Among them, around 1.1 million hematologic neoplasms were diagnosed.[1] Lymphoid neoplasms are characterized as a group of such blood cancers that originate from lymphocytes. They are categorized into two major subgroups by lineage, B-cell neoplasms and T-/NK-neoplasms, and both presenting as either precursor neoplasms or as mature lymphomas/leukemias.[2] Among B-cell neoplasms, chronic lymphocytic leukemia (CLL) is the most prevalent leukemia in adults in the Western world, accounting for 25-30% of all leukemias in the United States (US).[3]

1.1.1 Clinical profile of chronic lymphocytic leukemia

According to the National Cancer Institute, there will be 20,160 new CLL cases in the US in the year 2022,[4] with an age-adjusted rate of new cases of 4.9 and a death rate of 1.1 per 100,000 per year in the US.[4] The median age at diagnosis of CLL is 72 years (range from 65 to 74 years old), and the male population shows a higher incidence than the female population (1.7:1).[4,5] However, studies have shown that female patients often present with more aggressive disease feature than males.[3,6] Up to now, several independent risk factors have been identified for CLL.[7] Around 10% of the cases have a family history of hematological malignancies,[8] which underlines a pronounced hereditary risk in comparison to other hematological malignancies.[8,9] Moreover, living or working on a farm, working as a hairdresser, sun exposure, atopic disorder, and hepatitis C virus infection are linked to a predisposing risk for CLL.[7] Monoclonal B-cell lymphocytosis (MBL), an asymptomatic proliferation of clonal B cells with a blood count of <5,000/µL which appears at an incidence of 12% in healthy humans older than 40 years, is thought to be an essential preleukemic state of CLL.[10,11]

1.1.1.1 Clinical presentation and diagnosis criteria

In general, early-stage CLL cases do not present any symptoms and are often found during a routine blood test with a leukocytosis.[5] When the disease progresses by the proliferation and accumulation of mature monoclonal CD5+ B cells in the peripheral blood (PB), bone marrow (BM), and secondary lymphoid tissues,[5,12] patients may experience unintentional weight loss, significant fatigue, fevers, or night sweats without other evidence of infections, as well as splenomegaly and/or lymphadenopathy, and symptomatic anemia and/or thrombocytopenia.[13]

With a B-cell count greater than 5000 B cells per µL PB, the diagnosis of CLL is generally established by immunophenotyping.[9,14] CLL cells express the T-cell antigen (CD5) and B-cell

antigens (CD19, CD20, and CD23), with lower levels of surface immunoglobulin expression in comparison to normal B cells.[15,16] CD200 expression could also distinguish CLL from other lymphomas.[17] Immunophenotyping of PB lymphocytes is important and usually sufficient to distinguish CLL from other subtypes of low-grade non-Hodgkin lymphomas.[14]

1.1.1.2 The therapeutic landscape of CLL

As a heterogeneous disease, CLL often presents an indolent clinical course that might not demand treatment for many years. Still, in some patients, the disease progresses fast and with a deadly course within several months.[18] Patients with atypical CLL had a significantly higher probability of disease progression.[19] Blood test shows a significantly increased number of leukocytes and detection of at least 5000 B lymphocytes per µL PB over three months.[20] *Rai*[21] and *Binet*[22] have introduced the clinical staging systems based on the manifestation of low platelet or red blood cell (RBC) counts. Over the last two decades, many biological and genetic markers have been described in CLL, which helped to improve predictions of disease progression or response to therapy.[23] Therefore, the CLL-International Prognostic Index (CLL-IPI) has been developed to score the prognostic factors.[24] It is based on a weighted ranking of five independent prognostic factors, including *TP53* dysfunction (*TP53* deletion and/or mutation), mutational status of immunoglobulin heavy chain variable (*IGHV*) genes, serum β2-microglobulin, clinical stage, and age.[5,24] The CLL-IPI also distinguishes four risk groups with different overall survival (OS) at 5 years.[5,24] Furthermore, physical fitness was determined using the Comorbidity Illness Rating Scale (CIRS).[25] In recent years, the treatment of CLL has been improved significantly (**Figure 1**).[25,26] Chlorambucil has been the standard treatment for CLL patients for many years.[27] The current standard protocols include chemotherapy with different agents (e.g., chlorambucil, bendamustine, cyclophosphamide, fludarabine), anti-CD20 monoclonal antibodies (e.g., rituximab, ofatumumab, obinutuzumab), target therapy with specific small molecules (e.g., Bruton's tyrosine kinase (BTK) inhibitors: ibrutinib, acalabrutinib, zanubrutinib; phosphatidylinositol 3-kinase (PI3K) inhibitors: idelalisib; B-cell lymphoma-2 (BCL-2) inhibitors: venetoclax).[5,28] These substances are used either as a single agent or in combination strategies.[5,28,29] There are chemo-immunotherapies, such as the combination of fludarabine, cyclophosphamide, and rituximab (FCR),[30] or of bendamustine with rituximab (BR).[25,31] Besides, allogeneic hematopoietic stem cell transplantation (allo-HSCT) may benefit some patients with relapsing or refractory CLL.[5] Another potential therapeutic option currently tested in clinical trials is the treatment with genetically modified T cells expressing chimeric antigen receptors (CAR-T-cell therapy) targeting CD19 expressing B cells.[32] Despite the advances in the treatment of CLL, it remains an incurable disease.[33]
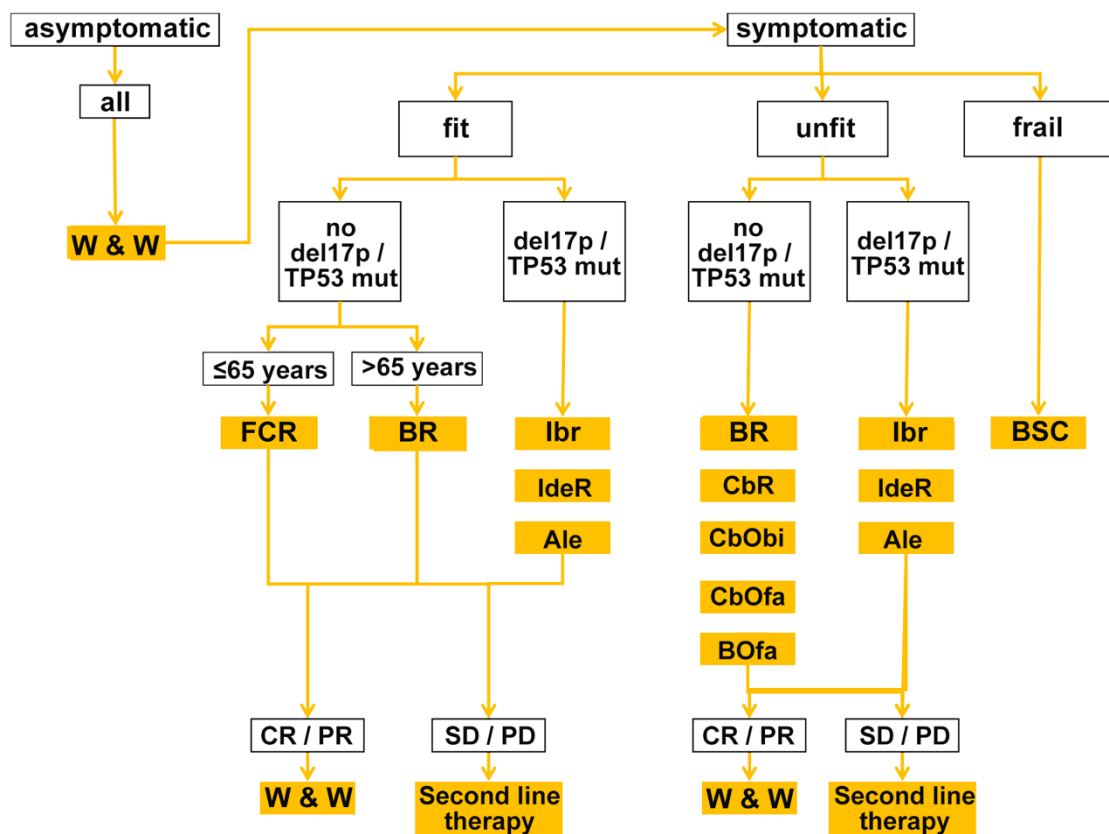
Figure 1. The First-line treatment of chronic lymphocytic lekemia (modified according to the AWMF Clinical Practice (S3) Guideline for CLL and according to the Onkopedia guideline for CLL).[26] Physical fitness was determined using the Comorbidity Illness Rating Scale (CIRS). Patients with a score of or below 6 were labelled as "fit", patients with a score above 6 as "unfit". w & w: watch and wait; Ale: alemtuzumab; B: bendamustine; BSC: best supportive care; C: cyclophosphamide; Cb: chlorambucil; F: fludarabine; Ibr: ibrutinib; Ide: idelalisib; Obi: obinutuzumab; Ofa: ofatumumab; P: prednisone; R: rituximab; PD: progressive disease; PR: partial remission; SD: stable disease.

1.1.2 The pathogenesis of CLL

1.1.2.1 The cellular origin of CLL

CLL is characterized by the monoclonal expansion of mature CD5+CD19+ B cells in PB, BM, and lymphoid tissues.[34] Human CLL B cells express functional B-cell receptor (BCR) on the surface by productive immunoglobulin gene rearrangements.[11,35–37] According to the mutational status of *IGHV* genes, CLL patients can be categorized into two major subtypes: the more aggressive *IGHV* unmutated CLL (U-CLL) and the more indolent *IGHV* mutated CLL (M-CLL).[38,39] These mutations occur in the germinal center (GC) during the transition from naive B cells into memory B cells, suggesting that the *IGHV* mutated subtype is derived from GC or post-GC B cell, while *IGHV* unmutated subtype comes from pre-GC B cell.[40] The identification of these two subsets has improved the understanding of the cell origin of CLL. Further transcriptome analyses suggested that U-CLL originates from unmutated mature CD5+ B cells, while M-CLL derives from an unrecognized CD5+CD27+ post-GC B cell subset that can be rapidly reactivated to produce high-affinity antibodies.[41] However, the cellular origin of CLL is still controversial and more studies are required to characterize its leukemogenic process. Of note, about 1% of CLL cells from both groups express almost the same BCRs, and over 20% of CLL cases present the specific stereotyped BCRs, suggesting that the similarity of these BCRs could be the result of antigen selection during the development of CLL.[11,42,43] However, the data from a recent study suggests that BCRs of CLL cells induce antigen-independent signaling in CLL B cells, thus providing new insight into the CLL pathogenesis with regard to the role of autonomous BCR stimulation.[11,44]

Nevertheless, CLL is not always a monoclonal disease.[11] Two or more different neoplastic B cell clones have been shown to be presented in 3.4% of typical CLL patients and 13.8% of atypical CLL patients,[45] as well as in some MBL, often representing the preleukemic state of CLL.[45–47] Although it is not clear at which stage the first oncogenic event takes place,[11] it has been shown that pluripotent hematopoietic stem cells (HSCs) from CLL patients have the capacity to develop into CLL B cells, suggesting that the initial leukemogenic event in CLL involves multipotent, self-renewing HSCs.[5,48] In support, CLL-HSCs could engraft successfully in immunodeficient mice and trigger the proliferation of clonal B cells that frequently expressed the classic phenotypic surface antigens of CLL, CD5 and CD23.[48] In addition, HSCs aging is considered to be a contributing factor in the pathogenesis of CLL.[11]

Overall, it is accepted that U-CLL cells originate from mature CD5+CD27- B cells, whereas M-CLL cells are derived from CD5+CD27+ post-GC B cells. Moreover, the efficient engraftment of HSCs from CLL patients in immunodeficient mice implies that the alterations in genetic and epigenetics at the very early stage resulting in CLL may already exist at the pluripotent stage of HSCs (**Figure 2**).[40,49]
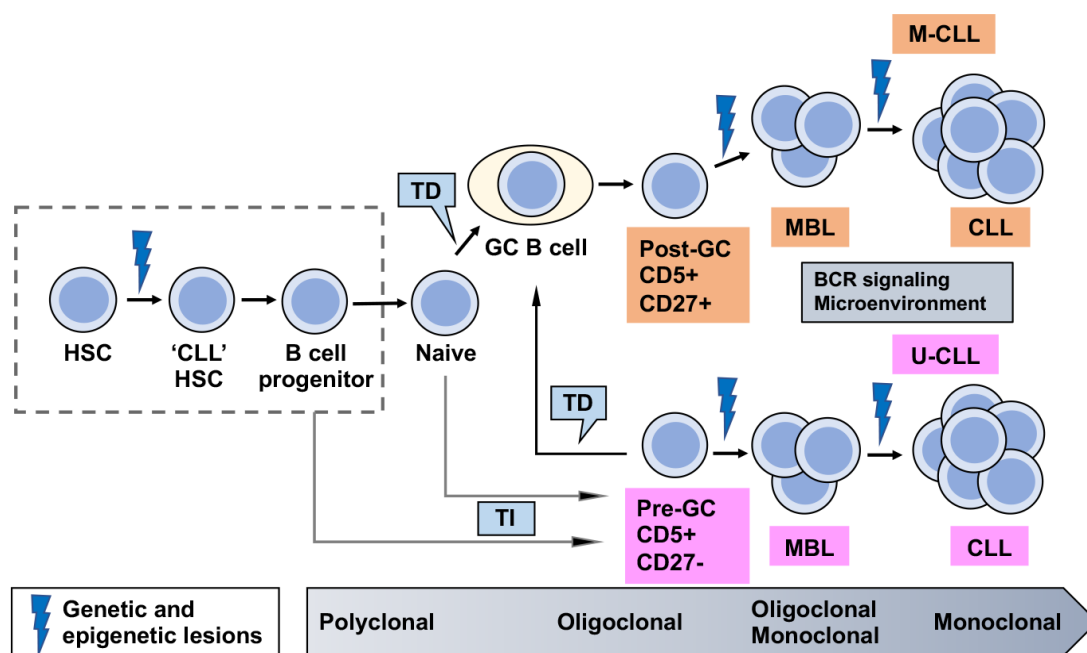
Figure 2. Concepts of the cellular origin of CLL (modified from *Fabbri & Dalla-Favera, 2016*).[40] HSCs may provide growth/survival advantages for B cells by acquisition of genetic and epigenetic lesions, which in the setting of T-cell-independent (TI) or T-cell-dependent (TD) immune stimulation may eventually progress to CLL. *IGHV* mutated CLL seem to originate from post germinal center (post-GC) CD5+CD27+ B cells, which are like memory B cells and are most likely derived from CD5+CD27- B cells that have experienced the GC reaction. *IGHV* unmutated CLL seem to originate from pre-GC CD5+CD27- B cells, which may derive from naive B cells or from a distinct lineage of precursor B cells. Additional aberrations in genetic and epigenetic, BCR stimulation and micromilieu interactions will ultimately contribute to the emerge of monoclonal CLL.

1.1.2.2 The cytogenetics and genomics in CLL

The cytogenetic landscape of CLL was studied in the early 1990s, which provided useful clinical and prognostic information in patients.[50,51] With the development of the fluorescence in situ hybridization (FISH) test, comprehensive analyses of chromosomal gains and losses were achieved.[52] In 2000, *Döhner et al.* reported that 82% of CLL patients carry at least one of four recurrent aberrations detected by FISH and associated with clinical outcomes.[18] A deletion of chromosome 13 long arm (*del13q*) is the most frequently detected abnormality that has been detected in about 55% of cases with a median survival of 133 months, followed by the acquisition of chromosome 12 (Trisomy 12, *tri12*) in 10-20% of cases with a median survival of 114 months. About 10% of CLL cases harbor deletion of chromosome 11q (*del11q*) with a median survival of 79 months and 5-8% of cases harbor deletion of chromosome 17p (*del17p*) with a median survival of 32 months. In contrast, a normal karyotype is presented in 18% of CLL cases with a median survival of 111 months.[9,18,23] In addition, about 16% of CLL patients carry

a complex aberrant karyotype which is often linked to an inferior clinical outcome.[53] Still, some cytogenetic abnormalities are not included in the standard FISH test, including deletion of 6q21 (*del6q21*), a gain of 2p, and recurrent translocations, e.g., t(14;19)(q32;q13). All of them are linked to poor prognosis (**Figure 3**).[18,54–56]
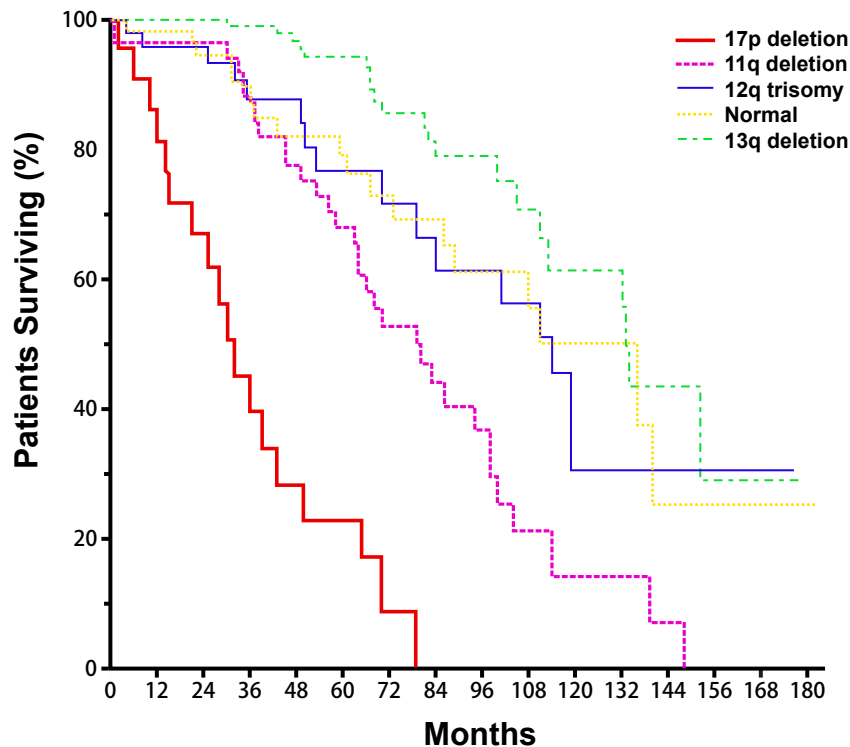
Figure 3. Survival data of CLL patients in five cytogenetic categories from the date of diagnosis (adapted from *Döhner et al. 2000*).[18] The median survival for the five CLL groups: a. 17p deletion, 32 months; b. 11q deletion, 79 months; c. 12q trisomy, 114 months; d. normal karyotype, 111 months; and 13q deletion, 133 months.

In the last years, next-generation sequencing (NSG)-based techniques have expanded the mutational catalogue in CLL.[51] For instance, *del13q* leads to the loss of *DLEU* and micro RNAs (miRs, miR-15a and miR-16-1) in around 68% of CLL cases.[57,58] MiR-15a/16-1-deletion has been shown to regulate the expression of genes (e.g., *CCND1*, *CCND3*, *CHK6*, and *BCL-2*) controlling cell-cycle progression, resulting in an acceleration of proliferation in both human and mouse B cells.[59] The *del11q* leads to the loss of the *ATM* gene that encodes the ATM serine/threonine kinase involved in the DNA damage response. Generally, *del17p* deletes the tumor suppressor gene *TP53*. Over 80% of CLL cases with a *del17p* also carry mutations in the remaining *TP53* allele, disrupting the function of the P53 pathway.[9,60] These genetic mutations are strongly related to more rapid disease progression and chemotherapy resistance. Moreover, recurrent somatic gene mutations have been identified in *NOTCH1, SF3B1, XPO1,*

KLHL6, and *MYD88*.[9,61] *NOTCH1* mutations are among the most frequently detected mutations in 10-14% of newly diagnosed CLL cases, and about 80% of *NOTCH1* mutated cases are U-CLL.[23,62] There is also a striking association of *NOTCH1* mutations with *tri12*.[63] Unlike mutations in *TP53* and *NOTCH1*, which could be expected based on prior knowledge about tumor biology to some degree, aberrations in genes involved in the splicing machinery (e.g., *SF3B1*) were less expected.[64] *SF3B1* encodes the subunit 1 of the splicing factor 3b protein complex, catalyzing removing introns from precursor messenger RNA (mRNA).[65] *SF3B1* mutations can be found in about 10% of newly diagnosed CLL patients, but with a higher frequency in advanced disease.[66] *XPO1* mutations which also affect spliceosomal subunits have been detected in around 5% of CLL patients.[23,61] Similarly to *NOTCH1*, *XPO1* mutations are mainly detected in U-CLL patients, whereas mutations in *KLHL6* and *MYD88* are predominant in M-CLL patients.[61] Altogether, the comprehensive analysis of the whole-genome sequencing, combining with CLL clinical characteristics and outcomes, advanced the identification of clinically relevant mutations in CLL.[61]

1.1.2.3 The microenvironment of CLL

In addition to the alterations in genetics, the tumor microenvironment that promotes tumor growth and protects cancer cells from apoptosis or immune surveillance has become a central hallmark of cancer.[67,68] Particularly in CLL, the survival and proliferation of CLL cells are highly dependent on external factors, although these malignant B cells have some intrinsic genetic features promoting their accumulation.[68] The BCR signaling that is central to the CLL microenvironment has been reported to be critical in pathogenesis.[69,70] Interestingly, a subset of IgG-expressing CLL cases share remarkably similar BCRs (stereotyped BCRs).[71] Further, studying the capability of different types of antigen/BCR interactions in the pathogenesis of CLL has provided a better understanding of how BCR interactions/signals affect CLL development and progression.[72] Cell-autonomous BCR interaction and interactions with low-affinity autoantigens that are considered primarily a feature of U-CLL BCRs, involving binding to endogenous antigenic elements, are preferred in the U-CLL pathogenesis.[72] Antigen-induced BCR activation leads to phosphorylation and recruitment of immunoreceptor tyrosine-based activation motifs (ITAMs) tyrosines by the SRC family kinases, including LYN, FYN, and BLK.[73] BCR downstream kinases, like BTK and PI3K, are recruited by subsequent phosphorylation cascades. Activation of BCR signaling with further activation of downstream signaling cascades eventually mediates cell proliferation, survival, and migration.[69] Moreover, ZAP70 tyrosine kinase has been shown to enhance BCR signaling capacity.[74] Overexpression of ZAP70 is associated with an adverse disease feature and a poor outcome. Besides, the expression of CD38 is linked to BCR activation.[69] CD38-CD31 interactions appear to promote CLL cell

survival and contribute to pathways involved in migration and homing.[69,75,76] Overall, increased understanding of the importance of BCR signaling in CLL provides new opportunities for target therapy.

Besides the BCR pathway, the other aspects (non-transformed elements) of the CLL micro-milieu, including nurse-like cells (NLCs) from monocyte lineage, stromal cells, and T cells, can also affect the CLL cell migration, homing, and proliferation.[68] NLCs are tumor-associated macrophages deriving from monocytic lineage. Monocytes differentiated NLCs can promote CLL B cells survival and proliferation in a co-culture system in vitro.[77] In CLL patients, NLCs in the lymph nodes and BM are associated with the viability of leukemic cells.[78] NLCs express high levels of genes encoding adhesion/migration molecules, including B-cell activating factor (BAFF), a proliferation-inducing ligand (APRIL), and CD14. They interact with CLL cells through secreted cytokines and chemokines to enhance homing, survival, and proliferation of CLL cells.[79,80] Therefore, NLCs are wildly used as an in vitro co-culture model for the assessment of substances targeting the interaction of CLL cells and their micromilieu.[68] Like NLCs, stromal cells recruit CLL cells into the tissue environments by secreting chemokines and inducing up-regulation of factors that promote CLL cell survival and proliferation by direct contact.[68,81,82] Stromal cells are recognized as "feeder" layers for normal hematopoietic progenitor cells.[68] In vitro, some CLL cells can migrate towards the bone marrow stromal cell (BMSC) layer.[83] In addition, CLL-derived exosomal protein and miR have been reported to enhance proliferation, migration, and secretion of inflammatory cytokines in stromal cells.[84] Furthermore, injecting CLL cells together with CLL-derived exosomes into immunodeficient mice promoted tumor growth.[68,84]

Importantly, CLL cells also stay in close contact with T cells in the micromilieu, and T cells are involved in providing regulatory signals within the tissue.[68,85] CLL-related T cells with increased expression of the exhaustion markers (CD244, CD160, and PD1) are also known for their functional defects, as "exhaustion".[86] They can also express the inhibitory receptor, cytotoxic T-lymphocyte associated antigen-4 (CTLA-4; CD152). Disrupting the immune control state of the CLL micromilieu by inhibiting CTLA-4 or the PD-1/PD-L1 axis may be of clinical significance.[87] Other cellular components in the CLL micromilieu include NK cells with reduced capacity to lyse leukemia cell lines associated with a lack of cytoplasmic granules,[88] myeloid-derived suppressor cells (MDSCs) that play a role in the defective T and NK cells of the CLL micromilieu,[89] and endothelial cells as well as follicular dendritic cells, which are important for homing.[68] These cellular components as well as the BCR pathway work together and provide an environment for CLL cell survival and proliferation (**Figure 4**). This provides rationales to target these interactions and involved signaling pathways.
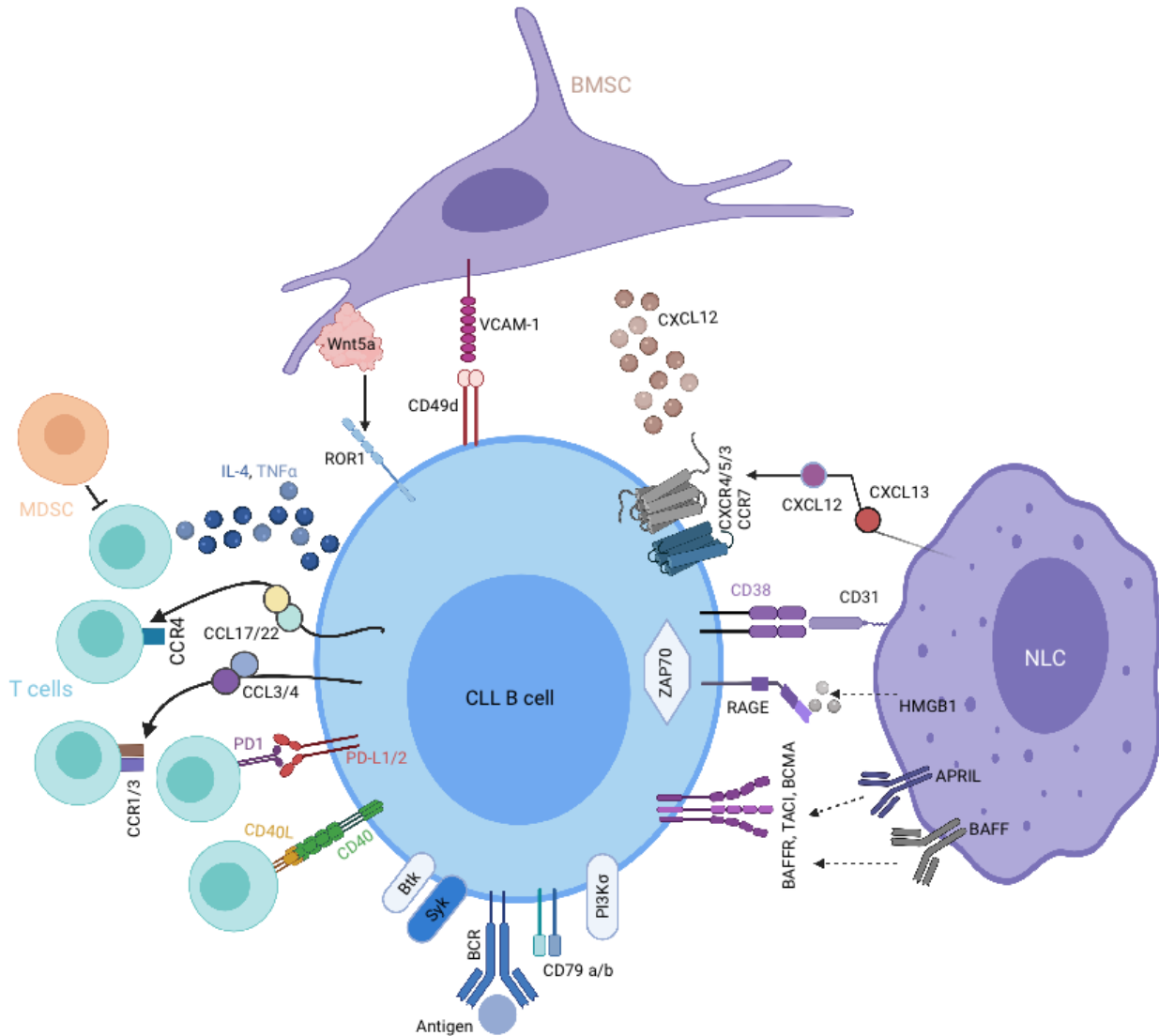
Figure 4. CLL and its microenvironment (adapted from *Choi et al. 2016*).[68] The interaction between CLL cells and their micromilieu facilitates leukemic cell survival, proliferation, homing and tissue retention. The connection between CLL cells and bone marrow stromal cells (BMSCs) or nurse-like cells (NLCs) is regulated by chemokines, chemokine receptors, kinases, and adhesion molecules expressed by leukemic or cells from the micromillieu. The NLCs express CXCL12 and CXCL13, while BMSCs exclusively express CXCL12. NLCs and BMSCs attract CLL cells via interaction of CXCR4/5 receptors, which are higher expressed in CLL cells in comparison to normal B cells. CXCR3 and CCR7 on leukemic B cells are involved in lymphatic tissue homing. NLCs express some of the proteins belonging to TNF family like BAFF and APRIL providing pro-survival signals to CLL cells by binding to the respective receptors BAFFR, TACI, and BCMA. CLL cells express CD49d and interact with VCAM-1 expressed on BMSCs to facilitate cell-cell adhesion. The receptor ligand interaction of CD38-CD31 results in ZAP-70 phosphorylation. The recruitment of ZAP-70 and other kinases of the activated BCR complex increase the ability of antigen response in B cells. The BCR complex stimulation induces activation of downstream signaling, promoting CLL cell survival and proliferation. CLL cells secret CCL3, CCL4, and CCL22 chemokine, which may facilitate to the recruit immune cells. The interaction of CD40 and CD40L were found in the proliferation center of CLL. PD-L1/2 in leukemic splenocytes could cooperate with PD1. MDSC, myeloid-derived suppressor cells.

1.2 The oncogene T-cell leukemia/lymphoma 1A

1.2.1 The T-cell leukemia/lymphoma 1 family genes

The lymphoid proto-oncogene T-cell leukemia/lymphoma 1 family of genes encode small and non-enzymatic proteins that play different roles in mammalian physiology. These genes may be linked to reproduction as well as the development and function of immune cells.[90–93] Three structurally homologous members are known in humans: the mature T-cell proliferation 1 (*MTCP1*), the T-cell leukemia/lymphoma 1A (*TCL1A*), and the T-cell leukemia 1B (*TCL1B*, also called *TML1*). The coding genes are located at 14q32 (*TCL1A* and *TCL1B*) and Xq28 (*MTCP1*).[90–93] The encoded products consist of 106 (MTCP1), 114 (TCL1A), and 128 (TCL1B) amino acids with predicted protein molecular weight of 13 (MTCP1), 14 (TCL1A), and 15 (TCL1B) kDa, respectively.[94–96] Human TCL1 family proteins share a quite high sequence homology: 40% identity and 61% homology between *MTCP1* and *TCL1A*, 36% identity and 63% homology between *MTCP1* and *TCL1B*.[97] These proteins share a common three-dimensional structure consisting of an orthogonal eight-stranded barrel with a unique topology.[97–100] MTCP1 (and probably TCL1B) is a monomeric protein, while TCL1A forms a tight dimer in the crystal and in solution with no intrinsic enzymatic activity or DNA binding domains, which suggests that it mediates its function via protein-protein interactions.[101] Notably, the expression of TCL1A has been implicated in different cancer entities, including hematological malignancies and solid tumors.[102]

1.2.2 The expression patterns of TCL1A

Physiologically, the expression of TCL1A is mainly detected in early embryogenesis, fetal tissues (liver, kidney, thymus, and lung), developing lymphocytes, and adult testis, suggesting that it functions in stem cells and progenitor cells.[103] It has been reported that the absence of TCL1A protein in female mice leads to reduced fertility, indicating its importance in early embryogenesis.[103] In the immune system, TCL1A can be detected in different B-cell developmental stages including pre-B cells, surface IgM expressing B cells, and GC B cells. Its expression decreases in more mature B cells and it is silenced in memory B cells and plasma cells.[104–106] While in T cells, TCL1A is expressed in very early CD4-CD8-CD3- thymocytes, but not in more mature T cells in normal biological conditions.[96,106,107] The expression of TCL1A in healthy tissues implies a potential role of TCL1A in B- and T-cell differentiation.

In the neoplastic context, TCL1A was first identified in T-prolymphocytic leukemia (T-PLL), where high TCL1A levels correlate with higher WBC counts, faster tumor cell proliferation, and consequently a more aggressive disease course.[96,108] Nearly all T-PLL cases harbor the chromosomal aberrations inv(14) or t(14;14), causing a constitutive expression of *TCL1A* through

10

its locus juxtapositioning to T-cell receptor (TCR) gene enhancers.[109] In addition, TCL1A is overexpressed in some other diseases, including Epstein-Barr virus-infected B-cell lymphoma, B-cell CLL, ataxia telangiectasia, seminoma, dysgerminoma, or acquired immune deficiency syndrome-related lymphoma.[104,110] In B-cell malignancies, it has been shown that the expression pattern of TCL1A varies as a function of the developmental stage of the B cells.[110,111] Similarly, high levels of TCL1A are associated with aggressive disease in CLL.[111]

1.2.3   The oncogenic potential and downstream signaling of TCL1A

The oncogenic potential of TCL1A is demonstrated in mouse models. In the *Eµ-TCL1A* transgenic (tg) mice, where human *TCL1A* has been placed under the control of a murine *VH-promoter/IgH-µ* enhancer to target *TCL1A* expression to immature and mature B cells, produce expansions that mimic the biology and course of human CLL.[112] And the transgenic mice that carry the *TCL1A* gene under the transcriptional control of the *Lck* promoter (*Lck-TCL1A*) can develop a T-PLL-like disease.[113] These *TCL1A*-tg mice often present enlarged spleens, lymph nodes, and livers, as well as elevated WBC counts. Another *TCL1A*-tg model, *pEµ-B29-TCL1A* produces GC-derived B-cell tumors mimicking Burkitt lymphoma, follicular lymphoma, and diffuse large B-cell lymphoma.[114] Particularly, the well-established *Eµ-TCL1A* model for CLL has been crossbred with various other alleles. In 2014, *Simonetti et al.* published a comprehensive overview comparing these CLL mouse models, concerning disease phenotype, penetrance, and severity (**Figure 5**).[115] These genetically modified mice present a marked expansion of the CD5+CD19+ population in the peritoneal cavity starting at 2 months of age, and this population becomes evident in the spleen by 3-5 months and in the bone marrow by 5-8 months. Eventually, these mice develop a CLL-like disease resembling human B-CLL.[112]

The overexpression of TCL1A in B- and T-cell tumors and other lymphomas in *TCL1A*-tg mice indicates the contributing role of TCL1A in the pathogenesis of hematological disorders. Nevertheless, the deregulation of TCL1A is not only seen in leukemias like CLL and T-PLL, but also found in several solid tumors like cancers from the bladder, prostate, colon, liver, kidney, thyroid gland, and breast.[116] TCL1A is not expressed in these tissues in physiological conditions. The re-expression of TCL1A in these solid tumors indicates the role of TCL1A in stemness programs.[97] Given the important role of TCL1A in tumor initiation, progression, and maintenance, investigating the downstream signaling of TCL1A can help to better understand the pathogeneses of these tumors.

TCL1A lacks enzymatic activity and reveals no DNA-binding motif. The serine/threonine kinase AKT was the first protein described to interact with TCL1A which increases AKT kinase

activity and mediates its translocation to the nucleus.[117] AKT is a central integrative node that relays important growth signals in normal and in transformed lymphocytes.[117] It seems that TCL1A facilitates AKT-dimerization, hence the phosphorylation of AKT, leading to increased phosphorylation of AKT downstream targets involved in cell survival and proliferation.[117] Furthermore, the serine/threonine-protein kinase ATM, which usually induces cell cycle arrest, DNA repair, or apoptosis upon DNA damage through the NFκB pathway activation, is another important interaction partner of TCL1A.[118] Additionally, TCL1A has been reported to activate NFκB by physical interaction with p300/CREB binding protein.[118] Moreover, TCL1A can also specifically bind subunits of the AP-1 complex and inhibit the transcriptional activity of AP-1.[119] Importantly, AP-1 is known to control many cellular processes including apoptosis.[120] This suggests that TCL1A inhibits the AP-1-regulated pro-apoptotic factors and promotes survival via activating the NFκB pathway simultaneously.

In short, the identified TCL1A-binding partners suggest that TCL1A as a small molecule has various targets and different functions. Therefore, further studies are needed to improve the understanding of the molecular concept around TCL1A.
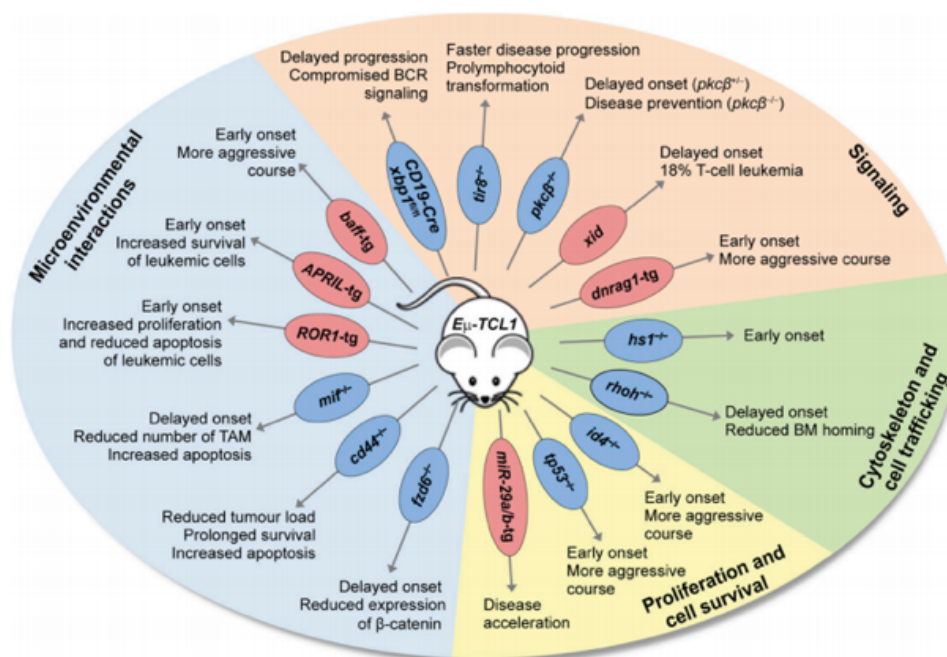
Figure 5. Study of pathogenic mechanisms of CLL in the _TCL1A_-driven leukemia models (_Simonetti et al. 2014_).[115] Several different mouse models have been crossed with _Eμ-TCL1A_ mice to study the function of specific molecules in the pathogenesis of CLL in a _TCL1A_ oncogenic background.

1.2.4   The mechanisms of TCL1A (dys)regulation

The silencing of TCL1A is tightly regulated during embryonic development and T/B-cell differentiation. Although the TCL1A (dys)regulation mechanisms are not being understood completely, there are advances in understanding its transcriptional and post-transcriptional regulations, including genomic aberrations, epigenetic modifications, dysregulation of TCL1A-targeting miRs, as well as modulations via altered signals by the micromilieu.[102]

In murine embryonic stem cells (mESCs), *Tcl1a* was reported to play a role in self-renewal and Oct3/4 was shown to bind to the promoter region of *Tcl1a* and activate its transcription.[121–123] Furthermore, Kruppel-like factors (Klf) 2, 4, and 5 were found to bind to the promoter region of *Tcl1a* and regulate its expression in mESCs.[123] In somatic cells, there is a TATA box with cis-regulatory elements within the 5'-promoter region of *TCL1A* for several transcription factors (TFs),[124] including nuclear receptor subfamily 4 group A member 1 (NR4A1, also called Nur77) with its nerve growth factor-responsive element (NBRE), but also nuclear factor NF-κB, forkhead box protein O3 (FOXO3, also called FKHRL1), P53, and the TF SP1.[97,124]

There are also suppressive relationships of TFs binding to *TCL1A* promoter, most of them are implicated by indirect evidence from associated data, such as FKHRL and P53.[124] Nevertheless, a negative regulation has been demonstrated to work via AKT and its substrate NR4A1. NR4A1 is activated by phosphorylated AKT and prevented from binding to the NBRE of the *TCL1A* promoter, leading to transcriptional suppression of *TCL1A*.[124] This implicates that TCL1A-induced increase of lymphocyte activation causes subsequent repression of this oncogene under normal conditions, which might be disturbed in malignant B cells or T cells. Additionally, a novel CREB/TORC2 regulatory mode of TCL1A has been described to be of importance in GC B cells.[125] Besides, different miRs have been implicated to negatively regulate TCL1A at the post-transcriptional level. MiR29 and miR181 were shown to repress TCL1A in CLL.[125,126] Higher TCL1A levels were observed in CLL cases with aggressive disease features characterized by chromosomal loss of 11q22 (*ATM*) and 17p (*TP53*),[127,128] with an implied co-deletion of TCL1A repressive miRs miR34b/c and miR3676, respectively.[127,128] Our group found miR484 as a new inhibitory regulator of TCL1A in CLL.[129] Moreover, our lab has shown that direct cell-cell contact of the leukemic cells with BMSCs leads to upregulation of TCL1A,[129] which is linked to decreased levels of TCL1A-repressive miRs (miR29b, miR181b, miR34b, and miR484).[130,131]

Overall, a better understanding of the (dys)regulation modes of TCL1A could benefit future approaches to interfere with TCL1A-driven malignant transformation.

1.2.5 Mass spectrometric analysis identified epigenetic factors as novel TCL1A interacting partners in primary CLL cells

Despite intensive efforts to clarify the molecular mechanisms of TCL1A's oncogenic function, the identification of specific TCL1A-mediated pathways remains a challenge. TCL1A shows no intrinsic enzymatic activity and has no DNA-binding motif suggesting that it mediates its activity in a chaperone-like approach via protein-protein interactions. Indeed, previous studies have demonstrated that TCL1A can activate the AKT kinase and other targets through defined protein-protein interactions, resulting in NFκB-dependent and independent pro-survival effects.[117,129,132] Our lab has generated evidence that implicates TCL1A as a modulator of BCR and TCR signaling, through which it acts lymphocyte permissive at the levels of AKT kinase activation and/or permissive kinase substrate biases.[108,111] More recent discoveries indicate that TCL1A might be involved in DNA damage/repair pathways and, importantly, epigenetic events.[118,133]

The mutual cause-effect interplay between TCL1A and epigenetic processes has been underappreciated, but there are emerging data around this aspect. First, the expression of the TCL1A gene is controlled epigenetically, e.g., TCL1A expression is elevated due to hypomethylation of its promoter regions in CLL.[134] Similarly, TCL1A was shown to be a downstream effector of lysine demethylase 3A (KDM3A) in embryonic stem cells.[135] There, KDM3A demethylates dimethyl (me2) of histone3 (H3) on lysine 9 (K9; H3K9me2) at *TCL1A* promoter regions and by that positively regulates its expression, ultimately thought to promote stem cell self-renewal and pluripotency via the TCF3/NANOG/TCL1A signaling axis.[135,136] On the other hand, TCL1A can control the global DNA methylation landscape by suppressing the activity of the de novo DNA methyltransferases Dnmt3a/b through direct protein-protein interaction.[133]

Importantly, our mass-spectrometry (MS) based screen for new TCL1A interaction partners identified a panel of chromatin-modifying enzymes as novel TCL1A interactors in B cells (**Figure 6, Table 1**), suggesting that TCL1A may be involved in the epigenetic modification. Moreover, epigenetic regulators in general and histone-modifying enzymes in particular, are much less well investigated in CLL.

Table 1. Patient characteristics of samples used in MS analysis

Patient ID	Age	Karyotype	ZAP70 (%)	CD38 (%)	IGHV	Binet stage	WBC (x10⁹/L)	LDT (months)
CLL1	74	Normal	neg	pos	M	A	174.54	>12
CLL2	65	Normal	1	31	M	A	109.05	>12
CLL3	43	del(13q)	3	1	M	A	94.99	>12
CLL4	79	normal	3	6	U	C	94.57	>12
CLL5	55	normal	2.8	0.7	U	B	189.33	

CLL6	71	del(13q)	2.8	28.7	M	C	71.42	>12
CLL7	58	del(13q)	13	0.4	M	C	300	>12
CLL8	72	del(17p)	4	80	M	A	62.06	>12
CLL9	56	del(11q), CAK	41	41	U	B	81.39	n.a.
CLL10	67	del(11q), del(13q)	2	73	U	B	77.41	<12
CLL11	45	del(11q)	25.5	9.5	U	A	101.84	

IGHV: *IGHV* mutation status; M: *IGHV* mutated; U: *IGHV* unmuted; CAK: complex aberrant karyotype
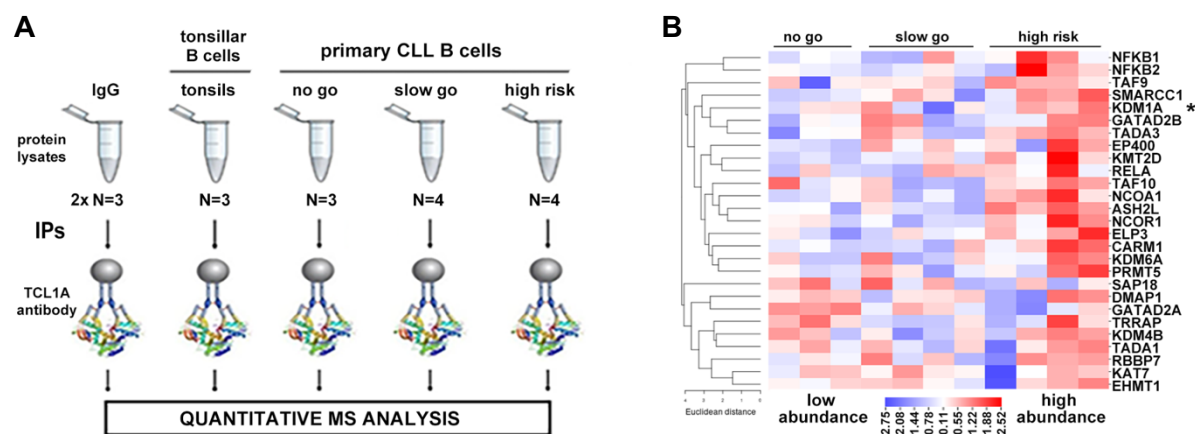
Figure 6. TCL1A interacts with epigenetic factors in CLL B cells. (A) Experimental setting of mass-spectrometry (MS) of TCL1A co-immunoprecipitations (co-IPs) in human CLL B cells (non-malignant B cells from tonsils as biological controls). IgG co-IPs in CLL B cells served as technical controls. Three subgroups based on CLL clinical status / (cyto)genetic risk: 1. "no go": early-stage CLL with an indolent clinical course under a 'watch & wait' strategy (all *IGHV* mutated N=3), 2. "slow go": advanced disease stage and need treatment, but without high-risk genetic lesions (*IGHV* mutated N=2, unmutated N=2), 3. high-risk cases with deletions or mutations of *TP53* or *ATM* (*IGHV* mutated N=1, unmutated N=3). Proteins that showed a significant enrichment between the IgG control and CLL samples (459 proteins)/tonsils (889 proteins) were considered TCL1A interacting partners (Welch test, FDR q-value≤0.05, fold change≥2.0). 318, 350, and 326 proteins were identified in "no go", "slow go", and "high-risk" groups, respectively. 217 interacting partners overlapped across all three risk categories. **(B)** Heatmap showing the epigenetic modifiers that interact with TCL1A. KDM1A (*) was found to interact with TCL1A in CLL cells.

1.3   Epigenetic regulation of gene expression

As a macromolecular complex of DNA and histones, chromatin provides the scaffolding for the packaging of the entire genome and contains the genetic material of eukaryotic cells.[137] Nucleosome, consisting of 147 base pairs (bp) of DNA, is the basic functional unit of chromatin.[137] Nucleosome is wrapped around a histone octamer, with two each of histones H2A, H2B, H3, and H4 (**Figure 7**).[137] Generally, chromatin can be divided into two main regions: euchromatin, regions of DNA containing genes that are actively transcribed; and heterochromatin

which is greatly condensed and contains inactive genes.[137] Studies on the coordinated regulation of the nucleosome have shown that all the nucleosome components can be covalently modified. The modification alters the organization and function of these basic chromatin tenants.[137,138] Epigenetics, the chromatin-based events that regulate DNA-templated processes, can be modified in different manners, including DNA modifications and histone modifications. These modifications are highly regulated by chromatin-modifying enzymes.[137] An important DNA modification is DNA methylation, which has a variety of biological functions.[139] There have been rapid advances in the understanding of the epigenetic mechanisms of DNA methylation and histone post-transcriptional modifications (PTM) concerning their contribution to oncogenesis.[140]
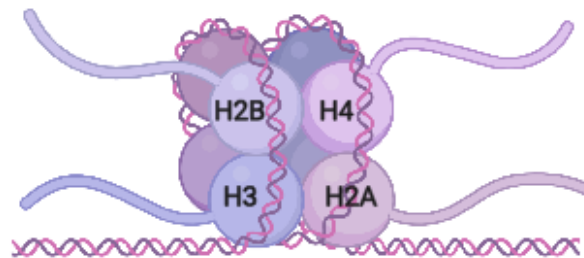
Figure 7. The structure of nucleosomes. A nucleosome is formed by 146 bp of DNA bound to a histone octamer.

During the last decades, the gene expression architecture has been clarified (**Figure 8**).[141] Nucleosome positions change dynamically during cell replication and with gene expression changes.[141] Active gene promoters, which are cytosine-guanine dinucleotides (CpG)-rich and lack DNA methylation, have nucleosome-depleted regions (NDRs) upstream of their transcription start sites (TSS). The nucleosomes next to NDRs are marked by the tri-methylation (me3) of histone 3 on lysine 4 (H3K4me3), which may facilitate the initiation of transcription by destabilizing nucleosomes.[141] More histone marks have been reported to be involved in promoting transcription, including H3K4me1, H3K9me1, H3K27me1, H3K36me3, H4K20me1, and H3 acetylation on lysine 27 (H3K27ac).[141,142] H3K4me1 and H3K27ac are defined as active enhancer marks.[143] In contrast, H3K9me2, H3K9me3, H4K20me3, and H3K27me3 marks are repressive histone modifications.[142] And DNA methylation stabilizes epigenetic gene silencing with promoter CpG islands.[141] This is generally linked to inactive X-linked genes in normal conditions, but also common in aberrant gene silencing in cancer.[141]
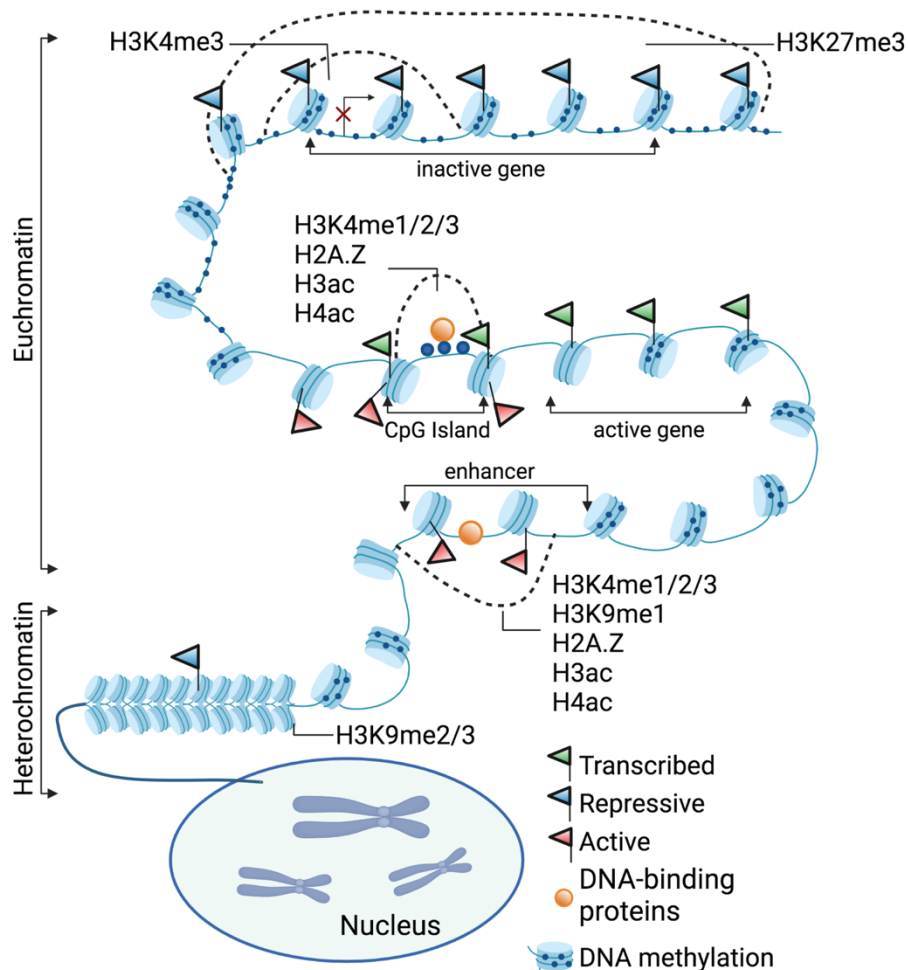
Figure 8. The structure of the epigenome in normal human cells (adapted from *Baylin S et al., 2011*).[141] The normal packaging state of DNA is maintained by the balanced state of chromatin, nucleosome positioning, and DNA methylation. Chromosomes are divided into accessible regions of euchromatin and poorly accessible regions of heterochromatin. Heterochromatic regions are marked with di-/tri-methylation of histone H3 on lysine 9 (H3K9me2/H3K9me3). DNA methylation is missing in regions such as CpG islands, promoters and possibly enhancers. The H3K27me3 is present in broad domains containing inactive genes. The transcription start site regions of active genes are marked by H3K4me1/2/3, histone acetylation, and histone variant H2A.Z.

1.3.1   DNA methylation

DNA methylation is a biological process whereby methyl groups are added to the DNA molecule at the carbon-5 position of the cytosine base (5-methylcytosine; 5mC) primarily in the context of CpG, mediated by the DNA methyltransferase enzymes (DNMTs) (**Figure 9**).[144] DNA methylation plays an essential role in cell biology, including regulation of gene expression, centromere stability and chromosome segregation in mitosis, inactivating X-chromosome, and monoallelic silencing of imprinted genes.[144] It is well established that DNA methylation is frequently changed in cancer, including DNA hypomethylation events at centromeres and

oncogenes in combination with focal DNA hypermethylation linked to repression of critical gene regulatory elements (**Figure 10**).[144] It is of importance to understand the dynamic DNA methylation patterns in normal cell biology and disease development.
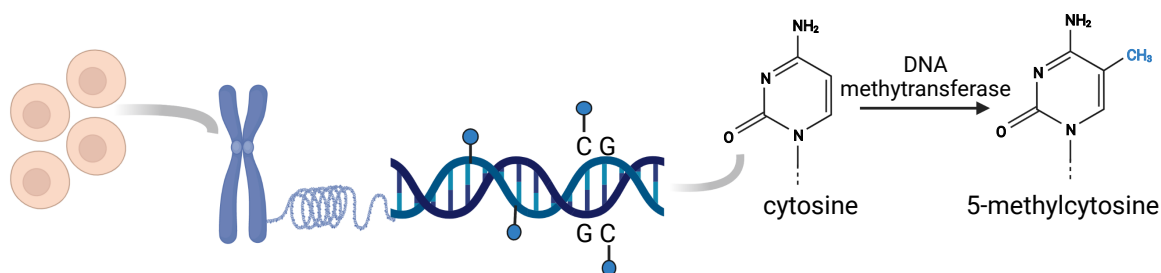
Figure 9. The process of DNA methylation (adapted from *Skvortsova K et al., 2019*).[144] DNA methyltransferase enzymes (DNMTs) catalyze the addition of a methyl group to the fifth carbon position of cytosines primarily within CpG dinucleotide contexts (5-methylcytosine; 5mC).
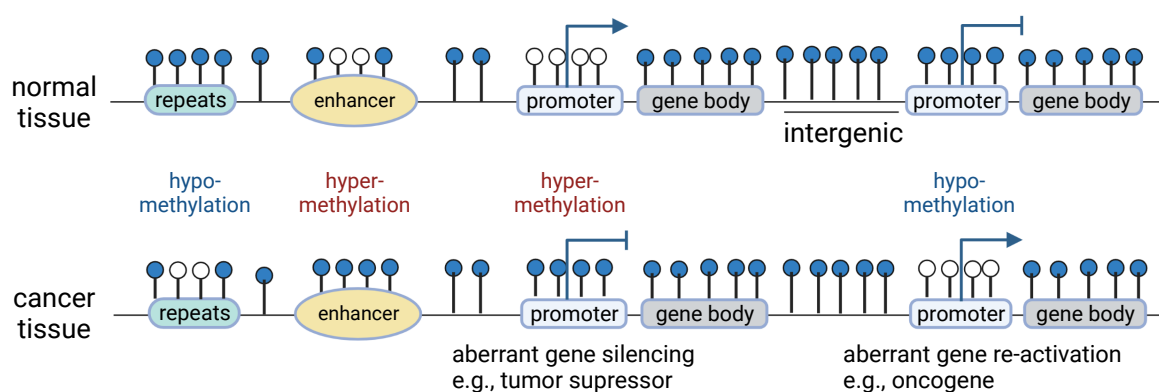
Figure 10. Distinct DNA methylation profiles in normal and cancer genomes (adapted from *Skvortsova K et al., 2019*).[144] Normal (top) and cancer (bottom) cells present different DNA methylation patterns throughout the genome, including all gene regulatory elements. Cancer cells show abnormal increased DNA methylation at enhancers and promoters. This change in distribution leads to a suppression of tumor suppressor genes and activation of oncogenes, driving tumorigenesis. White circle, unmethylated; blue circle, methylated.

1.3.2 Histone modification

In addition to DNA methylation, on which cancer epigenetics has been largely focused, histone modifications are important determinants of epigenetic state.[145] It has been known that histones are post-translationally modified since the early 1960s.[146] Since then, it is well noted that PTMs of histones play a key role in mediating a diversity of biological processes, through chromatin modification leading to the expression or repression of target genes.[147] With the development of chromatin immunoprecipitation (ChIP) technologies, including ChIP with DNA microarray analysis (ChIP-chip) and ChIP-sequencing (ChIP-seq), different alteration patterns

of histone PTMs have been associated with cancer, at the global level across the genome and specific gene loci.[146] The most described histone modifications are acetylation, methylation, and phosphorylation. Histone acetylation is generally associated with transcriptional activation, particularly at enhancers, promoters, and the gene body.[148] Furthermore, the alterations in global histone acetylation, predominantly acetylation of H4K16, have been linked to phenotypes of different cancers,[149] which could also be predictive of their clinical outcomes.[150] Histone phosphorylation, which takes place on serines, threonines, and tyrosines, mainly in the N-terminal histone tails, is highly dynamic as that like histone acetylation.[150] Kinases adding and phosphatases removing the modification, control the modification levels.[150] However, histone methylation mainly appears on the side chains of lysines and arginines, which does not have an impact on the charge of the histone protein.[151] Unlike histone acetylation and phosphorylation, histone methylation can be a transcriptional repressor or activator.[151] Besides, the histones can be methylated in multiple degrees, with lysine forming mono-, di- or trimethylation (me1/2/3), whereas arginine methylation occurs in mono- or dimethylated (symmetric or asymmetric) forms.[152] Histone methylation is a dynamic process with crucial roles in development and differentiation, and aberrant methylations are likely to play a role in the pathogenesis of tumors.[153] Of note, numerous enzymes that are responsible for placing as "writers" and removing as "erasers" epigenetic marks have been identified (**Figure 11**).[146] Mutations in these enzymes are among the most common mutated targets in cancers.[146] Overall, the epigenetic layers of chromatin dynamics and histone modulations added to the complexity of our understanding of the oncogenic transformation.
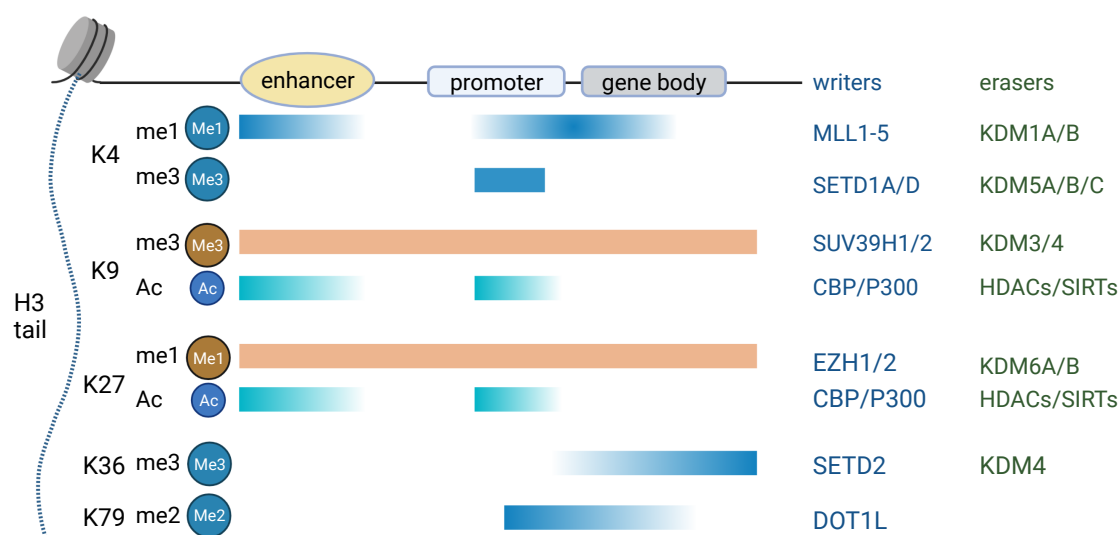
Figure 11. Histone writers and erasers (adapted from *Audia J et al., 2016*).[146] Histone H3 tail lysine residues are frequently subjected to post-translational modifications (PTMs). Typically, the distribution of these H3 PTMs is indicated along the length of gene loci. Blue (methylation) or green (acetylation) indicate histone marks associated with active genes, whereas orange indicates silent genes. Examples of some writers and erasers, which may propagate a mark or act as an effector protein, are listed on the right.

1.3.3 Epigenetic disturbances in CLL

The disturbance of epigenetic mechanisms is also central in the pathogenesis of CLL, although this is inferred primarily from genomic profiling data and direct experimental evidence that is better established for DNA methylation than for histone modulation.[154–157] The global DNA methylation profile of CLL cells is relatively stable over time and highly similar in resting (peripheral blood) and proliferative (lymph node) compartments, suggesting aberrant methylation as an early leukemogenic event.[158] *Chen et al.* have also reported that aberrant methylation of genomic DNA can be detected before disease onset in a CLL mouse model (*Eµ-TCL1A* mice).[154] In human CLL, tumor clones seem to derive from a spectrum of B-cell maturation stages and their DNA methylation pattern predicts two clinically relevant major molecular subtypes of CLL, derived from naïve- or memory-like developmental stages.[155] The global epigenetic changes observed in CLL ultimately lead to misexpression of genes crucially involved in its pathogenesis, such as DAPK1, LEF1, MYB, HOXA4, or ZAP70.[156,159,160]

The other branch of covalent modifications in chromatin remodeling, namely acetylation or methylation of histones, has moved into focus in the CLL field. Pilot studies demonstrated differential expression of histone PTMs in CLL and acute myeloid leukemia (AML).[161] More recent findings indicate that altered histone profiles can distinguish between healthy individuals and CLL patients.[162] Similarly, chromatin accessibility signatures were shown to predict *IGHV-* specific CLL subsets.[163] A comprehensive analysis of the epigenome of CLL samples with complete genetic characterization and samples spanning the normal B-cell developmental stages has also improved our understanding of the biological basis and clinical courses of CLL.[164] Alterations in the CLL-specific transcriptome are associated with deregulated chromatin features and activity changes of a TF network downstream of microenvironmental signaling cascades.[165]

Furthermore, recent studies have explored the roles of histone-modifying enzymes in regulating transcriptional expression in CLL. The global levels of histone deacetylase (HDAC) have been described as an independent prognostic marker for treatment-free survival (TFS) and OS.[166,167] *Zhou et al.* reported global hypoacetylation of H3/H4, hypermethylation of H3K9, and upregulation of SIRT1 and EZH2 in CLL cases.[167,168] While recurrent deletions and mutations of the histone methyltransferase SETD2 were also found in CLL.[169] Interestingly, pharmacological HDAC inhibition by valproate was shown to increase the expression of CD20 in vitro but not in vivo, where the H3K9ac was induced.[170] In fact, valproate induced H3K9ac and EZH2-mediated H3K27me3 at the promoter region of *CD20* in vivo.[167,170] These findings indicate the requirement or benefit of combination treatments in CLL. Indeed, one study has shown that a combination of HDAC inhibitor with BTK inhibitor ibrutinib induces synergistic effects on cell death and improves OS in vivo.[171] EZH2 is overexpressed in CLL cases with

poor prognosis and is associated with H3K27me3.[172] EZH2 inhibition led to apoptosis in vivo.[167,173] In addition, it was shown that the anti-apoptotic effect of EZH2 can be regulated via microenvironmental mechanisms.[173]

In short, recent studies have provided valuable knowledge on the chromatin landscape of CLL, including currently still understudied histone modifications. A better understanding of CLL epigenetics and epigenomics could help to find novel biomarkers or drug targets.

1.4 The lysine-specific demethylase KDM1A

Histone methylation was considered to be a stable and static modification for many years.[153] Nonetheless, various pathways were suggested as potential demethylation mechanisms for both lysine and arginine in 2002.[174,175] Initially, the transfiguration of arginine to citrulline through a deimination process was shown as a way to antagonize arginine methylation,[176] which indicated that methylation was irreversible. More recently, the Jumonji domain-containing 6 protein (JMJD6) was reported to demethylate histones H3R2 and H4R3.[176] In 2004, *Shi Y et al.* identified the first lysine demethylase which was found to utilize flavin adenine dinucleotide (FAD) as a co-factor and was termed as lysine-specific demethylase 1A (KDM1A), also known as LSD1.[177] It specifically removes mono- and di-methyl groups from lysine 4 or 9 in H3 (H3K4me1/2, H3K9me1/2), leading to transcriptional alterations.[178]

1.4.1 The structure of KDM1A

KDM1A consists of 852 amino acids coding 3 main domains: 1) Swi3p/Rsc8p/Moira (SWIRM), small alpha-helical domain in the N-terminal, the critical domain for the protein-protein interactions contributes to the protein stability;[179] 2) In the C-terminal, there is an amine oxidase-like (AOL) domain that shares 20% sequence similarity with FAD-dependent oxidase;[180] 3) A central protruding Tower domain is formed by a big insertion that separates the AOL domain into two halves (**Figure 12**).[180,181] The complex structure of KDM1A that allows its interaction with various cellular proteins is most likely the basis of its functional diversity.[181] Particularly, the AOL domain, responsible for targeting substrate proteins, was defined as the catalytic center modulating the enzymatic activity.[180,181] The Tower domain divides the AOL domain into two sections. One forms a non-covalent FAD-binding site, similar to other amine oxidases. The other forms a more open active funnel-shaped site for substrate recognition and binding, enabling KDM1A to store more surrounding residues near the target lysine, e.g., accommodating long histone tails by interacting with the first 20 amino acids of H3.[181,182] Moreover, the flexible region in the N-terminal is a non-catalytic domain that is involved in protein-protein interactions and subject to PTMs.[181,183,184] The SWIRM domain, located far away from the

FAD-binding site and the catalytic center, forms a functional structure interface together with the AOL domain, contributing to the involvement of protein interactions.[180,181]

Figure 12. Overview of the structural domain of KDM1A (modified from *Gu et al. 2020*).[181] KDM1A contains the catalytic amine oxidase-like domain (AOL, light blue), a SWIRM domain (yellow), and a Tower domain (dark blue). The N-terminal flexible region and the C-terminal tail are in gray.

1.4.2   The biological function of KDM1A

The demethylase KDM1A was first recognized as the interacting partner of the corepressor (CoREST) transcription repressor complex and the histone deacetylase HDAC1/2.[185–187] In the complexes with CoREST and Nucleosome Remodeling and Deacetylase (NuRD), KDM1A as a transcription repressor demethylates H3K4me1 and H3K4me2, which imply activation of chromatin transcription state, respectively.[177,187–189] But as a co-activator, KDM1A can interact with the androgen (AR) and estrogen (ER) receptors and modify the specificity of its substrate through demethylation of the transcription repressive marks H3K9me1 and H3K9me2.[190,191] Besides, the splicing variant of KDM1A (KDM1A+8a) that contains four additional amino acids (exon 8a) has been shown to promote the transcription of neuronal-regulated genes by targeting methylation of H4K20.[187,192] Taken together, the histone demethylase KDM1A as transcriptional coregulator can be transcription repressor or activator via demethylating different histone marks (**Figure 13**).

Moreover, KDM1A also demethylates non-histone proteins, including P53, DNMT1, STAT3, E2F1, RB1, MEFD2, MTA1, ERα, HSP90, HIF-1α, and AGO2 (**Figure 14**).[187,193] The demethylase activity of KDM1A changes the stability of these proteins and modulates their function. Particularly, KDM1A enhances the functional activity of STAT3 and P53 without affecting their expression levels, whereas it destabilizes the protein MYPT1 and stabilizes E2F1, MEFD2, and HIF-1α proteins.[187] Demethylation of non-histone lysine residues induced by KDM1A may affect different cellular processes. Understanding the influences of KDM1A in cell biology is an emerging field in cancer biology.[187] In addition, KDM1A can be targeted by post-translational modifications that change its activity or stability, subsequently modifying its transcription regulation.[187,194,195] Phosphorylation of KDM1A at serine 112 by Protein kinase C alpha (PKCα) is crucial for its binding and demethylation activity.[196] KDM1A acetylation by the acetyltransferase MOF has been identified to be involved in the regulation of KDM1A and epithelial to mesenchymal transition (EMT).[197]

Over the last years, reports on the diversity of functions have indicated that KDM1A may have additional biological functions beyond catalytic demethylation. KDM1A accelerates the protein

degradation of F-box and WD repeat-containing protein 7 (FBXW7)[198] or p62[199] via protein-protein interactions, resulting in different bioconsequences.[181]

In general, KDM1A could elicit different biological functions via catalytic and non-catalytic mechanisms.
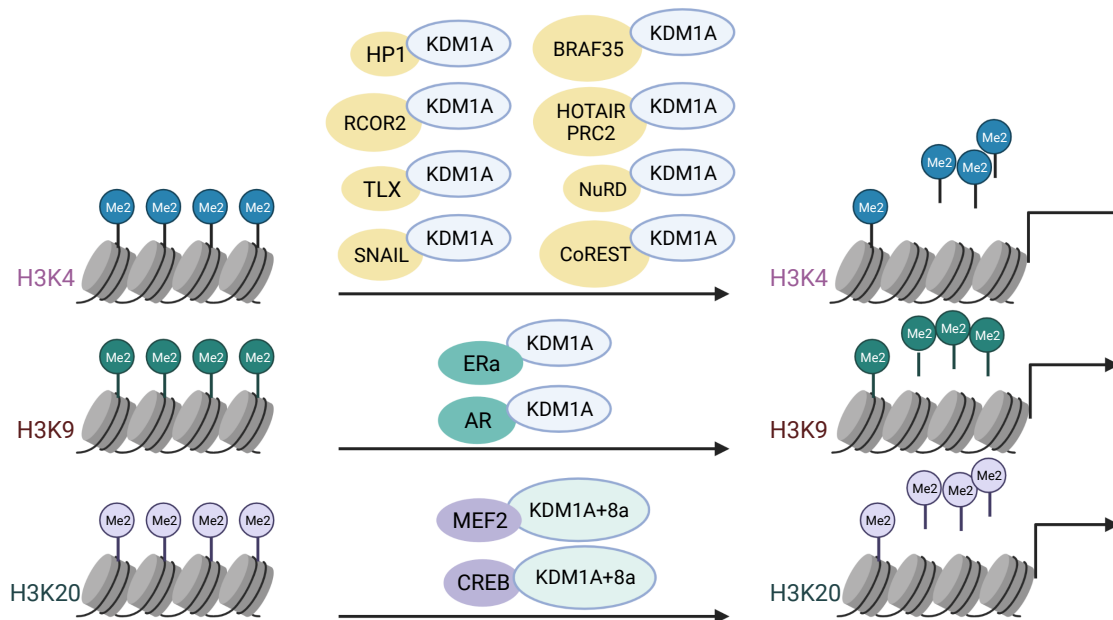
Figure 13. Transcriptional role of KDM1A (adapted from *Majello et al. 2019*).[187] Top: KDM1A is recruited at the target gene by indicated transcription factors where it represses the transcription through removing methyl from the activation mark H3K4me2. Middle: KDM1A demethylates the repressive mark H3K9me2 as coactivator with the androgen or estrogen receptor. Bottom: KDM1A+8a, a neuronal-specific isoform interacting with CREB and MEF2, catalyzes the demethylation of the repressive mark H4K20me2.
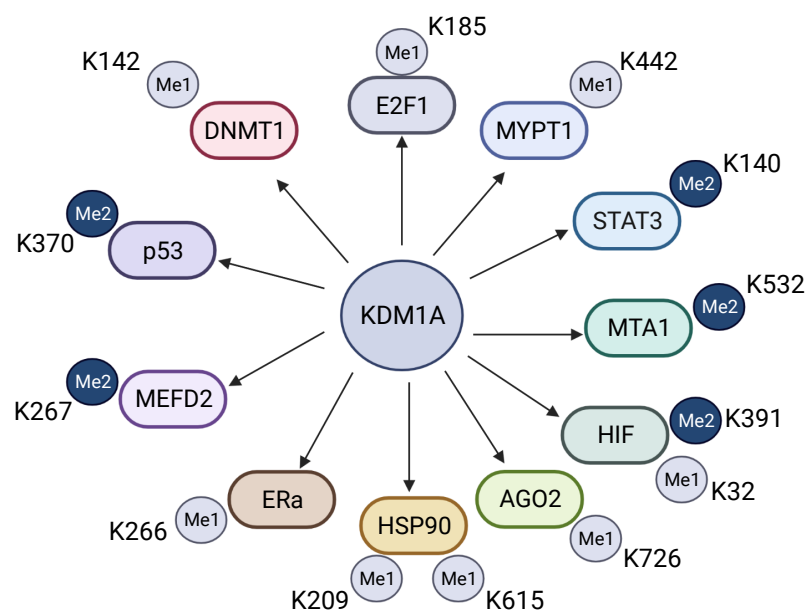
Figure 14. KDM1A demethylates non-histone proteins on specific lysine residues (adapted from *Majello et al. 2019*).[187]

1.4.3 The regulation of KDM1A

KDM1A can be regulated both transcriptionally and post-transcriptionally.[200] The miR-137 targets the mRNA of KDM1A and suppressed its expression in neuroblastoma and colon cancer cells.[201,202] While an essential regulator of neural stem cell self-renewal, tailless-like (TLX) represses miR-137 expression by recruiting KDM1A to the genomic region of miR-137, suggesting that miR-137 controls the dynamics between neural stem cell proliferation and differentiation during neural development by forming a feedback regulatory loop with TLX and KDM1A.[200,203] KDM1A can be phosphorylated by PKCα in a circadian manner and the complex of phosphorylated KDM1A with pioneer-like transcription factor CLOCK:BMAL1 facilitates E-box-mediated transcriptional activation.[204] Interestingly, hyperphosphorylated KDM1A has been observed in nocodazole synchronized cells.[205] The impacts of this phosphorylation on the cell cycle as well as on chromatin states remain unknown.[200,206] However, the regulation of KDM1A is in a cell cycle-dependent manner.[200] At G1, S, and G2 phases of the cell cycle, KDM1A is localized in the nuclei of cells, consistent with its chromatin-modifying activity. But when cells go through mitosis, KDM1A is moved from the chromatin and is mainly present in the cytoplasm.[206]

Moreover, it has been reported that KDM1A is controlled by the ubiquitin-proteasome system and it is prone to proteasomal degradation upon CoREST loss in vivo.[186,207] *Wu Y. et al.* demonstrated that the formation of a Snail-KDM1A-CoREST complex plays a key role in maintaining the stability and proper function of these proteins.[207] They further showed that ubiquitin-specific peptidase 28 (USP28) stabilizes KDM1A via inhibiting its ubiquitination.[208]

1.4.4 How is KDM1A causally implicated in cancer?

KDM1A has been proposed as a therapeutic target in many cancers, such as prostate, lung, brain, and breast cancers, and some hematologic malignancies.[209] Its overexpression has been reported to correlate with a poor prognosis.[210] KDM1A is involved in cancer stem cell self-renewal, cell proliferation and differentiation, cancer cell metabolic programming, epithelial-mesenchymal transition as well as in metastasis.[187] As a result, numerous pharmaceutical compounds that target KDM1A have been developed and some are undergoing clinical investigation, particularly for small cell lung cancer (SCLC) and AML.[187,210] In addition, germline truncating and missense KDM1A mutations have been recently reported in multiple myeloma.[187] Functionally, KDM1A interacting with different factors might present distinct molecular mechanisms in various types of tumors.

In a mouse model of the human mixed-lineage leukemia (MLL) rearranged AML, Kdm1a was identified as a regulator of leukemic stem cell potential.[211] By promoting the expression of

genes associated with the oncogenic program, Kdm1a prevents differentiation and apopto-sis.[211] Fittingly, the inhibition of Kdm1a caused exhaustion of the leukemia-initiating cell pop-ulation, emphasizing the promising potential of pharmacologic KDM1A inhibition in AML.[211] In hepatocellular carcinoma cells, KDM1A depletion activates mitochondrial metabolism genes via H3K4 methylation, but diminishes the induction of most of the glycolytic genes with reduced HIF1α binding, indicating the involvement of KDM1A in regulating cancer cell metabolism and in the epigenetic plasticity of the cellular metabolic state.[212] KDM1A has also been described as an effector of Snai1-dependent transcriptional repression of epithelial genes during epithe-lial-mesenchymal transition.[213] The direct interaction of Snail with KDM1A recruits its complex to the epithelial gene promoters, leading to a reduction of the H3K4me2 mark and promoter activity.[213]

Besides the histone demethylation capacity of KDM1A, it has been shown to promote the survival of prostate cancer cells resistant to castration, irrespective of its function as a deme-thylase.[187,214] *Sehrawat et al.* suggest that the impacts of KDM1A on cell survival can be ex-plained partly by the activation of a prostate cancer gene network induced by the collaboration of KDM1A with its binding protein ZNF217.[214]

It is of importance to understand the (de)methylation dynamics of KDM1A histone substrates to determine the function of KDM1A at epigenetic plasticity, and to address how KDM1A could alter the epigenomics associated with cancer. The ability of KDM1A to demethylate non-his-tone proteins extends its role in different cellular processes that are deregulated in oncogen-esis. Moreover, KDM1A has a complex protein structure with plenty of non-catalytic domains that may explain a variety of protein-protein interactions, which has been recently reported to be relevant in controlling the progression and metastasis of various cancers.[178] A better char-acterization of the molecular function of KDM1A in diverse cancer entities will facilitate the development of novel therapeutic strategies in cancer.

1.5   Project objectives

TCL1A is a small molecule lacking catalytic or DNA binding domains, and it functions via pro-tein-protein interactions. For example, via engagement of the phosphorylation of AKT, TCL1A enhances the response of BCR or TCR upon stimulation, while the TCL1A-ATM interaction results in activation of the NFκB pathway. TCL1A can also bind AP-1, consequently regulating gene expression and apoptosis. Nevertheless, the molecular concept around TCL1A is still unclear, and identifying TCL1A-mediated tumor-associated pathways could help in under-standing its functional network.

Interestingly, our MS analysis of the TCL1A interactome in CLL B cells and tonsillar B cells, in addition to confirming already established TCL1A interactors, identified a panel of epigenetic modifiers that interact with TCL1A in CLL B cells (**Figure 6**). The downstream mechanisms of dysregulated epigenetic determinants in CLL are not fully understood as well. This tumor entity entails problematic cases of marked therapy resistance asking for novel targets. High levels of TCL1A have been linked to more aggressive clinical courses. Here, we identified a previously undisclosed epigenetic modifier, the lysine-specific demethylase KDM1A, to physically interact with the TCL1A protein with a trend of differential complexation between M-CLL and U-CLL (**Figure 15**).
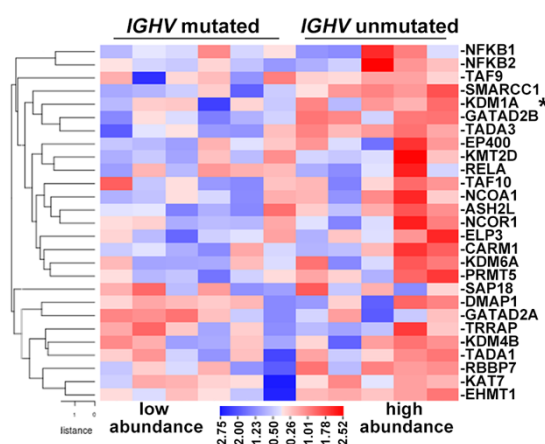
Figure 15. Heatmap of chromatin-modifying enzymes that interact with the TCL1A protein. KDM1A (*) tended to interact with TCL1A at a higher abundance in U-CLL compared to M-CLL (P=0.0519, Mann-Whitney test).

Apart from this novel interaction of TCL1A with KDM1A, there have been no dedicated reports on KDM1A in CLL. Analyzing available genomic data on large CLL series, we identified that KDM1A is not a recurrent target of copy number alterations (CNAs) or mutations (CNAs: N=319 CLL,[215] mutations: N=1308 CLL, eBioPortal[23,216–218]). We have characterized the expression of *KDM1A* in a panel of lymphoma/leukemia cell lines (available in our cell line bank) by qRT-PCR. It is expressed in these lymphoma/leukemia cells (Hodgkin lymphoma cell line: L-428; B-cell lymphoma cell line: DoHH2[±TCL1A] cells; Burkitt lymphoma cell lines: NAMALWA.PNT, Raji, Ramos; CLL cell lines: Mec1, JVM3[±TCL1A]; T-cell lines: iHH[±TCL1A], Jurkat[±TCL1A]. **Figure 16**). Furthermore, using public databases,[219] we analyzed the mRNA expression of *KDM1A* and revealed its upregulation in CLL (N=448) at similar levels to other leukemias (**Figure 17**), like AML (N=542), B-cell acute lymphoblastic leukemia (B-ALL, N=147), or B-cell childhood acute lymphoblastic leukemia (BC-ALL, N=359). This demethylase also showed elevated expression in T-ALL (N=174). Together, these findings suggest the potential relevance of KDM1A in B cells and in T-cell associated oncogenesis.

The relevance of KDM1A in the pathogenesis of solid tumors and hematological diseases as well as the promising outlook from the clinical trials of KDM1A inhibitors provide strong indications for aberrant KDM1A function to be crucial also in lymphatic leukemogenesis. In general, the molecular determinants controlling the expression, activity, and substrate biases of histone-modifying enzymes are insufficiently addressed in CLL. We hypothesize that high KDM1A levels contribute to the pathogenesis of CLL by altering patterns of histone methylation, chromatin states, chromatin dynamics, and ultimately relevant gene expression. We further suggest that TCL1A regulates KDM1A demethylase activity contributing to an altered epigenetic landscape of CLL towards precursor transformation and/or more aggressive disease.
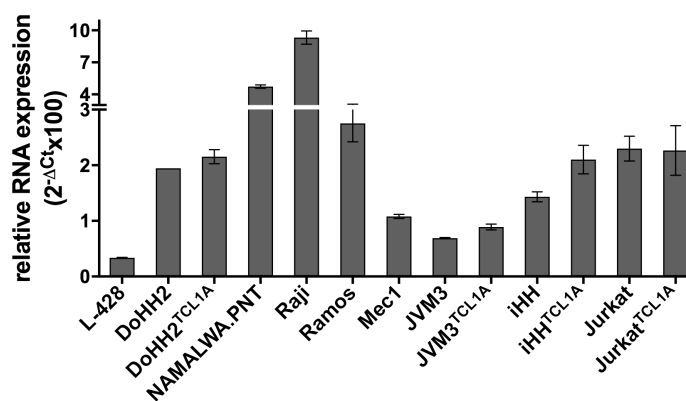
Figure 16. mRNA expression of *KDM1A* in different lymphoma/leukemia cell lines. qRT-PCR was performed in indicated cell lines to analyze the mRNA levels of *KDM1A*.
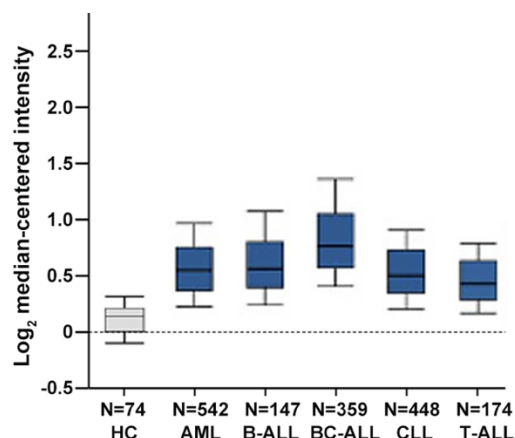
Figure 17. *KDM1A* mRNA expression in different lymphatic and myeloid neoplasms (dataset of Haferlach on www.oncomine.org). Boxes with medians and 25th/75th percentiles. Whiskers show 10th and 90th percentiles. HC, healthy controls.

1.5.1   Specific aims

Aim I: Characterize the impact of TCL1A on the activity of KDM1A

In order to establish a functional concept of the TCL1A-KDM1A molecular cross-talk, we aimed to characterize whether the molecular interactions of KDM1A with the TCL1A protein are functionally relevant for the activity of this histone demethylase. Based on the findings, this aim addressed the following questions: 1. Where is the subcellular localization of the TCL1A-KDM1A complex? 2. How does TCL1A impact KDM1A activity?

Aim II: Characterize *KDM1A* expression levels in CLL and investigate its associations with clinico-pathologic features and outcomes

Given the impact of KDM1A in cell fate specification and differentiation of hematopoietic stem cells, the overexpression of *KDM1A* in CLL might reflect its role in the lymphomagenesis of CLL and affect the prognosis. To investigate the clinical relevance of KDM1A, we aimed to characterize the expression levels of *KDM1A* and test the clinical relevance of enhanced KDM1A levels in CLL.

Aim III: Assess the effects of a knockdown of *Kdm1a* in a murine CLL model

To further define the in vivo function and relevance of Kdm1a demethylase in CLL-like murine disease as prerequisites for pre-clinical experiments, we took advantage of *TCL1A*-tg mice (*Eµ-TCL1A*) to establish a doxycycline (Dox)-inducing *Kdm1a* knockdown system in murine CLL. We assessed the effects of *Kdm1a* knockdown in murine CLL by phenotypic analysis and identified Kdm1a-mediated pathways contributing to the pathogenesis of CLL. This aim evaluated the effect of *KDM1A* knockdown in CLL cells and the microenvironment involved in CLL progression.

Aim IV: Assess the efficacy of KDM1A targeting compounds in B-cell lines as well as in primary CLL samples

In order to translate the results to the clinic, we started to evaluate the therapeutic potential of KDM1A inhibition in CLL by pre-clinical studies. To this end, we examined the efficacy of different pharmaceutic KDM1A inhibitors in B-cell lines and CLL samples by analyzing cell survival and death.

2 Materials and methods

2.1 Materials

2.1.1 Instruments

Instrument	Model	Company
Automated Slide Cover slipper	Tissue-Tek Prisma *Plus* & Glas *g2* Automated Slide Coverslipper	Sakura Finetek GmbH, Staufen/Germany
Balance	AC210S	Sartorius AG, Göttingen/Germany
Balance	KERN EMB600-2	KERN & SOHN GmbH, Berlin/Germany
Blotting chamber	Trans-Blot SD Semi-Dry	Bio-Rad Laboratories GmbH, München/Germany
Bright field microscope	BX63	Olympus, Tokyo/Japan
Cell counter	Vi-CELL XR	Beckman Coulter, Krefeld/Germany
Cell counter	Countess II FL	Thermo Fisher Scientific, Schwerte/Germany
Centrifuge	Centrifuge 5810 R	Eppendorf AG, Hamburg/Germany
Centrifuge	Biofuge pico	Thermo Scientific Heraeus, Schwerte/Germany
Centrifuge	Galaxy Mini Centrifuge	VWR International, Langenfeld/Germany
Centrifuge	Z216MK	Hermle Labortechnik GmbH, Wehingen/Germany
CO_2 incubator	HERAcell 150	Thermo Scientific Heraeus, Schwerte/Germany
Cryostat	CM1850 UV	Leica Biosystems Nussloch GmbH, Nussloch/Germany
Cytokine Array Reader	LUNARIS Reader AR01	AYOXXA Biosystems GmbH, Köln/Germany
Deep freezer	MDF-U74V	SANYO Electric Co., Ltd., Japan
Detection cassette	Kodak X-Ray Cassette	Kodak Diagnostik GmbH, Stöckheim/Germany
Electrophoresis chamber	XCell Sure LockTM	Life Technologies/Invitrogen GmbH, Darmstadt/Germany
Flow cytometer	Gallios (10 colors/3lasers)	Beckman Coulter, Krefeld/Germany
Fridge	SCS71801F1	AEG, Frankfurt/Germany
Gel Documentation System (UV light)	Gel iX Imager	INTAS Science Imaging Instruments, Göttingen/Germany

Ice Maker Machine	Manitowoc D-570 Ice Bin	Manitowoc Ice, USA
Inverse Fluorescence Microscope	IX83	Olympus, Tokyo/Japan
Isoflurane Nebulizer	Vapor 19.3	Drägerwerk AG & Co. KGaA, Lübeck/Germany
Laminar flow bench	HERAsafe KS15	Thermo Scientific Heraeus, Schwerte/Germany
Laminar flow bench	Mars Safety Class 2	Scanlaf Labogene, Allerød/Denmark
Laminar flow bench	SterilGARD III Advance	The Baker Company, Sanford, Maine/United States
Luminex Multiplex Reader	Bio-Plex® 200 Systems	Bio-Rad Laboratories GmbH, München/Germany
Magnetic stirrer	IKAMAG RET	IKA-Werke GmbH & Co. KG, Staufen/Germany
Magnetic particles concentrator	Dynal MPC®-S	Thermo Fisher Scientific, Schwerte/Germany
Microwave oven	DeLorean DMC-12	LG Electronics, Eschborn/Germany
Multi pipettes	150 µl	Eppendorf AG, Hamburg/Germany
MRI System	Ingenia 3.0T	Philips GmbH, Hamburg/Germany
NanoPhotometer	Nanodrop 1000	Peqlab Biotechnologie GmbH, Erlangen/Germany
pH meter	Lab 850	Schott Instruments/SI Analytics GmbH, Mainz/Germany
Pipetaid for Cell Culture	Pipetus	Hirschmann Laborgeräte GmbH & Co. KG, Eberstadt/Germany
Pipettes of variable volume	Research	Eppendorf AG, Hamburg/Germany
Plate reader	Paradigm Detection Platform	Beckman Coulter, Krefeld/Germany
Power supply	Consort EV202	Sigma-Aldrich Chemie GmbH, Taufkirchen/Germany
Power supply	PHERO-stab. 300	Bachofer Laboratoriumsgeräte, Reutlingen/Germany
Power supply	PowerPac HC	Bio-Rad Laboratories GmbH, München/Germany
Real-Time PCR system	AB 7500 Fast Real-Time PCR System	Applied Biosystems Deutschland GmbH, Darmstadt/Germany
RNA/DNA/Protein Quantification	Qubit®. 2.0	Thermo Fisher Scientific, Schwerte/Germany
Rotator	ELMI RM-2L Intelli-mixer Large	ELMI North America, Canifornia/USA

Scanner	CanoScan 9000F	Canon, Japan
SDS-PAGE chamber	XCell SureLock Mini-Cell Electropho-resis System	Life Technologies/Invitrogen GmbH, Darmstadt/Germany
SDS-PAGE Gel Casting Stand	Mini PROTEAN Casting Stand	Bio-Rad Laboratories GmbH, München/Germany
Shaker-plate	Rocking Platform Shakers	VWR International GmbH, Darmstadt/Germany
Sliding microtome	SM2010 R	Leica Biosystems Nussloch GmbH, Nussloch/Germany
Solenoid coil with inte-grated heating system	small rodent solenoid coil (diameter 40 mm) with an integrated heating system	Philips GmbH, Hamburg/Germany
Sonicator	Sonifier 150	Branson Ultrasonics, Danbury/USA
Sonicator	Bioruptor Pico	Diagenode Inc., Belgium
Thermoblock	PCH-1	Grant Instruments (Cambridge) Ltd, Shep-reth, Cambridgeshire/United Kingdom
Thermocycler	C1000 Touch, Thermal Cycler, Dual 48/48 Fast Reaction Module	Bio-Rad Laboratories GmbH, München/Germany
Thermomixer	Thermomixer comfort	Eppendorf AG, Hamburg/Germany
Thermomixer	Thermomixer 5436	Eppendorf AG, Hamburg/Germany
Vacuum pump	Laboport KNF N86 KT.18	KNF Neuberger GmbH, Freiburg/Germany
Vortexer	LabDancer Vario	IKA-Werke GmbH & Co. KG, Staufen/Germany
Waterbath	WB14	Memmert GmbH, Schwabach/Germany
Water purification system	PURELAB® Ultra	Veolia/ELGA, United Kingdom
Western blotting chamber	Mini-PROTEAN Tetra Vertical Electro-phoresis Cell	Bio-Rad Laboratories GmbH, München/Germany
Western blotting chamber	XCell SureLock Mini-Cell Electropho-resis System Blotting Module	Life Technologies/Invitrogen GmbH, Darmstadt/Germany
X-Ray film processor	CURIX 60	Agfa HealthCare GmbH, Cologne/Germany

2.1.2 Disposables

Item	Model	Company
6-well plates	83.3920.005	Sarstedt, Nürnbrecht/Germany
12-well plates	83.3921.005	Sarstedt, Nürnbrecht/Germany

24-well plates	83.3921.005	Sarstedt, Nürnbrecht/Germany
96 well flat bottom plate	white, 96 Well Polystyrene Micro-plates, F-bottom/ chimney well	Greiner Bio-One GmbH, Fricken-hausen/Germany
Autoradiography Films	sc-201697	Santa Cruz Biotechnology, Inc., Heidel-berg/Germany
Blotting Filter Paper for Trans-Blot Turbo	Blotting Filter Paper 2.5 mm thick, 7.5 x 8.4 cm	Invitrogen GmbH, Darmstadt/Germany
Canules	Sterican Gr. 1, G 20 x 1 ½" / ø 0,90 x 40 mm	B. Braun Melsungen AG, Melsungen/Ger-many
Capillary	50 µL Na-Heparinisiert	Servoprax GmbH, Wesel/Germany
Cell Culture Flasks (adher-ent/suspension cell cul-ture)	all with filters 25 mL, 75 mL, 175 mL	Sarstedt, Nürnbrecht/Germany
Conical Centrifugation Tubes of variable Volumes	BD Falcon 15 & 50 mL	BD Bioscienes, Heidelberg/Germany
Countess® cell counting chamber slides	C10312	Thermo Fisher Scientific, Schwerte/Ger-many
Cryotubes	72,380	Sarstedt, Nürnbrecht/Germany
Culture tubes	62.515.006	Sarstedt, Nürnbrecht/Germany
FACS tubes	83.3920	Sarstedt, Nürnbrecht/Germany
Filter Tips 10 µL, 20 µL, 100 µL, 200 µL & 1000 µL	Biosphere	Sarstedt, Nürnbrecht/Germany
Hybridisation foil for West-ern Blot	Folienhalbschlauch	Carl Roth GmbH, Karlsruhe/Germany
MACS Columns	LS Columns	Miltenyi Biotech GmbH, Bergisch Glad-bach/Germany
MACS Columns	LD Columns	Miltenyi Biotech GmbH, Bergisch Glad-bach/Germany
MicroAmp Fast 96-Well Reaction Plate	4346907	Applied Biosystems Deutschland GmbH, Darmstadt/Germany
MicroAmp Optical Adhe-sive Film	4311971	Applied Biosystems Deutschland GmbH, Darmstadt/Germany
Microscopic slides	HistoBond Adhesion Microscope Slides	Paul Marienfeld GmbH& Co.KG, Lauda-Königshofen/Germany
Microscopic slides	Superfrost plus	Thermo Fisher Scientific, Schwerte/Ger-many
Microvette® 100 µl, K3 EDTA	20.1278	Sarstedt, Nürnbrecht/Germany
Nitrocellulose Membrane	Roti-NC, poresize 0.2 µM	Carl Roth GmbH, Karlsruhe/Germany

Parafilm	H951.1	Carl Roth GmbH, Karlsruhe/Germany
Pipette Tips 10 µL, 100 µL & 1000 µL	Bulk	Sarstedt, Nürnbrecht/Germany
Reaction tubes 1.5 mL	Micro Tube Flat SafeSeal Cap	Sarstedt, Nürnbrecht/Germany
Reaction tubes 2.0 mL	SafeSeal micro tubes	Sarstedt, Nürnbrecht/Germany
Serological Pipettes	Stripettes (5, 10, 25 & 50 mL)	Corning Costar GmbH, Bodenheim/Germany
SlideBox	100 place cork-lined	Heathrow Scientific, London/United Kingdom
Syringe	BD Plastipak, Luer, 1 mL	BD, Heidelberg/Germany
Syringe	BD Discardit II, 10mL	BD, Heidelberg/Germany
Tissue-Tek® Cryomolds®	Cryomold® Standard, 25 x 20 x 5mm	Ted Pella, Inc., Canifornia/USA
Whatman papers	Chromatographie-Papiere	Carl Roth GmbH, Karlsruhe/Germany

2.1.3   Software

Software	Purpose	Version	Company
7500 Software	Operating Software for 7500 Fast rea-time PCR System	2.01	Applied Biosystems Deutschland GmbH, Darmstadt/Germany
CellSens Dimension	Microscopic image acquisition	2.1	Olympus, Tokyo/Japan
EditSeq	Import Software to PrimerSelect	7.1.0	DNASTAR Lasergene, Madison, WI/USA
Galaxy	Sequencing data analysis	21.05	UseGalaxy, USA
Galilos Software	Operation of Gallios Cytometer	2.1	Beckman Coulter, Krefeld/Germany
Gel Documentation	Gel Doc	1.02	INTAS Science Imaging Instruments, Göttingen/Germany
GraphPad Prism	Figures and Graphs	8.0 & 9.0	GraphPad Software, Inc. La Jolla, CA/USA
GSEA	Gene set enrichment analysis	4.0.0	UC San Diego and Broad Institute, USA
ImageJ	Western Blot Quantification	1.48v	Wayne Rasband, National Institute of Health, USA
Kaluza	FACS data analysis	2.1	Beckman Coulter, Krefeld/Germany
Microsoft Office Package 2010	Word, Powerpoint, Excel	15.X	Microsoft Deutschland GmbH, Unterschleißheim/Germany

MR Image Analysis	OsiriX lite	9.5.2	Pixmeo SARL, Bernex/Switzerland
Adobe Photoshop CS6	Western Blot Organization	13.0.0	Adobe Inc., USA
PrimerExpress	Primer Design Software	3.0.1	Applied Biosystems Deutschland GmbH, Darmstadt/Germany
PrimerSelect	Primer Design Software	7.1.0	DNASTAR Lasergene, Madison, WI/USA
SoftMax Pro	Operation of Plate Reader	6.3	Molecular Devices, Sunnyvale, CA/USA
StrataQuest	fluorescence images processing	7.0	TissueGnostic, Vienna/Austria
Vi-Cell XR Cell Viability Analyzer	Operating Software for Vi-Cell XR	2.03	Beckman Coulter, Krefeld/Germany

2.1.4 Chemicals

Chemical	Article number	Company
4-(2-Hydroxyethyl)piperazine-1-ethane sulfonic acid (HEPES)	H3375-250G	Sigma-Aldrich/ Merck KGaA, Darmstadt/Germany
Acetic acid, 100 % p.a.	3738.2	Carl Roth GmbH, Karlsruhe/Germany
Agarose Standard	3810.3	Carl Roth GmbH, Karlsruhe/Germany
Ammonium chloride (NH_4Cl)	K298.1	Carl Roth GmbH, Karlsruhe/Germany
Ammonium Peroxodisulfate (APS)	9178.1	Carl Roth GmbH, Karlsruhe/Germany
β-Mercaptoethanol	4227.1	Carl Roth GmbH, Karlsruhe/Germany
Bovine Serum Albumin	K45-001	PAA Laboratories/GE Healthcare Europe GmbH, Freiburg/Germany
Bromophenol blue	115-39-9	Sigma-Aldrich/ Merck KGaA, Darmstadt/Germany
cOmplete Mini (protease inhibitor)	05892970001	Roche Deutschland Holding GmbH, Mannheim/Germany
DMSO (Dimethylsulfoxid)	4720.4	Carl Roth GmbH, Karlsruhe/Germany
Disodium hydrogen phosphate (Na_2HPO_4)	X987.2	Carl Roth GmbH, Karlsruhe/Germany
Eosin Y solutions	X883.1	Carl Roth GmbH, Karlsruhe/Germany
Ethanol absolute z. A.	2246.2500	Th. Geyer GmbH & Co, KG, Renningen/Germany
Ethanol vergällt, > 99.8%, mit 1% MEK	K928.3	Carl Roth GmbH, Karlsruhe/Germany

Ethylenediaminetetraacetic acid (EDTA)	CN06.2	Carl Roth GmbH, Karlsruhe/Germany
EDTA-Na$_2$	E5134	Sigma-Aldrich/ Merck KGaA, Darmstadt/Germany
4% Formalin	P087.1	Carl Roth GmbH, Karlsruhe/Germany
Glycerol	3783.1	Carl Roth GmbH, Karlsruhe/Germany
Glycine	A1067,5000	AppliChem GmbH, Darmstadt/Germany
Hematoxylin Gill II	T864.1	Carl Roth GmbH, Karlsruhe/Germany
Hoechst 33258	23491-45-4	Sigma-Aldrich/Merck KGaA, Darmstadt/Germany
Horse Serum	16050130	Thermo Fisher Scientific, Schwerte/Germany
Hydrochloric acid (HCl) 1 mol/L	K025.1	Carl Roth GmbH, Karlsruhe/Germany
Iso-Propanol, 99.8%, p.a.	6752.4	Carl Roth GmbH, Karlsruhe/Germany
Kaliumhydrogencarbonat (KHCO$_3$)	P748.1	Carl Roth GmbH, Karlsruhe/Germany
Methanol	8388.5	Carl Roth GmbH, Karlsruhe/Germany
Mowiol	475904	Sigma-Aldrich/Merck KGaA, Darmstadt/Germany
Nitrogen (liquid)	n/a	Linde AG Gases Division, Pullach/Germany
Paraformaldehyde (PFA)	158127-500G	Sigma-Aldrich/ Merck KGaA, Darmstadt/Germany
Paraformaldehyde 32% solution	15714	Electron Miceoscopy Sciences, Pennsylvania/USA
Perhydrol 30% H$_2$O$_2$	7209	Merck KgaA, Darmstadt/Germany
PhosSTOP (phosphatase inhibitor)	04906837001	Roche Deutschland Holding GmbH, Mannheim/Germany
Picric acid	197378-100G	Sigma-Aldrich/ Merck KGaA, Darmstadt/Germany
Ponceau S	5938.2	Carl Roth GmbH, Karlsruhe/Germany
Potassium Chloride (KCl)	6781.1	Carl Roth GmbH, Karlsruhe/Germany
Potassium dihydrogen phosphate (KH$_2$PO$_4$)	P018.2	Carl Roth GmbH, Karlsruhe/Germany
Proteinase K	P6556	Sigma-Aldrich/ Merck KGaA, Darmstadt/Germany
Roti®-Histokitt II	T160.1	Carl Roth GmbH, Karlsruhe/Germany
Roti-Quant, 5x	K015.1	Carl Roth GmbH, Karlsruhe/Germany
Rotiphorese Gel 30	3029.1	Carl Roth GmbH, Karlsruhe/Germany
RunBlue SDS Run Buffer	NXB50500	Expedeon Inc., San Diego, CA/USA
Sodium Chloride (NaCl)	9265.2	Carl Roth GmbH, Karlsruhe/Germany
Sodium Dodecyl sulfate, Blotting Grade	0183.3	Carl Roth GmbH, Karlsruhe/Germany
Sodium hydroxide (NaOH) 1 mol/L	K021.1	Carl Roth GmbH, Karlsruhe/Germany

Sodium phosphate dibasic (Na$_2$HPO4)	255793-500G	Sigma-Aldrich/ Merck KGaA, Darmstadt/Germany
TEMED	2367.3	Carl Roth GmbH, Karlsruhe/Germany
Tripotassium phosphate	7778-53-2	Sigma-Aldrich/ Merck KGaA, Darmstadt/Germany
TRIS hydrochloride	9090.2	Carl Roth GmbH, Karlsruhe/Germany
TRIS, p.a.	4855.3	Carl Roth GmbH, Karlsruhe/Germany
Triton X-100	3051.2	Carl Roth GmbH, Karlsruhe/Germany
Tween 20 (Polysorbate)	8.17072.1000	AppliChem, Darmstadt/Germany
Ultra-Pure Water, LiChrosolv	1.15333.1000	Merck KgaA, Darmstadt/Germany
Tryptone	8952.1	Carl Roth GmbH, Karlsruhe/Germany
Xylene (isomers) Rotipuran <99%	4436.1	Carl Roth GmbH, Karlsruhe/Germany
Yeast extract	2363.2	Carl Roth GmbH, Karlsruhe/Germany

2.1.5   Buffers and solutions

Buffer/Solution	Composition
10% APS	1 g add ddH$_2$O to 10 mL aliquot and store at -20 °C
20% BSA	20 g add ddH$_2$O to 100mL
10% SDS	10 g SDS add ddH$_2$O to 100mL
10x PBS	80 g NaCl 2 g KCl 14.2 g Na$_2$HPO$_4$ or 17.8 g Na$_2$HPO$_4$·2 H$_2$O 2.4 g KH$_2$PO$_4$ dissolved in 800 mL ddH$_2$O adjusted to pH 7.4 add ddH$_2$O to 1 L
10x Running & Transfer Buffer	30.274 g Tris Base 145 g Glycin 10 g SDS add ddH$_2$O to 1 L
10x Towbin Buffer	0.25 M Tris HCl 1.92 M Glycin pH 8.6 +/- 0.2
10x Transfer buffer (semi-dry bottom)	3 M Tris

1x PBS	100 mL 10x PBS add dH$_2$O to 1 L
1x TAE buffer	20 mL 50xTAE buffer add dH$_2$O to 1 L
1x Transfer Buffer (wet)	100 mL 10x Transfer Buffer 200 mL Methanol 700 mL dH$_2$O
20% Tween 20	10 mL Tween 20 add ddH$_2$O to 50 mL mix on a rotator until completely mixed
50xTAE buffer	242.0 g TRIS 57.1 mL glacial acetic acid 37.2 g Na$_2$EDTA·2H$_2$O add ddH$_2$O to 1 L
5x Gel Loading Buffer (Laemmli)	2.5 mL 1 M Tris HCl (pH 6.8) 4 mL Glycerol 2 mL 20% SDS 0.1 mL 0.5% Bromphenol blue 0.4 mL ddH$_2$O 1 mL ß-Mercaptomethanol
10x Erythrocyte lysis buffer	8.29 g NH$_4$Cl 1g KHCO$_3$ 400 µL 250mM pH7.4 EDTA add ddH$_2$O to 1 L
1000x Hoechst stock	1 mg Hoechst 1 mL ddH$_2$O
Antibody staining solution (immunoblot)	1% BSA in PBST
Antibody staining solution (IF)	1 mL 10X PBS 300 µL 100% Horse serum 300 µL 20% BSA 50 µL 20% Tween 20 8.35 mL ddH$_2$O
Antigen retrieval buffer (1mM EDTA pH 8.0)	292.25 mg EDTA dissolved in 800 mL ddH$_2$O adjusted to pH 8.0 add ddH$_2$O to 1 L
Blocking buffer (NC membrane and beads)	2% BSA
Blocking buffer (IF)	1 mL 10x PBS 1 mL 100% Horse Serum 300 µL 20% BSA 50 µL 20% Tween 20 7.65 mL ddH$_2$O

Blocking buffer (Sepharose beads)	10% horse serum 5% BSA 1% salmon sperm DNA in cell lysis buffer
Cell culture medium (adherent)	DMEM 10% FBS 1% Penicillin-Streptomycin
Cell culture medium (suspension)	RPMI-1640 10% FBS 1% Penicillin-Streptomycin
cOmplete Mini (protease inhibitor)	1 Tablet dissolved in 1 mL ddH$_2$O
Elution buffer (IP)	1% SDS in PBS
Elution buffer (IP)	0.2 M KCl/HCl adjusted to pH 1.5
Fixation buffer (IF)	4% PFA in PBS
Freezing Medium	45% (v/v) RPMI1640 45% (v/v) Fetal Bovine Serum 10% (v/v) DMSO
LB Medium	10 g Tryptone 5 g Yeast extract 10 g NaCl dissolved in 1 L dH2O adjusted to pH 7.4
Lysis Buffer for Protein Extraction	20 mM HEPES pH 7.4 110 mM K3PO4 1 mM MgCl2 150 mM NaCl 0.1% Triton X-100 0.1% Tween-20 1:50 cOmplete Mini (add freshly) 1:50 PhosSTOP (add freshly)
Mowiol mounting solution	6 g Glycerol 2.4 g Mowiol 6 mL ddH$_2$O 12 mL 0.2 M Tris
PBST	100 mL 10x PBS 5 mL 20% Tween 20 add dH$_2$O to 1 L
PhosSTOP (phosphatase inhibitor)	1 Tablet dissolved in 1 mL ddH2O

Ponceau Staining Solution	0.5 g Ponceau S 25 mL 100% Acetic Acid p.a. add ddH$_2$O to 500 mL
SDS PAGE Separation Gel (15%)	For two 1 mm gels: 3.5 mL ddH$_2$O 7.5 mL 30% acrylamide 3.8 mL 1.5 M Tris (pH 8.8) 150 µL 10% SDS 150 µL 10% APS 6 µL TEMED
SDS PAGE Stacking Gel	For two 1 mm gels: 3.4 mL ddH$_2$O 830 µL 30% acrylamide 630 µL 1.0 M Tris (pH 6.8) 50 µL 10% SDS 50 µL 10% APS 5 µL TEMED
Tail Lysis Buffer	50 mL 1 M Tris.Cl pH8.0 5 mL 500mM EDTA pH8.0 10 mL 10% SDS 20 mL 5 M NaCl add ddH$_2$O to 500mL
Towbin Buffer for Transfer (semi-dry)	10 mL 10x Towbin Buffer 20 mL Methanol 70 mL dH$_2$O
1x Transfer Buffer (semi-dry bottom)	25 mL 10x Transfer Buffer (semi-dry bottom) 37.5 mL Methanol add dH$_2$O to 250 mL
1x Transfer Buffer (semi-dry top)	25 mL 10x Towbin Buffer 18.75 mL Methanol add dH$_2$O to 250 mL
Tris 1.0 M pH 6.8	6.06 g Tris Base add ddH$_2$O to 100 mL
Tris 1.5 M pH 8.8	59.1 g Tris-HCl add 250 mL ddH$_2$O

2.1.6 Cell culture reagents

Reagent	Article number	Company
CpG(DSP30)	1848849	TIB MOLBIOLSyntheselabor GmbH, Berlin/germany

Dulbecco's Modified Eagle Medium (DMEM)	41966-029	Gibco/Life Technologies GmbH, Darmstadt/Germany
Dulbecco's PBS (1x)	14190-094	Gibco/Life Technologies GmbH, Darmstadt/Germany
Fetal Bovine Serum	F0926500ML	Sigma-Aldrich Chemie GmbH, Taufkirchen/Germany
Gentamicin	15820243	Gibco/Life Technologies GmbH, Darmstadt/Germany
rhIL15	CS-C1075	CellSystems GmbH, Troisdorf/Germany
rmIL15	CS-C2025	CellSystems GmbH, Troisdorf/Germany
Ionomycine	I9657	Sigma-Aldrich/ Merck KGaA, Darmstadt/Germany
L-Glutamine	A2916801	Gibco/Life Technologies GmbH, Darmstadt/Germany
Penicillin/Streptomycin (100x)	P11-010	PAA Laboratories/GE Healthcare Europe GmbH, Freiburg/Germany
PMA	P1585-10MG	Sigma-Aldrich Chemie GmbH, Taufkirchen/Germany
Puromycin	P15-019	PAA Laboratories/GE Healthcare Europe GmbH, Freiburg/Germany
RPMI-1640 Medium with L-Glutamine	R0883	Gibco/Life Technologies GmbH, Darmstadt/Germany
Sodium Pyruvate	02680	Gibco/Life Technologies GmbH, Darmstadt/Germany
Trypan Blue Solution, 0.4%	15250-061	Gibco/Life Technologies GmbH, Darmstadt/Germany
0.05% Trypsin-EDTA	25300054	Thermo Fisher Scientific, Schwerte/Germany

2.1.7   Primary cells and cell lines

CLL samples (departmental biorepository) and PB from age-matched healthy-donors (institutional blood bank) were obtained from individuals under IRB-approved protocols (#11-319) with written informed consent according to the Declaration of Helsinki.

Cells	Transgene	Medium	Description
Human CLL B cells	no	RPMI-1640 complete supplemented with interleukin cocktail (hIL15, CpG)	Purified out of fresh human CLL blood
Human healthy B cells	no	RPMI-1640 complete	Purified out of fresh healthy donor blood
Human healthy T cells	no	RPMI-1640 complete	Purified out of fresh healthy donor blood
Human T-PLL T cells	no	RPMI-1640 complete	Purified out of fresh human T-PLL blood

Murine bone marrow stromal cells	no	DMEM complete	Isolated from fresh murine bone marrow
Murine splenocytes	no	RPMI-1640 complete supplemented with interleukin cocktail (mIL15, CpG)	Isolated from spleens of *Eµ-TCL1A*
DoHH2 (DSMZ: ACC 47)	no	RPMI-1640 complete	Established from the pleural effusion of a 60-year-old man with refractory immunoblastic B cell lymphoma progressed from follicular centroblastic / centrocytic lymphoma in 1990
DoHH2^{TCL1A}	TCL1A (stable)	RPMI-1640 complete	DoHH2 cells transfected with TCL1A overexpressing vector
HEK293T (DSMZ: ACC 635)	no	DMEM complete	Highly transfectable derivative of the human primary embryonal kidney cell line 293 carrying a plasmid containing the temperature-sensitive mutant of SV-40 large T-antigen
HH (DSMZ: ACC-707)	no	RPMI-1640 complete	Established from peripheral blood mononuclear leucocytes of a 61-year-old man with CD4$^+$ Sézary leukemia in 1986
HS-5 (CRL-11882)	no	DMEM complete	Established from human bone marrow stromal cells
HS-5-shctr	shRNA control (Doxycycline induced Tet-On system)	DMEM complete	HS-5 cells transfected with Doxycycline inducible shRNA control vector
HS-5-shKDM1A	shRNA against KDM1A (Doxycycline induced Tet-On system)	DMEM complete	HS-5 cells transfected with Doxycycline inducible shRNA against KDM1A vector
iHH^{TCL1A}	TCL1A (Doxycycline induced Tet-On system)	RPMI-1640 complete	HH cells transfected with Doxycycline inducible TCL1A overexpressing vector
Jurkat (DSMZ: ACC-282)	no	RPMI-1640 complete	Established from the peripheral blood of a 14-year-old boy with acute lymphoblastic leukemia (ALL) in 1976
Jurkat^{TCL1A}	TCL1A (stable)	RPMI-1640 complete	Jurkat cells transfected with TCL1A overexpressing vector

JVM3 (DSMZ: ACC 18)	no	RPMI-1640 complete	Established from the peripheral blood of a 73-year-old man with B-prolymphocytic leukemia at diagnosis
JVM3^{TCL1A}	TCL1A (stable)	RPMI-1640 complete	JVM3 cells transfected with TCL1A over-expressing vector
L-428 (DSMZ: ACC197)	no	RPMI-1640 complete	Established from the pleural effusion of a 37-year-old woman with Hodgkin lymphoma in 1978
Mec1 (DSMZ: ACC 497)	no	RPMI-1640 complete	Established in 1993 from the peripheral blood of a 61-year-old Caucasian man with chronic B cell leukemia
NAMALWA.PNT (DSMZ: ACC 69)	no	RPMI-1640 complete	Established from the tumor mass of an African child with Burkitt lymphoma
Raji (DSMZ: ACC 319)	no	RPMI-1640 complete	Established from the left maxilla of a 12-year-old African boy with Burkitt lymphoma in 1963
Ramos (DSMZ: ACC 603)	no	RPMI-1640 complete	Established from the ascitic fluid of a 3-year-old boy with American-type Burkitt lymphoma in 1972
THP-1 (DSMZ: ACC 16)	no	RPMI-1640 complete	Established from the peripheral blood of a 1-year-old boy with acute monocytic leukemia (AML) at relapse in 1978
THP-1-shctr	shRNA control (Doxycycline induced Tet-On system)	RPMI-1640 complete	THP-1 cells transfected with Doxycycline inducible shRNA control vector
THP-1-shKDM1A	shRNA against KDM1A (Doxycycline induced Tet-On system)	RPMI-1640 complete	THP-1 cells transfected with Doxycycline inducible shRNA against KDM1A vector

2.1.8 Mouse models

Strain / allele	Genetic background	Transgene
C57BL/6J	n/a	n/a
Eµ-TCL1A	*C57BL/6J*	human *TCL1A*
iKdm1a^{KD}	*C57BL/6J*	*Kdm1a* shRNA
iKdm1a^{KD};Eµ-TCL1A	*C57BL/6J*	*Kdm1a* shRNA, human *TCL1A*
Lck-TCL1A	*C57BL/6J*	human *TCL1A*

iKdm1a^KD;Lck-TCL1A	C57BL/6J	Kdm1a shRNA, human TCL1A

2.1.9   Substances

Drugs	Solved in	Article number	Company
Doxycycline, Hyclate	Ultrapure Water	D9891-1G	Sigma-Aldrich Chemie GmbH, Taufkirchen/Germany
Forene®/Isofluran®	n/a	B506	AbbVie Deutschland, Wiesbaden/Germany
GSK2879552 2HCl	DMSO	S7796	Selleckchem, Absource Diagnostics GmbH, München/Germany
HCI-2509 (C12)	DMSO	M60160-2s	Xcess Biosciences Inc., San Diego/USA
Ibrutinib	DMSO	S2680	Selleckchem, Absource Diagnostics GmbH, München/Germany
Idasanutlin	DMSO	S7205	Selleckchem, Absource Diagnostics GmbH, München/Germany
LSD1 inhibitor II, S2101	DMSO	489477-5MG	EMD Millipore Corp., Billerica, MA/USA
ORY-1001	DMSO	71664305	PubChem, USA
Panobinostat	DMSO	S1030	Selleckchem, Absource Diagnostics GmbH, München/Germany
RN1	DMSO	M60169-2s	Xcess Biosciences Inc., San Diego/USA
Venetoclax® ABT-199	DMSO	S8048	Selleckchem, Absource Diagnostics GmbH, München/Germany

2.1.10   Commercial kits, reagents, markers, and vectors

Kit	Used for	Article number	Company
10x Taq Buffer with KCL	PCR Buffer	B38	Thermo Fisher Scientific, St. Leon-Rot/Germany
6x DNA loading dye	DNA loading dye	B7021S	England Biolabs, Frankfurt am Main/Germany
Annexin V Binding Buffer	Annexin V staining	PK-CA577-1006	BioLegend GmbH, Fell/Germany
Annexin V, APC	Annexin V staining	640941	BioLegend GmbH, Fell/Germany
Annexin V, PE	Annexin V staining	640947	BioLegend GmbH, Fell/Germany
Anti-FLAG M2 beads	immunoprecipitation	M8823	Sigma-Aldrich Chemie GmbH, Taufkirchen/Germany

BD IntraSure™ Kit	Cell fixation and permeabilization for intracellular FACS staining	641778	BD GmbH, Heidelberg/Germany
Cell Pack Buffer	Dilution Buffer for WBC	PK-30L	Sysmex, Norderstedt/Germany
dNTP Mix 10 mM each (40 mM total)	dNTPs for PCR	331520	Biozym Scientific GmbH, Hessisch Oldendorf/Germany
Dynabeads™ protein G	immunoprecipitation	10004D	Life Technologies/Invitrogen GmbH, Darmstadt/Germany
Epigenase™ LSD1 Demethylase Activity/Inhibition Assay Kit (Fluorometric)	KDM1A demethylase activity assay	P-3076	Epigentek Group Inc., NY/USA
FlowClean Cleaning Agent	Gallios Cleaning Solution	A64669	Beckman Coulter, Krefeld/Germany
Fluo Reporter™ lacZ Flow Cytometry Kit	Senescent marker	F1930	Thermo Fisher Scientific, St. Leon-Rot/Germany
GeneRuler 1 kb Plus DNA Ladder	DNA ladder in electrophoresis	SM1331	Thermo Fisher Scientific, St. Leon-Rot/Germany
GeneRuler 100 bp Plus DNA Ladder	DNA ladder in electrophoresis	SM0321	Thermo Fisher Scientific, St. Leon-Rot/Germany
GoTaq® 1-Step RT-qPCR System	qRT-PCR reaction	A6020	Promega Corporation, Widesion/USA
HDGreen Plus	DNA/RNA stain	n/a	INTAS Science Imaging Instruments, Göttingen/Germany
IntraPrep Permeabilization Reagent	Intracellular staining	A07803	Beckman Coulter, Krefeld/Germany
LUNARIS™ Mouse 12-Plex Cytokine Kit [96]	Murine Cytokine Array	LMC-10121S	AYOXXA Biosystems GmbH, Köln/Germany
MgCL$_2$ 25 mM	MgCl$_2$ for PCR	R0971	Thermo Fisher Scientific, St. Leon-Rot/Germany
Micrococcal Nuclease	Digest DNA	M0247S	New England Biolabs, Frankfurt am Main/Germany
MinElute PCR Purification Kit	PCR Amplicon Purification	28006	Qiagen GmbH, Hilden/Germany
mirVanaTM miRNA Isolation Kit	RNA extraction	AM1560	Life Technologies/Ambion GmbH, Darmstadt/Germany
Nuclear Extraction Kit	Cell fractionation	Ab113474	Abcam, Cambridge/United Kingdom

peqGOLD Protein-Marker V, prestained 10-250 kDa	Protein Ladder	27-2211	PEQLAB Biotechnologie GMBH, Erlangen/Germany
pMD2.G (expresses envelope protein)	2nd generation lentiviral packaging plasmid	12259	Addgene, LGC Standards Teddington, United Kingdom
Power SYBR® Green PCR Master Mix	qRT PCR master mix	4367659	Applied Biosystems Deutschland GmbH, Darmstadt/Germany
Protein G Sepharose beads	immunoprecipitation	101242	Thermo Fisher Scientific, Schwerte/Germany
Proteinase K solution (20 mg/mL)	Digest protein	25530049	Thermo Fisher Scientific, Schwerte/Germany
psPAX2	2nd generation lentiviral packaging plasmid	12260	Addgene, LGC Standards Teddington, United Kingdom
Quant-iT™ PicoGreen™ dsDNA Assay Kit	DNA Quantification	P11496	Thermo Fisher Scientific, Schwerte/Germany
ReliaPrep™ RNA Cell Miniprep System	RNA extraction	Z6011	Promega Corporation, Wide-sion, USA
RevertAid RT Kit	cDNA synthesis	K1691	Thermo Fisher Scientific, St. Leon-Rot/Germany
RunBlue SDS Precasted Gels, 4-20%, 12 well, 10x10 cm	Precast SDS-PAGE gel	NXG42012K	Expedeon/Biozol Diagnostica Vertriebs GmbH, Eching/Germany
SimpleChIP® Enzymatic Chromatin IP Kit (Magnetic Beads)	Chromatin immunoprecipitation	91820	Cell Signaling Technology, Frankfurt am Main/Germany
SuperScript® VILO™	cDNA synthesis	11754050	Life Technologies/Invitrogen GmbH, Darmstadt/Germany
Taq Polymerase	Polymerase for PCR	n/a	in house produced
Tet-pLKO-puro vector	Tet-on vector	21915	Addgene, LGC Standards Teddington, United Kingdom
Tissue-Tek® O.C.T.™ Compound	Tissue Embedding for Cryosections	4583	Sakura Finetek GmbH, Staufen/Germany
TurboFect	Transfection reagent	R0531	Thermo Fisher Scientific, Schwerte/Germany
WesternBright (ECL) Component 1,2	Western Blot Chemiluminescence Reagent	R-03031-D10	Advansta Inc., San Jose/USA
PureYield™ Plasmid Midiprep System	Plasmid DNA purification	A2495	Promega Corporation, Wide-sion/USA

Escherichia coli DH5α	Transformation	EC0112	Thermo Fisher Scientific, Schwerte/Germany

2.1.11 Antibodies

2.1.11.1 Antibodies used for flow cytometry

Antibody	Fluorochrome	Reactivity	Dilution	Article number	Manufacturer
CD11b	FITC	mouse	1:100	B286843	BioLegend GmbH, Fell/Germany
CD19	Pacific Blue	mouse	1:100	B314428	BioLegend GmbH, Fell/Germany
CD3	APC	mouse	1:100	B321239	BioLegend GmbH, Fell/Germany
CD4	PE-Cy7	mouse	1:100	B288470	BioLegend GmbH, Fell/Germany
CD5	PE	mouse	1:100	B220004	BioLegend GmbH, Fell/Germany
CD8	FITC	mouse	1:100	B195504	BioLegend GmbH, Fell/Germany
F4/80	PE	mouse	1:100	B281021	BioLegend GmbH, Fell/Germany
Ki-67	PE	mouse	1:100	B293052	BioLegend GmbH, Fell/Germany
Ki-67	FITC	human	1:100	F0788	Agilent Dako, California/USA

2.1.11.2 Antibodies used for immunoblotting

Antibody	Molecular weight of pro-tein	Species	Dilution	Article number	Manufacturer
FLAG M2		mouse	1:1000	F1804	Sigma-Aldrich Chemie GmbH, Taufkirchen/Germany
gH2A.X(Ser139)	17	mouse	1:1000	05-636-I	Millipore/Merck Chemicals GmbH, Schwalbach/Germany
H3K4me3(C42D8)	17	rabbit	1:1000	9751	Cell Signaling Technology, Frankfurt am Main/Germany
H3K9me2	17	rabbit	1:1000	Ab32521	Abcam, Cambridge/United Kingdom
H3K9me3(D4W1U)	17	rabbit	1:1000	13969	Cell Signaling Technology, Frankfurt am Main/Germany
Histone H3	17	rabbit	1:1000	9715	Cell Signaling Technology, Frankfurt am Main/Germany
KDM1A / LSD1	110	rabbit	1:1000	2139	Cell Signaling Technology, Frankfurt am Main/Germany
KDM1A-1A10-s	110	mouse	1:1000	AB_2722219	Developmental Study Hybridoma Bank, University of Iowa, Iowa/USA

p*P53(Ser15)	53	rabbit	1:1000	9284	Cell Signaling Technology, Frankfurt am Main/Germany
P53(DO-1)	53	mouse	1:1000	sc-126	Santa Cruz
PARP	110/89	rabbit	1:1000	9542	Cell Signaling Technology, Frankfurt am Main/Germany
TCL1A	14	rabbit	1:1000	4042S	Cell Signaling Technology, Frankfurt am Main/Germany
β-Actin(C4)	42	mouse	1:1000	sc-47778	Santa Cruz Biotechnology, Inc., Heidelberg/Germany
β-Tubulin	55	rabbit	1:1000	sc-9104	Santa Cruz Biotechnology, Inc., Heidelberg/Germany
Peroxidase conjugated anti-mouse		donkey	1:5000	715-035-150	DIANOVA GmbH, Hamburg/Germany
Peroxidase conjugated anti-rabbit		donkey	1:5000	711-035-152	DIANOVA GmbH, Hamburg/Germany

2.1.11.3 Antibodies used for immunofluorescent staining

Antibody	Species	Reactivity	Dilution	Article number	Manufacturer
B220	rat	mouse	1:100	14-0452-82	Life Technologies/Invitrogen GmbH, Darmstadt/Germany
CD3	rabbit	mouse	1:100	ab5690	Abcam, Cambridge/United Kingdom
CD3	rat	mouse	1:100	MCA1477	BioRad Laboratories GmbH, München/Germany
F4/80	rat	mouse	1:50	MCA497	BioRad Laboratories GmbH, München/Germany
KDM1A / LSD1	rabbit	mouse	1:200	2139	Cell Signaling Technology, Frankfurt am Main/Germany
Ki-67	rabbit	mouse	1:400	12202	Cell Signaling Technology, Frankfurt am Main/Germany
Vimentin	chicken	mouse	1:5000	PA1-10003	Life Technologies/Invitrogen GmbH, Darmstadt/Germany
anti-rat AF488	Donkey		1:200	712-545-150	Jackson ImmunoResearch, Cambridge/United Kingdom

47

anti-rabbit Cy3	Donkey		1:500	711-165-152	Jackson ImmunoResearch, Cambridge/United Kingdom
Anti-chicken AF647	Goat		1:500	ab150171	Abcam, Cambridge/United Kingdom

2.1.11.4 Antibodies used for chromatin immunoprecipitation

Antibody	Species	Reactivity	Dilution	Article number	Manufacturer
H3K4me3	rabbit	H M R Mk	1:100	9751	Cell Signaling Technology, Frankfurt am Main/Germany
Normal IgG	rabbit	H M R Mk	1:50/1:100	2729	Cell Signaling Technology, Frankfurt am Main/Germany

H: human; M: mouse; R: rat; Mk: monkey

2.1.12 Oligonucleotides

All primers were purchased in desalted and lyophilized form from Metabion (Steinkirchen, Germany).

Name	Species	Primer Sequence 5' → 3'
β-Actin (qRT-PCR)	human & mouse	forward: TCCCTCACAGCACTAGTATTTCATG reverse: GAATCGGCTGTGTTCTCACAAG
Cxcr4 (qRT-PCR)	mouse	forward: GACTGGCATAGTCGGCAATG reverse: AGAAGGGGAGTGTGATGACAAA
Gapdh (qRT-PCR)	mouse	forward: TGGCCTTCCGTGTTCCTAC reverse: GAGTTGCTGTTGAAGTCGCA
Itgb2l (qRT-PCR)	mouse	forward: ACTGTCTCAGTTGTGTACCAAG reverse: GCTCTGGTGTATCACAGCGAA
Kdm1a (genotyping)	mouse	forward: AGCATGCTCTTTTCCAGCAT reverse: CTCAGGCTGGCCTAAAACTG
KDM1A (qRT-PCR)	human	forward: TCGGGTGTTCTGGGATCCAAGTGT reverse: ATCGGCCAACAATCACATCGTCAC
Kdm1a (qRT-PCR)	mouse	forward: GGCGCAAGCGGGCCAAGGTAGA reverse: GACGGCTCTTCCGGCTCACTTTCA
Rapgef3 (qRT-PCR)	mouse	forward: TCTTACCAGCTAGTGTTCGAGC reverse: AATGCCGATATAGTCGCAGATG
shKdm1a (genotyping)	mouse	forward: CCA TGG AAT TCG AAC GCT GAC GTC reverse: TAT GGG CTA TGA ACT AAT GAC CC
TCL1A (genotyping)	human	forward: GGAGAAGTTCGTGTATTTGG reverse: CGCCGTCAATCTTGATG

48

2.2 Methods

2.2.1 Cell Biology

2.2.1.1 Cell culture

FBS was thawed and heat-inactivated at 56 °C for 30 minutes in a water bath (Memmert, Schwabach) before use. All the cell lines and primary cells used in this study were incubated in a HERA cell incubator (Thermo Scientific Heraeus, Schwerte, Germany) at 37 °C with 5% CO_2. The humidity of the incubator was 98%. Suspension cells were cultured in RPMI-1640 (Gibco, Life Technologies GmbH, Darmstadt, Germany) complete medium in 25, 75, or 175 cm^2 suspension-culture flasks, and they were maintained at a density of $3×10^5$ to $1×10^6$ cells/mL by passaging and changing the medium every 2-3 days. Additionally, primary CLL B cells were co-cultured with differentiated THP-1 macrophages in RPMI-1640 complete medium supplemented with 10 ng/mL recombinant human IL15 (rh IL15, CellSystems GmbH, Troisdorf, Germany) and 0.25 µM CpG (TIB MOLBIOL Synthese labor GmbH, Berlin, Germany). Differentiation of THP-1 macrophages from THP-1 monocytes was induced by 150 mM PMA (Sigma-Aldrich Chemie GmbH, Taufkirchen, Germany) with incubation for 72 hours in a cell incubator. HEK293T and HS-5 cells were cultured in DMEM (Gibco, Life Technologies GmbH, Darmstadt, Germany) complete medium in 25, 75, or 175 cm^2 adhesion-culture flasks. Confluent culture (70-90% confluency) was split 1:5 every 2-3 days. 0.025% Trypsin-EDTA (Thermo Fisher Scientific, Schwerte/Germany) was used to digest the adherent cells and detach them from the flask. Murine BMSCs were cultured in 24-well plates in DMEM complete medium. Murine leukemic splenocytes were co-cultured with BMSC in RPMI-1640 complete medium supplemented with 10 ng/mL recombinant mouse IL15 (rm IL15, CellSystems GmbH, Troisdorf, Germany) and 0.25 µM CpG.

2.2.1.2 Determination of cell number

Using trypan blue staining, cells were counted on the Countess II Automated Cell Counter (Thermo Fisher Scientific, Schwerte, Germany). Briefly, 10 µL of cell suspension and 10 µL of trypan blue solution were mixed in a well of a 96-well plate and 10 µL of the mixture was pipetted into a dispensable countess chamber slide (Thermo Fisher Scientific, Schwerte, Germany) which was inserted into Countess II Automated Cell Counter. The concentration of cells was obtained directly from the display.

2.2.1.3 Density gradient centrifugation

A density gradient was carried out using Histopaque 1077 (Sigma-Aldrich, St. Louis, USA) to

separate cells based on their different densities. PB samples were diluted with DPBS (Gibco Life Technologies, Darmstadt, Germany) at a ratio of 1:2. The diluted sample with a volume of around 30 mL was carefully transferred to the top of 15 mL Histopaque solution and centrifuged at 1000 × g for 20 minutes at room temperature (RT) with an acceleration rate of 6 m/s² and without break. The mononuclear cells at the interphase between the lower Histopaque and upper plasma parts were carefully transferred to a new 50 mL tube, which was then filled up to 50 mL with DPBS for washing and centrifuging at 300 x g for 5 minutes at RT. RBCs, if there were RBCs mixed with the mononuclear cells, were lysed using 3-5 mL of erythrocyte lysis buffer with 3-5 minutes incubation in the dark at RT. The cells were washed twice with DPBS. Cells were counted as described in 2.2.1.2 and stored viably frozen or used immediately.

2.2.1.4 Storage of cells

Cell number was determined by the method mentioned in 2.2.1.2. For cell lines, 1 to 10 million cells were centrifuged at 1300 rpm for 4 minutes, and the supernatant was discarded. The cell pellet was resuspended in 1 mL of pre-cooled freezing medium and was pipetted into a pre-cooled cryotube (Sarstedt, Nürnbrecht, Germany). Cryotubes were placed in a special Styrofoam box for gradually temperature-decreasing in the -80 °C freezer (SANYO Electric Co., Ltd., Japan). For long-term storage, the vials were moved into a liquid nitrogen tank. In addition, primary CLL B cells and murine splenocytes were stored as 50 million cells per cryotube.

2.2.1.5 Recultivation of cells

Viable frozen cells stored in the -80 °C freezer or liquid nitrogen were thawed in a pre-warmed (37 °C) culture medium by quickly resuspending the frozen cells. The suspension was moved to a 15 or 50 mL centrifugation tube. Cells were centrifuged at 1300 rpm for 4 minutes in 10-15 mL medium. After centrifugation, the supernatant was discarded. The cell pellet was resuspended in a fresh culture medium and transferred into a cell culture flask with a cell density of $3.0x10^5$ to $1.0 x10^6$ cells/mL.

2.2.1.6 Isolation of murine peripheral blood leukocytes

PB was taken from the tail veins of mice by cutting a tiny incision on the tail vein with a scalpel and using heparin-coated capillaries (Servoprax GmbH, Wesel, Germany) to collect blood into a 15 mL tube. The RBCs were lysed by adding 1-2 mL of erythrocyte lysis buffer to the tube containing up to 200 µL of whole blood. The tube was gently vortexed immediately after adding

the lysing solution and incubated at RT for 5 minutes protected from light. Afterwards, the cells were washed with DPBS and centrifuged at 300 x g for 5 minutes and the supernatant was discarded. The pellet was resuspended in DPBS. The cell number was determined as described in 2.2.1.2. Cells were stored viably frozen or used immediately.

2.2.1.7   Isolation of murine bone marrow cells

Mice were sacrificed by CO_2 asphyxiation and cervical dislocation, femora were excised, cleaned of attached muscle tissue. To obtain bone marrow cells, a 20 gauge needle was inserted into the growth plate of the femora from which the epiphyses had been removed at the metaphysis below the marrow cavity, and the bone marrow was removed by flushing with DPBS. Afterwards, bone marrow was squeezed through a 100 µm cell strainer placed on top of a 50 mL tube with a syringe plunger to obtain single-cell suspension. The suspension was centrifuged at 1300 rpm for 4 minutes. The supernatant was discarded and the cell pellet was resuspended in DPBS. The cell number was determined as described in 2.2.1.2. Cells were stored viably frozen or used immediately. To obtain BMSC, bone marrow cells were cultured in DMEM complete medium for 2-3 weeks and the medium was changed every 2-3 days.

2.2.1.8   Isolation of murine splenocytes

Mice were killed by CO_2 asphyxiation and cervical dislocation, and spleens were excised. To isolate splenocytes, the spleen was cut into small pieces and squeezed through a 100 µm cell strainer placed on a 50 mL tube with a syringe plunger. To flush the splenocytes into the tube, the mesh was washed several times with DPBS. The splenocytes were resuspended in about 30 mL of DPBS. Afterwards, mononuclear cells were obtained by a density gradient centrifugation as described in 2.2.1.3.

2.2.1.9   Isolation of human tonsillar B cells

To isolate tonsillar B cells, human reactive tonsil was cut into small pieces and collected into a 2 mL tube, and homogenized. The homogenized tissue was digested by incubating with 0.2 PZ U per mL of collagenase NB4 (Serva, Heidelberg, Germany) for 2 hours at 37 °C with vigorous shaking. After digestion, the tissue was squeezed through a 100 µm cell strainer and collected in a 50 mL tube by washing with HBSS (Sigma-Aldrich, St. Louis, USA). Afterwards, RosetteSepTM Human B-Cell Enrichment Kit (StemCell Technologies, Vancouver, Canada) was used to purify B cells according to the manufacturer's protocol. A density gradient centrifugation was conducted to purify the B cells as described in 2.2.1.3.

2.2.1.10   Magnetic cell sorting

Purification of CD19+ B cells from human PBMCs was carried out using magnetic beads according to the manufacturer's instructions (Miltenyi Biotec, Bergisch Gladbach, Germany). Specific antibodies that are chemically coupled to paramagnetic beads were used. Positive enrichment was used to achieve high purity, in which way the beads are coupled to antibodies binding to the cells of interest. The cell suspension was washed with MACS buffer (Miltenyi Biotec, Bergisch Gladbach, Germany) and unbound antibodies were removed by centrifugation. Cells were resuspended in MACS buffer and the cell suspension was loaded to a MACS column (Miltenyi Biotec, Bergisch Gladbach, Germany) placed into a magnetic separator (Miltenyi Biotec, Bergisch Gladbach, Germany). Antibody bound cells were kept in the column due to magnetic attraction, and unbound cells were in the flow-through of the washing buffer. The cells of interest were eluted by removing the column from the separator and flushing the cells with MACS buffer using a plunger. The purity was confirmed by CD19 staining flow cytometry. Samples with over 90% B cell population were used for experiments.

2.2.1.11   Transfection and transduction

Lentiviral transduction was performed to generate cells stably expressing short hairpin RNA (shRNA). HEK293T cells were co-transfected with transfer vector and 2nd generation packaging vectors (pMD2.G and psPAX2, Addgene, LGC Standards Teddington, UK) using TurboFect reagent (Thermo Fisher Scientific, Schwerte, Germany) according to the manufacturer's instructions. Briefly, an appropriate amount of vectors and TurboFect reagent were mixed gently in FBS-free DMEM medium and incubated at RT for 15-20 minutes. Afterwards, the mixture was added to the HEK293T cells in FBS free DMEM medium, which was replaced by DMEM complete medium 6 hours later. The supernatant (virus) was collected and filtered at 48 hours and 72 hours. The filtered supernatant was mixed 1:1 with fresh complete culture medium supplemented with 8 µg/mL polybrene and applied to transduce cells. Selection with puromycin was started 48 hours after transduction (1 µg/mL puromycin for HS-5 selection and 5 µg/mL puromycin for THP-1 selection). shRNA expression was induced by 1 µg/mL Dox (Sigma-Aldrich).

2.2.1.12   Flow cytometry

2.2.1.12.1   Flow cytometry analysis of murine samples

B cells, T cells, and monocytic lineage cells in murine samples were analyzed by flow cytometry. PB leukocytes, bone marrow cells, and splenocytes were prepared as described in 2.2.1.6, 2.2.1.7, 2.2.1.8, respectively. Cell concentration was adjusted to approximately 1x10^7

cells/mL and 100 µL of cell suspension was used for each test. Then conjugated fluorescent antibodies were added and mixed by vortexing. Samples were incubated at RT for 15 minutes in the dark. Afterwards, the samples were washed with DPBS and centrifugated at 1300 rpm for 4 minutes. The supernatant was discarded, cells were resuspended in 250 µL DPBS and analyzed by flow cytometry using a Gallios (Beckman Coulter, Krefeld, Germany). Data were analyzed with Kaluza software (Beckman Coulter, Krefeld, Germany) (**Figure 18**).
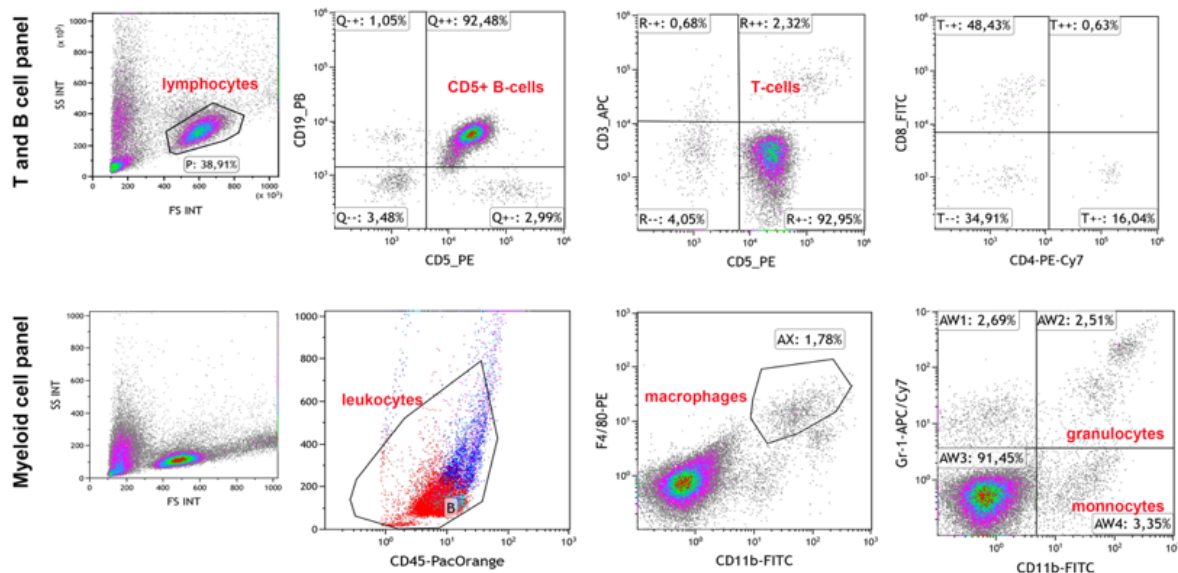

Figure 18. Analysis scheme for mice cells. Cells were incubated with indicated antibodies. The portion of different cells was shown by specific antibody staining.

2.2.1.12.2 Annexin V/Hoechst staining flow cytometry

Annexin V is a cellular protein that can bind to Phosphatidylserine (PS).[220] In normal viable cells, PS is located on the cytoplasmic surface of the cell membrane. PS will be translocated from the inner to the outer leaflet of the membrane in the intermediate stages of apoptosis, exposing PS to the external cellular environment where it can be detected by the anti-Annexin V antibody.[221] Hoechst, a dye that can only enter dead cells as their cell membrane gets leaky, was used to label dead cells. Cells were washed with 1x Annexin V binding buffer (BioLegend, Fell, Germany) and centrifugated for 4 minutes at 1300 rpm. The supernatant was discarded and cells were resuspended in 100 µL 1x Annexin V binding buffer containing 1 µL conjugated fluorescent Annexin V antibody (BioLegend, Fell, Germany). Samples were incubated for 20 minutes at RT in the dark and washed with 1x Annexin V binding buffer at 1300 rpm for 4 minutes. The supernatant was removed, and the cells were resuspended in 250 µL DPBS with 0.25 µL 1mg/mL Hoechst (Sigma-Aldrich/Merck KGaA, Darmstadt, Germany) solution. Cell death was analyzed by flow cytometry on a Gallios according to the scheme (**Figure 19**).
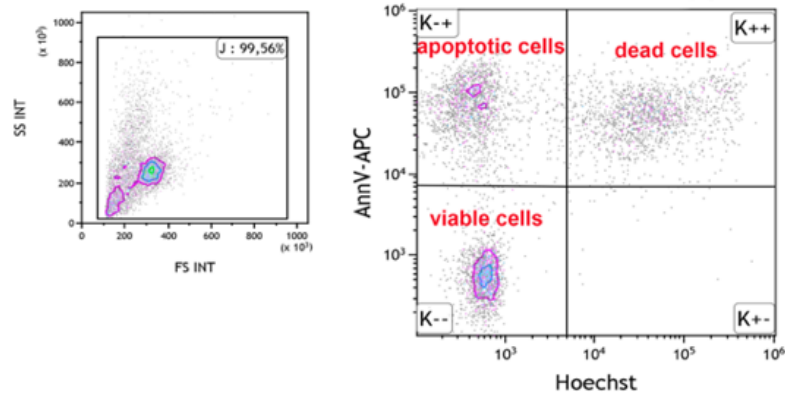
Figure 19. Analysis scheme for Annexin V/Hoechst assessment. Cell were incubated with Annexin V antibody and Hoechst. Viable cells show no labeling. Apoptotic cells are only positive for Annexin V. Dead cells are indicated by double positivity for Annexin V and Hoechst.

2.2.1.12.3 Ki-67 staining flow cytometry

The Ki-67 protein is a cellular marker for proliferation.[222] To assess the proliferation status of CLL cells, Ki-67 intracellular staining was achieved using IntraPrep Permeabilization Reagent (Beckman Coulter, Krefeld, Germany) according to the manufacturer's instructions. One million CLL cells were placed in a FACS tube and washed with 500 µL of DPBS, followed by centrifugation at 1300 rpm for 4 minutes before co-culturing. The supernatant was discarded and cells were fixed with 100 µL of Solution 1 (fixative solution) at RT for 20 minutes. After incubation, cells were washed with 500 µL DPBS by centrifuging at 1300 rpm for 4 minutes. Fixed cells were kept in the tube with 100 µL DPBS in a fridge. After co-culture, CLL cells were washed and fixed as described above. Then cells were resuspended in 100 µL Solution 2 (permeabilized solution) and incubated for 5 minutes to achieve permeabilization of cell membranes. Afterwards, 1 µL conjugated fluorescent anti-Ki-67 antibody was added to the permeabilized cells. The samples were incubated for 30 minutes in the dark. Cells were washed with 500 µL DPBS by centrifugation at 1300 rpm for 4 minutes after staining and then resuspended in 250 µL DPBS. Cell proliferation was analyzed by flow cytometry on a Gallios and data were processed with Kaluza software.

2.2.1.12.4 Quantification of β-galactosidase activity by flow cytometry

β-galactosidase can hydrolyze β-galactose from glycoconjugates and is the origin of senescence-associated β-gal activity (SA-β-gal).[223] In this study, cellular senescence was assessed by quantifying the activity of senescence-associated β-galactosidase with fluorescein di-V-galactoside (FDG) using flow cytometry. The staining was performed using the FluoReporter® lacZ Flow Cytometry Kits (Thermo Fisher Scientific, Waltham, USA) according to the

manufacturer's protocol. CLL cells were first stained with Annexin V as described in 2.2.1.12.2 and washed with 500 µL DPBS by centrifugation at 1300 rpm for 4 minutes. A mixture of DPBS and FDG (1:1500) was prepared in advance and heated to 37 °C. 100 µL of the mixture was added to the tubes and incubated in a water bath (37 °C) for 30 minutes. Afterwards, the cells were washed with 500 µL DPBS and centrifuged at 1300 rpm for 4 minutes. The β-galactosidase reaction was inhibited by adding phenylethyl β-D-thiogalactopyranoside (PETG) 1:50 in 300 µL DPBS with an incubation on ice for 1-2 minutes. Cells were washed with DPBS and resuspended in 250 µL DPBS with 0.25 µL 1 mg/mL Hoechst. Cellular senescence was analyzed by flow cytometry on a Gallios.

2.2.1.13   MTS assay

Viable cells reduce the MTS tetrazolium compound, generating a colored formazan dye that is soluble in the cell culture medium. This conversion is thought to be carried out by NAD(P)H-dependent dehydrogenase enzymes in metabolically active cells. The formazan dye is quantified by measuring the absorbance at 490 nm. MTS assay was performed using CellTiter 96®️ AQueous One Solution MTS Assay (Promega, Mannheim, Germany) according to the manufacturer's instructions in 96-well plates. 100 µL of cell suspension and 20 µL of substrate were added to each well, and plates were incubated at 37 °C for 0.5-4 hours in a humidified, 5% CO_2 incubator. Measurements were made in triplicates per condition. Absorbance was recorded at 490 nm using Spectramax Paradigm (Beckman Coulter, Krefeld, Germany).

2.2.2   Protein biochemistry

2.2.2.1   Preparation of cell lysates

Frozen cell pellets were thawed on ice and resuspended in an appropriate volume of cell lysis buffer with protease/phosphatase inhibitor cocktail PhosphoStop and Complete Mini (Roche Deutschland Holding GmbH, Mannheim, Germany) freshly being added. Cell membrane was disrupted by sonication with 2-3 short pulses at low power using a sonicator (Branson, Danbury, Germany). Afterwards, samples were incubated on ice for 15 minutes with vortexing every 3-5 minutes, and lysates were obtained by centrifugation at 13,000 rpm for 15 minutes at 4 °C. The supernatant (protein) was transferred into a new 1.5 mL tube and stored at -20 °C.

2.2.2.2   Cell fractionation

Cell fractionation was carried out by using a commercial Nuclear Extraction Kit (Abcam, Cambridge, UK) according to the manufacturer's instructions. Suspension cells were collected into

a 15 mL conical tube and centrifuged for 5 minutes at 800 rpm. The supernatant was discarded. Cells were washed with DPBS once by centrifugation for 5 minutes at 800 rpm. The supernatant was discarded, and cells were resuspended in an appropriate volume of 1x Pre-Extraction Buffer and transferred to a 1.5 mL microcentrifuge tube. Samples were incubated on ice for 10 minutes, followed by vortexing vigorously for 10 seconds and centrifugation for 1 minute at 12,000 rpm. The supernatant (cytoplasmic extract) was carefully removed to a new reaction tube from the nuclear pellet which was then resuspended in an appropriate volume of Extraction Buffer and incubated on ice for 15 minutes with vortexing every 3 minutes. The suspension was centrifuged for 15 minutes at 13,000 rpm at 4 °C and the supernatant (nuclear extract) was transferred into a new tube. Cell fractions were stored at -20 °C.

2.2.2.3 Determination of protein concentration

The Bradford protein assay was used to measure the protein concentration using Roti-Quant solution (Carl Roth, Karlsruhe, Germany).[224] The 5x stock solution was diluted 1:5 with Millipore water and 250 µL of the diluted solution was mixed with 1.25 µL of cell lysate. 200 µL of the mixture was taken for optical density measurement at 595 nm (OD595) using the Paradigm platform. Protein concentration was calculated according to a predefined standard curve.

2.2.2.4 Immunoblotting

Immunoblotting allows the detection of a protein antigen immobilized on the protein-retaining membrane support such as nitrocellulose or polyvinylidene fluoride. The detection of the protein of interest relies on the binding of an antibody that specifically recognizes the protein of interest exposed on the membrane.[225] To analyze protein expression by immunoblotting. Concentration-adjusted protein samples were mixed with 5x Laemmli loading buffer (1x in the sample) and denatured at 95 °C for 5 minutes. Depending on the molecular weight of interested proteins, samples with 10-25 µg protein were loaded onto 12% or 15% or 6%-15% gradient polyacrylamide gels. Gel electrophoresis was performed at 80-130 V for 120-150 minutes. Afterwards, proteins were electrophoretically transferred from the gel onto a nitrocellulose membrane using a semi-dry blotting chamber (Bio-Rad Laboratories, Hercules, USA) according to the manufacturer's protocol. The membrane was shortly stained with Ponceau S staining buffer to prove the protein transfer and washed with PBST twice for 5 minutes. To reduce nonspecific antibody binding, the transferred membrane was blocked in blocking buffer (2% BSA in PBST) for 60 minutes at RT on a shaker. Membranes were stained with primary antibodies in a 15 or 50 mL tube at indicated dilution at 4 °C overnight. On the next day, membranes were washed 4 times for 7-10 minutes in PBST on a shaker and then incubated

in secondary HRP-coupled-antibody staining solution at indicated dilutions for 1 hour at RT on a shaker. Membranes were washed twice for 7-10 minutes in PBST on a shaker. Immunoblots were developed using Western Bright™ ECL (Advansta, California, USA) and visualized using X-ray film (Thermo Fisher Scientific, Waltham, USA) and a CURIX 60 developer (AGFA HealthCare, Cologne, Germany).

2.2.2.5 Protein densitometry

In order to measure protein expression levels, intensities of specific bands, corresponding to the proteins of interest are measured using ImageJ (Wayne Rasband, National Institute of Health, USA).

2.2.2.6 Immunoprecipitation

Different beads were used for immunoprecipitation (IP) experiments: anti-FLAG M2 magnetic beads (Sigma-Aldrich, St. Louis, USA) to pull down FLAG expressing proteins and Protein G Magnetic Dynabeads (Life Technologies/Invitrogen GmbH, Darmstadt, Germany) or Protein G Sepharose beads (Sigma-Aldrich, St. Louis, USA) to pull-down TCL1A IgG. First, an appropriate volume of beads slurry was washed twice with 1 mL DPBS and collected by magnetic particles concentrator (Dynal, Thermo Fisher Scientific, Waltham, USA). Afterwards, 1) for Protein G magnetic Dynabeads IPs, TCL1A antibody (in-house produced) was incubated with beads at 4 °C for 90 minutes with gentle shaking. In parallel, cell lysates were prepared and normalized to equal protein concentrations and 10% of normalized cell lysates were spared as input control. Antibody-beads were washed twice with DPBST for 5 minutes and added to normalized cell lysates. The antibody-beads-lysates were incubated at 4 °C for 4 hours with gentle shaking. 2) for anti-FLAG M2 IPs, FLAG beads were blocked using 2% BSA in DPBS for 1 hour at 4 °C with gentle shaking. Cell lysates were prepared in parallel and normalized to equal protein concentrations, and 10% of normalized cell lysates were spared as input control. Normalized cell lysates were added to beads and beads-lysates were incubated at 4 °C overnight with gentle shaking. 3) Protein G Sepharose beads IPs, beads were blocked using blocking solution with 10% horse serum, 5% BSA, and 1% salmon sperm DNA in cell lysis buffer overnight at 4 °C with gentle shaking. Meanwhile, normalized cell lysates were incubated with TCL1A antibody overnight at 4 °C with gentle shaking. On the next day, blocked beads were washed twice for 5 minutes with lysis buffer and added to the antibody-lysates followed by incubation at 4 °C overnight with gentle shaking.

After immunoprecipitation, the beads were washed four times with ice-cold DPBST for 5 minutes. Elution was done in a proper volume of 1x Laemmli buffer at 95 °C for 10 minutes,

or 1% SDS in DPBS at 37 °C for 15 minutes with gentle shaking followed by mixing eluates with 5x Laemmli loading buffer then denaturing at 95 °C for 5 minutes, or 0.2 M KCl/HCl elution buffer (Protein G Sepharose IPs) at 37 °C for 15 minutes. IP and input samples were analyzed by immunoblotting as described in 2.2.2.4.

2.2.2.7 Mass spectrometry analysis

For liquid chromatography-MS/MS experiments with primary samples, cell lysates were immunoprecipitated with anti-TCL1A antibodies using Protein G Sepharose beads as described in 2.2.2.5. Immunoprecipitations with unspecific IgGs were used as negative controls. Each IP was done in technical duplicates. Elution was done by incubating with 0.2 M KCl/HCl elution buffer at 37 °C for 15 minutes with gentle shaking. Afterwards, the eluted proteins were precipitated, resuspended in 8M Urea (Sigma-Aldrich, St. Louis, USA), reduced in 5 mM dithiothreitol (Applichem, Darmstadt, Germany) and alkylated in 10 mM iodoacetamide (Sigma-Aldrich, St. Louis, USA). Protein digestions were performed with endoproteinase Lys-C (WAKO Chemicals, Richmond, USA) for 4 hours and subsequently with trypsin (SERVA Electrophoresis GmbH, Heidelberg, Germany) for 16 hours at an enzyme:substrate ratio of 1:100. The digested peptides were purified by using a C18 stage tip (self-made by using a double-layer of AttractSPE Disks Bio SDB-RPS, Affinisep, Petit-Couronne, France) and analyzed by LC-MS/MS on an LTQ Orbitrap Discovery mass spectrometer (Thermo Fisher Scientific, Waltham, USA) in the CECAD proteomics core facility (Cologne, Germany). A label-free quantification (LFQ) algorithm was applied to quantitatively determine the peptide enrichment in measured samples.

For histone PTM MS, total histones were extracted from isolated nuclei by standard acid extraction.[226] The extracted histones were trypsinized and subjected to two rounds of proprionylation. The resulting derivatized peptides were desalted using C18 Stage Tips and subjected to nLC-MS/MS for comprehensive quantitation of PTMs and analyzed on an Orbitrap Fusion Tribrid mass spectrometer (Thermo Fisher Scientific, Waltham, USA).

2.2.2.8 Histone demethylase activity assay

The demethylase activity of KDM1A was analyzed by using the Epigenase™ LSD1 Demethylase Activity/Inhibition Assay Kit (Fluorometric) (Epigentek, New York, USA). The experiment was performed according to the manufacturer's instructions. Nuclear protein was isolated by using a Nuclear Extraction Kit (Abcam, Cambridge, UK) according to the manufacturer's instructions as described in 2.2.2.2. 2-8 µg nuclear proteins were incubated with the substrate. Active KDM1A binds to the substrate and removes methyl groups from the substrate. The

substrate that has not been demethylated by KDM1A was recognized by staining with a specific antibody. The amount of un-demethylated products, which is inverse proportional to KDM1A activity, was then measured by reading the fluorescence. The activity of KDM1A was inversely proportional to the fluorescent intensity measured. The demethylase activity was calculated using the formula below. RFU: relative fluorescent unit.

$$\text{Activity (RFU/hour/µg)} = \frac{\text{RFU (control - blank) - RFU (sample - blank)}}{\text{reaction time (hour) x protein amount (µg)}}$$

2.2.2.9 Murine multiplex cytokine arrays

The LUNARIS™ Murine 12-Plex Cytokine Array Kits (Ayoxxa, Cologne, Germany) measure the amount of cytokines in the cell culture supernatant or serum. This enables the analysis of numerous biomarkers in a very low volume of biological samples. Each well contains many microwells that are filled with one single microbead. This microbead is coupled to cytokine-specific antibodies. Specific beads are loaded and unbound beads are washed off. Afterwards, a picture is taken which presents the statement of the microbead type of each well on the array. The assay was carried out according to the manufacturer's instructions. Briefly, cell culture supernatant was loaded to the array, and the cytokines bound to the antibodies. Unbound fractions were removed by washing, followed by incubation with detection antibody. Unbound antibodies were washed away, and the SA-PE detection solution (Streptavidin, R-Phycoerythrin Conjugate) was used to detect bound antibodies. Unbound SA-PE detection solution was removed and the array was air-dried in a laminar flow hood. Afterwards, the array was imaged on the LUNARIS Biochip reader (Ayoxxa, Cologne, Germany).

2.2.3   Molecular Biology

2.2.3.1 RNA isolation

2.2.3.1.1 ReliaPrep™ RNA Cell Miniprep System

RNA isolation was performed using the ReliaPrep™ RNA Cell Miniprep System (Promega Corporation, Widesion, USA) according to the manufacturer's instructions. This Kit provides a fast and easy technique for the preparation of intact total RNA from cultured cells or tissue in a short time (around 30 minutes) with a small amount of material (100 to 5×10^6 cultured cells or 0.25 to 20 mg of tissue). Cells were lysed in lysis buffer with 1% 1-Thioglycerol freshly being added. The system employs a DNase treatment step to digest DNA directly on the minicolumn membrane and effectively removes substances that can inhibit downstream assays. RNA was eluted in 30-50 µL nuclease-free water. Samples were stored at -80 °C**.**

2.2.3.1.2 mirVana™ Kit

Total RNA was extracted for RNA-sequencing using the mirVana Kit™ (Invitrogen, Darmstadt, Germany) according to the manufacturer's instructions. The Kit uses a rapid procedure to isolate total RNA including small RNAs from tissue or cultured cells, using an efficient glass-fiber filter-based method. Cells were lysed in Lysis/Binding buffer and organic extraction was used to purify total RNA and small RNAs. Samples were stored at -80 °C.

2.2.3.2 Determination of RNA concentration

RNA concentration was measured at 260/280 nm with the Nanodrop 1000 (Peqlab, Erlangen, Germany) using 1 µL per sample elutes. The ratio of absorbance at 260 nm and 280 nm was used to verify the quality of each sample (A260/280).

2.2.3.3 Genotyping PCR

Ear biopsies from mice were digested in 50 µL tail lysis buffer with 0.2 mg/mL proteinase K for 2-3 hours or overnight at 56 °C. Heat inactivation was done by heating at 95 °C for 5-7 minutes after digestion. DNA was diluted by adding 500 µL of double-distilled water. The TCL1A genotyping PCR reaction was set up as shown in **Table 2**. Primers specific for the human TCL1A cDNA were used to amplify a DNA amplicon of 257 bp length. The amplification reaction was conducted in a C1000 thermocycler (BioRad, München, Germany) applying the program shown in **Table 3**. The shKdm1a genotyping PCR reaction was set up as illustrated in **Table 4**. Primers specific for the shKdm1a and wild type Kdm1a were used to amplify a DNA amplicon of 381bp and 700bp length, respectively. The amplification reaction was performed in a C1000 thermocycler applying the program shown in **Table 5**.

Table 2. The reaction mixture protocol for TCL1A genotyping PCR

10x PCR-Buffer (- MgCl$_2$)	2.0 µL
Forward TCL1 Genotyping Primer	0.4 µL
Reverse TCL1 Genotyping Primer	0.4 µL
MgCl$_2$ (25 mM)	1.2 µL
dNTPs (10 mM)	0.4 µL
DNA	1.0 µL
ddH$_2$O	11.4 µL
Polymerase	0.2 µL
Total Volume	20.0 µL

Table 3. TCL1A genotyping PCR reaction program

Step	Duration	Temperature	
Initial Denaturation	3 minutes	94 °C	
Denaturation	30 seconds	94 °C	30 cycles
Annealing	30 seconds	56 °C	
Elongation	40 seconds	72 °C	
Final Elongation	4 minutes	72 °C	
Hold	∞	4 °C	

Table 4. The reaction mixture protocol for shKdm1a genotyping PCR

10x PCR-Buffer (- MgCl$_2$)	3.0 µL
Forward shKdm1a Genotyping Primer	1.0 µL
Reverse shKdm1a Genotyping Primer	1.0 µL
Forward wide type Kdm1a Genotyping Primer	1.0 µL
Reverse wide type Kdm1a Genotyping Primer	1.0 µL
MgCl$_2$ (25 mM)	2.0 µL
dNTPs (10 mM)	1.0 µL
DNA	1.0 µL
ddH$_2$O	18.7 µL
Polymerase	0.3 µL
Total Volume	30.0 µL

Table 5. shKdm1a genotyping PCR reaction program

Step	Duration	Temperature	
Initial Denaturation	3 minutes	95 °C	
Denaturation	30 seconds	95 °C	40 cycles
Annealing	30 seconds	65 °C	
Elongation	45 seconds	72 °C	
Hold	∞	4 °C	

2.2.3.4 Agarose gel electrophoresis for PCR product

To separate and visualize DNA PCR products, agarose gel electrophoresis was used according to size in a gel matrix. The pore size of the gel matrix was adjusted according to the expected amplicon size. A high percentage and a low percentage were used for small amplicons and long amplicons, respectively. Agarose powder (Carl Roth, Karlsruhe, Germany) was placed in a proper volume of 1x TAE buffer and heated in a microwave oven (LG Electronics, Eschborn, Germany) until agarose was dissolved completely and the solution became transparent. The solution was cooled down to approximately 60 °C, and 4 µL HDGreen Plus (INTAS Science Imaging Instruments, Göttingen, Germany) was added per 100 mL agarose gel solution. The solution was carefully mixed and poured into the Biometra Compact casting form (Analytik Jena, Jena, Germany) containing combs. After polymerization, the gel was used

immediately or stored in a plastic bag at 4 °C for future use. The gel was placed in a Biometra Compact running chamber (Analytik Jena, Jena, Germany) filled with 1x TAE buffer for gel electrophoresis. DNA loading dye (New England Biolabs, Frankfurt am Main, Germany) was added to the PCR products and 10-30 µL was loaded per lane. Separation of the products was achieved by running the gel for around 30-40 minutes at 120-170 V using a PHERO-stab 300 power supply (Bachofer Laboratoriumsgeräte, Reutlingen, Germany). Imaging of the gel was conducted using a Gel iX Imager (INTAS Science Imaging Instruments, Göttingen, Germany).

2.2.3.5 Primer design

Primers were designed with PrimerSelect (DNASTAR Lasergene, Madison, Germany). cDNA sequences were taken from the ENSEMBL Genome Browser database (www.ensembl.org) and primers were tested for specificity using the BLAST database (http://blast.ncbi.nlm.nih.gov/Blast.cgi).

2.2.3.6 cDNA Synthesis

The RevertAid RT Kit (Thermo Fisher Scientific, Waltham, USA) was used to generate complementary DNA (cDNA) according to the manufacturer's instructions. Random hexamer primer anneals to complementary RNA sequences allowing strand elongation by reverse-transcriptase. 0.5-1 µg of isolated RNA was used for each reaction. Reactions were mixed according to **Table 6**.

Table 6. Reaction mix protocol for RevertAid RT Kit

RNA (up to 1 µg)	x µL
Random Hexamer primer	1 µL
5x Reaction Buffer	4 µL
RiboLock RNase Inhibitor (20 U/µL)	1 µL
10 mM dNTP Mix	2 µL
RevertAid RT (200 U/µL)	1 µL
Millipore water	x µL
Total volume	20 µL

2.2.3.7 Quantitative real-time PCR

Quantitative real-time PCR (qRT-PCR) was conducted using an ABI 7500 Fast Real-Time PCR System (Applied Biosystems, Darmstadt, Germany) and GoTag® qPCR Master Mix (Promega Corporation, Widesion, USA). A fluorescent dye SYBR Green binds to double-stranded DNA (dsDNA), which measures the increasing amplicons generated from the cDNA

template during PCR.[227] Fluorescence intensity was measured after each elongation step.

With a melting curve analysis, the DNA is melted by slowly increasing the temperature (gradually from 50 °C to 95 °C) and fluorescence intensity was continuously recorded. The reaction was set as shown in **Table 7**. The PCR program presented in **Table 8** was applied.

Table 7. Reaction mix protocol for qRT-PCR

RT primer premix [10 nM]	5 µL
cDNA [10 ng/µL]	1 µL
GoTag qPCR Master Mix	10 µL
Ultra-Pure Water	4 µL
reaction volume	20 µL

Table 8. qRT-PCR Reaction Scheme

Step	Duration	Temperature	
Initial Denaturation	10 min	95 °C	
Denaturation	30 sec	95 °C	40 cycles
Annealing	30 sec	60 °C	
Elongation	30 sec	72 °C	
Final Elongation	30 sec	72 °C	

2.2.3.8 Gene expression profiling (GEP)

GEP was carried out using the Affymetrix GeneChip® Human Exon 1.0 ST Array as previously described in CLL B cells from 337 previously untreated patients of the CLL8 trial.[228,229] Patient characteristics are summarized in **Table 9**.

Table 9. Patient characteristics of samples used in GEP analyses

Baseline characteristics	Cluster 1	Cluster 2	Cluster 3	Total	p-value
All patients (ITT), N	**128**	**100**	**109**	**337**	**-**
Age at study entry (years)	**128**	**100**	**109**	**337**	**Median test**
Median (range)	61 (35-81)	61 (36-78)	62 (39-75)	61 (35-81)	0.697
Age group (years), N (%)	**128**	**100**	**109**	**337**	**Chi²**
≤ 60	63 (49.2)	50 (50.0)	49 (45.0)	162 (48.1)	
> 60 & ≤ 65	34 (26.6)	30 (30.0)	28 (25.7)	92 (27.3)	0.802
> 65 & ≤ 70	21 (16.4)	14 (14.0)	24 (22.0)	59 (17.5)	
> 70	10 (7.8)	6 (6.0)	8 (7.3)	24 (7.1)	
Gender, N (%)	**128**	**100**	**109**	**337**	**Chi²**
Female	40 (31.3)	21 (21.0)	20 (18.3)	81 (24.0)	0.048
Male	88 (68.8)	79 (79.0)	89 (81.7)	256 (76.0)	

Binet stage, N (%)	128	100	109	337	Chi²
A	9 (7.0)	4 (4.0)	8 (7.3)	21 (6.2)	
B	80 (62.5)	62 (62.0)	64 (58.7)	206 (61.1)	0.809
C	39 (30.5)	34 (34.0)	37 (33.9)	110 (32.6)	
Deletion in 17p, N (%)	**127**	**100**	**108**	**335**	**Chi²**
No	120 (94.5)	91 (91.0)	96 (88.9)	307 (91.6)	0.291
Yes	7 (5.5)	9 (9.0)	12 (11.1)	28 (8.4)	
Deletion in 11q, N (%)	**127**	**100**	**108**	**335**	**Chi²**
No	89 (70.1)	80 (80.0)	70 (64.8)	239 (71.3)	0.049
Yes	38 (29.9)	20 (20.0)	38 (35.2)	96 (28.7)	
Trisomy 12, N (%)	**127**	**100**	**108**	**335**	**Chi²**
No	113 (89.0)	87 (87.0)	97 (89.8)	297 (88.7)	0.807
Yes	14 (11.0)	13 (13.0)	11 (10.2)	38 (11.3)	
Deletion in 13q, N (%)	**127**	**100**	**108**	**335**	**Chi²**
No	48 (37.8)	39 (39.0)	41 (38.0)	128 (38.2)	0.981
Yes	79 (62.2)	61 (61.0)	67 (62.0)	207 (61.8)	
Type according to hierar-chical model, N (%)	**127**	**100**	**108**	**335**	**Chi²**
17p deletion	7 (5.5)	9 (9.0)	12 (11.1)	28 (8.4)	
11q deletion	37 (29.1)	19 (19.0)	34 (31.5)	90 (26.9)	
Trisomy 12	13 (10.2)	8 (8.0)	9 (8.3)	30 (9.0)	0.382
No abnormalities	24 (18.9)	19 (19.0)	18 (16.7)	61 (18.2)	
13q deletion (single)	46 (36.2)	45 (45.0)	35 (32.4)	126 (37.6)	
***IGHV* mutational status, N (%)**	**124**	**97**	**106**	**327**	**Chi²**
Unmutated	84 (67.7)	57 (58.8)	74 (69.8)	215 (65.7)	0.212
Mutated	40 (32.3)	40 (41.2)	32 (30.2)	112 (34.3)	
***TP53* mutational status, N (%)**	**125**	**99**	**107**	**331**	**Chi²**
Unmutated	114 (91.2)	87 (87.9)	87 (81.3)	288 (87.0)	0.079
Mutated	11 (8.8)	12 (12.1)	20 (18.7)	43 (13.0)	
***TP53* mutation and/or dele-tion, N (%)**	**125**	**99**	**107**	**331**	**Chi²**
No	114 (91.2)	85 (85.9)	86 (80.4)	285 (86.1)	0.059
Yes	11 (8.8)	14 (14.1)	21 (19.6)	46 (13.9)	
Serum β₂-microglobulin (mg/l)	**111**	**93**	**102**	**306**	**Median test**

64

Median (range)	2.6 (0.9-8.0)	3.3 (1.1-7.9)	2.9 (1.4-9.2)	2.8 (0.9-9.2)	0.027
Serum β₂-microglobulin (mg/l) N (%)	**111**	**93**	**102**	**306**	**Chi²**
≤ 3.5	87 (78.4)	52 (55.9)	70 (68.6)	209 (68.3)	0.003
> 3.5	24 (21.6)	41 (44.1)	32 (31.4)	97 (31.7)	
Leukocyte count (x 10⁹/L)	**124**	**98**	**108**	**330**	**Median test**
Median (range)	62.2 (6.7-181.0)	99.0 (14.0-494.4)	142.3 (21.8-867.0)	94.9 (6.7-867.0)	< 0.001
Leukocyte count (x 10⁹/L), N (%)	**124**	**98**	**108**	**330**	**Chi²**
< 50.0	53 (42.7)	17 (17.3)	13 (12.0)	83 (25.2)	< 0.001

2.2.3.9   RNA sequencing (RNA-seq)

RNA was isolated from murine splenic leukocytes using the mirVana Kit and was subjected to the library preparation and sequenced on the NovaSeq 6000 according to the manufacturer's instructions for polyA-RNA sequencing which was done by the Cologne Center for Genomics (CCG, University Cologne, Germany).

2.2.3.10   Chromatin immunoprecipitation-sequencing (ChIP-seq)

ChIP experiments were performed using the SimpleChIP enzymatic chromatin IP kit (Cell Signaling Technology, Frankfurt am Main, Germany) according to the manufacturer's instructions. Splenic leukocytes (10 million per mL) were crosslinked with 1% methanol-free formaldehyde (Electron Microscopy Sciences, Pennsylvania, USA) in culture medium for 9 minutes at RT with gentle shaking. Cells were washed twice with ice-cold DPBS by centrifugation at 500 x g for 5 minutes at 4 °C after quenching with glycine for 5 minutes at RT. Nuclei were extracted and chromatin was treated with 0.15 µL micrococcal nuclease (New England Biolabs, Frankfurt am Main, Germany) per 100 µL buffer at 37 °C for 15 minutes followed by sonication shearing using a Bioruptor Pico sonicator (Diagenode Inc., Belgium). Chromatin size was verified by agarose gel electrophoresis after chromatin digestion and DNA purification. Anti-H3K4me3 (#9751, Cell Signaling) antibodies were used for ChIP. After reverse cross-linking and DNA purification, ChIP-DNA and whole nuclear DNA as control were subjected to the library preparation and sequenced using the Illumina TruSeq in CCG.

2.2.4   Microbiology

2.2.4.1 Microorganisms, culturing medium, and antibiotics

Escherichia coli DH5α (Thermo Fisher Scientific, Schwerte, Germany), LB Medium, and ampicillin (Carl Roth GmbH, Karlsruhe, Germany) were used in this study.

2.2.4.2 Bacterial transformation

100 ng of plasmid DNA and 100 µL on ice thawed competent *Escherichia coli DH5α* cells were mixed. The mixture was incubated on ice for 30 minutes, followed by a short heat shock at 42 °C for 1 minute and then was chilled on ice for 5 minutes. After transformation, cells were resuspended in 900 µL fresh LB medium and incubated at 37 °C for 1 hour with gentle shaking. Afterwards, cells were mixed with 3-4 mL LB medium (mini-culture) containing 100 µg/mL Ampicillin and transferred to a culture tube to be incubated at 37 °C overnight with shaking at 180 rpm.

2.2.4.3 Culture of transformed *Escherichia coli* cells

A maxi-culture was conducted by adding the mini-cultured *Escherichia coli* cells to the main culture of 250 mL LB medium containing 100 µg/mL Ampicillin and incubation overnight at 37 °C with shaking at 180 rpm.

2.2.4.4 Purification of plasmid DNA

The PureYield™ Plasmid Midiprep System (Promega Corporation, Widesion, USA) was used to purify the plasmid DNA from Escherichia coli DH5α culture according to the manufacturer's instructions. Using the vacuum protocol, plasmid isolation was completed in a short time. The PureYield™ System clears lysate with a fixed-angle centrifugation step, followed by binding and washing using a vacuum. Elution with a vacuum leads to a better DNA recovery and yield.

2.2.4.5 Determination of plasmid DNA concentration

DNA concentration was measured at 260/280 nm with the Nanodrop 1000 using 1 µL per sample elutes. The ratio of absorbance at 260 nm and 280 nm was used to verify the quality of each sample (A260/280).

2.2.5 Animal experiments

2.2.5.1 Laboratory mice

Mice stayed in the animal facility of the University Hospital of Cologne according to the national regulations for animal experiments recommended by the GV-SOLAS (http://www.gv-solas.de) in individually ventilated cages (IVC) under specific pathogen-free conditions. Animal experiments were approved under the LANUV permission 84-02.04.2014.A146, 81-02.04.2019.A009, and 84-02.04.2016.A243.

2.2.5.1.1 *Eµ-TCL1A* mouse model

Eµ-TCL1A mice were obtained from Professor Croce (Philadelphia, USA).110 In this model, human TCL1A has been engaged under the control of a mouse VH-promoter/IgH-µ enhancer to target TCL1A expression to immature and mature B cells, which are widely used as a disease model mimicking human CLL.

2.2.5.1.2 *Lck-TCL1A* mouse model

Lck-TCL1A mice were obtained from Jackson Laboratory (Bar Harbor, ME, USA).[113] In this model, human TCL1A oncogene was expressed in animals under the proximal T-cell specific p56 (*Lck*) promoter element. These mice develop a T-PLL-like disease with a CD4-/CD8+ phenotype at the age of around 10-15 months. Therefore, *Lck-TCL1A* mice serve as the standard in vivo model for studying T-PLL.

2.2.5.1.3 *iKdm1a^KD* mouse model

An inducible *Kdm1a* knockdown *(iKdm1a^KD)* mouse model was obtained from Professor Schüle (Freiburg, Germany), in which *Kdm1a*-specific shRNA sequences are driven off a Dox-inducible Rosa26 promoter (**Figure 20**).[230] While untreated animals are of wild-type phenotype, Dox induces pan-organismal downregulation of Kdm1a protein, mimicking systemic administration of a specific KDM1A inhibitor.

Figure 20. Schematic representation of the TET-ON system used to induce the *Kdm1a*-specific shRNA in vivo (adapted from *A Sprüssel et al. 2012*).[230]

2.2.5.1.4 *iKdm1a^{KD}; Eµ-TCL1A* mouse model

To study Kdm1a inhibition in the context of CLL*, iKdm1a^{KD};Eµ-TCL1A* mice were obtained by the crossbreeding of *Eµ-TCL1A* and *iKdm1a^{KD}* mice. Mice were fed with Dox-food to induce the knockdown of *Kdm1a*, mimicking systemic inhibition of Kdm1a in murine CLL.

2.2.5.1.5 *iKdm1a^{KD};Lck-TCL1A* mouse model

To study Kdm1a inhibition in the context of T-PLL*, Lck-TCL1A* were crossbred with *iKdm1a^{KD}* mice. Dox-food was used to induce the knockdown of *Kdm1a*, mimicking systemic inhibition of Kdm1a in murine T-PLL.

2.2.5.2 Procedures of animal experiments

2.2.5.2.1 Blood sample collection from mice

For monitoring leukemia development, blood was taken from *Eµ-TCL1A*, *Lck-TCL1A*, *iKdm1a^{KD};Eµ-TCL1A*, and *iKdm1a^{KD};Lck-TCL1A* mice by cutting a tiny incision on the tail vein with a scalpel and using heparin-coated capillary to collect 20-40 µL of blood into a 1.5 mL microtube. Blood samples were used for blood routine examination and phenotypic analysis by flow cytometry.

2.2.5.2.2 Narcotization of mice

The mice that were under experiments were narcotized in an inhalation cabinet using Isofluran (AbbVie, Wiesbaden, Germany) with an Isofluran nebulizer Vapor 19.3 (Dräger, Lübeck, Germany) and O_2. Mice were narcotized with 1.5-2.5% Isoflurane plus 2.5-3 L/minute O_2 in an inhalation exposure chamber when they were going through the Magnetic resonance imaging (MRI) scanning.

2.2.5.2.3 Magnetic resonance imaging and spleen volumetry

MRI was used to image and measure the spleen size of mice in a non-invasive way. MRI scans were performed in the Department of Radiology of the University Hospital of Cologne using the clinical Ingenia 3.0T MRI system (Philips, Hamburg, Germany). The system was equipped with a small rodent solenoid coil and an integrated heating system (Philips Research Europe, Hamburg, Germany) to keep the body temperature of the mouse during the MRI procedure. Before imaging, the mice were narcotized using Isolfluran inhalation as described in 2.2.4.2.2 and kept under the same conditions during the examination. Imaging was carried out

with the following parameters: turbo spin-echo (TSE) factor: 10, repetition time (TR): 2674 ms, echo time (TE): 65 ms, flip angle: 90°, slice thickness: 1.0 mm (without gap), voxel size (reconstructed): 0.16 x 0.16 x 1.0 mm, matrix: 256 x 256, the field of view (FOV): 40 x 40 mm, and the number of acquisition (NSA): 6. MRI data were exported in the Digital Imaging and Communications in Medicine format (DICOM). The spleen volume was analyzed using OsiriX lite (Pixmeo, Bernex, Switzerland). The splenic region of interest (ROI) in each section was made and then the volume was calculated by the function "ROI Volume" computing the relevant spleen volume in cm^3 (**Figure 21**).
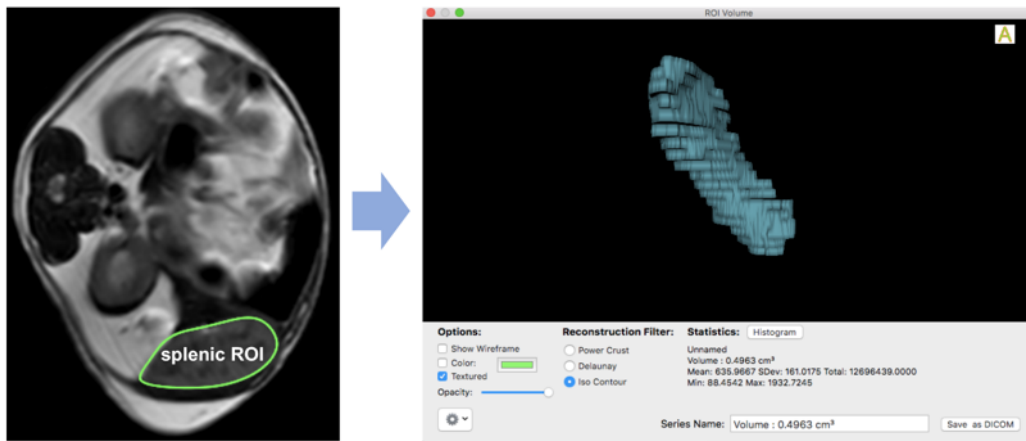
Figure 21. Determination of the spleen volume by MRI. Mice were imaged using MRI scanning. DICOM files were analyzed by using OsiriX lite software (Pixmeo, Bernex). The splenic ROI was made in each section allowing the computation of the spleen volume as shown.

2.2.5.2.4 Sacrificing mice

Mice were sacrificed by CO_2 asphyxiation and cervical dislocation.

2.2.5.2.5 Isolation of murine bone marrow cells and splenocytes

The isolation was processed as described in 2.2.1.7 and 2.2.1.8, respectively.

2.2.5.2.6 Preparation of tissue

A small piece of the spleen was kept in a block and fixed in 4% formalin (Carl Roth, Karlsruhe, Germany) for at least 24 hours at RT. Formalin-fixed tissue specimens were washed using running tap water for 1-2 hours followed by dehydration in 70% ethanol (Th. Geyer GmbH, Renningen, Germany) for 30 minutes. Then the tissue can be stored in 70% ethanol in the fridge. Tissue specimens were embedded into paraffin in the department of Dermatology (University of Cologne) and Formalin-Fixed Paraffin-Embedded (FFPE) tissue was stored at RT

for future sectioning. Another small piece of the spleen was placed upright in a plastic Cryomold (Ted Pella, Inc., California, USA) filled with Tissue-TEK (Sakura, Staufen, Germany). The samples were snap-frozen on a metal block in liquid nitrogen and then were transferred to a -80 °C freezer for future cryosectioning.

2.2.5.3 Histology

2.2.5.3.1 Sectioning on a microtome

FFPE tissue specimens were cut into 4 µm thick sections using a sliding microtome (Leica Biosystems, Nussloch, Germany). The cut tissue was floated over a water bath to eliminate wrinkles and distortion, and mounted on a slide. All the slides were stored at RT for future staining.

2.2.5.3.2 Hematoxylin and Eosin staining

Hematoxylin and eosin (H&E) staining has been used for decades and remains a key procedure for identifying various types of tissue or morphological alterations. Hematoxylin has a deep blue-purple color, staining the nucleic acids. Eosin dye is pink and stains proteins in a non-specific way. Typically, nuclei are recognized by blue staining, while the cytoplasm and extracellular matrix structures have differential degrees of pinkish color.[231] Sections were hydrated for 30 seconds in tap water followed by staining in Hemalum solution acid acc. to Mayer (Carl Roth, Karlsruhe, Germany) for 5 minutes and washed shortly in dH_2O. Afterwards, slides were rinsed with warm tap water until tissue sections appear blue color. Then slides were stained with Eosin Y staining solutions (Carl Roth, Karlsruhe, Germany) for 5 minutes and washed shortly in dH_2O. Tissue sections were dehydrated in 70%, 90%, and 100% ethanol (Carl Roth, Karlsruhe, Germany) for each 1 minute, and were incubated for 1 minute in Xylene (Carl Roth, Karlsruhe, Germany). Subsequently, slides were mounted using Roti®-Histokitt II mounting solution (Carl Roth, Karlsruhe, Germany) and coverslipped.

2.2.5.3.3 Microscopy of H&E stained slides

After the mounting solution was dried, slides were scanned using a BX63 motorized bright field microscope (Olympus, Tokyo, Japan) and the CellSens Dimension software (Olympus, Tokyo, Japan) under 40X resolution.

2.2.5.4 Tissue cytometry

2.2.5.4.1 Cryosectioning

Tissue-TEK embedded tissue was assembled in the cryostat CM1850 UV (Leica Biosystems, Nussloch, Germany) and 6 µm thick tissue sections were cut. Sections were mounted on Superfrost microscopic slides (Fisher Scientific, Schwerte, Germany). The slides were stored at -80 °C for future staining.

2.2.5.4.2 Immunofluorescent (IF) staining

Tissue sections were fixed for 15 minutes in 4% PFA (Carl Roth GmbH, Karlsruhe, Germany) at 4 °C and washed 3 times for 5 minutes at RT in PBS with gentle shaking. Afterwards, antigen retrieval was done in 1 mM EDTA at 60 °C in a water bath for 15 minutes followed by 3 times washing for 5 minutes in PBS. In order to block unspecific binding, sections were blocked with blocking reagent (Perkin Elmer, USA) for 1 hour at RT. The solution was carefully removed. Primary antibodies were diluted in staining buffer. The antibody solution was applied onto each section to cover the whole tissue and the slides were incubated overnight in a wet chamber at 4 °C. On the following day, the primary antibody staining solution was removed and the slides were washed 3 times for 5 minutes in PBST. Afterwards, the slides were incubated with fluorescence conjugated secondary antibodies and 1 µg/mL Hoechst to stain the nucleus for 60 minutes at RT in a wet chamber. Slides were washed 3 times for 5 minutes and air-dried in the dark. The dried slides were mounted using mowiol mounting solution and coverslips. Then the mounted slides were stored at 4 °C in the dark.

2.2.5.4.3 Microscopy of IF stained slides

After the mounting solution was dried, slides were scanned using an IX83 motorized inverted fluorescence microscope (Olympus, Tokyo, Japan) and the CellSens Dimension software (Olympus, Tokyo, Japan) under 60X resolution. The images were processed using the StrataQuest software (TissueGnostics, Vienna, Austria).

2.2.5.4.4 Imaging process of the IF staining microscopy

The microscopic pictures of the immunofluorescent staining were processed with StrataQuest software using the nuclear marker as the master channel to identify all cells. A secondary measure mask, derived from the nuclear mask, was used to measure cytoplasmic reactivity. For markers expressed in the nucleus (e.g., Ki-67), the nuclear mask was used to quantify the signal. Cutoffs were set interactively using the "forward connection" feature in the software,

which links each dot in the scattergram to the corresponding event in the image. The quantified results were plotted as density plots (**Figure 22**).
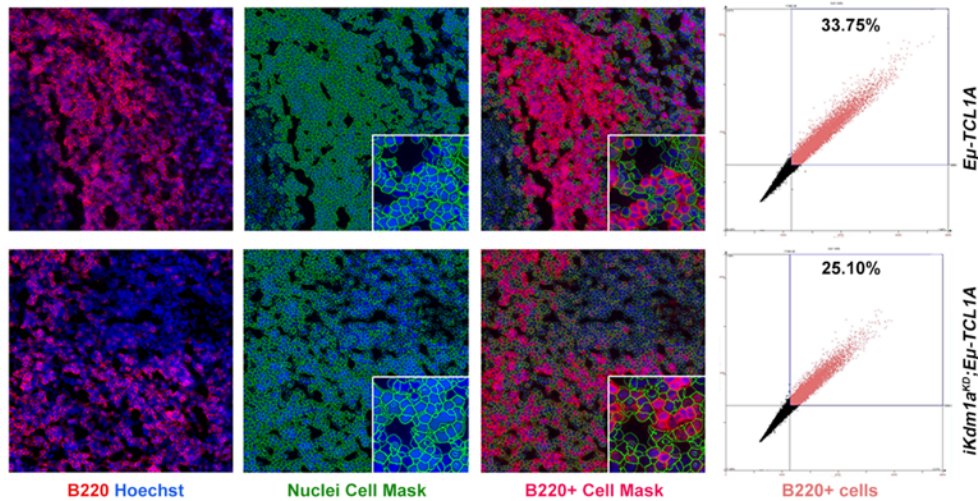

Figure 22. An example of the analysis process of the microscopic images using StrataQuest. Nuclear Cell Mask and Cell Mask of positive stained cells were sketched with cutoffs that removed background. Density plots showing the quantified results.

2.2.6 Bioinformatics and statistics

2.2.6.1 Analysis of MS data

The Perseus software (Max Planck Society, Munich, Germany) was used for the analysis of primary samples. Proteins with less than 25 valid values among all samples were sorted out and missing values were replaced by random numbers based on a normal distribution (width 0.3; downshift: 1.8). To identify specific TCL1A interacting proteins, a Welch test was performed to compare the log2 of LFQ intensities of the different groups with the log2 of LFQ intensities of IgG (cut-off: fold change > 2, q < 0.05). The identified TCL1A interacting partners within each group were subsequently compared between the different groups using a Welch test (cut-off: fold change > 2, q < 0.05).

For histone PTM MS, data were acquired using a data-independent acquisition method (DIA) and analyzed using EpiProfile v.2.0.[232] The peptide relative ratio was calculated using the total area under the extracted ion chromatograms of all peptides with the same amino acid sequence with all modified forms as 100%. For isobaric peptides, the relative ratio of two isobaric forms was estimated by averaging the ratio for each fragment ion with a different mass between the two species.

2.2.6.2 Analysis of GEP data of CLL tumor cells from the CLL8 clinical trial

The expression intensities derived from the Affymetrix GeneChip® Human Exon 1.0 ST Array, were restricted to "core" probe sets and averaged on gene levels. A Log2-transformed summary measure of gene expression provided by the robust multi-array average (RMA) algorithm was used for data normalization. The uni-variate permutation test with the Benjamini-Hochberg correction for multiple testing was used to calculate the differential gene expression. Agglomerative hierarchical clustering was done by using Pearson's correlation coefficient for distance measures and average linkage as agglomeration rules. The Affymetrix Power Tools (http://www.affymetrix.com/partners_programs/programs/developer/tools/powertools.affx) and BRB-Array tools (http://linus.nci.nih.gov/BRB-ArrayTools.html) were used for analyses, including normalization. The genesis clustering software was used for clustering and visualization.

2.2.6.3 RNA-seq data processing

RNA-seq data were processed using a high-throughput Next-Generation Sequencing analysis pipeline.[233] FastQC (v0.10.1) was used for basic read quality check and read statistics were acquired with SAMtools v0.1.19.[234] Then reads were mapped to the mouse reference (version 93) using Tophat v2.0.10,[235] and gene quantification was carried out using a combination of Cufflinks v2.1.1[236] and the DESeq2 package v1.4.5,[237] with genomic annotation from the Ensembl database, version 93. Afterwards, the results were uploaded into an in-house MySQL database and joined with BiomaRt v2.20.0[238] annotations from Ensembl, version 93. Lists of differentially expressed genes were defined by a final database export using 5 and 0.01 as cutoffs for DESeq2-based fold changes and P-values, respectively.

2.2.6.4 ChIP-seq data analysis

ChIP-seq reads were mapped to a mouse reference genome provided by the Mouse Genome Sequencing Consortium (GRCm39/mm39) using Bowtie2 v. 2.2.9,[239] and aligned reads from biological replicates were pooled together. Peaks were called for pooled samples with MACS2 v. 2.2.6[240] using the corresponding inputs and default parameters. Differential peaks were identified using MACS2 bdgdiff default parameters. Heatmaps and average profile plots were generated using coverage normalized to signal per million reads (SPMR) using deeptool.[241] Peak annotation according to GENCODE gene annotation vM27 of the corresponding peaks sets was performed using annotatePeaks.pl function of HOMER v4.11.1[242] and custom R 4.0.0 scripts. Analysis of TF motifs at each peak set was performed using findMotifsGenome.pl of HOMER v4.11.1.[242]

2.2.6.5 General statistics

Results are presented as mean ± standard error of the mean (SEM) or standard deviation (SD). The student's t-test and Mann-Whitney test (GraphPad Prism, La Jolla, Version 8.0 & 9.0) were used to determine statistical significance. P values < 0.05 were considered statistically significant.

3 Results

3.1 Aim I: Characterize the impact of TCL1A on the activity of KDM1A

3.1.1 TCL1A interacts with KDM1A in the nucleus of B cells

To validate the result of our MS analysis that TCL1A interacts with KDM1A in CLL B cells (**Figure 15**), co-IP experiments using anti-TCL1A/TCL1A^{FLAG} antibodies were carried out in primary human CLL cells, leukemic B cells from a CLL mouse model, and CLL-like cell lines JVM3$^{GFP/TCL1A}$ under relevant conditions. For this, primary CLL B cells were co-cultured with differentiated THP-1 cells for 36 hours in advance, supplemented with 10 μg/L of rhIL-15 and 0.25 μM of CpG. Splenic lymphocytes were isolated from leukemic *Eμ-TCL1A* mice. It is known that TCL1A as well as KDM1A are involved in the DNA damage response (DDR).[243,244] In order to decipher a potential interaction during active DDR, we additionally treated murine splenic lymphocytes and JVM3 cells with VP-16 (etoposide) for different time points (0/1/3 hours). These co-IPs confirmed the MS results that TCL1A interacts with KDM1A in primary CLL cells (**Figure 23A, Table 10**) and in *Eμ-TCL1A* leukemic cells (**Figure 23B**). As an epigenetic factor, KDM1A was supposed to have a function in the nucleus. Cell fractions were extracted from JVM3$^{GFP/TCL1A}$ cells by using a nuclear extraction kit. Immunoblots showed that cell fractions are separated efficiently as defined by staining with Histone 3 as a nuclear protein and β-Tubulin as a cytoplasmic protein. The TCL1A^{Flag} protein was pulled down and the resulting immune complexes were precipitated with anti-FLAG M2 magnetic beads. KDM1A and TCL1A proteins are presented in both the cytoplasm and nucleus. However, TCL1A^{Flag} IP demonstrated the KDM1A-TCL1A interaction only to be present in the nucleus (**Figure 23C**), which might be important for TCL1A affecting the epigenetic function of KDM1A.
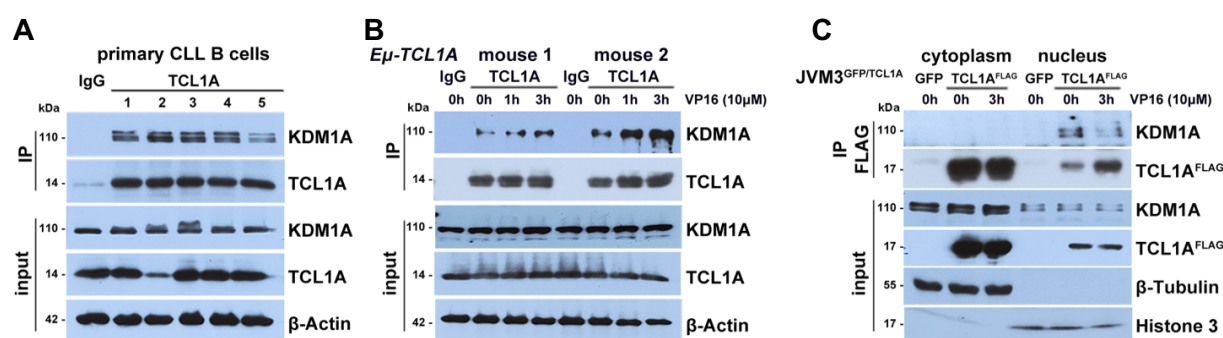
Figure 23. TCL1A interacts with KDM1A in B cells. (A,B) Co-IPs and immunoblots confirmed TCL1A-KDM1A interaction in primary CLL samples (N=5) and in splenic lymphocytes from leukemic *Eμ-TCL1A* mice (N=2), respectively. (C) Co-IPs and immunoblots showing the interaction of TCL1A with KDM1A in the nuclear fraction of CLL-like B cells (N=3 independent experiments).

Table 10. Patient characteristics of samples used in TCL1A co-IP experiment

Patient ID	Age	Karyotype	ZAP70 (%)	CD38 (%)	IGHV	Binet stage	WBC (x10⁹/L)	LDT (months)
CLL12	78	del(13q)	neg		M	A	253.7	>12
CLL13	53	del(13q)	1.72	32.69	U	A	159.86	
CLL14	64	complex karyotype			na	A	111.38	
CLL15	54				U	B	435.1	
CLL16	57	tri12			na	A	209	

IGHV: *IGHV* mutation status; M: *IGHV* mutated; U: *IGHV* unmuted

3.1.2 TCL1A enhances the histone demethylase activity of KDM1A and alters histone post-translational modifications in B cells

The interaction of TCL1A with KDM1A might control their subcellular localization thus limiting or facilitating their access to histones. However, it is also likely that TCL1A operates as a chaperone to regulate post-translational modifications of histones by directly binding the enzymatic KDM1A F-box domains thus affecting its conformation and demethylase activity. Alternatively, TCL1A might modulate KDM1A's activity indirectly by permitting/inhibiting access to co-factors or by accelerating/mitigating degradation. To address whether TCL1A affects the catalytic activity of KDM1A, a KDM1A histone demethylase activity assay was performed in B cell lines in the context with or without the presence of TCL1A. Higher histone demethylase activity of KDM1A was observed in *TCL1A*-tg cell lines (JVM3 P=0.048, DoHH2 P=0.008, **Figure 24**). Furthermore, MS analysis of histone PTM was performed in the B-cell lymphoma cell lines DoHH2$^{\pm TCL1A}$ to characterize the impact of TCL1A on histone PTM. Differential histone PTMs in TCL1A negative and positive cells were observed (**Figure 25A-B**). Significantly lower H3K9me2/3 levels were presented in *TCL1A*-tg DoHH2 cells (H3K9me2 P=0.013, H3K9me3 P<0.001, **Figure 25C**). Additionally, immunoblotting confirmed a decreased H3K9 methylation level in *TCL1A*-transgenic B-cell lines (**Figure 26**).
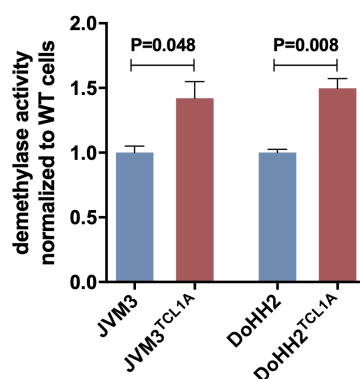
Figure 24. TCL1A enhances the demethylase activity of KDM1A in B cells. Demethylase activity assay demonstrate higher histone demethylase activity in TCL1A positive cells. Mann-Whitney test was used to assess statistical significance (N=4 independent experiments).

Given that TCL1A is expressed in over 90% of the CLL cases and its overexpression marks responsive BCR pathway and adverse clinical outcome.[111] These results suggest that the increased TCL1A levels in CLL might affect the epigenetic signature of B cells by modulating demethylase activity of KDM1A.
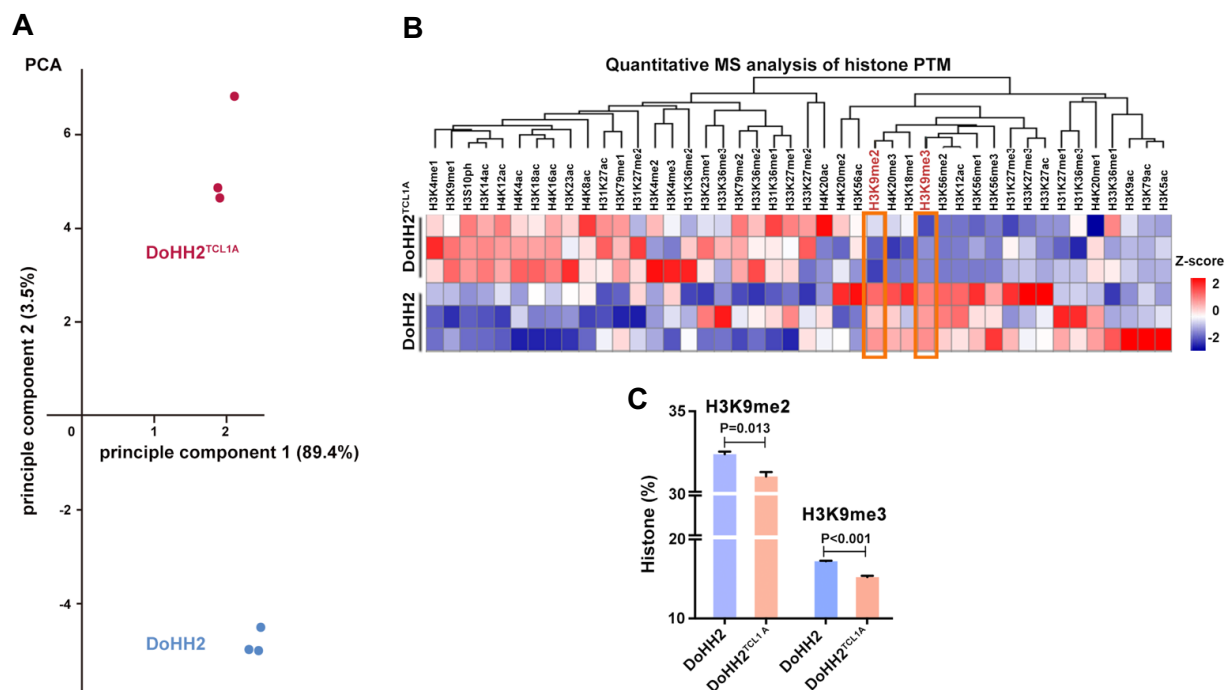

Figure 25. TCL1A affects histone post-translational modifications (PTM) in DoHH2 cells. Quantitative mass-spectrometry (MS) analysis of histone post-translational modifications analysis was performed in DoHH2±TCL1A cells (N=3 independent experiments). (A) Principal component analysis (PCA) analysis of MS data distinct groups by the presence of TCL1A (blue DoHH2, red DoHH2^TCL1A). Each data point represents one independent experiment. (B) Heatmap showing the differential histone marks in TCL1A positive and negative cells. (C) Significantly lower H3K9me2/3 was observed in *TCL1A*-tg B cells. Mann-Whitney test.
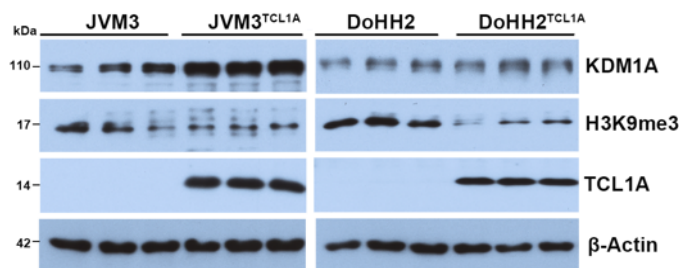
Figure 26. Immunoblots showing lower levels of H3K9me3 in TCL1A-transgenic B cell lines in comparison to parental lines. Immunoblotting was performed in JVM3±TCL1A and DoHH2±TCL1A cells, each lane represents one individual sample.

3.2 Aim II: Characterize *KDM1A* expression levels in CLL and investigate its associations with clinico-pathologic features and outcomes

We next aimed to characterize the expression of KDM1A and its biological relevance in CLL.

3.2.1 KDM1A is upregulated in primary CLL cells

An association of KDM1A with cancer was first reported a few years ago. It has been found to possess oncogenic properties in a range of solid tumors, e.g., of the prostate, bladder, lung, liver, and in neuroblastomas.[187] Recently, KDM1A also has been strongly implicated in the pathogenesis and maintenance of several hematological malignancies.[187] To investigate the KDM1A levels in primary cells, CLL B cells were collected and their cellular proteins were extracted for detection of KDM1A and TCL1A protein levels by immunoblotting. B cells from age-matched healthy donors (HD) were used as control. Indeed, immunoblotting and densitometry analysis showed that the protein levels of KDM1A are higher in CLL samples compared to that in HD B cells (P=0.004, **Figure 27, Table 11**).

Given an established oncogenic relevance of KDM1A[245] also in hematopoietic tumorigenesis, we speculate here that the observed KDM1A overexpression could contribute to the pathogenesis of CLL.
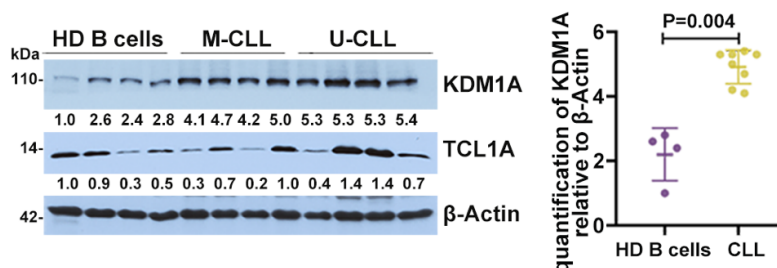
Figure 27. The protein levels of KDM1A in CLL and healthy B cells. Immunoblots (left) and densitometry (right) analysis demonstrated that the protein levels of KDM1A are higher in CLL samples (N=8) compared to healthy donors (HD, N=4) B cells. Mann-Whitney test.

Table 11. Patient characteristics of samples used in immunoblotting for detection of KDM1A

Patient ID	Age	Karyotype	ZAP70 (%)	CD38 (%)	IGHV	Binet stage	WBC (x10^9/L)	LDT (months)
CLL12	78	del(13q)	neg		M	A	253.7	>12
CLL17	61	del(13q)			U	A	133.5	<12
CLL18	53	del(13q), t(6;8)			U	B	199	
CLL19	76	del(13q)		pos	U	B	71.2	
CLL20	80				na	B	222	
CLL21	85				U	A	66.3	
CLL22	71		neg		M	A		>12
CLL23	62	mutation in BIRC3			M		89.7	

IGHV: *IGHV* mutation status; M: *IGHV* mutated; U: *IGHV* unmuted

3.2.2 Higher *KDM1A* levels are associated with adverse prognostic features in CLL

To explore the role of elevated *KDM1A* expression in human CLL, we analyzed GEP data of patients (N=337) enrolled in the CLL8 trial. This prospective study compared outcomes after fludarabine and cyclophosphamide treatment with or without rituximab (FC vs. FCR).[229] We identified 586 differentially expressed genes (DEGs) between patients with low vs. high *KDM1A* expression (low vs. high quartile) and defined three clusters (cluster 1, 2, 3, Fold change>1.55, FDR q<0.02) using the top 449 DEGs (**Figure 28A, Table 9**). *KDM1A* levels were significantly higher in cluster 3 than in cluster 1 (P<0.001, **Figure 28B**). Among the top up/down-regulated genes that are associated with high *KDM1A* levels, *SLAMF6* expression levels positively correlated with higher *KDM1A* levels (FDR q<1e-07, **Figure 28A**). SLAMF6 plays a key role in the interactions between T follicular helper cells and germinal center B cells.[246] It has been reported that anti-SLAMF6 treatment reduces the number of CLL cells.[247] While genes of the *FOS* family, which are subunits of AP-1 TF, *FOS* and *FOSB* expression levels inversely correlated with high *KDM1A* levels (**Figure 28A**). Low or very low expression levels of the *FOS* gene family have been shown to predict a poor prognosis in CLL.[248] Kyoto encyclopedia of genes and genomes (KEGG) pathway analysis revealed that DNA replication, DNA repair pathways, and BCR signaling pathways are enriched in *KDM1A* high quartile, while the cytokine receptor interaction pathway is enriched in the *KDM1A* low quartile (**Figure 29**).

There were higher WBC counts (P<0.001) and higher serum thymidine kinase levels (P=0.009) at presentation in patients of cluster 3 (**Figure 30A-B**). Higher *TCL1A* levels (P<0.001), higher rates of *TP53* aberrations (deletion or mutation, P=0.022) and shorter telomere lengths (P=0.003) were also detected in this *KDM1A^{high}* cluster 3 (**Figure 30C-E**). Importantly, when assessing the prognostic impact for CLL patients within these clusters, we found significantly shorter progression-free survival (PFS) for patients (both treatment arms) of cluster 3 compared to cluster 1 (median PFS 32.4 months (cluster 3) vs. 46.6 months (cluster 1), HR: 1.487 (95% CI: 1.096-2.018), P=0.011, **Figure 31A**). This prognostic impact derived predominantly from patients of the FC trial arm (median PFS 29.1 months (cluster 3) vs. 34.1 months (cluster 1), HR: 1.587 (95% CI: 1.047-2.406), P=0.029, **Figure 31B**). While no significant effect on PFS was observed for patients in the FCR cohort (42.4 months (cluster 3) vs. 55.2 months (cluster 1), P=0.16, **Figure 31C**). Addition of rituximab to fludarabine and cyclophosphamide improved the progression-free survival in CLL patients.[249]

Taken together, KDM1A shows an upregulation in CLL and gene expression signatures associated with higher *KDM1A* levels mark a more aggressive disease with adverse clinical outcomes.

A Top 449 differentially expressed genes for *KDM1A* low vs. high quartile in 337 CLL patients

cluster   1   2   3

FOS
FOSB
TNF
GUCY
HSPA1A
HSPA1B
GABARAPL1
C13orf15
NR4A3
NR4A2

CYB5A
AIM2
SLAMF6
CR2
SAMD9L
PCMTD1
FIG4
LARS
ACADM
UGDH

KDM1A

fold change>1.55, q<0.02

B *KDM1A* levels

P<0.001

Log$_2$ expression

cluster   N=128   N=100   N=109
          1   2   3
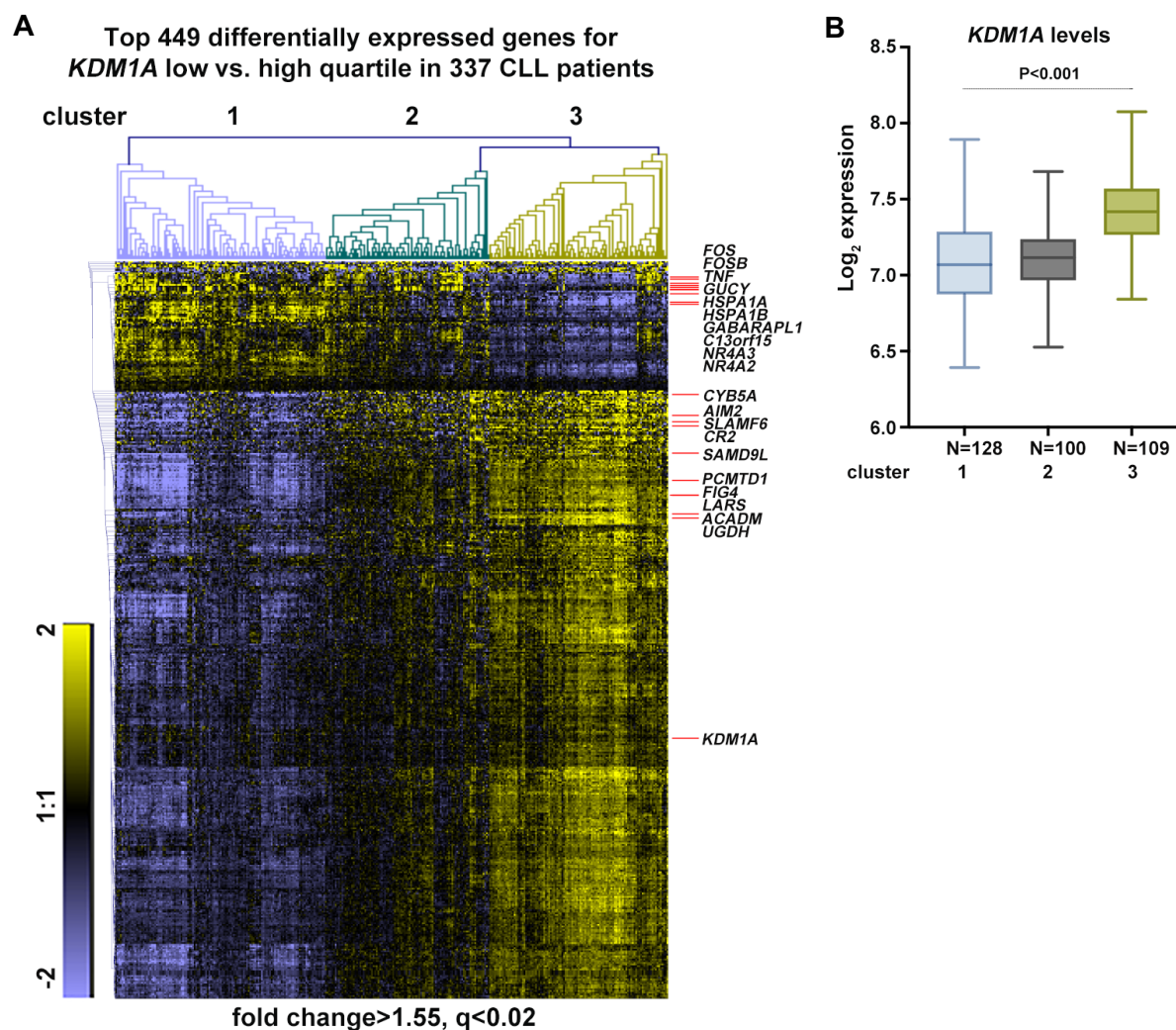
Figure 28. Gene clusters in CLL patients. Gene expression profiling (GEP) of previously un-treated CLL patients (N=337) from the CLL8 trial. KDM1A specific signatures were explored based on the differential expression for KDM1A (low quartile vs. high quartile). (A) Heatmap showing clusters (euclidean distance and average linkage) of the top 449 differentially expressed genes (fold change>1.55, q<0.02), top 10 up or down-regulated genes and KDM1A are indicated (cluster 1 N=128, cluster 2 N=100, and cluster 3 N=109). (B) CLL patients of cluster 3 (clusters defined in Figure 25A, N=109) showing significantly higher KDM1A expression levels compared to cluster 1 (N=128), P<0.001, Mann-Whitney test.

A

KEGG pathways correlated with high *KDM1A* levels
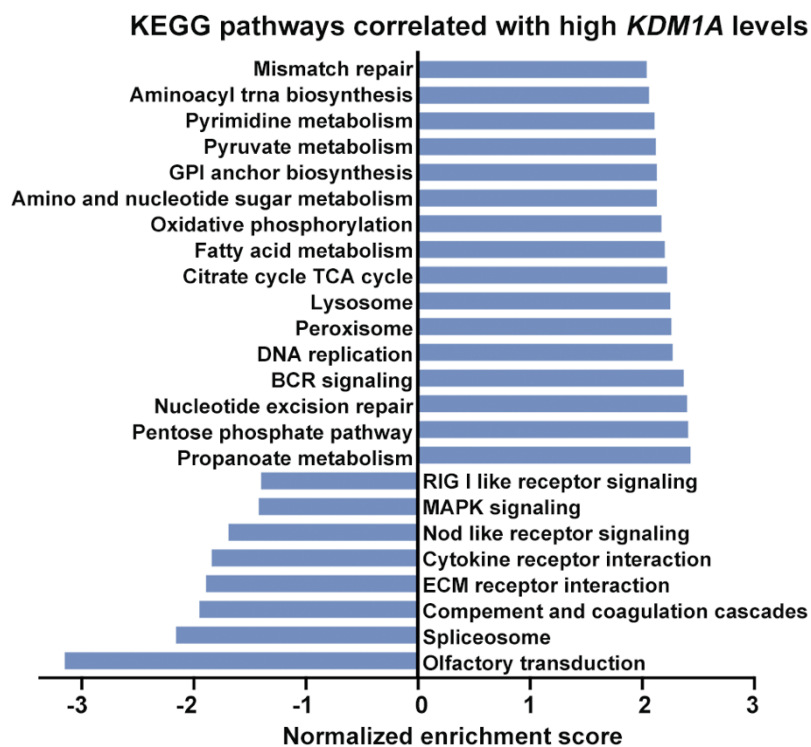
B
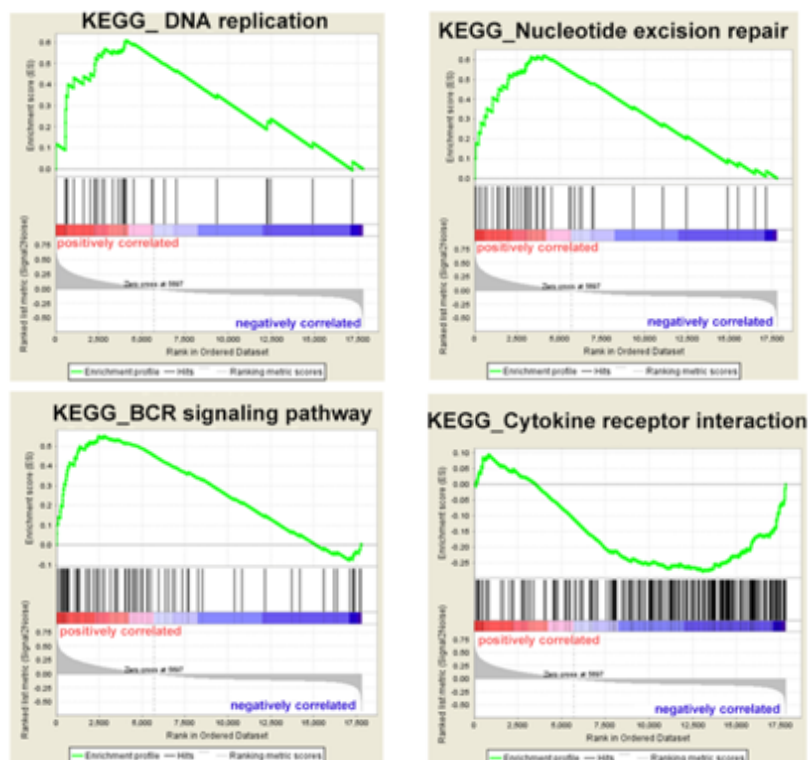
Figure 29. KEGG pathway analysis of differentially expressed genes. (A) Bar displaying top KEGG pathways correlated with high *KDM1A* levels. (B) Enrichment plots of indicated pathways.
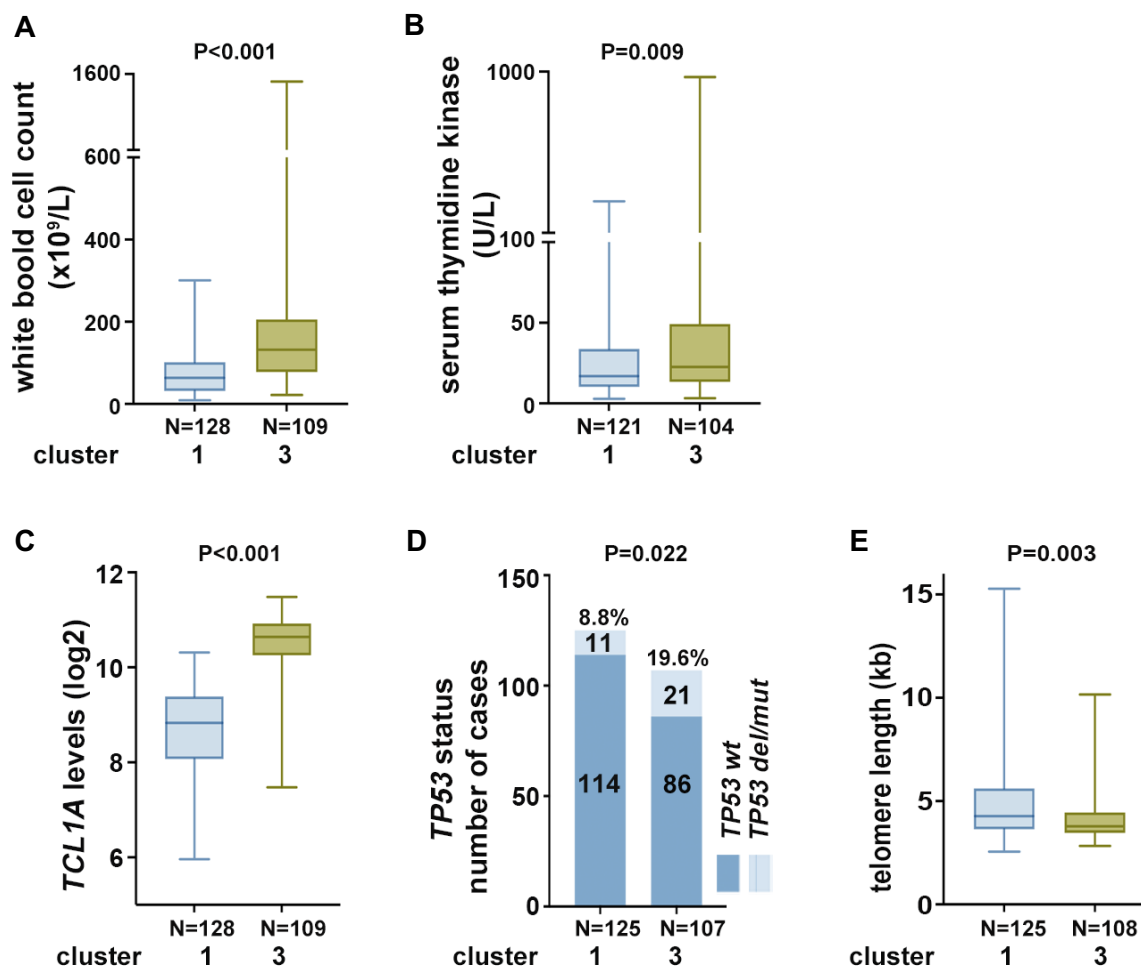
Figure 30. Higher *KDM1A* levels are associated with adverse prognostic features in CLL patients.
(A) Patients in the cluster 3 (N=109) showed higher WBC counts than patients in the cluster 1 (N=128).
P<0.001, Mann-Whitney test. (B) Significantly higher thymidine kinase serum levels in patients of the
cluster 3 (N=104) vs. cluster 1 (N=121), P=0.009, Mann-Whitney test. (C, D, E) Patients in cluster 3
showed (C) higher *TCL1A* levels (cluster 1 N=128, cluster 3 N=109, P<0.001, Mann-Whitney test), (D)
higher incidence of *TP53* deletion/mutation (*TP53 del/mut*, cluster 1 114/125, cluster 3 86/107, P=0.022,
Fisher's exact test), *wt*: wild type, and (E) shorter telomere length (cluster 1 N=125, cluster 3 N=108,
P=0.003, Mann-Whitney test). Boxes show median and the min-max.
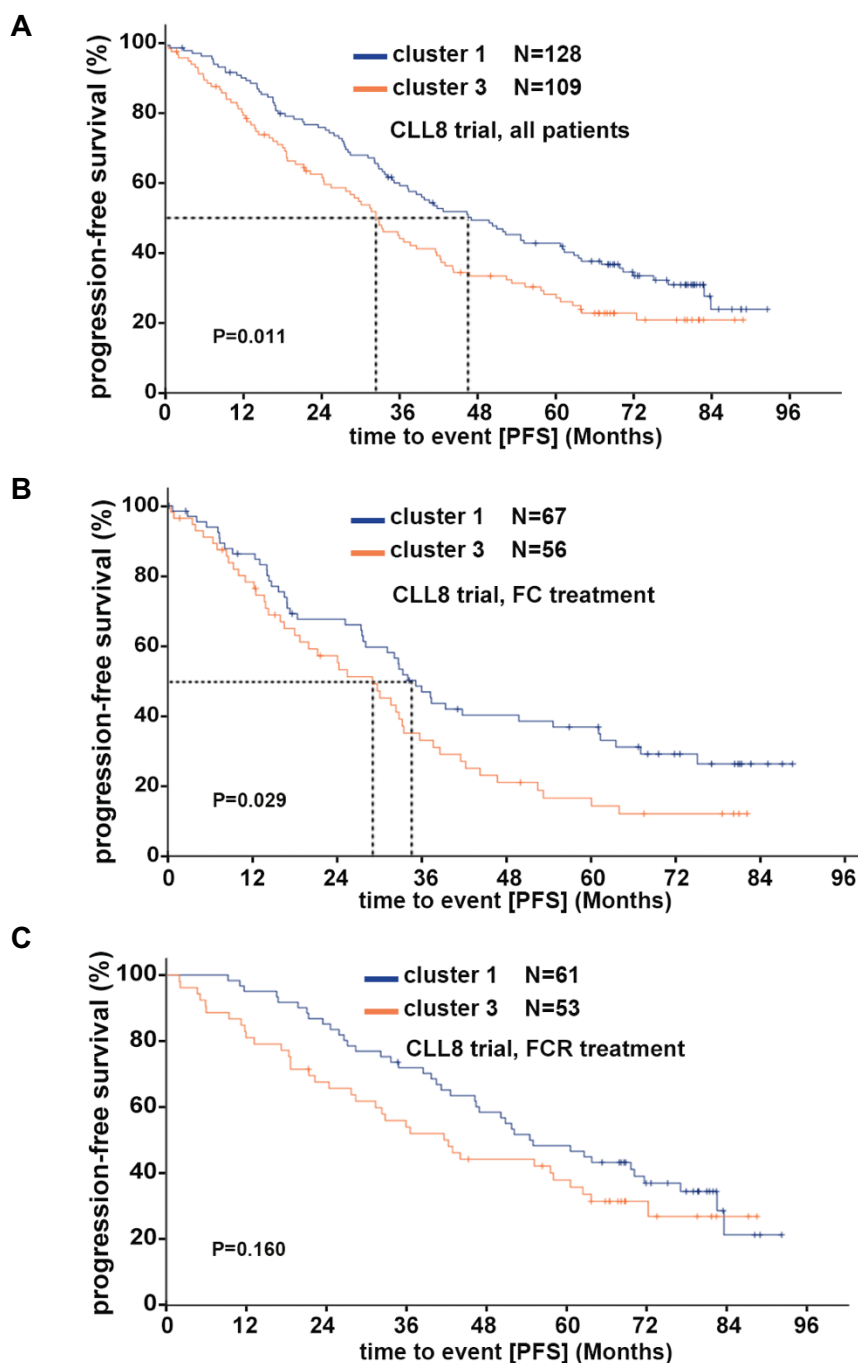
Figure 31. Survival analysis of CLL patients. The Kaplan-Meier curves comparing progression-free survival (PFS) of CLL patients in cluster 3 (orange) vs. cluster 1 (blue). Survival data were acquired from the CLL8 trial. Comparisons were made among patients (A) in both arms, cluster 3 (N=109, median 32.4 months) vs. cluster 1 (N=128, median 46.6 months), HR: 1.487 (95% CI: 1.096-2.018), P=0.011. (B) in the fludarabine/cyclophosphamide (FC) cohort, cluster 3 (N=56, median 29.1 months) vs. cluster 1 (N=67, median 34.1 months), HR: 1.587 (95% CI: 1.047-2.406), P=0.029. (C) in the fludarabine/cyclophosphamide/rituximab (FCR) cohort, cluster 3 (N=53, median 42.4 months) vs. cluster 1 (N=61, median 55.2 months), HR: 1.318 (95% CI: 0.879-2.172), P=0.160. Log-rank test was used to assess statistical significance.

3.3 Aim III: Assess the effects of a knockdown of *Kdm1a* in a murine CLL model

To evaluate the therapeutic potential of KDM1A inhibition, this aim focuses on analyzing the functional role of Kdm1a on CLL cell growth and the identification of its molecular targets in a murine model of CLL. *Kdm1a* was knocked down by using a genetically modified mouse model that ubiquitously expresses shRNAs against *Kdm1a* under the *ROSA26* promoter in a doxycycline (Dox)-inducible manner (*iKdm1a^{KD}*). These mice were crossbred with *Eµ-TCL1A* mice to get *iKdm1a^{KD};Eµ-TCL1A* mice, which were treated with Dox to induce whole-organismal *Kdm1a* knockdown in murine CLL (**Figure 32**).
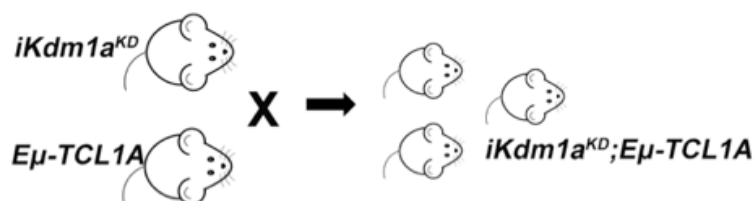
Figure 32. Establishment of the inducible *Kdm1a* knockdown CLL mouse model. Inducible *Kdm1a* knockdown mice (*iKdm1a^{KD}*) were crossbred with *Eµ-TCL1A* mice to achieve *Kdm1a* knockdown in *Eµ-TCL1A* mice in a Dox-inducible manner (*iKdm1a^{KD};Eµ-TCL1A*).

3.3.1 Knockdown of *Kdm1a* reduces tumor burden in a CLL mouse model

For the validation of the model, *iKdm1a^{KD};Eµ-TCL1A* leukemic mice and *Eµ-TCL1A* control mice were treated with Dox-containing food (1 mg Dox/kg food) for short term (shorter than 2 weeks) or long term (longer than 4 weeks) to induce the knockdown of *Kdm1a* (*iKdm1a^{KD}*) in murine CLL. To confirm the depletion of *Kdm1a* in *iKdm1a^{KD};Eµ-TCL1A* mice, peripheral blood leukocytes, splenic mononuclear cells, and bone marrow leukocytes were isolated from these Dox-exposed *iKdm1a^{KD};Eµ-TCL1A* and *Eµ-TCL1A* control animals. qRT-PCR analysis demonstrated that Dox-food for both short and long-term treatment efficiently knocked down *Kdm1a* in peripheral blood leukocytes, splenic mononuclear cells, and bone marrow leukocytes (all $P<0.05$, **Figure 33**).

To dissect the role of the induced Kdm1a knockdown on CLL pathogenesis, we treated leukemic *iKdm1a^{KD};Eµ-TCL1A* and *Eµ-TCL1A* with Dox-containing food. To determine the time of Dox application, a blood test was performed every week to monitor the disease progression. Dox-food was applied when WBC counts reached $50x10^3$ /µL. Interestingly, the WBC counts of *iKdm1a^{KD};Eµ-TCL1A* mice remained relatively stable, whereas in contrast, *Eµ-TCL1A* mice showed strongly increasing WBC and died from leukemia within 8 weeks ($P=0.01$, **Figure 34A**). In addition, *iKdm1a^{KD};Eµ-TCL1A* mice also presented significantly lower levels of CD19+CD5+ leukemic cells after Dox-induced *Kdm1a*-KD ($P=0.013$, **Figure 34B**). PB platelet counts dropped in *iKdm1a^{KD};Eµ-TCL1A* mice confirming previous observations in *iKdm1a^{KD}*

mice (**Figure 35A**),[230] while there were no significant differences in erythroid PB parameters upon Dox-exposure between *Eµ-TCL1A* and *iKdm1a^KD;Eµ-TCL1A* leukemic mice (**Figure 35B**).

Dox-exposed *iKdm1a^KD;Eµ-TCL1A* mice showed a significant reduction of CLL-cell content of suspended spleens and bone marrow as compared to *Eµ-TCL1A* animals (all P<0.05, **Figure 36A**). Quantification of cell infiltration in the spleen by immunofluorescent staining followed by data processing with StrataQuest demonstrated a decreased intensity of KDM1A and infiltration of B cells in *iKdm1a^KD;Eµ-TCL1A* mice (**Figure 36B**), supporting that *Kdm1a* depletion reduces tumor burden in the spleen. Still, both models developed splenomegaly to a similar extent (**Figure 37**). This might be due to splenic stress erythropoiesis in *iKdm1a^KD* mice (**Figure 38**) as reported before.[230] Furthermore, immunostaining of Ki-67 and B220 revealed less proliferating B cells in spleens of *iKdm1a^KD;Eµ-TCL1A* mice (**Figure 39**). An increased population of apoptotic CLL cells in the spleen was detected in *iKdm1a^KD;Eµ-TCL1A* mice (**Figure 40**). Strikingly, leukemic *iKdm1a^KD;Eµ-TCL1A* mice showed a significantly longer overall survival as compared to *Eµ-TCL1A* animals (median 67 days vs. 39 days, P=0.018, **Figure 41**).

Collectively, systematical knockdown of *Kdm1a* in *Eµ-TCL1A* leukemic mice reduced tumor cells in peripheral blood, spleen, and bone marrow, via leukemic cell death, which translated into increased animal survival. These findings implicate the therapeutic potential of targeting KDM1A in CLL.
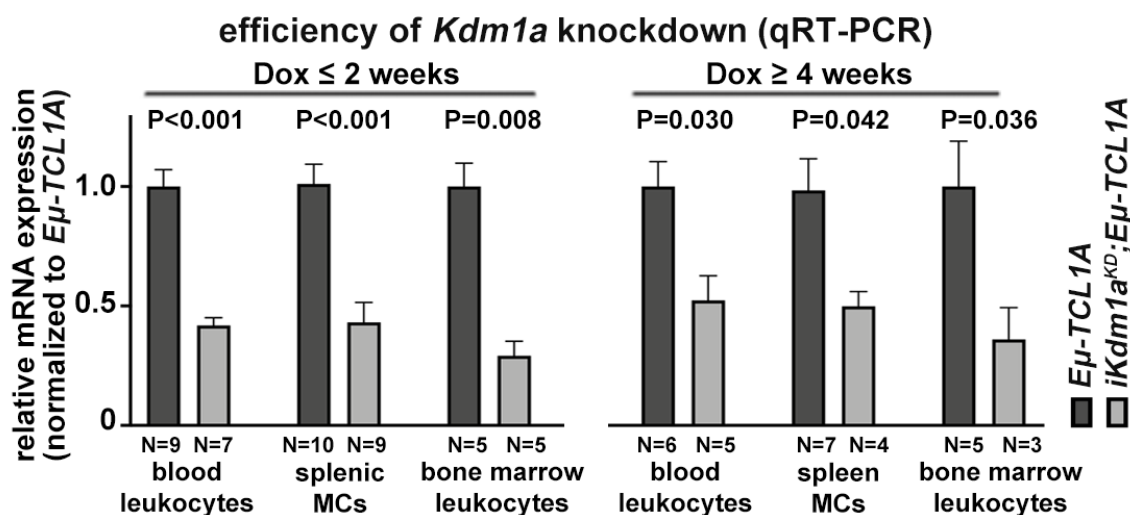

Figure 33. The mRNA expression of *Kdm1a* in leukemic mice under Dox treatment analyzed by qRT-PCR. In vivo *Kdm1a* knockdown was achieved in peripheral blood leukocytes, splenic mononuclear cells (MCs), and bone marrow leukocytes by daily Dox application via the food (1g Dox / kg food) for short term (≤ 2 weeks, left) or long term (≥ 4 weeks, right). Mean±SEM, Mann-Whitney test.
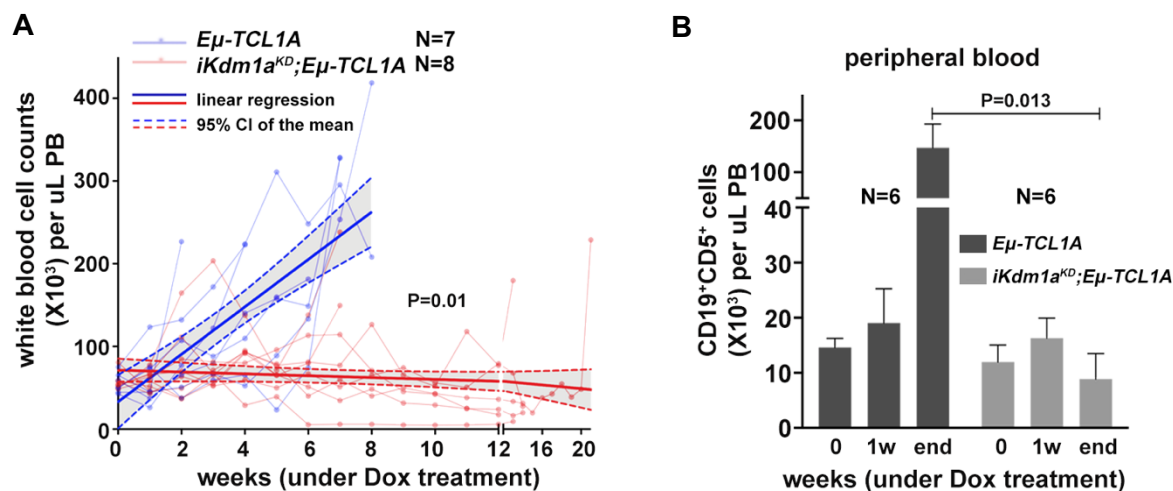
Figure 34. The knockdown of *Kdm1a* reduces the CLL burden in peripheral blood. *Eμ-TCL1A* and *iKdm1a^KD;Eμ-TCL1A* leukemic mice were treated with Dox food when WBC counts were ≥ 50x10^3 /μL. (A) *iKdm1a^KD;Eμ-TCL1A* leukemic mice (N=8) showed a significantly lower WBC count in comparison to *Eμ-TCL1A* (N=7) under Dox treatment. A two-way ANOVA test was used to assess the statistical significance. (B) The WBC count and flow cytometric analysis of peripheral blood showed a decrease in the total number of leukemic CD19+CD5+ B cells. "end": the endpoint defined by internationally endorsed principles. Mean±SEM, Mann-Whitney test.
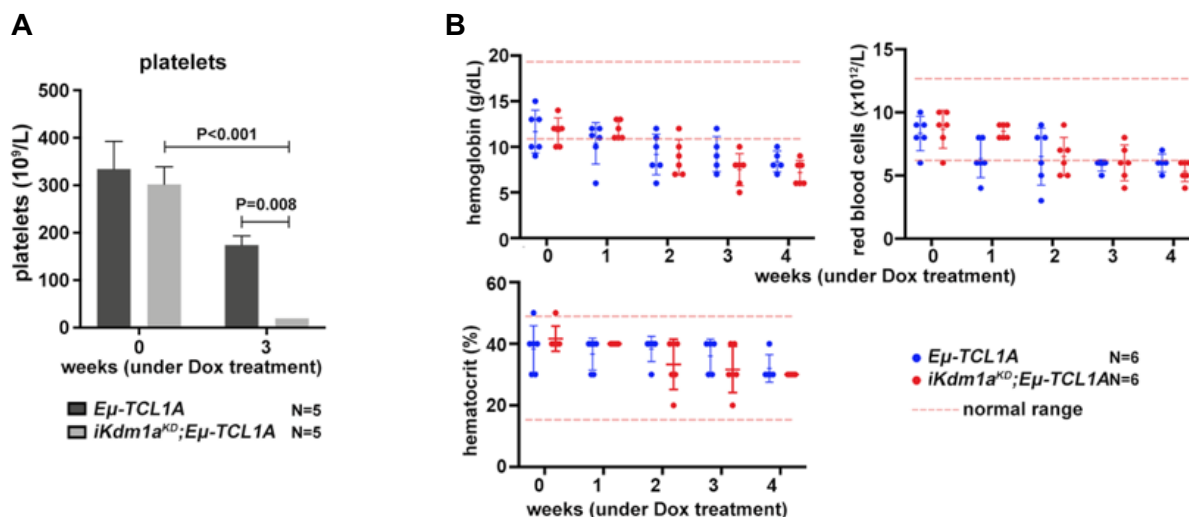
Figure 35. The effect of *Kdm1a* knockdown on other blood cell counts. (A) *Kdm1a* knockdown significantly reduced platelet count in peripheral blood compared with *Eμ-TCL1A* control mice. N=5 of each group, Mean±SEM, Mann-Whitney test. (B) Peripheral blood erythroid parameters. No significant difference was found in hemoglobin, red blood cell count, and hematocrit between *Eμ-TCL1A* (blue) and *iKdm1a^KD;Eμ-TCL1A* (red) under Dox treatment.
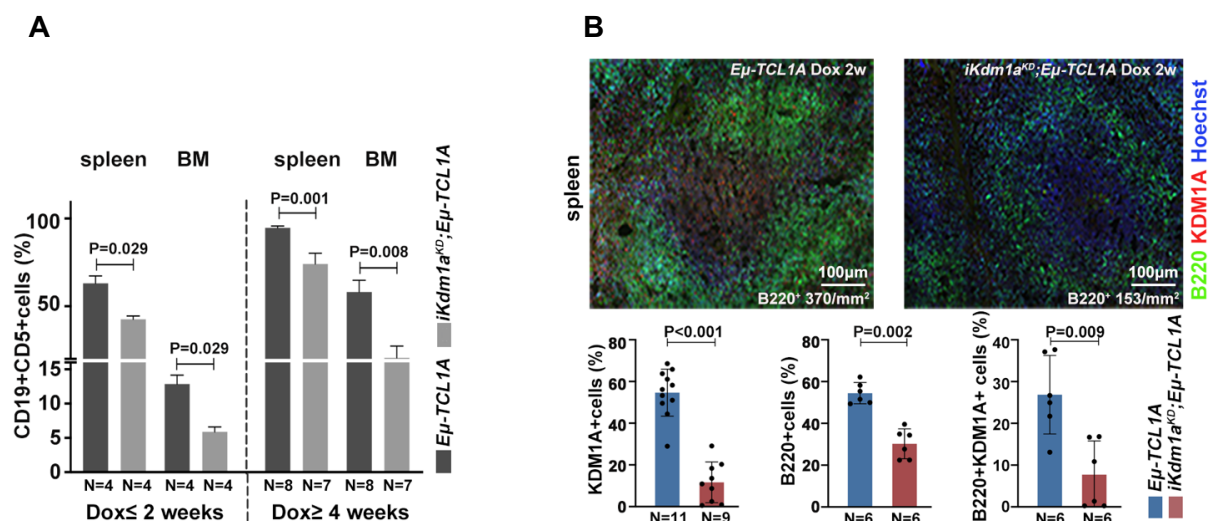
Figure 36. Kdm1a knockdown reduces the CLL burden in spleen and bone marrow. (A) Flow cytometric analyses of splenocytes and bone marrow samples demonstrate a reduced percentage of CD19+CD5+ leukemic B cells in *iKdm1a^{KD};Eμ-TCL1A* mice under short term (≤ 2 weeks, left) or long term (≥ 4 weeks, right) Dox treatment. Mean±SEM, Mann-Whitney test. (B) Top: Representative images of immunofluorescent B220/KDM1A/Hoechst staining of spleen sections from *Eμ-TCL1A* and *iKdm1a^{KD};Eμ-TCL1A* mice under Dox treatment for 2 weeks (B220 green, KDM1A red, Hoechst blue). Immunofluorescent images were taken at 60x magnification using an IX83 fluorescent invert microscope. Bottom: Quantification of B220/KDM1A signal of spleen sections by StrataQuest confirmed the decreased signal of KDM1A and identified a reduced percentage of B220+ B cells in the spleen. Mean±SD, Mann-Whitney test.
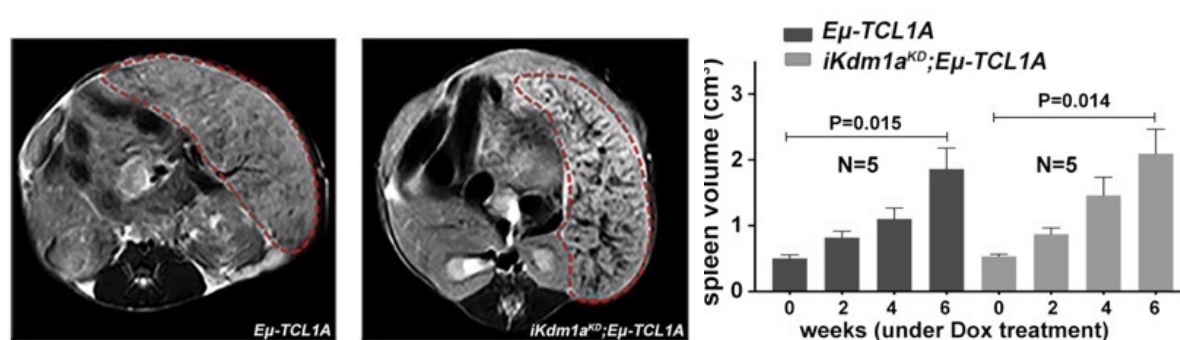

Figure 37. MRI scanning and volumetric analysis of spleens. (A) Representative MRI images of mice abdomen, with red dashed line indicating the enlarged spleens of *Eμ-TCL1A* and *iKdm1a^{KD};Eμ-TCL1A* mice treated with Dox for 6 weeks. (B) The bar chart displays the volume of spleens before and under Dox treatment at 2, 4, and 6 weeks. N=5 of each group, Mean±SEM, Student's t-test.
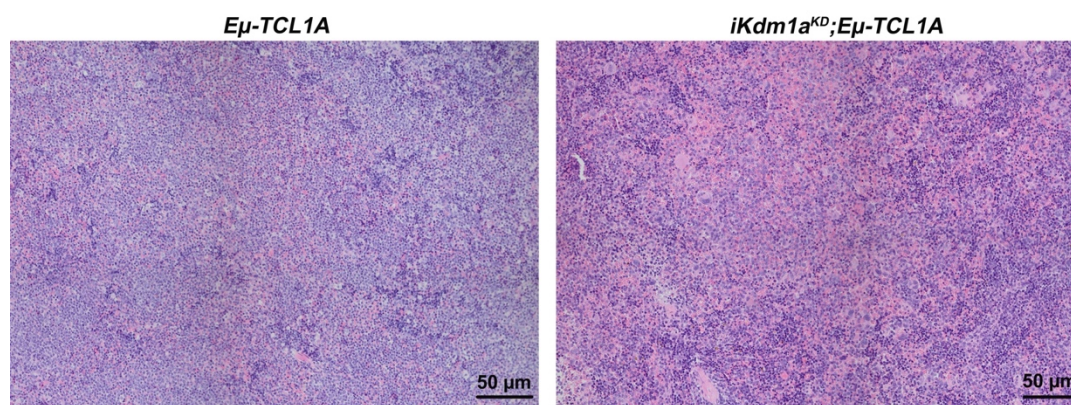
Figure 38. Splenic stress erythropoiesis in *Kdm1a* knockdown mice. Representative Hematoxylin and Eosin staining of splenic sections showing prominent expansion of the red pulp in *iKdm1a^{KD};Eµ-TCL1A* (right) vs. *Eµ-TCL1A* (left) mice. Scale bar is 50 µm.
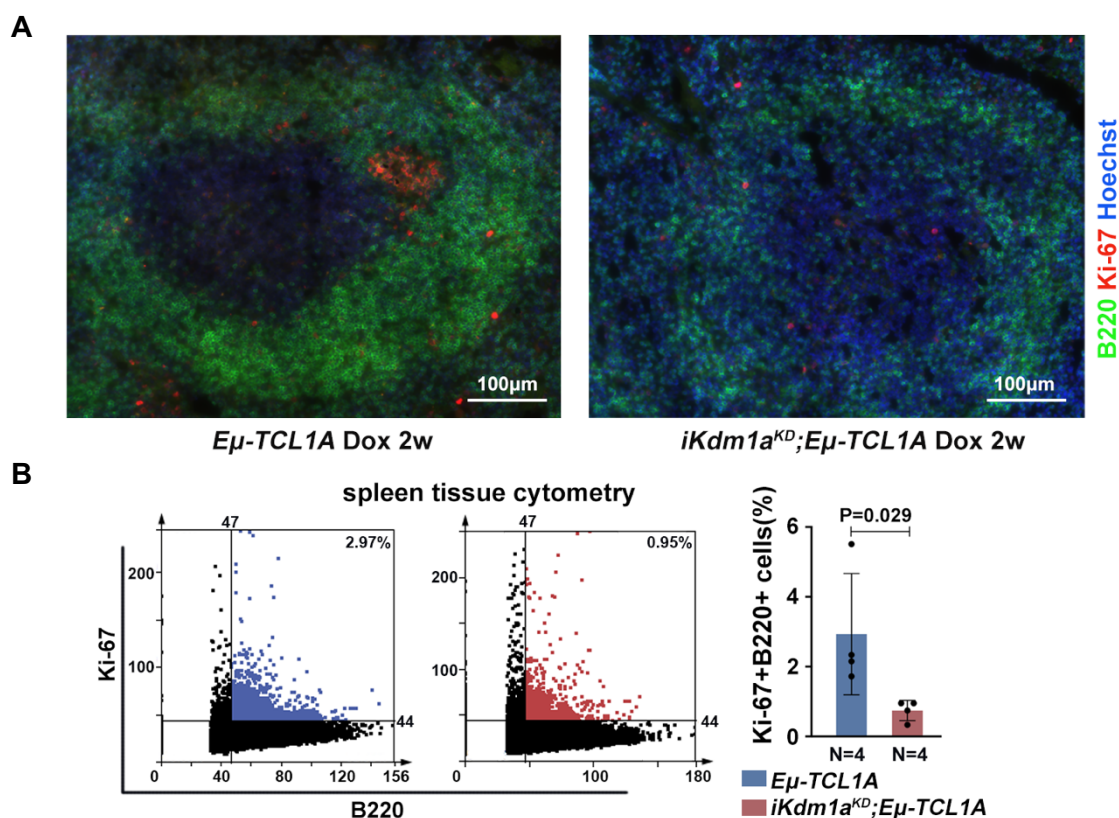

Figure 39. *Kdm1a* knockdown leads to a reduced proliferation rate in splenic B cells. (A) Representative images of Ki-67 (red) / B220 (green) immunofluorescent staining in spleens sections. Slides with immunofluorescent staining were scanned at 60x magnification using an IX83 fluorescent invert microscope. (B) Tissue cytometer analysis of B220/Ki-67 immunofluorescent signals of spleen sections by StrataQuest. Left: Representative tissue cytometry plots showing Ki-67+B220+ B cells in spleens (*Eµ-TCL1A* blue, *iKdm1a^{KD};Eµ-TCL1A* red). Right: Quantified signal implicates decreased Ki-67 expression in B cells in spleens *iKdm1a^{KD};Eµ-TCL1A* mice. N=4 of each group, Mean±SD, Mann-Whitney test.
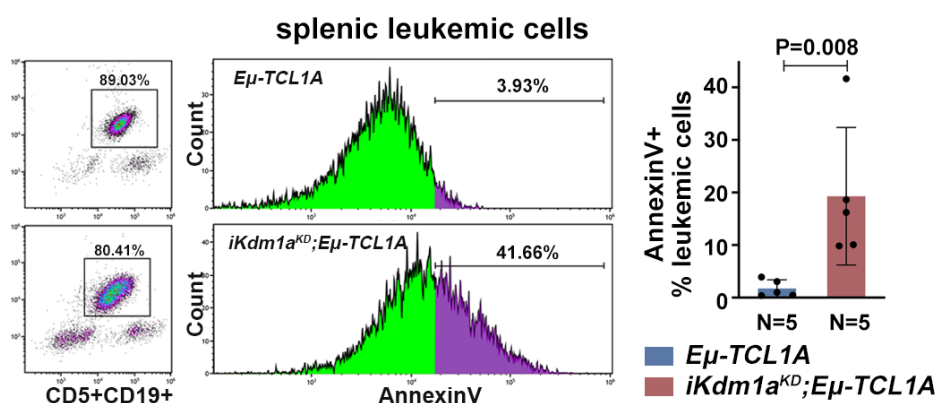
Figure 40. *Kdm1a* knockdown results in an increased apoptotic rate in splenic leukemic B cells. Left: Flow cytometric analysis of apoptotic B cells in spleens using Annexin V staining. Representative density plots and histograms show a smaller population of CD19+CD5+ leukemic B cells and an increase of apoptotic leukemic cells in *iKdm1a^{KD};Eμ-TCL1A* mice after 2 weeks of Dox treatment. Right: Bar chart demonstrating an increased percentage of apoptotic CD19+CD5+ leukemic B cells in spleens from *iKdm1a^{KD};Eμ-TCL1A* mice. N=5 of each group, Mean±SD, Mann-Whitney test.
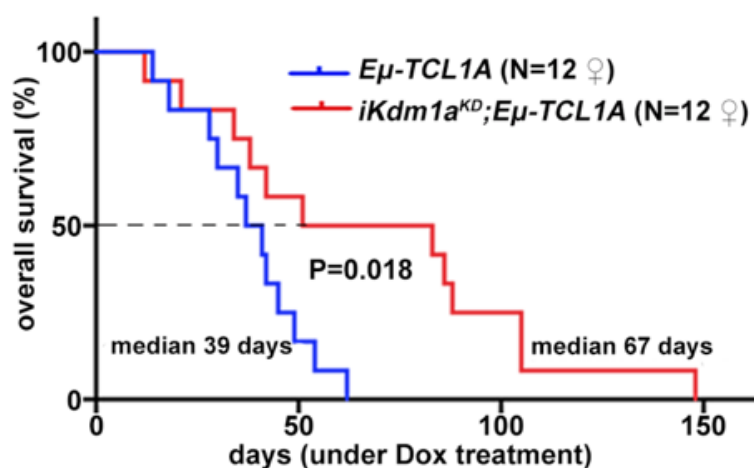

Figure 41. *Kdm1a* knockdown in murine CLL is associated with a better animal survival. Kaplan-Meier survival curve of *Eμ-TCL1A* (N=12, female, blue) and *iKdm1a^{KD};Eμ-TCL1A* (N=12, female, red) leukemic mice under Dox treatment. Log-rank (Mantel-Cox) test was used to assess statistical significance.

3.3.2   Targeting *KDM1A* in the micromilieu impairs survival support for CLL cells

CLL cell sustenance and leukemic progression are maintained by vital interactions with elements of the microenvironment, such as T cells,[250] macrophages,[251] or stromal cells.[250] The animal model of systemic *Kdm1a*-KD allows to address the role of KDM1A in non-CLL cells and to draw parallels to the whole-organismal effects of its pharmacologic targeting. KDM1A inhibition has been shown to influence non-tumor cell compartments, like CD8+ T cells,

mediating their infiltration and re-invigoration at the tumor site in Breast cancer.[252,253] Moreover, KDM1A was shown to promote myeloid differentiation.[211,254] In our model, we could observe a reduction of CD3+ T-cell numbers in the blood (4 weeks Dox-exposure, P=0.028) and spleens (at the endpoint, P=0.032) of *iKdm1a^(KD);Eµ-TCL1A* mice vs. *Eµ-TCL1A* animals (**Figure 42A**), with a reversed ratio of CD4+/CD8+ T cells that was skewed in *Eµ-TCL1A* leukemic mice (**Figure 42B**). Immunostaining of spleen sections demonstrated a decreased infiltration of CD3+ T cells in the germinal center in *iKdm1a^(KD);Eµ-TCL1A* mice (**Figure 42C-D**). In addition, an increased percentage of CD11b+F4/80+ monocytes/macrophages was present in PB and spleens of Dox-exposed *iKdm1a^(KD);Eµ-TCL1A* mice (**Figure 43A-B**). There were no significant differences in splenic Vimentin+ fibroblast counts between both models, despite decreased Kdm1a protein levels in *iKdm1a^(KD);Eµ-TCL1A* fibroblasts (**Figure 44**).

To corroborate the conclusion that the anti-leukemic impact of a *Kdm1a*-KD originates from combined effects on leukemic cells and milieu components, we employed reciprocal co-culture systems. Primary murine CLL cells were co-cultured with primary murine BM stromal cells (BMSCs) for 48 hours supplemented with 10 µg/L of recombinant mouse IL-15 and 0.25 µM of CpG. Both cell types were isolated from Dox-exposed *iKdm1a^(KD);Eµ-TCL1A* and *Eµ-TCL1A* leukemic animals. We observed a decreased viability of co-cultured primary murine CLL cells upon *Kdm1a*-KD (i) in murine BMSCs, (ii) in the leukemic cells, or (iii) in both compartments as compared to *Eµ-TCL1A* leukemic cells co-cultured with *Kdm1a* wild-type (*Kdm1a^(WT)*) BMSCs (**Figure 45**).

Next, we sought to verify these findings in a human in vitro system by co-culture of human CLL cells together with HS-5 fibroblastic cells or differentiated THP-1 macrophages. For this, we transfected a vector containing Dox-inducible shRNAs against *KDM1A* into HS-5 and THP-1 cells. *KDM1A* knockdown was induced in HS-5 stromal cells by Dox treatment for seven days, which was confirmed by immunoblotting (**Figure 46A**). Although no difference in cell number or viability of HS-5 cells was observed upon *KDM1A* knockdown (**Figure 46B**), there was a reduced potency of *KDM1A*-KD stromal cells to support the survival of CLL cells in vitro (**Figure 46C, Table 12**). *KDM1A*-KD in THP-1 monocytes was achieved by treatment with Dox for five days and was also confirmed by immunoblotting (**Figure 47A**). Interestingly, *KDM1A-KD* led to a decreased proliferation of THP-1 monocytes (**Figure 47B**) and a decreased ability of differentiated THP-1 macrophages to induce proliferation in CLL cells, as determined by Ki-67+ staining (**Figure 47C, Table 13**).

Together, these findings suggest a pro-leukemic relevance of KDM1A in CLL via its effects in supporting cells of the micromilieu in addition to tumor-cell intrinsic mechanisms.
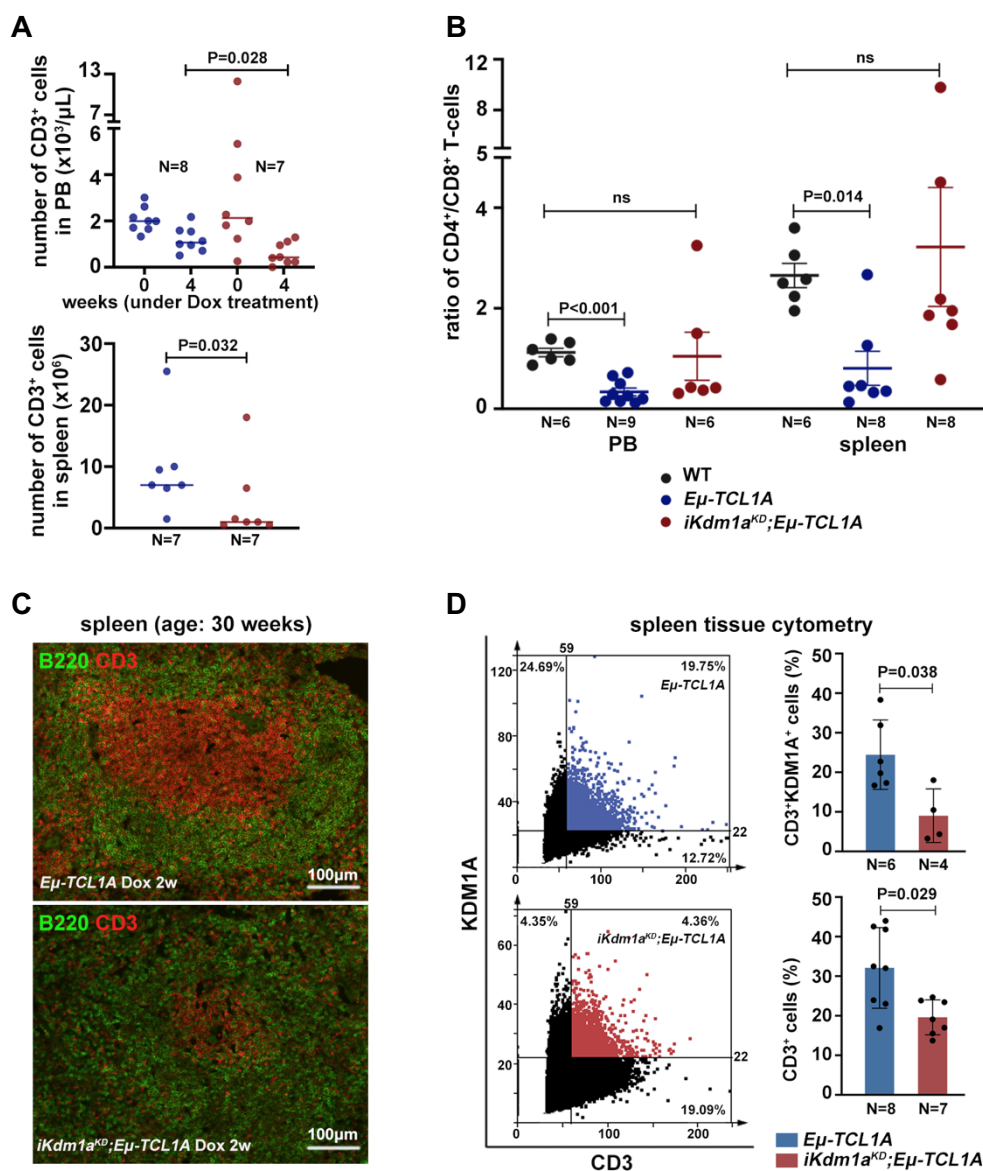
Figure 42. The effect of *Kdm1a* knockdown on the T-cell compartment. *Eµ-TCL1A* mice and *iKdm1a^KD;Eµ-TCL1A* mice were treated with Dox-food when WBC counts were ≥50x10³ /µL (A, B) or ≥30x10³ /µL (C, D). (A) *iKdm1a^KD;Eµ-TCL1A* mice show a reduced absolute number of CD3+ T cells in peripheral blood (upper) and spleen (lower). Mann-Whitney test. (B) Flow cytometric analyses revealed a significantly reduced ratio of CD4+/CD8+ T cells in PB and spleen in *Eµ-TCL1A* leukemic mice, but not in *iKdm1a^KD;Eµ-TCL1A* mice. (C) Representative images of immunofluorescent B220/CD3 staining showing a reduced density of CD3+ T cells in the germinal center of spleens from *iKdm1a^KD;Eµ-TCL1A* mice. (D) Tissue cytometer analysis of B220/CD3 immunofluorescent staining of spleen sections by StrataQuest. Left: Representative tissue cytometry plots of CD3 and KDM1A staining. Right: Quantification of CD3/KDM1A signal demonstrating a decreased CD3+ T-cell infiltration in the spleen of *iKdm1a^KD;Eµ-TCL1A* mice. Mann-Whitney test.
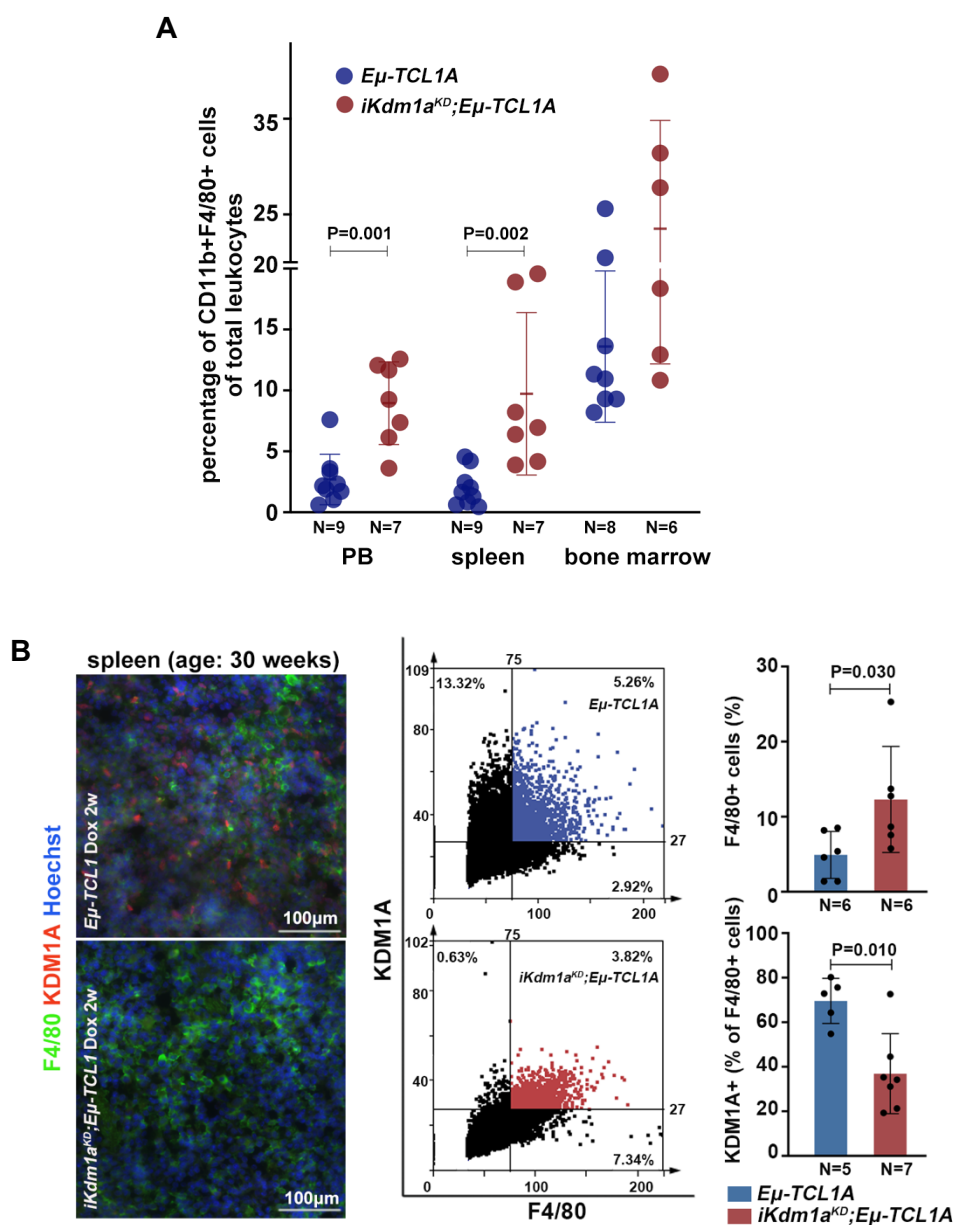
Figure 43. *Kdm1a* **knockdown leads to an increase of macrophages in blood and spleen.** *Eµ-TCL1A* mice and *iKdm1a[KD];Eµ-TCL1A* mice were treated with Dox-food when WBC counts were ≥50x10^3/µL (A) or ≥30x10^3/µL (B). (A) Flow cytometric staining of CD11b+F4/80+ showed a significantly higher percentage of macrophages in the blood and spleen of *iKdm1a[KD];Eµ-TCL1A*. Mann-Whitney test. (B) Left: Representative immunofluorescent staining of F4/80/KDM1A in spleen sections after 2 weeks of Dox treatment. Middle: Representative tissue cytometry plots of F4/80/KDM1A signal. Right: Quantification of F4/80/KDM1A signal displaying an increase of F4/80+ macrophages and decreased KDM1A signal in macrophages in *iKdm1a[KD];Eµ-TCL1A* mice. Mann-Whitney test.
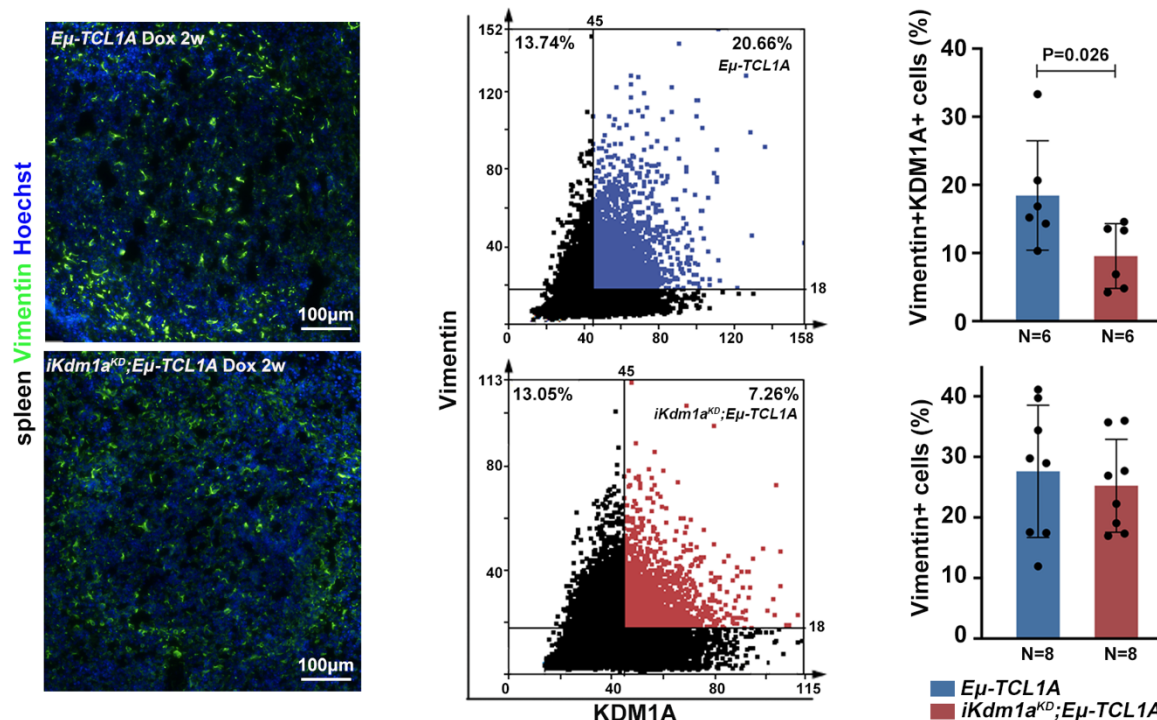
Figure 44. *Kdm1a* knockdown does not influence splenic fibroblast numbers. Left: Representative immunofluorescent staining of Vimentin in spleen sections. Middle: Representative tissue cytometry plots of Vimentin/KDM1A signal. Right: Quantification of Vimentin/KDM1A signal displaying a decrease of KDM1A signal in Vimentin+ fibroblasts in *iKdm1a^{KD};Eµ-TCL1A* mice (top). No difference in cell number of Vimentin+ fibroblasts between *iKdm1a^{KD};Eµ-TCL1A* and *Eµ-TCL1A* animals (bottom). Mean±SD, Mann-Whitney test.
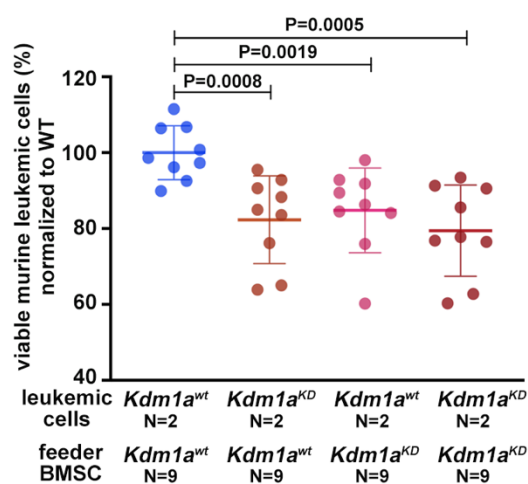

Figure 45. *Kdm1a* knockdown in BMSCs impairs their support on leukemic cells. Murine CLL cells were co-cultured with murine bone marrow stromal cells in the presence of CpG and IL-15 for 48 hours. Flow cytometric analysis using Annexin V staining demonstrates lower cell viability of *iKdm1a^{KD};Eµ-TCL1A* leukemic cells co-cultured with *Eµ-TCL1A* or *iKdm1a^{KD};Eµ-TCL1A* BMSCs and of *Eµ-TCL1A* leukemic cells co-cultured with *iKdm1a^{KD};Eµ-TCL1A* BMSCs, compared to *Eµ-TCL1A* leukemic cells co-cultured with *Eµ-TCL1A* BMSCs. Mann-Whitney test.
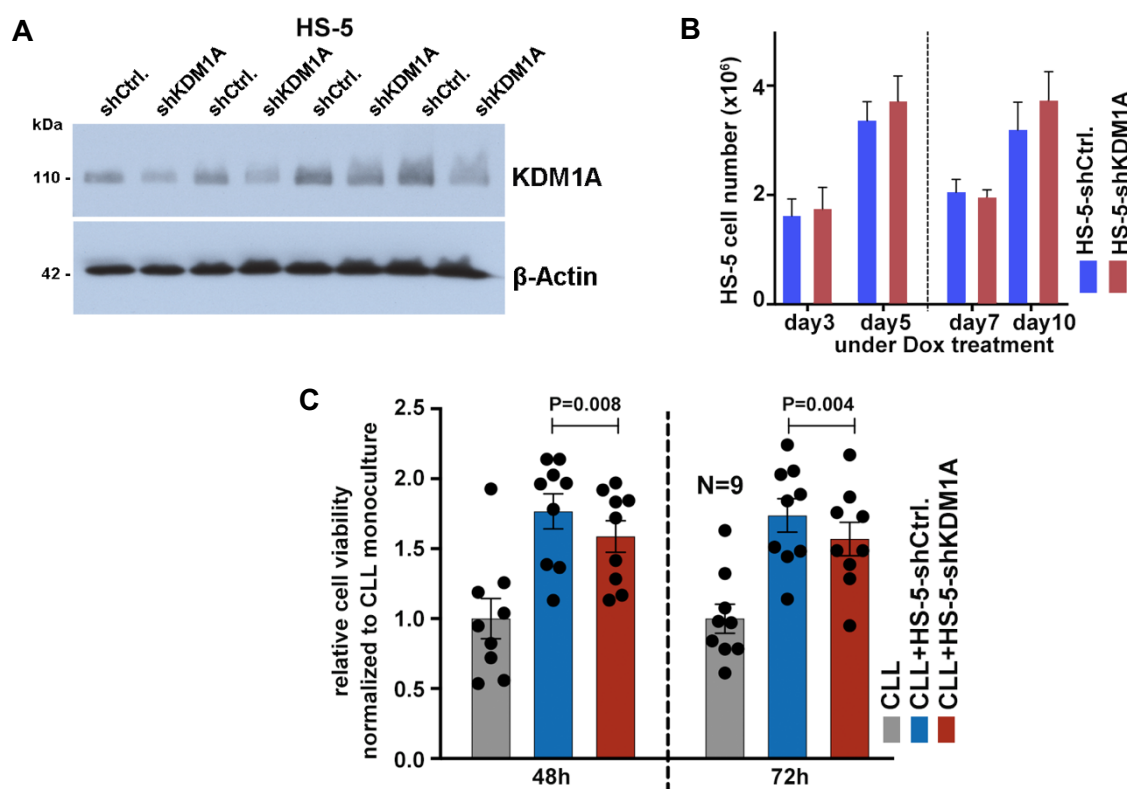
Figure 46. KDM1A knockdown in HS-5 stromal cells impairs their support on CLL cells survival.
(A) Immunoblots showing the efficiency of KDM1A knockdown in the HS-5 cell line. (B) Bar charts showing no significant differences in the cell count of HS-5 cells upon *KDM1A*-KD. (C) Human primary CLL cells were co-cultured with HS-5-shCtrl. or HS-5-shKDM1A stromal cells for 48 hours or 72 hours. Flow cytometric analysis using Annexin V staining demonstrates reduced cell viability of CLL cells co-cultured with HS-5-shKDM1A cells compared to that with HS-5-shCtrl. cells. Mean±SEM, Student's t-test.

Table 12. Patient characteristics of samples used in HS-5 co-culture experiments

Patient ID	Age	Karyotype	ZAP70 (%)	CD38 (%)	IGHV	Binet stage	WBC (x10^9/L)	LDT (months)
CLL18	53	del(13q), t(6;8)			U	B	199	
CLL19	76	del(13q)		pos	U	B	71.2	
CLL20	80				na	B	222	
CLL21	85				U	A	66.3	
CLL22	71		neg		M	A		>12
CLL23	62	Mutation in BIRC3 Gen			M		89.7	
CLL33	80	complex karyotype			M	A		
CLL34	69	isolated 13q14			M	B	69.5	<12
CLL 35	58					A	209.3	

IGHV: *IGHV* mutation status; M: *IGHV* mutated; U: *IGHV* unmuted
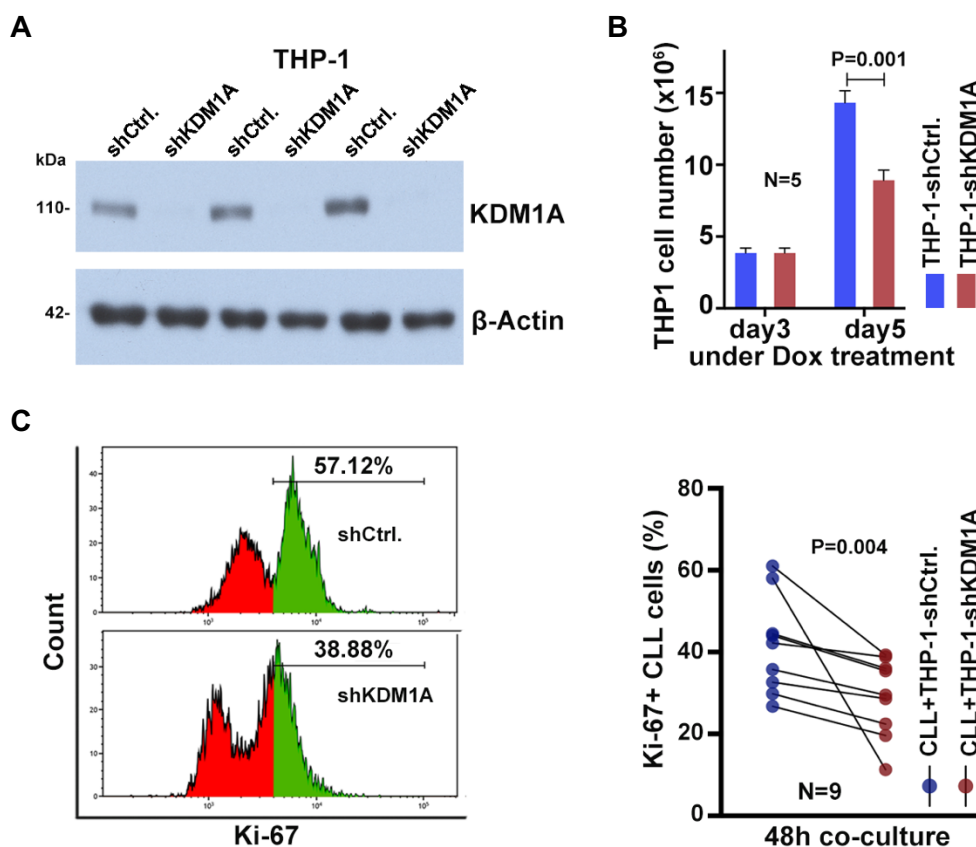
Figure 47. *Kdm1a* knockdown in THP-1 macrophages decreases their ability to induce the proliferation of CLL cells. (A) Immunoblots showing the efficiency of KDM1A knockdown in the THP-1 cell line. (B) THP-1 cells with KDM1A knockdown show a significantly lower cell count after five days of culturing compared to the control cell line. Mean±SEM, Mann-Whitney test. (C) Left: Representative flow cytometric histogram of Ki-67 expression in primary CLL cells, co-cultured for 48 hours with differentiated THP-1-shCtrl. or THP-1-shKDM1A cells supplemented with CpG and IL-15. Right: Ki-67 levels of CLL cells co-cultured with differentiated THP-1-shCtrl. or THP-1-shKDM1A cells. Knockdown of KDM1A in THP-1 cells reduces the percentage of proliferating CLL B cells. CLL N=9, the black lines connect the same patient samples cultured with different THP-1 cells. Student's t-test.

Table 13. Patient characteristics of samples used in THP-1 co-culture experiments

Patient ID	Age	Karyotype	ZAP70 (%)	CD38 (%)	IGHV	Binet stage	WBC (x10^9/L)	LDT (months)
CLL12	78	del(13q)	neg		M	A	253.7	>12
CLL15	54				U	B	435.1	
CLL17	61	del(13q)			U	A	133.5	<12
CLL18	53	del(13q), t(6;8)			U	B	199	
CLL19	76	del(13q)		pos	U	B	71.2	
CLL20	80				na	B	222	
CLL21	85				U	A	66.3	
CLL22	71		neg		M	A		>12
CLL23	62	mutation in BIRC3 gene			M		89.7	

IGHV: *IGHV* mutation status; M: *IGHV* mutated; U: *IGHV* unmuted

3.3.3 Depletion of *Kdm1a* in murine CLL implicates its role as a transcriptional repressor

To assess changes in gene expression caused by *Kdm1a* knockdown, we performed RNA-sequencing of splenic mononuclear cells (mean purity 70% B cells) from Dox-exposed leukemic *Eµ-TCL1A* vs. *iKdm1a^{KD};Eµ-TCL1A* mice. Principle component analysis (PCA) of gene expression levels shows separate clustering of the two genotypes (**Figure 48A**). We have identified 1013 genes to be differentially expressed between the two genotypes. 81% of the differentially expressed genes (DEGs) were upregulated in *iKdm1a^{KD};Eµ-TCL1A* cells (fold change>1.5, q≤0.01, **Figure 48B**), suggesting that *Kdm1a* suppresses global transcriptional activity in murine CLL. In line with our previous data, that *Kdm1a* knockdown induces apoptosis in leukemic B cells (**Figure 40**), programmed cell death genes were overrepresented in *iKdm1a^{KD};Eµ-TCL1A* cells, identified by KEGG pathway analysis and gene-set enrichment analysis (GSEA, Hallmark gene sets, **Figure 49A-B**). Pro-apoptotic molecules that were upregulated involved *Casp3*, *Cdk6*, *Mapk9*, and *Gadd45g* (**Figure 49C**). Additionally, we have identified differentially expressed genes involved in cell adhesion and migration (**Figure 50A**), like *Intgb2l*, *rapgef3*, and *Cxcr4*, all downregulated in splenic mononuclear cells and peripheral blood leukocytes of Dox-exposed *iKdm1a^{KD};Eµ-TCL1A* mice (**Figure 50B**).
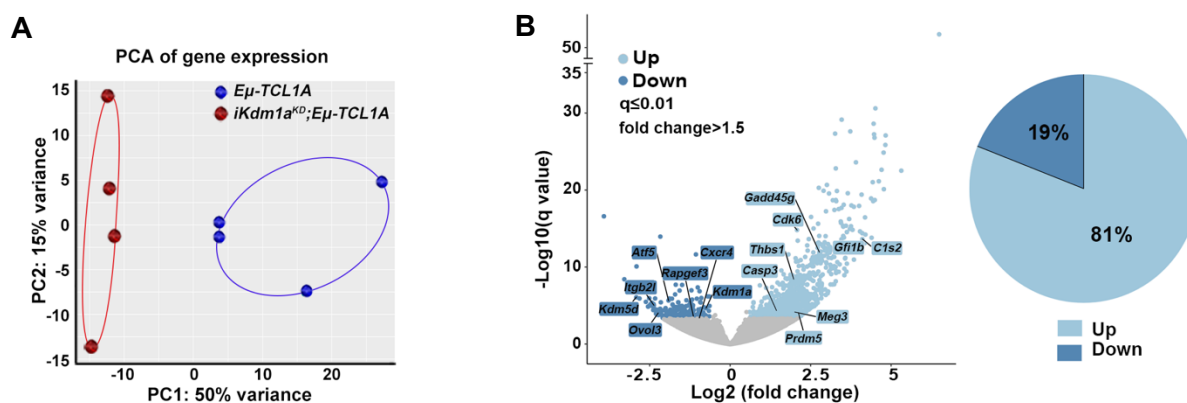

Figure 48. *Kdm1a* acts as a gene repressor in *Eµ-TCL1A* mice. *Eµ-TCL1A* and *iKdm1a^{KD};Eµ-TCL1A* leukemic mice were treated with Dox for 2 weeks. Gene expression of splenocytes from leukemic mice (>70% B cells content) was analyzed by RNA sequencing (RNA-seq) using Illumina TruSeq stranded (NEB) protocol. **(**A) Principal component analysis (PCA) of RNA-seq data displaying distinct groups by genotype. Each data point represents one mouse. (B) Left: Volcano plot showing differential gene expression between *Eµ-TCL1A* and *iKdm1a^{KD};Eµ-TCL1A* mice (light blue: upregulated in *iKdm1a^{KD};Eµ-TCL1A*, dark blue: downregulated in *iKdm1a^{KD};Eµ-TCL1A*). Right: Pie chart displaying the percentage of up or down-regulated genes. 1013 out of 30262 genes are differentially expressed between *Eµ-TCL1A* and *iKdm1a^{KD};Eµ-TCL1A* mice, fold change>1.5, q≤0.01, with most of these being upregulated in *iKdm1a^{KD};Eµ-TCL1A*.
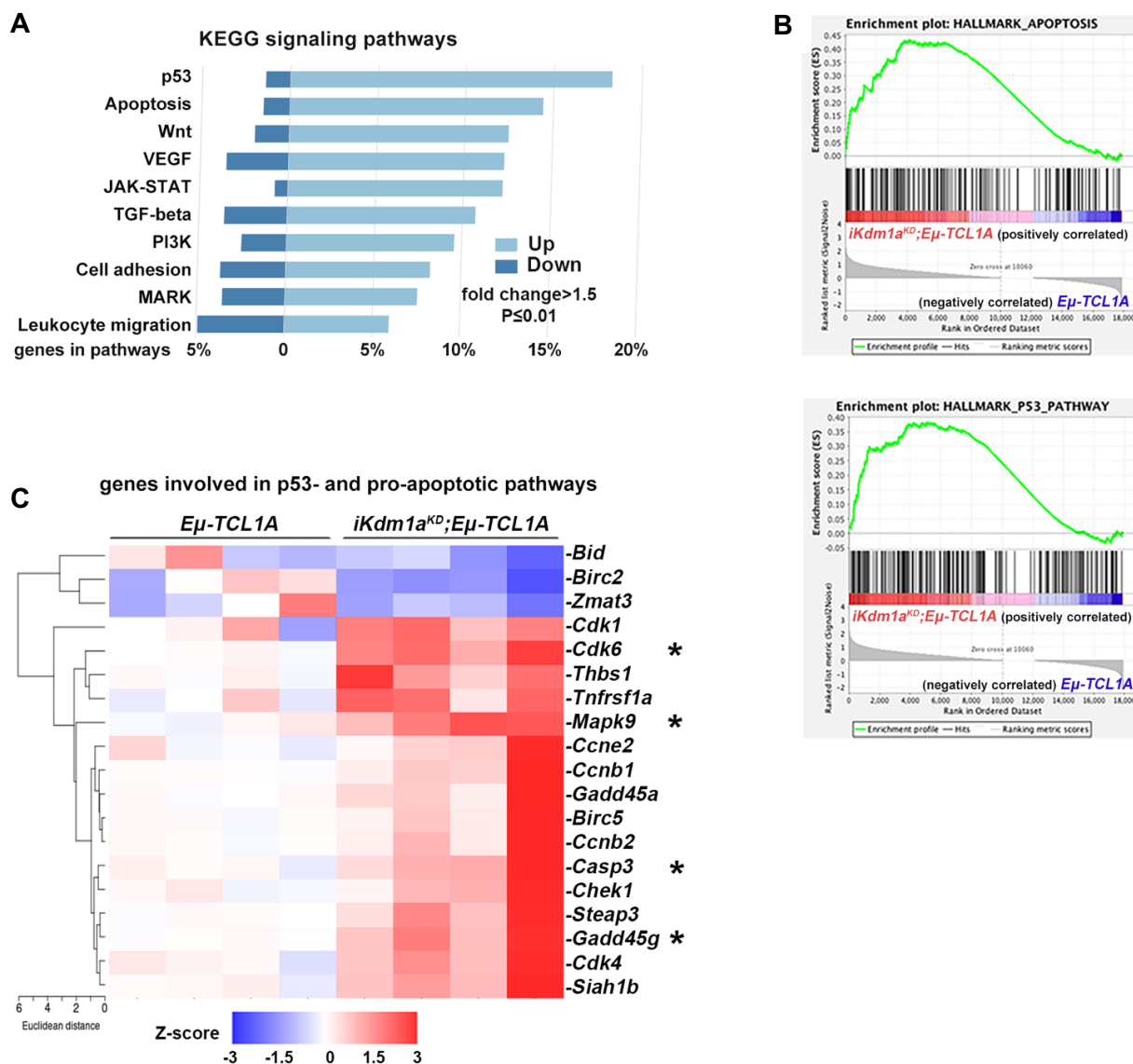
Figure 49. ***Kdm1a* knockdown leads to an upregulation of p53 and pro-apoptotic pathways.** (A) GSEA of differentially expressed genes between *Eμ-TCL1A* and *iKdm1a^KD;Eμ-TCL1A* splenic lymphocytes*. The bars represent the percentage of genes from the data set that mapped to the corresponding KEGG pathway. Light blue: upregulated genes and dark blue: downregulated genes in *iKdm1a^KD;Eμ-TCL1A.* Fold change≥1.5, P≤0.01. (B) Enrichment plots of GSEA of apoptosis (top) and p53 (bottom) pathways. (C) Heatmap of genes differentially expressed between *Eμ-TCL1A* and *iKdm1a^KD;Eμ-TCL1A* mice involved in p53 and pro-apoptotic pathways. * Pro-apoptotic markers that are upregulated in splenic mononuclear cells of *iKdm1a^KD;Eμ-TCL1A* mice.
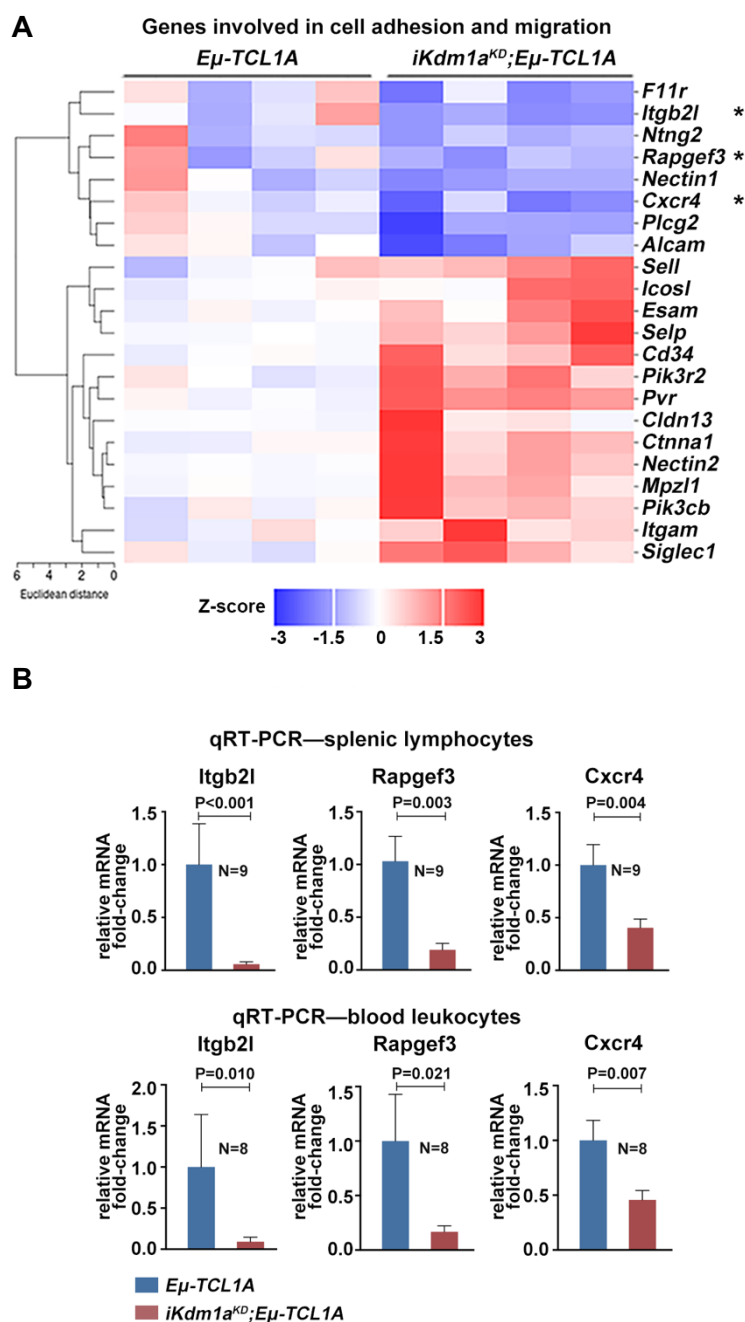
Figure 50. The knockdown of *Kdm1a* results in a downregulation of molecules involved in cell adhesion and migration. (A) Heatmap of differentially expressed genes involved in the cell adhesion and migration pathways. * Molecules involved in cell adhesion and migration that are downregulated in splenic mononuclear cells of *iKdm1a^KD^;Eµ-TCL1A* mice. (B) qRT-PCR analysis validating the reduced expression of Intgb2l, Rapgef3, and Cxcr4 in splenic lymphocytes and peripheral blood leukocytes of *iKdm1a^KD^;Eµ-TCL1A* mice. Mean±SEM, Student's t-test.

98

3.3.4 *Kdm1a* knockdown alters the H3K4me3 epigenetic profile in leukemic mice

Because *Kdm1a* knockdown resulted in an upregulation of the majority of the DEGs, we hypothesized that the knockdown of *Kdm1a* might enrich the regulatory elements of these genes with the H3K4 methylation, leading to their activation. To investigate the epigenetic regulation mediated by Kdm1a in murine CLL, we performed H3K4me3 ChIP followed by high throughput sequencing (ChIP-seq) from splenic mononuclear cells (>85% CD19+CD5+ B cells) of leukemic *Eµ-TCL1A* and *iKdm1a^{KD};Eµ-TCL1A* mice treated with Dox for 2 weeks. *Kdm1a* knockdown in splenic mononuclear cells was confirmed by qRT-PCR analysis (**Figure 51**). Overall, we identified 38880 and 40041 enriched regions in *Eµ-TCL1A* and *iKdm1a^{KD};Eµ-TCL1A* splenic lymphocytes, respectively (**Figure 52A**). 5327 of these were specific for *Eµ-TCL1A* and 14824 regions were only enriched in *iKdm1a^{KD};Eµ-TCL1A* (**Figure 52B**). Consistent with the known role of H3K4me3,[255] H3K4me3 was enriched at promoter regions (**Figure 53**). The distribution of enriched H3K4me3 regions at the genome level did not show a significant difference between *Eµ-TCL1A* and *iKdm1a^{KD};Eµ-TCL1A* CLL cells (**Figure 53**), suggesting that the genomic distribution of H3K4me3 might be stable. Nevertheless, there was differential H3K4me3 enrichment with higher occupancies at specific regions in *iKdm1a^{KD};Eµ-TCL1A* cells (**Figure 54**).

When we evaluated TF binding motifs that were enriched at H3K4me3 binding sites in *iKdm1a^{KD};Eµ-TCL1A* cells, we identified three highly enriched motifs. These were associated with Krüppel Like Factor family members KLF3 and KLF1 binding motifs, and Sp2 (**Figure 55**). KLFs are known in regulating proliferation, differentiation, and apoptosis in many tissues.[256] And it has been reported that KLF3 is essential for normal B cell development and for programming of marginal zone B-cell fate.[257,258] Furthermore, KEGG pathway analysis using genes associated with the *iKdm1a^{KD};Eµ-TCL1A*-specific H3K4me3 regions showed, among others, enrichment for gene sets related to apoptosis and chemokine signaling (**Figure 56**). In term overrepresentation analysis (gene ontology consortium, subontology "biological process"), 'regulation of leukocytes' cell-cell adhesion process appeared to be significantly enriched (**Figure 57**). These findings are in line with the data from RNA-seq analysis that *Kdm1a*-KD regulates genes involved in apoptotic and cell migration/adhesion pathways (**Figure 49**).

In addition, a total of 543 genes were both upregulated by *Kdm1a*-KD and associated with H3K4me3 binding sites (**Figure 58A**), of which 19 were TFs (**Figure 58B**). This suggests that the transcriptional effects by *Kdm1a*-KD are also mediated secondarily through H3K4me3-conveyed regulation of TF expression. Fittingly, an increase of H3K4me3 marks in regions surrounding genes upregulated in *iKdm1a^{KD};Eµ-TCL1A* splenocytes was observed (**Figure 59**). Examples include the apoptotic executioners *Casp3* and *Mapk9*, the TFs *Gata1* and *Gfi1b*, and the tumor suppressor *Trim16* (**Figure 60**).

In summary, our data suggest that *Kdm1a* acts as a transcriptional repressor in CLL by modifying H3K4, with pronounced effects on defined cell death and motility genes.
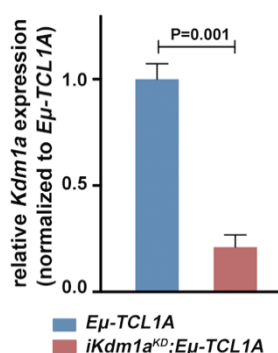

Figure 51. mRNA levels of *Kdm1a* in splenic lymphocytes of mice included in the ChIP experiments. qRT-PCR analysis demonstrating significantly lower *Kdm1a* levels in splenic lymphocytes from *iKdm1a^{KD};Eµ-TCL1A* vs. *Eµ-TCL1A* mice. N=3 of each group. Mean±SEM, Student's t-test.
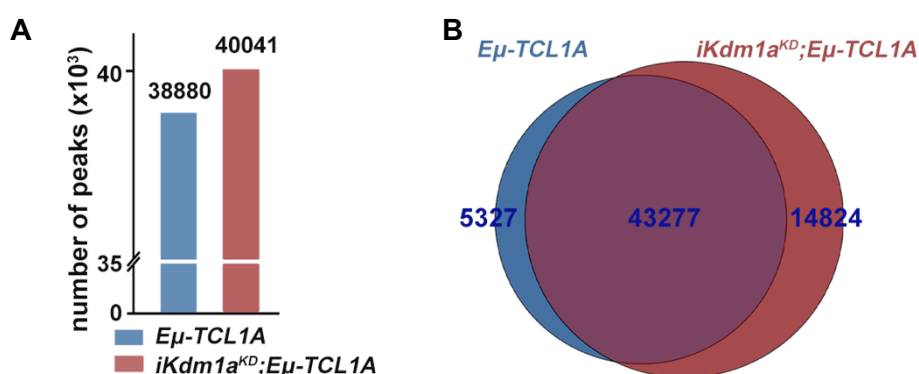
Figure 52. Overview of ChIP-seq data. (A) Bar chart showing the number of peaks in two groups. (B) Venn diagram presenting the number of common and specific peaks between two groups.
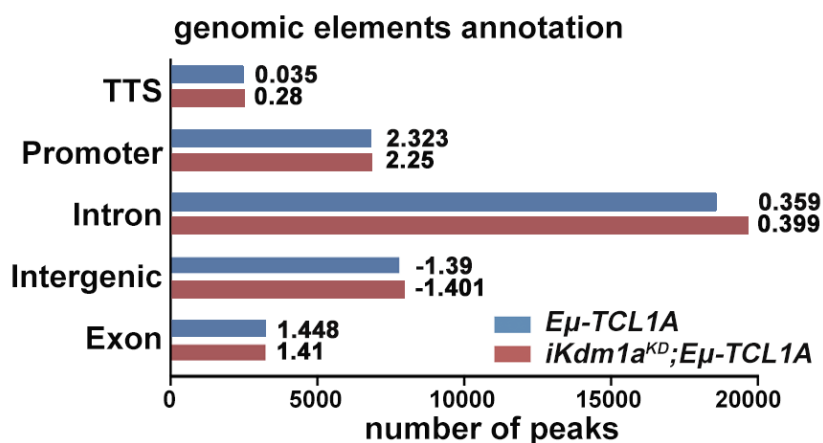
Figure 53. Genomic elements annotation of H3K4me3 peaks. Bar chart displaying the distribution of H3K4me3 regions. Numbers next to bars indicate log2 (observation/expectation) enrichment.
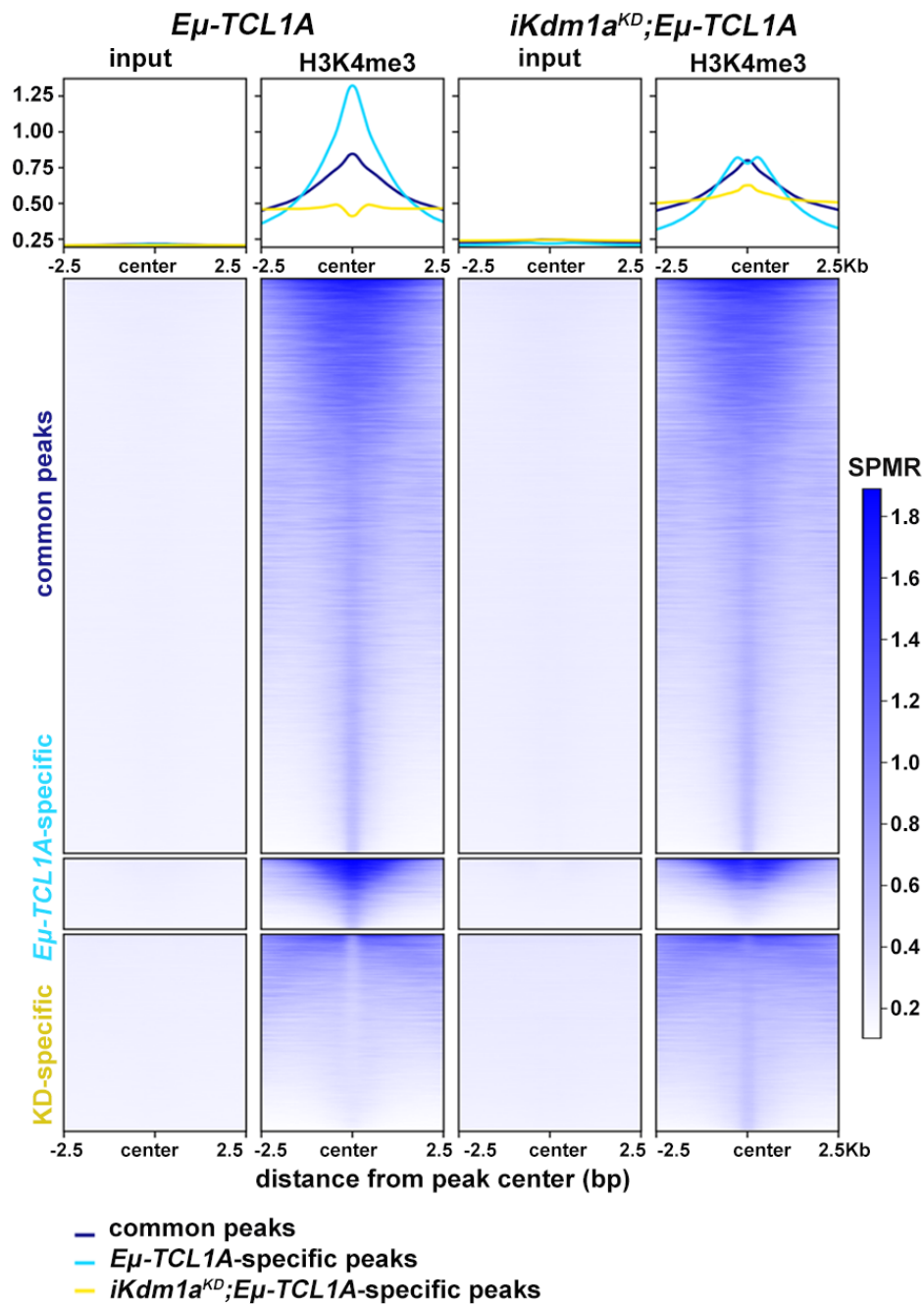
Figure 54. H3K4me3 binding occupancy at common and specific regions. Signal is displayed from -2.5 kb to +2.5 kb surrounding the center of each peak. SPMR: signal per million reads.
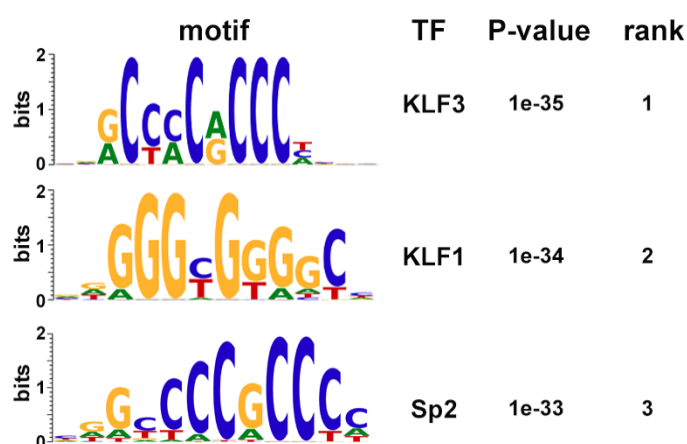
Figure 55. Motif analysis. Top enriched motifs in *iKdm1a^{KD};Eμ-TCL1A*-specific H3K4me3 regions were associated with best matching transcription factor binding motifs.
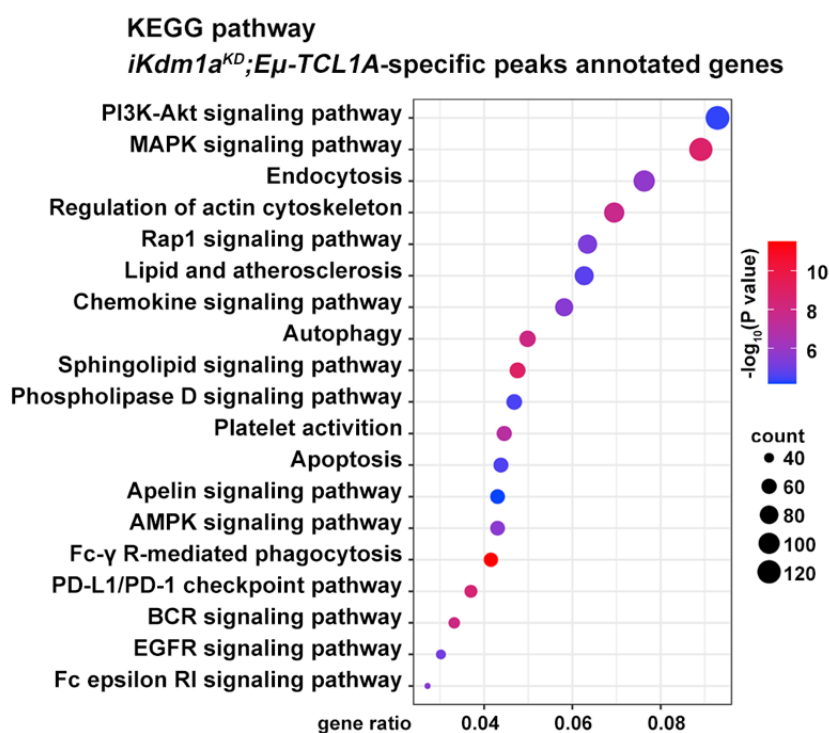
Figure 56. KEGG pathway enrichment bubble plot. KEGG pathways analysis of genes associated with *iKdm1a^{KD};Eμ-TCL1A*-specific H3K4me3 regions.
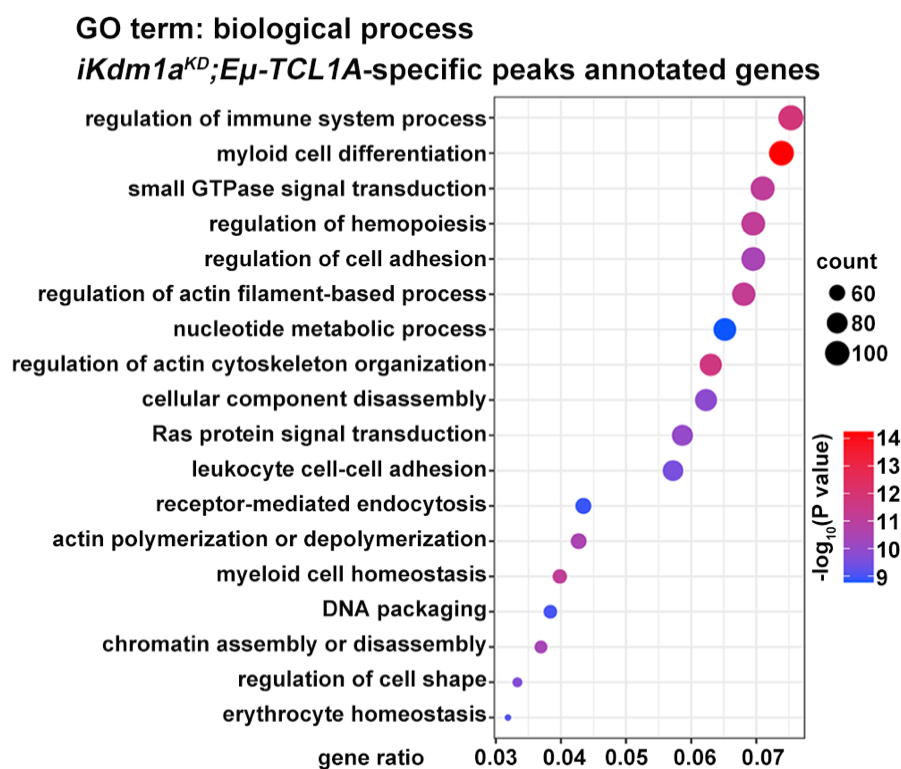
Figure 57. Biological process of GO term enrichment bubble plot. Gene ontology (GO) analysis of genes associated with *iKdm1a^KD;Eμ-TCL1A*-specific H3K4me3 regions.
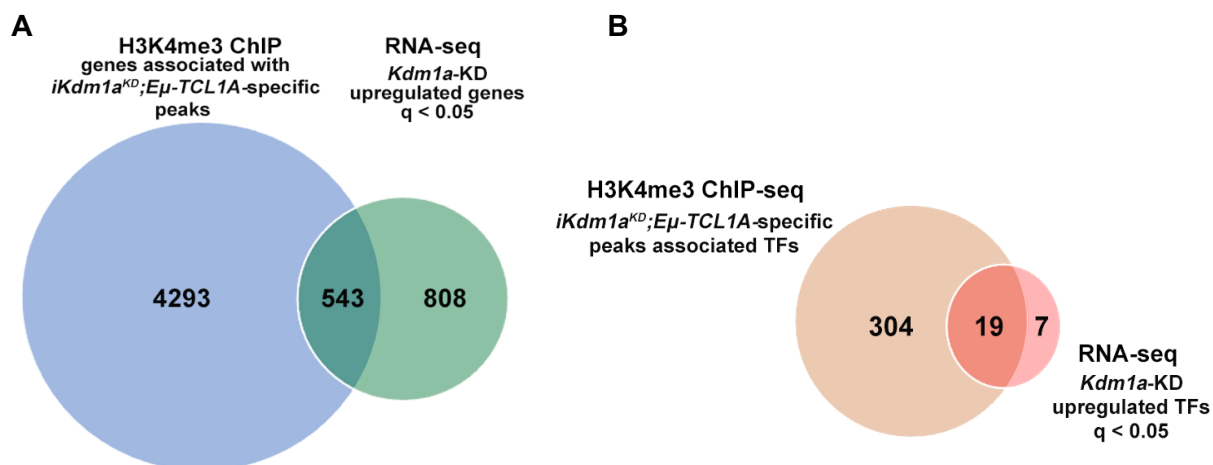
Figure 58. Integrative analysis of ChIP-seq and RNA-seq data. Overlap between genes (A) and transcription factor-encoding genes (B) upregulated by *Kdm1a*-KD and associated with *iKdm1a^KD;Eμ-TCL1A*-specific H3K4me3 regions.
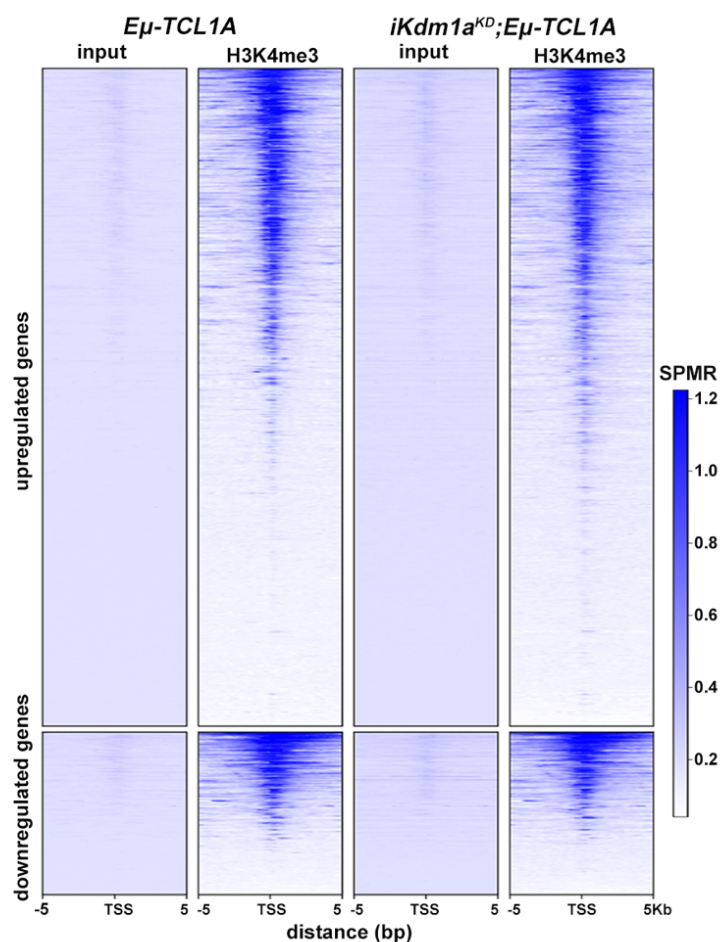
Figure 59. H3K4me3 binding occupancy at regions of differentially expressed genes in *Eµ-TCL1A* and *iKdm1a^{KD};Eµ-TCL1A* splenic mononuclear cells. Signal is displayed from -5 kb to +5 kb from the transcription start site (TSS).
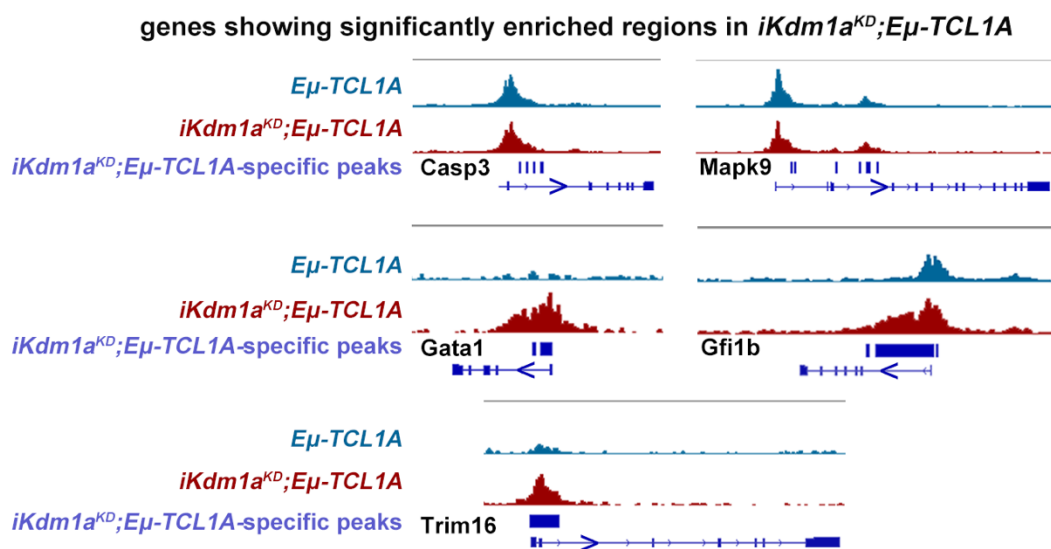
Figure 60. Gene tracks showing enriched H3K4me3 regions in splenocytes of *iKdm1a^{KD};Eµ-TCL1A*. Integrative Genomics Viewer (IGV) gene browser tracks of genes showing enriched H3K4me3 regions in *iKdm1a^{KD};Eµ-TCL1A*, including apoptotic makers *Casp3* and *Mapk9*, transcription factor encoding genes *Gata1* and *Gfi1b*, as well as tumor suppressor *Trim16*.

3.4 Aim IV: Assess the efficacy of KDM1A targeting compounds in B-cell lines as well as in primary samples

As higher KDM1A levels are associated with poor clinical outcomes and genetic knockdown of *Kdm1a* in the murine CLL model decreased the tumor burden and prolonged animal survival, targeting KDM1A with pharmacological inhibitors could provide a potential treatment option for CLL. Therefore, we aimed to assess the efficacy of KDM1A targeting compounds in CLL.

3.4.1 The KDM1A inhibitor C12 affects histone methylation and induces apoptosis in leukemic B cells

There are different KDM1A inhibitors being tested in several phase-I/II trials.[245] Among these, RN-1 (RN1), C12 (HCI-2509, SP-2509), S2101 (LSD1 inhibitor II), and GSK (GSK2879552) are potent inhibitors of KDM1A (**Figure 61, Table 14**). RN1 is a cell-permeable tranylcypromine analog that has been reported to act as a potent, irreversible inhibitor of KDM1A with a low IC 50 (0.07 µM).[259] C12 has demonstrated a promising anti-AML activity.[260] It has been reported that S2101 treatment decreases the levels of phosphorylated AKT and mTOR, and S2101 can inhibit ovarian cancer cell viability.[261] LSD1 inhibition with GSK has potent activity against MLL-AF9 leukemia.[262] Before investigating the effect of KDM1A inhibitors on primary CLL cells, we first tested these 5 different substances on multiple B cell lines. JVM3$^{\pm TCL1A}$ cells were treated with KDM1A inhibitors for 48 hours with a concentration of 10 µM. Of all five inhibitors, only compound C12 markedly decreased cell viability via reduction of metabolic activity and by induction of apoptosis (**Figure 62A**), accompanied by phosphorylation of P53 and cleavage of PARP (**Figure 62B**). C12 treatment increased H3K4 and H3K9 methylation irrespective of TCL1A status, while the other inhibitors increased H3-methylation preferably in the TCL1A-negative parental line (**Figure 62B**). We observed similar results in Mec1 cells (CLL cell line with *TP53* mutation) (**Figure 62C**) and in DoHH2$^{\pm TCL1A}$ lymphoma cells (**Figure 62D**).

Next, we tested these inhibitors in primary CLL samples that had been stimulated to induce proliferation (>35% proliferating cells), confirmed by Ki-67 staining flow cytometry (**Figure 63, Table 15**), for which we co-cultured CLL cells with differentiated THP-1 macrophages supplemented by 0.25 µM of CpG and 10 µg/L of rhIL-15 for 36 hours. The selected CLL samples were then treated with 10 µM of different substances for 72 hours. Only C12 notably reduced the cellular metabolic activity of these stimulated CLL cultures (**Figure 64A**). C12 induced apoptotic cell death, while RN1 induced the expression of early apoptotic Annexin-V (**Figure 64B-C**). Such a pattern is described for metabolically (hyper)active senescent cells that undergo apoptotic transition.[263,264] In agreement, RN1, but not C12, markedly induced cellular senescence as recorded by FDG staining flow cytometry (**Figure 64D**). In line with the data

from cell lines, H3K4me3 and H3K9me3 were most strongly increased in CLL cells treated with C12 (both P=0.008, **Figure 64E**). Consistently, only C12 was able to enhance P53 phosphorylation and PARP cleavage (P<0.05, **Figure 64E**).

Collectively, these data suggest that C12 increases methylation levels of H3K4/K9 and elicits apoptotic cell death towards B cells.
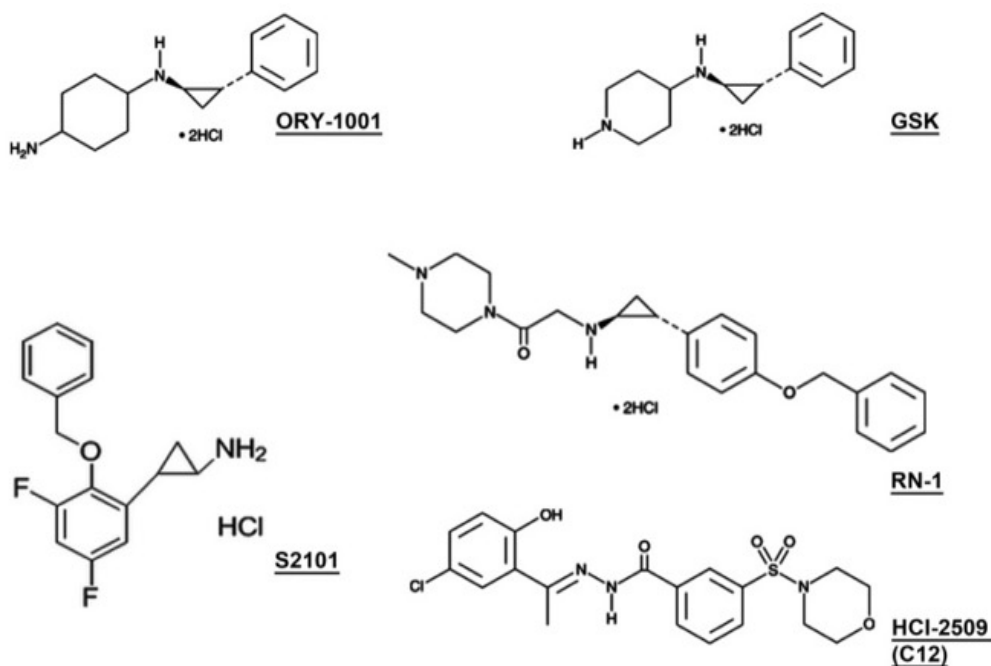
Figure 61. The chemical structures of selected KDM1A inhibitors used in this study.

Table 14. List of selected KDM1A inhibitors in this study

KDM1A inhibitor	IC50 (nM)	Disease setting	Cellular or functional effect
ORY (ORY-1001)	IC50 < 20 nM	AML SCLC	Promotes differentiation in vitro[245] Retards MLL-AF9 leukemogenesis in vivo[211] Phase I/II clinical trials in AML[265] Phase I clinical trial in SCLC[245]
RN1 (RN-1)	IC50 = 70 nM	AML Sickle cell disease	Impairs AML cell differentiation and growth, induces apoptosis in vitro and in vivo[266] Induces fetal hemoglobin synthesis[267]
C12 (HCI-2509)	IC50 = 13 nM	Ewing sarcoma lung adenocarcinoma AML	Impairs cell differentiation and tumor growth, induces apoptosis in vitro and in vivo[268–270] Synergy with panobinostat in vivo[260]
S2101 (LSD1 inhibitor II)	IC50 = 0.99 µM	Ovarian cancer	Inhibits ovarian cancer cell proliferation in vitro[261]
GSK (GSK2879552 2HCl)	IC50 = 1.7 µM	AML SCLC	Phase I clinical trials in AML and SCLC[245] Predominantly cytostatic effect in multiple cell lines in vitro and in vivo[271]
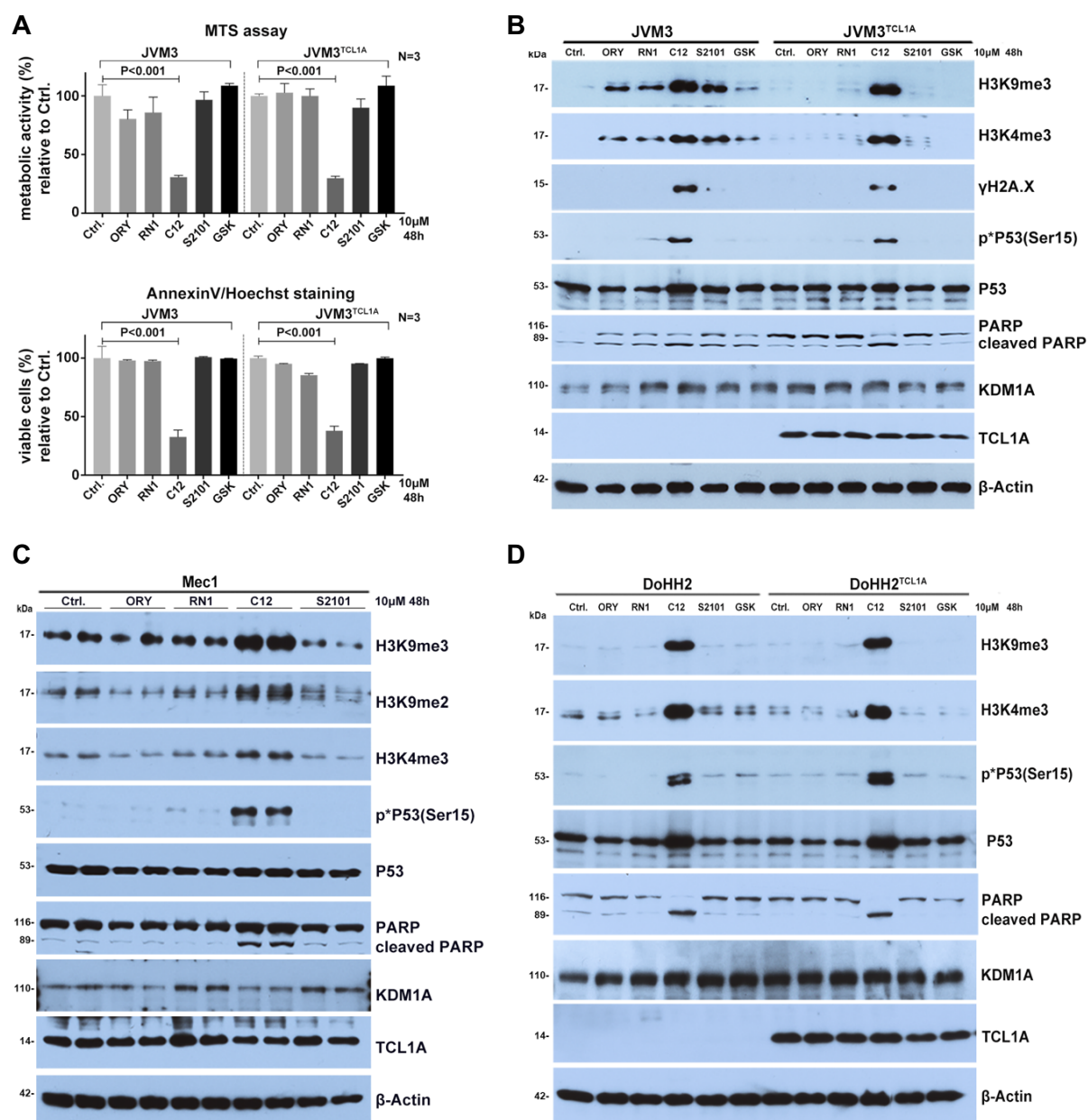
Figure 62. The KDM1A inhibitor C12 increases the methylation of H3K4/9 and apoptotic cell death in B-cell lines. (A) Metabolic activity and cell viability were assessed by MTS assay (top) and annexin V staining flow cytometry (bottom) in JVM3 cell lines treated with KDM1A inhibitors for 48 hours. The inhibitor C12 reduced metabolic activity and cell viability of JVM3$^{\pm TCL1A}$ cells. Mean±SEM, Student's t-test. (B) Immunoblots displaying an induction of apoptosis as shown by phosphorylation of P53 and cleavage of PARP, and an increase in tri-methylation of H3K4/9 by C12 in both JVM3$^{\pm TCL1A}$ cells. (C) Immunoblots displaying increased phosphorylation of P53, cleavage of PARP, and methylation of H3K4/9 by treatment with C12 in CLL-like Mec1 cells. (D) Immunoblots showing increased phosphorylation of P53, cleavage of PARP, and tri-methylation of H3K4/9 by treatment with C12 in both TCL1A negative and positive DoHH2 cells. N=3 independent experiments.

107
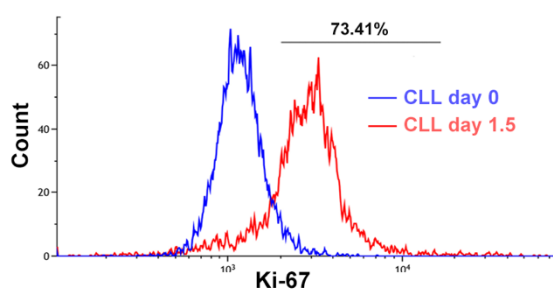
Figure 63. Representative flow cytometric histogram of Ki-67 expression in primary CLL cells co-cultured with differentiated THP-1 cells supplemented with CpG and IL-15 for 36 hours. Samples with more than 35% Ki-67 positive cells were selected for experiments, which were subsequently treated with KDM1A inhibitors for 72 hours (Selected samples are in **Table 15**).

Table 15. Patient characteristics of selected samples for testing KDM1A inhibitors

Patient ID	Age	Karyotype	ZAP70 (%)	CD38 (%)	IGHV	Binet stage	WBC (x10^9/L)	LDT (months)	Proliferation rate (%)
CLL12	78	del(13q)	neg		M	A	253.7	>12	41.94
CLL13	53	del(13q)	1.72	32.69	U	A	159.86		39.98
CLL23	62	mutation in BIRC3			M		89.7		53.94
CLL24	55	del(11q)	41	41	U	B	81.39		53.66
CLL25	71	del(13q)	2.80	28.70	M	C	71.42		73.16
CLL26	76		7.70	50.70	U	A			38.84
CLL27	62				M	C	395	<12	38
CLL28	49	del(13q)	neg	neg	M	B	315.49		63.72
CLL29	69	complex karyotype	neg	neg	M	B-C	205.5		79.42
CLL30	72	del(13q)	pos	pos	U	B	70.64	<6 month	82.76
CLL31	68	del(11q), del(13q)		pos		A	215.77	6-12	35.56
CLL32	57	del(13q), del(17p)	neg	neg	M	C	105.19		58.74

IGHV: *IGHV* mutation status; M: *IGHV* mutated; U: *IGHV* unmuted
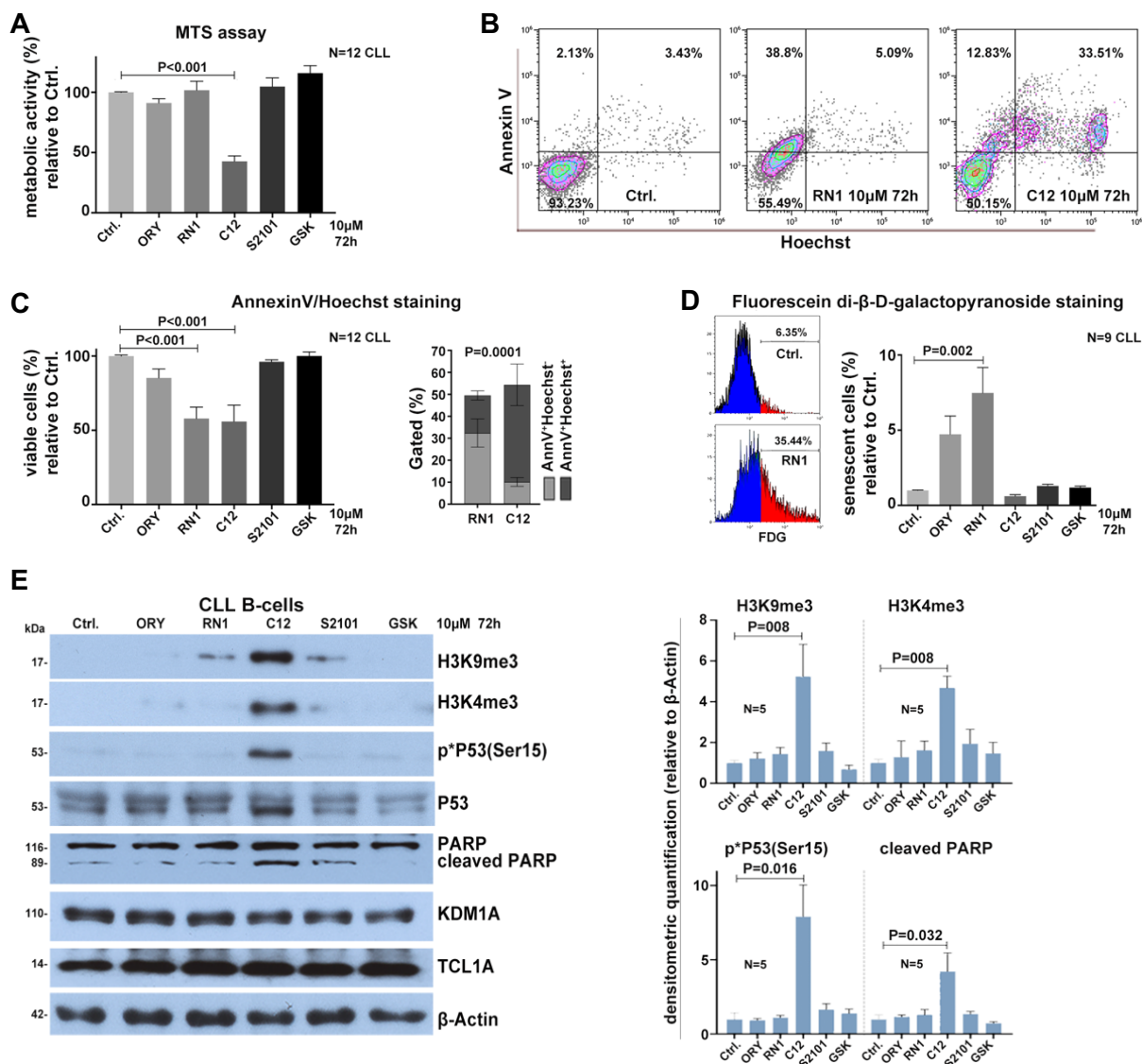
Figure 64. The KDM1A inhibitor C12 increases the methylation of H3K4/9 and induces apoptotic cell death in primary CLL cells. (A) The inhibitor C12 decreased the metabolic activity of CLL cells indicated by the MTS assay (N=12 CLL, P<0.001, Student t-test, Mean±SEM). (B) Representative flow cytometry plots of Annexin V/Hoechst staining in CLL samples. Left: 93.23% viable cells in control condition as determined by AnneV-. Middle: RN1 treatment induced early apoptotic change as shown by AnneV+. Right: C12 treatment induced apoptotic cell death shown by AnneV+/Hoechst+. (C) Left: The inhibitor C12 and RN1 compromised CLL cell viability analyzed by Annexin V staining (N=12 CLL. both P<0.001, Student's t-test, Mean±SEM). Right: Bar shows more AnneV+/Hoechst- (grey) and less AnneV+/Hoechst+ (dark grey) cells in RN1 treated CLL samples in comparison to C12 treatment (N=12, P=0.0001, a two way ANOVA test was used, Mean±SEM). (D) Left: Representative flow cytometry plots of Di-β-D-Galactopyranoside (FDG) staining in CLL samples (control and RN1 treatment). Right: The inhibitor RN1 promoted cellular senescence of CLL cells as analyzed by FDG staining (N=9 CLL, P=0.002, Student's t-test, Mean±SEM). (E) Left: Representative immunoblots showing that the inhibitor C12 induces phosphorylation of P53, cleavage of PARP, and higher tri-methylation levels of H3K4/9 in CLL cells. Right: Bar charts indicate densitometric quantification of immunoblots. Treatment with C12 induced significantly higher H3K9me3 (P=0.008), H3K4me3 (P=0.008), phosphorylated P53 (P=0.016), and cleaved PARP (P=0.032) in comparison to control (N=5 CLL, Mann-Whitney test, Mean±SEM).

3.4.2   KDM1A inhibition acts synergistically with antagonists of BCL-2 and MDM2 in B cells

The availability of targeted agents for the treatment of CLL, like the BTK inhibitor ibrutinib and the BCL-2 inhibitor venetoclax, has greatly increased over the past decade. However, many patients relapse under these therapies. Combination treatments have been considered as strategies to prevent resistance and minimize undesired toxic effects.[272] Combination therapies including BTK inhibitors, venetoclax,[272] and HDAC inhibitor (HDACi) have already shown great response rates.[273] Therefore, we evaluated if the inhibition of KDM1A might represent a potential combination partner for the treatment of CLL. To this end, we treated *TCL1A*-tg JVM3 cells with C12 in combination with ibrutinib, venetoclax, and the pan-HDACi panobinostat for 48 hours using indicated concentrations. Furthermore, we included the MDM2 inhibitor idasanutlin, which represents a novel therapeutic approach to induce P53-mediated apoptosis.[274] Annexin V staining flow cytometry was performed to analyze cell viability. The synergistic effect was analyzed and the synergy score was calculated using SynergyFinder 2.0 based on the zero interaction potency (ZIP) model.[275] Combinations of C12 with venetoclax or idasanutlin showed a synergistic anti-leukemic relationship (ZIP score >10, **Figure 65A-B**), while the combination of C12 with ibrutinib showed only additive effects (**Figure 66A**) and the co-treatment with panobinostat revealed no cooperating effect on inducing cell death (**Figure 66B**). These data indicate that the inhibition of KDM1A might be a suitable synergistic combination partner for targeted therapies in CLL.
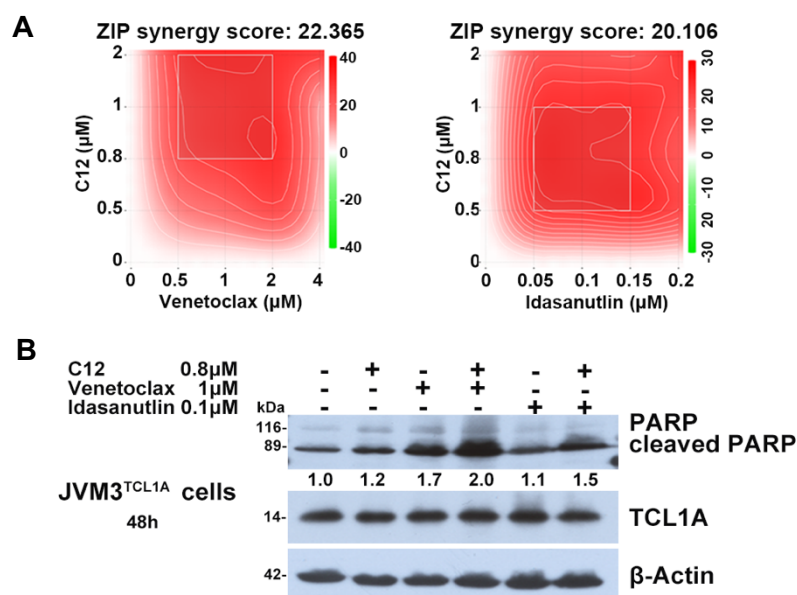
Figure 65. The KDM1A inhibitor C12 presents a synergistic effect with venetoclax and with idasanutlin in JVM3^TCL1A cells. (A) The two-dimensional contour plots showing the synergistic effect of the co-treatment of C12 with Venetoclax (left) and with Idasanutlin (right) in JVM3^TCL1A cells. (B) Immunoblots demonstrating a synergistic effect of the co-treatment of C12 with Venetoclax and with Idasanutlin in inducing cleavage of PARP in JVM3^TCL1A cells. N=3 independent experiments.
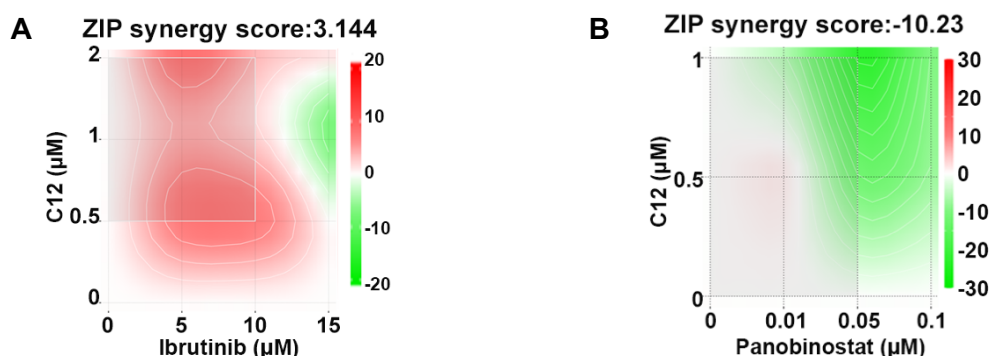
Figure 66. The two-dimensional contour plots showing (A) the additive effect of C12 with Ibrutinib. (B) the antagonistic effect of the combination treatment of C12 with Panobinostat in JVM3[TCL1A] cells. N=3 independent experiments.

3.4.3 Treatment with C12 decreases the amount of secreted cytokines in splenic leukocytes from leukemic mice

It is known that cytokines are important in the tumor microenvironment and could be targeted for immunotherapies. We have shown previously that *Kdm1a*-KD also has an effect on the CLL microenvironment in mice. KDM1A inhibition has been reported to impede the production of cytokines.[276,277] Therefore, we hypothesized that KDM1A inhibition may also affect the production of cytokines in CLL. To this end, splenic leukemic cells were isolated from *Eµ-TCL1A* leukemic mice and treated with the KDM1A inhibitor C12 at a concentration of 10 µM in vitro for 24 hours. 25 ng/mL PMA and 1 µg/mL ionomycin were applied to stimulate cytokine production for the last 6 hours (**Figure 67A**). Afterwards, a cytokine assay was performed to detect the amount of the secreted cytokines. Cells were viable after treatment with 10 µM C12 for 24 hours (**Figure 67B**). Interestingly, the C12 treatment decreased the amount of cytokines that had been triggered by PMA and ionomycin (**Figure 67C**). A recent study has demonstrated that KDM1A inhibition could reduce cytokine release in vitro.[278] This data suggests that KDM1A inhibition might lead to the blocking of cytokine production or release in splenic leukemic cells of CLL mice.

A

Eu-TCL1A
leukemic mice
N=3

splenocytes
(90% CD19+CD5+ cells)

C12   24h

6h
+/-(PMA & ionomycine)

supernatant

LUNARIS™ Mouse 12-Plex Cytokine Kit

Ayoxxa cytokine array

B

C
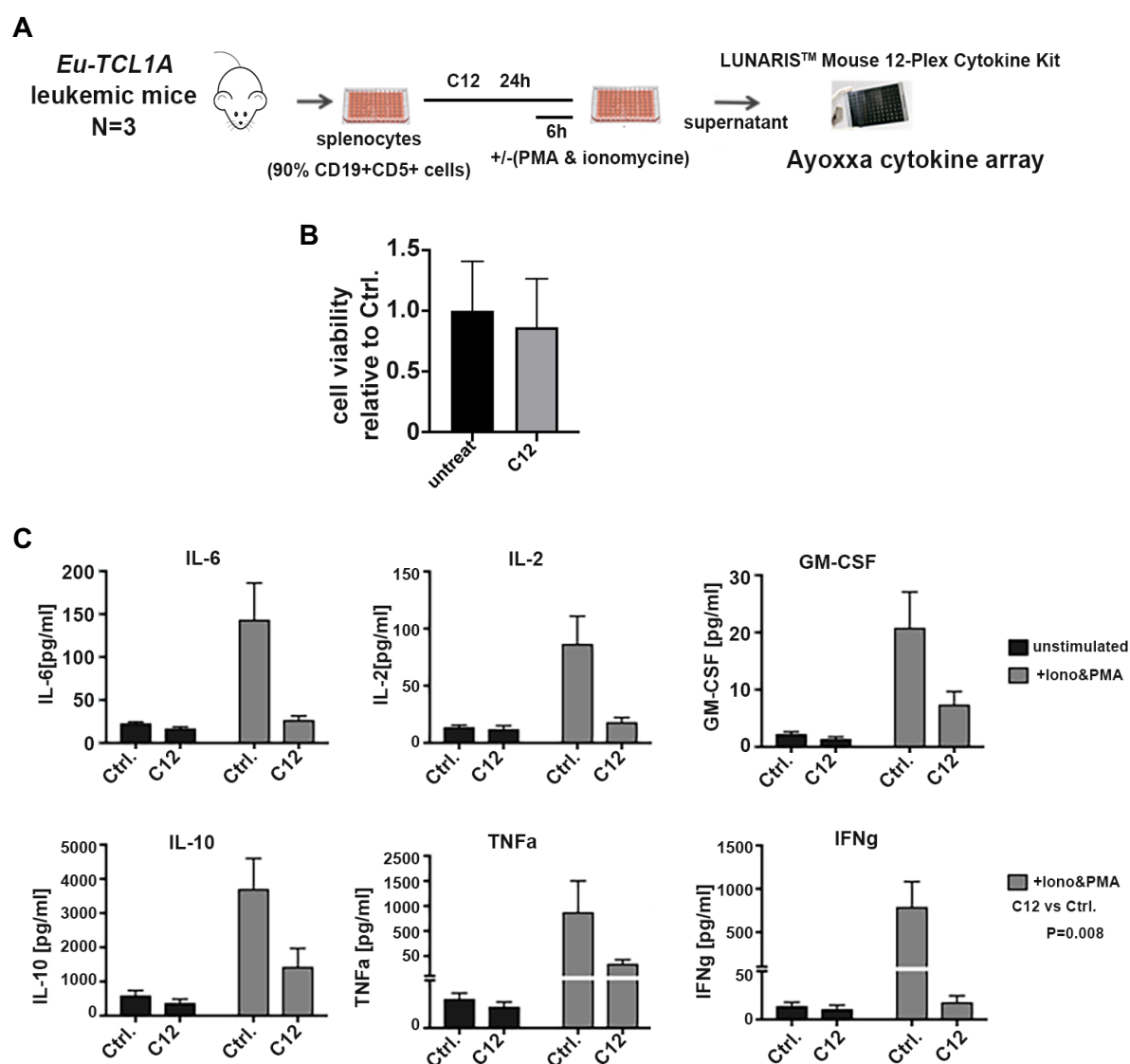
Figure 67. Treatment with C12 decreases the amount of secreted cytokines in murine CLL cells.
(A) Experiment set up: leukemic cells isolated from *Eµ-TCL1A* mice (N=3) were treated with the inhibitor
C12 for 24 hours with or without PMA & Ionomycine stimulation for the last 6 hours. Cultured superna-
tant was collected for cytokine array. (B) Cell viability was analyzed by annexin V/Hoechst staining flow
cytometry. (C) Cytokine array demonstrated that C12 decreases the amount of the secreted cytokines
stimulated by PMA & Ionomycine. Mean±SEM, Student t-test.

4 Discussion

As the most prevalent leukemia in adults in the Western world, CLL presents diverse clinical courses. With the identification of numerous genomic and molecular alterations in CLL, it is possible to define high-risk patients.[279] Treatment strategies for CLL have been improved with the development of novel therapies, which could further improve overall survival and the outcome of high-risk patients.[33] Nevertheless, CLL remains an incurable disease that requires a better understanding of underlying oncogenic potencies in different disease subsets.

The epigenetic layers of chromatin dynamics and histone modifications have recently been recognized as important characteristics of CLL.[167] Since the first publication of chromatin accessibility profiling in CLL in 2016,[163] few other studies have strengthened the concept of specific chromatin configurations and dynamic histone modifications underlying leukemic development, disease heterogeneity, and the relapsed/refractory state.[164,165,280,281] Moreover, currently applied treatments, such as ibrutinib, significantly reprogram chromatin accessibility models and patterns of histone marks.[282,283] Furthermore, to overcome the resistance to CD20 antibodies, BCR inhibitors, and BCL-2 inhibitors in CLL, the promise of targeted pharmacological epigenomics is primarily based on observations of enhanced target (re)expression and highly synergistic drug relationships towards re-established sensitivities.[167,284] Histone modifying enzymes represent the central target category for this. However, besides the data on HDACs, EZH2, SIRT1, or SETD2, histone-modifying enzymes in CLL are not well characterized for their deregulation, functional relevance, and target properties.[167]

Aberrant expression of the T-cell lymphoma/leukemia 1A proto-oncogene is a hallmark of CLL and high TCL1A levels are associated with aggressive disease features.[111] However, the molecular concept around TCL1A in the initiation and sustenance of tumors is still not clear. Despite intensive efforts to clarify the molecular mechanisms of TCL1A's oncogenic function, the identification of specific TCL1A-mediated pathways remains a challenge. TCL1A shows no intrinsic enzymatic activity and has no DNA-binding motif, suggesting that it mediates its activity in a chaperone-like fashion via protein-protein interactions. Indeed, previous studies have demonstrated that TCL1A can activate the AKT kinase and other targets through defined protein-protein interactions, resulting in NFκB-dependent and independent pro-survival effects.[117,118,129] Our lab has generated evidence that implicates TCL1A as a modulator of BCR and TCR signaling, through which it induces activation of AKT kinase and further induces the BCR/TCR associated kinase cascade.[108,132] More recent discoveries indicate that TCL1A might be involved in DNA damage/repair pathways and, importantly, epigenetic events.[118,133]

The mutual cause-effect interplay between TCL1A and epigenetic processes has been underappreciated, but there are emerging data around this aspect. First, the expression of the

TCL1A gene is controlled epigenetically, e.g., *TCL1A* expression is elevated due to hypomethylation of its promoter regions in CLL.[134] Similarly, TCL1A was shown to be a downstream effector of KDM3A (JMJD1A) in embryonic stem cells.[135] There, KDM3A demethylates H3K9me2 at *TCL1A* promoter regions and by that positively regulates its expression, ultimately thought to promote stem cell self-renewal and pluripotency via the TCF3/NANOG/TCL1A signaling axis.[135,136] On the other hand, TCL1A can control the global DNA methylation landscape by suppressing the activity of the de novo DNA demethylases Dnmt3a/b through direct protein-protein interaction.[133,154] A better understanding of functional networks around TCL1A, particularly with epigenetics, is needed to develop new treatment approaches in CLL.

Interestingly, our MS analysis of the TCL1A interactome has identified a panel of epigenetic modifiers that interact with TCL1A in CLL B cells (**Figure 6**). The chromatin-modifying enzyme lysine-specific demethylase KDM1A, as a novel interacting partner of the TCL1A protein, has been demonstrated to be involved in the development of various tumors including hematological malignancies. Overexpression of KDM1A has been reported in a variety of cancer types and correlated with poor overall survival in patients.[285–289] However, KDM1A is thought to support tumor progression by regulating gene expression in malignant cells and facilitating their adaptation to the tumor microenvironment.[289] Furthermore, pharmacological inhibition of KDM1A holds great promise as a new therapeutic strategy. KDM1A is considered a drug target in cancer, and many KDM1A inhibitors have been developed, some of them are currently undergoing clinical trials for the treatment of hematological cancers as well as solid tumors.[245,289] Therefore, this study aimed to characterize the interaction of TCL1A with KDM1A in CLL, further deciphering the role of KDM1A in its pathogenesis and providing a rationale of KDM1A inhibition for the treatment of CLL.

In the presented study, we establish an actionable oncogenic role of this lysine-specific demethylase. We identify KDM1A as a novel effector of the oncogenic chaperone TCL1A in B cells. Their protein interaction enhances the catalytic activity of KDM1A. Accordingly, MS-based analyses of histone PTMs demonstrate lower H3K9me2/3 upon expressing TCL1A in malignant B cells. In CLL, high levels of *KDM1A* and the associated gene expression signatures correlated with aggressive disease features and inferior clinical outcomes in 337 cases from the CLL8 trial cohort. Genetic *KDM1A* depletion in *Eµ-TCL1A* transgenic CLL mice suppresses leukemic growth via CLL-cell intrinsic as well as milieu-mediated mechanisms. Through integrated analyses of KDM1A-associated transcriptome and H3K4me3 alterations in murine CLL, we establish KDM1A as a transcriptional repressor, which specifically modifies histone methylation profiles to regulate defined B cell survival pathways. We finally

demonstrate that pharmacologic inhibition of KDM1A alters H3K4/9 methylation and induces apoptosis in CLL cells and therein also synergizes with BCL-2 inhibition and MDM2 inhibition.

As an epigenetic regulator, KDM1A is localized to the nucleoplasm and in addition to the cytoplasm. We investigated the subcellular localization of the TCL1A-KDM1A complex. Both TCL1A and KDM1A are present in the nucleus and cytoplasm, interestingly, they interact in the nucleus (**Figure 23C**), which might be important for KDM1A to exert its epigenetic function. Indeed, we observed higher histone demethylase activity of KDM1A in *TCL1A*-transgenic B cells (**Figure 24**), indicating that TCL1A may affect KDM1A's function via enhancing its demethylase activity. However, it is unknown how TCL1A interacts with KDM1A. TCL1A was previously demonstrated to propel the distribution of AKT complexes from cytoplasmic to nuclear sites.[132] It is therefore conceivable that TCL1A-bound KDM1A is either retained in the nucleus with chromatin accessibility as core demethylase or that in contrast, TCL1A-engagement promotes nuclear immigration of KDM1A. With further studies, we could employ a protein complementation assay to monitor the subcellular localization of TCL1A-KDM1A protein complexes. This allows the tracing of protein complexes in living cells by fluorescent microscopy.[290] TCL1A 'dimerization' constructs could also be applied to test for affected subcellular localization of KDM1A by such functionally 'hypomorphic' TCL1A.

Given the fact that over 90% of CLL cases express TCL1A and its high expression levels are associated with a poor clinical outcomes.[109] The identification of TCL1A-KDM1A interaction in the nucleus provided signs about a possible reinforcement impact of TCL1A on KDM1A's function in CLL. The overexpression of TCL1A may alter gene transcription via modulating the histone demethylase activity of KDM1A in CLL.

To study the clinical relevance of KDM1A in CLL, we categorized the expression of *KDM1A* and its biological relevance in CLL clinical courses. We could show that KDM1A protein levels are higher in CLL B cells compared to that in healthy B cells (**Figure 27**). Gene expression profiling data analysis demonstrated distinct gene clusters (cluster 1, 2, 3, **Figure 28A**) among patients with different *KDM1A* expression levels (low vs. high quartier). *KDM1A* levels are significantly higher in cluster 3 than in cluster 1 (**Figure 28B**). Interestingly, the expression of *SLAMF6* positively correlated with higher *KDM1A* levels, while the expression of the *FOS* family members *FOS* and *FOSB* are inversely associated with *KDM1A* levels. Previous studies have revealed that SLAMF6 plays a crucial role in the interactions of T-follicular helper cells with GC B cells and anti-SLAMF6 treatment reduces CLL cell number in a patient-derived xenograft.[246,247] Recently, low or very low expression levels of *FOS* gene family have been

reported as a marker of poor prognosis in CLL.[248] Together, these findings suggest that high *KDM1A* expression levels in CLL may relate to an inferior clinical course.

Furthermore, the enrichment of different pathways correlated with *KDM1A* expression levels. DNA replication, DNA repair pathways, and BCR signaling pathways are enriched in *KDM1A* high group, whereas the cytokine receptor interaction pathway is enriched in the *KDM1A* low group (**Figure 29**). Targeting DNA repair pathways and BCR signaling are therapeutic strategies for CLL.[291–293] This data suggests that *KDM1A* expression levels are linked to differential gene expressions and involved in functional pathways in CLL. It has been reported that, as a component of the NuRD multiprotein complex that combines functions including, e.g., HDAC1/2 with the nucleosome remodeling of the ATPases chromodomain helicase DNA-binding protein CHD3 and CHD4 and the methyl-CpG-binding domain proteins MBD2 or MBD3, KDM1A plays pivotal roles in the DNA damage repair process.[294] Interestingly, KDM1A was shown to promote histone ubiquitylation at sites of DNA damage downstream of E3 ligase recruitment, thereby promoting the DNA damage response.[244] Aberrantly expressed KDM1A has been shown to inhibit differentiation and contribute to cancer cell proliferation, cell metastasis and invasiveness in many cancers.[295] Our study indicates a role of KDM1A in CLL, although further functional studies are needed to investigate the mechanisms of its regulation in different pathways in the pathogenesis of CLL.

Moreover, significantly higher white blood cell count, higher serum thymidine kinase levels, higher *TCL1A* levels, and higher rates of *TP53* aberration (*TP53* mutation/deletion), which are related to more advanced CLL, were shown in patients in the cluster 3 (higher *KDM1A* expression, **Figure 30**). We also observed a shorter telomere length in this cluster (**Figure 30**). Telomere length is considered as a prognostic indicator and attrited telomeres were correlated with adverse survival in CLL.[296–299] Of note, we also observed shorter progression-free survival of patients in this cluster (**Figure 31**). The survival impact was shown in the FC cohort but not in the FCR arm of the trial (**Figure 31**). KDM1A has been shown to regulate cell proliferation/apoptosis in P53-dependent and -independent manners.[300] While rituximab depletes CD20 positive B cells in the immune system. In addition, various factors could have an impact on survival, e.g., telomere length has been shown to predict an outcome of FCR chemotherapy in CLL.[298] Therefore, more comprehensive studies are warned to identify independent prognostic markers in CLL.

Collectively, elevated KDM1A levels and the associated gene expression signatures mark a more aggressive disease with adverse clinical outcomes in CLL.

To interrogate the biological relevance of KDM1A in CLL's biology in vivo, the role of Kdm1a during murine CLL evolution was assessed on the backbone of the most widely accepted autochthonous model of CLL, the a *TCL1A*-tg mouse model named *Eµ-TCL1A*. As a highly informative model, it allowed the establishment of *Kdm1a's* leukemic relevance in the context of its catalytically activating interactor TCL1A. *Kdm1a* was knocked down systematically mimicking pharmacological inhibition of KDM1A in CLL patients. In the present study, we demonstrate that Kdm1a is important in CLL progression in vivo. Genetic *Kdm1a* knockdown in *Eµ-TCL1A* leukemic mice significantly reduced the leukemic burden in the peripheral blood (**Figure 34**) and lymphoid tissues (**Figure 36**), leading to prolonged animal survival (**Figure 41**). *Kdm1a*-KD induced apoptosis and impaired proliferation in leukemic B cells (**Figure 39-40**). It would be of interest to also analyze B-cell-specific Kdm1a function at different stages of *TCL1A*-driven leukemogenesis in a *Kdm1a* proficient non-leukemic environment in the future.

Next to the effect on B cells, with the advantage of whole-organismal *Kdm1a* knockdown, we could identify an important role of KDM1A in the microenvironment, which CLL cells heavily rely on. The interaction of CLL cells within the microenvironment can promote CLL cell survival and/or CLL progression.[68] CLL cells contact with T cells intimately in the microenvironment, where T cells play a role in providing critical regulatory signals.[85] In our study, we detected a lower number of T cells in the germinal centers in spleens of leukemic mice with *Kdm1a* knockdown (**Figure 42**). Interestingly, the skewed CD4+/CD8+ ratio observed in *Eµ-TCL1A* leukemic mice[301,302] was inverted when *Kdm1a* was knocked down. These indicate that KDM1A has an effect on the T-cell compartment in the CLL microenvironment. *Ye Qin et al.* reported that in triple-negative breast cancer (TNBC), KDM1A inhibits CD8+ T cells tracking in the microenvironment.[252] Others demonstrated that targeting nuclear KDM1A could inhibit metastatic cancer cells and reinvigorate exhausted T cells.[253] More recent exploration revealed the activation of antitumor T-cell immunity by KDM1A inhibition in TNBC.[303] Given that T cells are also of importance in CLL, further studies would be subject to characterize the mechanisms of the regulatory effect of KDM1A inhibition in regulating T-cell number, differentiation, and function.

Another component in the CLL microenvironment, tumor-associated macrophages derived from monocytic lineage are recognized as nurse-like cells which can promote the survival and proliferation of the CLL cells in vitro and in vivo.[77,78] We could show that the number of macrophages increased in peripheral blood and in the spleens of *iKdm1a*[KD] mice (**Figure 43**) as reported before,[211] however, the KDM1A deficient macrophages were significantly less efficient in stimulating CLL cells into proliferation in vitro (**Figure 47**). In solid tumors like breast cancer, KDM1A inhibition has been shown to abrogate the mesenchymal signature and promote an innate M1 macrophage-like tumoricidal immune response in the microenvironment.[304]

And KDM1A inhibitors that have the ability to target both FAD and CoREST could prime macrophages toward an anti-tumor M1-like phenotype in TNBC.[305] In general, macrophages are a large component of the microenvironment and are critical for tumor progression. KDM1A affects their differentiation and/or function, making KDM1A an important regulator in the CLL microenvironment.

In addition, the 'feeder' layer for CLL cells is thought to be stromal cells.[68] They can secrete chemokines to recruit CLL cells into the tissue environments and induce upregulation of elements to promote CLL cell survival and proliferation via cell-cell contact.[81] We have co-cultured murine bone marrow stromal cells with murine leukemic cells in vitro. *Kdm1a*-KD in murine BMSCs resulted in an impaired supporting effect on murine CLL cells (**Figure 45**). Furthermore, HS-5 stromal cells with decreased KDM1A expression presented compromised support on human CLL cells in vitro, although KDM1A-KD has no effect on the proliferation of stromal cells (**Figure 46**). These suggest that KDM1A might affect the supportive elements of stromal cells for CLL cells, e.g., production or secretion of chemokines.

Overall, KDM1A inhibition had been implicated in modulating the tumor micromilieu in other cancers, e.g., by affecting the stromal compartment as well as the infiltration of T cells and of macrophages.[252,253,304] Interpretations of such findings also need to provide room for consequences of a myeloid-biased differentiation triggered by KDM1A inhibition.[306] Further studies need to characterize the differentiation stages and functions of milieu components regulated by KDM1A to dissect the effect of the observed alterations of the micromilieu on CLL development. Nevertheless, we here provide the first evidence that a whole-organismal *Kdm1a*-KD in a CLL mouse model, mimicking pharmacological inhibition of KDM1A in CLL patients, not only causes apoptosis of leukemic cells, but also reshapes the composition of and impairs the support by the highly important micromilieu in CLL.

Given that KDM1A is elevated across numerous human cancers and we have shown that *Kdm1a* knockdown inhibits CLL progression in mice, we set out to characterize the molecular mechanism of *Kdm1a*-KD in murine CLL. Notably, our transcriptome analysis of murine CLL cells revealed that depletion of *Kdm1a* mainly led to an overall increase in gene expression (**Figure 48**), suggesting that *Kdm1a* acts as a suppressor of gene expression. We observed a significant upregulation of genes associated with p53 signaling and pro-apoptotic pathways (**Figure 49**), further supporting the pro-apoptotic effect of *Kdm1a*-KD in CLL cells. Very recently, *Jixing Zhao et al.* have reported that KDM1A inhibition regulates genes involved in apoptosis in glioblastoma cells.[307] Moreover, we showed that expression of the adhesion molecules *Intgb2l* and *Rapgef3* is downregulated in *iKdm1a^KD;Eμ-TCL1A* (**Figure 50**), both are important mediators of the interaction between malignant B cells and their

microenvironment.[308] The homing chemokine Cxcr4, whose overexpression correlates with a poor prognosis in CLL patients,[309] was downregulated as well. According to these data, Kdm1a is implicated in CLL progression via alteration of transcriptional gene expression, potentially by suppressing apoptotic pathways and increasing molecules involved in B-cell homing/adhesion.

Since KDM1A can act as a transcriptional repressor by removing methyl groups from H3K4, which was firstly reported to be associated with the co-repressor protein complex CoREST.[186] We hypothesized that *Kdm1a*-KD may enrich the regulatory elements of the upregulated genes with H3K4 methylation, leading to their activation. Indeed, ChIP-seq demonstrated that the enrichment of pro-apoptotic pathways can be, at least in part, explained by increased H3K4me3 at the involved gene regions (**Figure 60**). We also identified highly enriched motifs associated with KLF3 and KLF1 binding motifs (**Figure 55**). KLFs are known in regulating proliferation, differentiation, and apoptosis in many tissues.[256] It has been reported that KLF3 is essential for normal B-cell development and for directing marginal zone B-cell fate.[257,258] These results indicate a role of KDM1A for transcriptional regulation directly, or indirectly by altering epigenetic modifications in murine CLL. The further mining of the resources provided in this project is expected to reveal additional insights into transcriptional regulation mediated by KDM1A in CLL.

However, H3K4me3 enrichment remained at a low level in *iKdm1a^{KD};Eµ-TCL1A* splenocytes, indicating that the H3K4me3 pattern is not exclusively dependent on Kdm1a. Other KDM1A targets (e.g., H3K9, H3K27, H4K20)[187] may be involved as well. On the other hand, the transcriptional repression by Kdm1a in murine CLL might be not exclusively conferred through histone demethylation, as this enzyme also targets non-histone proteins like TFs.[187] These might explain the observed alterations in gene expression. KDM1A could also cooperate with other TFs in regulating gene transcription in murine CLL. Hence, more comprehensive and unbiased genome-wide and functional approaches should be employed in further studies to characterize the specific role of KDM1A in the initiation and progression of CLL.

Altogether, the presented results suggest that *Kdm1a* knockdown may work through diverse mechanisms including upregulating genes involved in pro-apoptotic pathways to prevent disease progression and downregulating genes encoding molecules involved in the interactions within the CLL microenvironment. These might be through inducing methylations of H3K4, or co-working with other transcription factors. Our data underscore the potential for KDM1A inhibition to treat CLL.

Given the enzymatic activity of KDM1A and its importance in cancers, there has been much interest in developing potent and specific pharmacologic inhibitors of KDM1A. The nonselective monoamine oxidase inhibitor tranylcypromine (trans-2-phenylcyclopropylamine) was the first drug reported to inhibit KDM1A.[310] To improve the potency and specificity of tranylcypromine against KDM1A, derivatives of tranylcypromine were subsequently developed.[311] And more compounds were designed and synthesized as selective KDM1A inhibitors, including reversible KDM1A inhibitors.[311–313] In our screen, consistent with in vivo study that *Kdm1a* depletion induces apoptosis in CLL cells accompanied by upregulation of p53 and apoptotic pathways, the inhibitor C12 was the most promising compound among the five included substances in inducing apoptosis and in increasing histone methylations in TCL1A positive or negative B-cell lines to a similar extent (**Figure 62**) and in CLL cells (**Figure 64**). Interestingly, treatment with RN-1 induced cellular senescence in CLL B cells (**Figure 64**). In trophoblast stem cells, KDM1A deletion or inhibition has been shown to trigger senescence.[314] More recently, *Y. He et al.* reported that KDM1A knockdown or inhibition can induce cell senescence in a manner independent of p53 in vitro and in vivo.[315] These suggest that KDM1A inhibition may elicit diverse functions in a context-dependent manner. However, the concentrations used for the induction of apoptosis are at a micromolar level that might have off-target effects,[316] which is most likely not achievable in patients and might be associated with pronounced toxicity. Other inhibitors that are clinically active in AML or other diseases[245] showed limited efficacy in our in vitro studies. This further indicates that cell-specific contexts are important for KDM1A inhibition by different compounds. Based on these findings, there is an urgent need for the development of more potent KDM1A inhibitors which show specific activity against CLL.

Combination treatment is one of the current therapeutic strategies in CLL. The combination treatment with the BTK inhibitor ibrutinib was investigated in high-risk CLL patients.[317,318] Another target agent, the BCL-2 inhibitor venetoclax in combination strategies, has also been investigated in CLL patients.[319,320] Interestingly, KDM1A inhibition has been recently combined with HDACi and EZH2 inhibitors in treatment for solid tumors and AML.[321–324] Therefore, we set out to evaluate the potential of combination treatment with KDM1A inhibitor in CLL. Besides ibrutinib, vanatoclax, and pan-HDACi panobinostat, we included an MDM2 inhibitor idasanutlin that could induce P53-mediated apoptosis.[274] In our study, KDM1A inhibitor C12 showed a synergistic effect with venetoclax and with idasanutlin (**Figure 65**). Venetoclax inhibits the pro-survival protein BCL-2, thereby inducing apoptosis in CLL. Idasanutlin could inhibit the p53 repressor MDM2, leading to non-genotoxic reactivation of p53.[274] These two substances synergized with the KDM1A inhibitor C12 and increased the cleavage of PARP in *TCL1A*-tg JVM3 cells, indicating potential combination strategies with KDM1A inhibition in CLL treatment. However, the BTK inhibitor ibrutinib presented an additive effect with C12 in

inducing apoptosis of CLL cells (**Figure 66A**). BTK is a key enzyme in the BCR signaling and plays an important role in the activation and survival of B cells.[325–328] It has been shown that ibrutinib modulates the microenvironment of CLL.[329] In this study, we tested a combination treatment of ibrutinib plus the KDM1A inhibitor C12 in the JVM3[TCL1A] cell line, with which the microenvironment was not involved. Further studies would be subjected to assess the efficacy of this combination in an in vitro co-culture system and in vivo experiments. Interestingly, pan-HDACi panobinostat and the KDM1A inhibitor C12 produced an antagonistic effect in JVM3[TCL1A] cells (**Figure 66B**). This combination has been reported to be synergistic efficiently in cultured primary AML cells as well as in vivo.[260] Once again, it suggests that cell-specific contexts are important for different treatment strategies. Nevertheless, these novel combinations are suggested to be of interest and more extensive testing is demanded in the future.

KDM1A has been previously reported to control the expression of pro-inflammatory cytokine genes.[330] KDM1A inhibition has been shown to impede the production of cytokines.[276,277] In the present study, KDM1A inhibition by the compound C12 could decrease the amount of cytokines that have been stimulated by PMA and ionomycin in splenocytes isolated from leukemic *Eµ-TCL1A* mice (**Figure 67**). However, little has been known about the molecular mechanism of KDM1A in mediating the production/secretion of cytokines in CLL cells. The role of KDM1A may be dependent on its enzymatic activity as a histone demethylase. In further studies, one could analyze the changes in histone methylation status in PMA and ionomycin-stimulated CLL cells with or without KDM1A inhibition.

In summary, this study indicates an oncogenic role of KDM1A in the pathogenesis of CLL. The ability of KDM1A inhibition to impede proliferation and to induce apoptosis of CLL cells, as well as its inhibitory impact on the microenvironmental support for CLL cells, makes KDM1A an intriguing candidate for therapeutic targeting. We propose that KDM1A inhibition alone or in combination should be further explored in CLL in a more clinically relevant setting.

5 Conclusions and outlook

CLL is the most common type of B-cell leukemia in Western countries. The identification of various genomic and molecular alterations has helped define high-risk patients. Importantly, treatment approaches for CLL are changing rapidly with the emergence of novel effective and well-tolerated therapies, which have been demonstrated to improve the overall survival of CLL patients as well as the outcome of patients with high-risk diseases. Nowadays, the therapeutic goal of the response has evolved from complete clinical remission to the eradication of the minimal residual disease.[31] Despite these advances, CLL remains an incurable disease. In order to develop new therapeutic approaches, there is a need to improve the understanding of the pathogenesis and identify targetable makers in this still incurable disease.

Chromatin dynamics and histone modifications are increasingly recognized as key features in different cancers, including CLL. Particularly, histone-modifying enzymes are still poorly characterized regarding their deregulation, function, and as therapeutic targets in this heterogeneous disease. T-cell lymphoma/leukemia 1A has also been reported as a hallmark in CLL and its overexpression was associated with a poor prognosis. However, the functional network of this oncogene in CLL is not completely understood, in particular, its interplay with epigenetics has been underappreciated. Thus, the characterization of novel epigenetic interaction partners of TCL1A could contribute to better understanding the initiation and sustenance of CLL.

As a new TCL1A interactor, the lysine-specific demethylase KDM1A specifically demethylates histone 3 (H3) on mono- or di-methylated lysine 4 (H3K4me1/2) as well as H3K9. It also demethylates non-histone proteins. Overexpression of KDM1A has been linked to a poor prognosis in different cancer entities including hematological malignancies. Numerous compounds targeting KDM1A have been developed and some are being tested in clinical interventional trials for cancer, particularly for acute leukemias. The role and molecular concept of KDM1A have not yet been described in CLL. Hence, the presented thesis aimed to decipher the role of KDM1A in CLL by testing its biological relevance and characterizing molecular mechanisms.

In the presented study, we established the oncogenic relevance and function of KDM1A in CLL based on the following findings:

- The oncogenic chaperone TCL1A interacts with KDM1A in protein complexes and enhances its demethylase activity in B cells. Fittingly, mass-spectrometry-based analyses of histone PTMs demonstrate lower H3K9me2/3 upon overexpression of TCL1A in malignant B cells.

- Higher *KDM1A* levels and the related gene expression signatures are associated with unfavorable disease characteristics and poorer clinical outcomes in a large prospective CLL cohort from the CLL8 trial.

- Induced genetic *Kdm1a* knockdown in the *Eµ-TCL1A*-transgenic CLL mouse model resulted in reductions of leukemic burden, which translated into longer leukemia-specific animal survival.

- Such systemic *Kdm1a* depletion suppressed leukemic growth via CLL-cell intrinsic modes (i.e. upregulation of p53 and pro-apoptotic pathways) as well as via milieu-mediated mechanisms. This *Kdm1a* loss reshaped the composition of the CLL microenvironment (e.g., T-, stromal, monocytic cells), paralleled by impaired support of these cells on CLL cell survival and proliferation.

- Through the integration of *KDM1A*-associated changes in transcriptomes (RNA-seq) and H3K4me3 binding site enrichments (ChIP-seq) in murine CLL, we establish KDM1A as a predominant transcriptional repressor, which regulates defined B cell survival and homing pathways via modifying histone methylation profiles.

- We finally demonstrate that pharmacologic inhibition of KDM1A by compound C12 increases H3K4/9 methylation and induces apoptosis in CLL cells. Following the concept that targeting histone-modifying enzymes is an effective strategy of drug (re)sensitization, C12 showed synergisms with BCL-2 inhibition and MDM2 inhibition.

This work established the pathogenetic role of KDM1A in CLL by its actions in the leukemic cells and in elements of the micromilieu. KDM1A regulates the expression of genes involved in apoptosis, proliferation, and migration. This is likely mediated by its impact on histones and the methylation of non-histone proteins. Our data point to a high therapeutic potential of drug-based inhibition of KDM1A in CLL. We consider our inducible pan-organismal depletion of *Kdm1a* in leukemic *Eµ-TCL1A* mice (*iKdm1a^{KD};Eµ-TCL1A*) as a relevant model as it mimics the systemic effects of pharmacologic KDM1A targeting. Overall, our study provides a strong rationale for KDM1A inhibition in CLL and will benefit the development of epigenetically relevant therapies for the treatment of this still incurable disease. Combination treatments may be more effective since the effect of mono-targeting therapy might be bypassed by the altered signaling and functions of CLL B cells. This has to be evaluated more thoroughly since promising results were obtained in pre-clinical studies.

In summary, this thesis has revealed a relevant pathogenetic role of KDM1A as a pro-oncogenic molecule in CLL cells and their microenvironment. From this, novel treatment rationales for targeting KDM1A and its networks are to be derived.

6   References

1.   World Health Organisation. Latest global cancer data. International Agency for Research on Cancer. Published 2020. Accessed November 15, 2021. Availble from: https://www.iarc.who.int/news-events/latest-global-cancer-data-cancer-burden-rises-to-19-3-million-new-cases-and-10-0-million-cancer-deaths-in-2020/.

2.   Swerdlow SH, Campo E, Pileri SA, et al. The 2016 revision of the World Health Organization classification of lymphoid neoplasms. *Blood.* 2016;127(20):2375-2390. doi:10.1182/blood-2016-01-643569.

3.   Mukkamalla SKR, Taneja A, Malipeddi D, et al. Chronic Lymphocytic Leukemia. [Updated 2021 Oct 1]. In: StatPearls. Treasure Island (FL): StatPearls Publishing; Available from: https://www.ncbi.nlm.nih.gov/books/NBK470433/.

4.   Chronic Lymphocytic Leukemia - Cancer Stat Facts. Accessed July 29, 2022. Available from: https://seer.cancer.gov/statfacts/html/clyl.html.

5.   Hallek M. Chronic lymphocytic leukemia: 2020 update on diagnosis, risk stratification and treatment. *Am J Hematol.* 2019;94(11):1266-1287. doi:10.1002/ajh.25595.

6.   Smith A, Howell D, Patmore R, et al. Incidence of haematological malignancy by sub-type: a report from the Haematological Malignancy Research Network. *British Journal of Cancer.* 2011;105:1684-1692. doi:10.1038/bjc.2011.450.

7.   Slager SL, Benavente Y, Blair A, et al. Medical History, Lifestyle, Family History, and Occupational Risk Factors for Chronic Lymphocytic Leukemia/Small Lymphocytic Lymphoma: The InterLymph Non-Hodgkin Lymphoma Subtypes Project. *Journal of the National Cancer Institute Monographs.* 2014;(48). doi:10.1093/jncimonographs/lgu001.

8.   Cerhan JR, Slager SL; Familial predisposition and genetic risk factors for lymphoma. *Blood* 2015; 126 (20): 2265–2273. doi:https://doi.org/10.1182/blood-2015-04-5.

9.   Hallek M, Shanafelt TD, Eichhorst B. Chronic lymphocytic leukaemia. *The Lancet.* 2018;391(10129):1524-1537. doi:10.1016/S0140-6736(18)30422-7.

10.   Nieto WG, Almeida J, Romero A, et al. Increased frequency (12%) of circulating chronic lymphocytic leukemia–like B-cell clones in healthy subjects using a highly sensitive multicolor flow cytometry approach. *Blood.* 2009;114(1):33–37. doi:https://doi.org/10.1182/blood-2009-01-197368.

11.   Kikushige Y, Miyamoto T. Hematopoietic Stem Cell Aging and Chronic Lymphocytic Leukemia Pathogenesis Hematopoietic stem cell aging and chronic lymphocytic leukemia pathogenesis. *Int J Hematol.* 2014;100(4):335-340. doi:10.1007/s12185-014-1651-6.

12.   Iril C, Ozman R, Milio E, Ontserrat M. Chronic Lymphocytic Leukemia. *N Engl J Med.* 1995;33(16):1052-1057.

13.   Hallek M. Chronic lymphocytic leukemia: 2017 update on diagnosis, risk stratification, and treatment. *Am J Hematol.* 2017;92(9):946-965. doi:10.1002/ajh.24826

14.   Hallek M, Cheson BD, Catovsky D, et al. Guidelines for the diagnosis and treatment of chronic lymphocytic leukemia: a report from the International Workshop on Chronic Lymphocytic Leukemia updating the National Cancer Institute-Working Group 1996 guidelines. *Blood.* 2008;111(12):5446-56. doi:10.1182/blood-2007-06-093906.

15.   Moreau EJ, Matutes E, A'Hern RP, et al. Improvement of the chronic lymphocytic leukemia scoring system with the monoclonal antibody SN8 (CD79b). *Am J Clin Pathol.* 1997;108(4):378-82. doi:10.1093/ajcp/108.4.378.

16.   Ginaldi L, de Martinis M, Matutes E, et al. Levels of expression of CD19 and CD20 in chronic B cell leukaemias. *J Clin Pathol.* 1998;51:364-369. doi:10.1136/jcp.51.5.364.

17.   Palumbo GA, Parrinello N, Fargione G, et al. CD200 expression may help in differential diagnosis between mantle cell lymphoma and B-cell chronic lymphocytic leukemia. *Leuk Res.* 2009;33(9):1212-6. doi:10.1016/j.leukres.2009.01.017.

18. Döhner H, Stilgenbauer S, Benner A, et al. *Genomic Aberrations and Survival in Chronic Lymphocytic Leukemia*. N Engl J Med. 2000;343(26):1910-6. doi:10.1056/nejm200012283432602.

19. Frater JL, McCarron KF, Hammel JP, et al. Typical and atypical chronic lymphocytic leukemia differ clinically and immunophenotypically. *Am J Clin Pathol*. 2001;116(5):655-64. doi:10.1309/7Q1J-1AA8-DU4Q-PVLQ.

20. Hallek M, Cheson BD, Catovsky D, et al. Special Report iwCLL guidelines for diagnosis, indications for treatment, response assessment, and supportive management of CLL. *Blood.* 2018;131(25):2745–2760. doi:https://doi.org/10.1182/blood-2017-09-806398.

21. Rai KR, Sawitsky A, Cronkite EP, et al. Clinical Staging of Chronic Lymphocytic Leukemia. *Blood.* 1975;46(2):219-34. PMID: 1139039.

22. Binet JL, Auquier A, Dighiero G, et al. A new prognostic classification of chronic lymphocytic leukemia derived from a multivariate survival analysis. *Cancer*. 1981;48(1):198-206. doi:10.1002/1097-0142(19810701)48:1<198::AID-CNCR2820480131>3.0.CO;2-V.

23. Landau DA, Tausch E, Taylor-Weiner AN, et al. Mutations driving CLL and their evolution in progression and relapse. *Nature*. 2015;526(7574):525–530. doi:10.1038/nature15395.

24. International CLL-IPI working group T. An international prognostic index for patients with chronic lymphocytic leukaemia (CLL-IPI): a meta-analysis of individual patient data. *Lancet Oncol*. 2016;17(6):779-790. doi:10.1016/S1470-2045(16)30029-8.

25. von Tresckow J, Eichhorst B, Bahlo J, Hallek M. The treatment of chronic lymphatic leukemia. *Dtsch Arztebl Int.* 2019;116(4):41-46. doi:10.3238/arztebl.2019.0041.

26. Chronic Lymphocytic Leukemia (CLL) — Onkopedia. Accessed November 17, 2021. Available from: https://www.onkopedia-guidelines.info/en/onkopedia/guidelines/chronic-lymphocytic-leukemia-cll/@@guideline/html/index.html.

27. Eichhorst BF, Busch R, Stilgenbauer S, et al. First-line therapy with fludarabine compared with chlorambucil does not result in a major benefit for elderly patients with advanced chronic lymphocytic leukemia. *Blood*. 2009;114(16):3382-3391. doi:10.1182/BLOOD-2009-02-206185.

28. Small S, Ma S. Frontline Treatment for Chronic Lymphocytic Leukemia/Small Lymphocytic Lymphoma (CLL/SLL): Targeted Therapy vs. Chemoimmunotherapy. *Curr Hematol Malig Rep.* 2021;16:325-335. doi:10.1007/s11899-021-00637-1/Published.

29. Al-Sawaf O, Zhang C, Tandon M, et al. Venetoclax plus obinutuzumab versus chlorambucil plus obinutuzumab for previously untreated chronic lymphocytic leukaemia (CLL14): follow-up results from a multicentre, open-label, randomised, phase 3 trial. *Lancet Oncol*. 2020;21(9):1188-1200. doi:10.1016/S1470-2045(20)30443-5.

30. Kutsch N, Busch R, Bahlo J, et al. FCR front-line therapy and quality of life in patients with chronic lymphocytic leukemia. *Leuk Lymphoma*. 2017;58(2):399-407. doi:10.1080/10428194.2016.1190966.

31. Eichhorst B, Fink AM, Bahlo J, et al. First-line chemoimmunotherapy with bendamustine and rituximab versus fludarabine, cyclophosphamide, and rituximab in patients with advanced chronic lymphocytic leukaemia (CLL10): an international, open-label, randomised, phase 3, non-inferiority trial. *Lancet Oncol*. 2016;17(7):928-942. doi:10.1016/S1470-2045(16)30051-1.

32. Davila ML, Brentjens R. Chimeric antigen receptor therapy for chronic lymphocytic leukemia: what are the challenges? *Hematol Oncol Clin North Am*. 2013;27(2):341-353. doi:10.1016/j.hoc.2012.12.004.

33. Sharma S, Rai KR. Chronic lymphocytic leukemia (CLL) treatment: So many choices, such great options. *Cancer*. 2019;125(9):1432-1440. doi:10.1002/cncr.31931.

34. Rozman C, Montserrat E. Chronic lymphocytic leukemia. *N Engl J Med*. 1995;333(16):1052-7. doi:10.1056/NEJM199510193331606.

35. Stevenson FK, Caligaris-Cappio F. Chronic lymphocytic leukemia: revelations from the B-cell receptor. *Blood*. 2004;103(12):4389-95. doi:10.1182/blood-2003-12-4312.

36. Caligaris-Cappio F, Ghia P. Novel Insights in Chronic Lymphocytic Leukemia: Are We Getting Closer to Understanding the Pathogenesis of the Disease? *Journal of Clinical Oncology.* 2008;26(27):4497-4503. doi:10.1200/JCO.2007.15.4393.

37. Chiorazzi N, Rai KR, Ferrarini M. Chronic Lymphocytic Leukemia. *N Engl J Med*. 2005;352:804-15.

38. Hamblin TJ, Davis Z, Gardiner A, et al. Unmutated Ig V(H) genes are associated with a more aggressive form of chronic lymphocytic leukemia. *Blood*. 1999;94(6):1848-54. PMID: 10477713.

39. Rosenwald A, Alizadeh AA, Widhopf G, et al. Relation of gene expression phenotype to immunoglobulin mutation genotype in B cell chronic lymphocytic leukemia. *J Exp Med*. 2001;194(11):1639-1647. doi:10.1084/jem.194.11.1639.

40. Fabbri G, Dalla-Favera R. The molecular pathogenesis of chronic lymphocytic leukaemia. *Nat Rev Cancer*. 2016;16(3):145-62. doi:10.1038/nrc.2016.8.

41. Seifert M, Sellmann L, Bloehdorn J, et al. Cellular origin and pathophysiology of chronic lymphocytic leukemia. *J Exp Med*. 2012;209(12):2183-2198. doi:10.1084/jem.20120833.

42. Widhopf GF, Rassenti LZ, Toy TL, et al. Chronic lymphocytic leukemia B cells of more than 1% of patients express virtually identical immunoglobulins. *Blood*. 2004;104(8):2499-2504. doi:10.1182/blood-2004-03-0818.

43. Stamatopoulos K, Belessi C, Moreno C, et al. Over 20% of patients with chronic lymphocytic leukemia carry stereotyped receptors: Pathogenetic implications and clinical correlations. *Blood*. 2007;109(1):259-270. doi:10.1182/blood-2006-03-012948.

44. Dühren-von Minden M, Übelhart R, Schneider D, et al. Chronic lymphocytic leukaemia is driven by antigen-independent cell-autonomous signalling. *Nature*. 2012;(489):309–312. doi:10.1038/nature11309.

45. Sanchez ML, Almeida J, Gonzalez D, et al. Incidence and clinicobiologic characteristics of leukemic B-cell chronic lymphoproliferative disorders with more than one B-cell clone. *Blood*. 2003;102(8):2994-3002. doi:10.1182/blood-2003-01-0045.

46. Dagklis A, Fazi C, Sala C, et al. The Immunoglobulin Gene Repertoire of Low-Count CLL-Like MBL Is Different from CLL: Diagnostic Considerations and Implications for Clinical Monitoring. *Blood*. 2008;112(11):779-779. doi:10.1182/blood.v112.11.779.779.

47. Lanasa MC, Allgood SD, Volkheimer AD, et al. Single-cell analysis reveals oligoclonality among low-count monoclonal B-cell lymphocytosis. *Leukemia*. 2010;24(1):133-140. doi:10.1038/leu.2009.192.

48. Kikushige Y, Ishikawa F, Miyamoto T, et al. Article Self-Renewing Hematopoietic Stem Cell Is the Primary Target in Pathogenesis of Human Chronic Lymphocytic Leukemia. *Cancer Cell*. 2011;20(2):246-59. doi:10.1016/j.ccr.2011.06.029.

49. Zhang S, Kipps TJ. The Pathogenesis of Chronic Lymphocytic Leukemia. *Annu Rev Pathol*. 2014;9:103-18. doi:10.1146/annurev-pathol-020712-163955.

50. Han T, Ozer H, Sadamori N, et al. Prognostic Importance of Cytogenetic Abnormalities in Patients with Chronic Lymphocytic Leukemia. *N Engl J Med*. 1984;310(5):288-292. doi:10.1056/nejm198402023100504.

51. Ljungström V, Baliakas P. Prognostic and Predictive Implications of Cytogenetics and Genomics. *Hematol Oncol Clin North Am*. 2021;35(4):703-713. doi:10.1016/j.hoc.2021.04.002.

52. Bentz M, Huck K, du Manoir S, et al. Comparative genomic hybridization in chronic B-cell leukemias shows a high incidence of chromosomal gains and losses. *Blood*. 1995;85(12):3610-8. PMID: 7780145.

53. Haferlach C, Dicker F, Schnittger S, Kern W, Haferlach T. Comprehensive genetic characterization of CLL: a study on 506 cases analysed with chromosome banding analysis, interphase FISH, IgV H status and immunophenotyping. *Leukemia*. 2007;21:2442-2451. doi:10.1038/sj.leu.2404935.

54. Cuneo A, Rigolin GM, Bigoni R, et al. Chronic lymphocytic leukemia with 6qÀ shows distinct hematological features and intermediate prognosis. *Leukemia*. 2004;18:476-483. doi:10.1038/sj.leu.2403242.

55. Kostopoulou F, Gabillaud C, Chapiro E, et al. Gain of the short arm of chromosome 2 (2p gain) has a significant role in drug-resistant chronic lymphocytic leukemia. *Cancer Med*. 2019;8(6):3131-3141. doi:10.1002/CAM4.2123.

56. Chapiro E, Radford-Weiss I, Bastard C, et al. The most frequent t(14;19)(q32;q13)-positive B-cell malignancy corresponds to an aggressive subgroup of atypical chronic lymphocytic leukemia. *Leukemia*. 2008;22(11):2123-2127. doi:10.1038/leu.2008.102.

57. Calin GA, Dumitru CD, Shimizu M, et al. Frequent deletions and down-regulation of micro- RNA genes miR15 and miR16 at 13q14 in chronic lymphocytic leukemia. *Proc Natl Acad Sci U S A*. 2002;99(24):15524-15529. doi:10.1073/pnas.242606799.

58. Dal Bo M, Rossi FM, Rossi D, et al. 13q14 Deletion size and number of deleted cells both influence prognosis in chronic lymphocytic leukemia. *Genes Chromosomes and Cancer*. 2011;50(8):633-643. doi:10.1002/gcc.20885.

59. Klein U, Lia M, Crespo M, et al. The DLEU2/miR-15a/16-1 cluster controls B cell proliferation and its deletion leads to chronic lymphocytic leukemia. *Cancer Cell*. 2010;17(1):28-40. doi:10.1016/j.ccr.2009.11.019.

60. Zenz T, Benner A, Döhner H, Stilgenbauer S. Chronic lymphocytic leukemia and treatment resistance in cancer: The role of the p53 pathway. *Cell Cycle*. 2008;7(24):3810-3814. doi:10.4161/cc.7.24.7245.

61. Puente XS, Pinyol M, Quesada V, et al. Whole-genome sequencing identifies recurrent mutations in chronic lymphocytic92nleukaemia. *Nature*. 2011;475(7354):101-5. doi:10.1038/nature10113.

62. Lionetti M, Fabris S, Cutrona G, et al. High-throughput sequencing for the identification of NOTCH1 mutations in early stage chronic lymphocytic leukaemia: Biological and clinical implications. *Br J Haematol*. 2014;165(5):629-639. doi:10.1111/BJH.12800.

63. Balatti V, Bottoni A, Palamarchuk A, et al. NOTCH1 mutations in CLL associated with trisomy 12. *Blood*. 2012;119(2):329-331. doi:10.1182/BLOOD-2011-10-386144.

64. Ljungström V, Baliakas P. Prognostic and Predictive Implications of Cytogenetics and Genomics. *Hematology/Oncology Clinics of North America*. 2021;35(4):703-713. doi:10.1016/j.hoc.2021.04.002.

65. Wahl MC, Will CL, Lührmann R. The spliceosome: design principles of a dynamic RNP machine. *Cell*. 2009;136(4):701-18. doi:10.1016/j.cell.2009.02.009.

66. Strefford JC, Sutton LA, Baliakas P, et al. Distinct patterns of novel gene mutations in poor-prognostic stereotyped subsets of chronic lymphocytic leukemia: the case of SF3B1 and subset #2. *Leukemia*. 2013;27:2196-2199. doi:10.1038/leu.2013.98.

67. Hanahan D, Weinberg RA. Hallmarks of cancer: the next generation. *Cell*. 2011;144(5):646-74. doi:10.1016/j.cell.2011.02.013.

68. Choi MY, Kashyap MK, Kumar D. The chronic lymphocytic leukemia microenvironment: Beyond the B-cell receptor. *Best Pract Res Clin Haematol*. 2016;29(1):40-53. doi:10.1016/j.beha.2016.08.007.

69. Stevenson FK, Krysov S, Davies AJ, Steele AJ, Packham G. B-cell receptor signaling in chronic lymphocytic leukemia. *Blood*. 2011;118(16):4313-4320. doi:10.1182/BLOOD-2011-06-338855.

70. Burger JA, Chiorazzi N. B cell receptor signaling in chronic lymphocytic leukemia. *Trends Immunol.* 2013;34(12):592-601. doi:10.1016/j.it.2013.07.002.

71. Agathangelidis A, Darzentas N, Hadzidimitriou A, et al. Stereotyped B-cell receptors in one-third of chronic lymphocytic leukemia: a molecular classification with implications for targeted therapies. *Blood*. 2012;119:4467-4475. doi:10.1182/blood-2011.

72. Iacovelli S, Hug E, Bennardo S, et al. Two types of BCR interactions are positively selected during leukemia development in the Eµ-TCL1 transgenic mouse model of CLL. *Blood*. 2015;125(10):1578-1588. doi:10.1182/BLOOD-2014-07-587790.

73. Young RM, Staudt LM. Targeting pathological B cell receptor signalling in lymphoid malignancies. *Nat Rev Drug Discov*. 2013;12(3):229-43. doi:10.1038/nrd3937.

74. Chen L, Huynh L, Apgar J, et al. ZAP-70 enhances IgM signaling independent of its kinase activity in chronic lymphocytic leukemia. *Blood*. 2008;111(5):2685-2692. doi:10.1182/blood-2006-12-062265.

75. Deaglio S, Vaisitti T, Bergui L, et al. CD38 and CD100 lead a network of surface receptors relaying positive signals for B-CLL growth and survival. *Blood*. 2005;105(8):3042-50. doi:10.1182/blood-2004-10-3873.

76. Poggi A, Prevosto C, Catellani S, Rocco I, Garuti A, Zocchi MR. Engagement of CD31 delivers an activating signal that contributes to the survival of chronic lymphocytic leukaemia cells. *Br J Haematol*. 2010;151(3):252-264. doi:10.1111/J.1365-2141.2010.08343.X.

77. Burger JA, Tsukada N, Burger M, et al. Blood-derived nurse-like cells protect chronic lymphocytic leukemia B cells from spontaneous apoptosis through stromal cell-derived factor-1. *Blood*. 2000;96(8):2655-63. PMID: 11023495.

78. Filip AA, Ciseł B, Koczkodaj D, et al. Circulating microenvironment of CLL: Are nurse-like cells related to tumor-associated macrophages? *Blood Cells Mol Dis.* 2013;50(4):263-270. doi:10.1016/J.BCMD.2012.12.003.

79. Cols M, Barra CM, He B, et al. Stromal endothelial cells establish a bidirectional crosstalk with chronic lymphocytic leukemia cells through the TNF-related factors BAFF, APRIL, and CD40L. *J Immunol*. 2012;188(12):6071-83. doi:10.4049/jimmunol.1102066.

80. Seiffert M, Schulz A, Ohl S, et al. CD14 is a novel monocyte-derived survival factor for chronic lymphocytic leukemia cells, which is induced by CLL cells in vitro and present at abnormally high levels in vivo. *Blood*. 2010;116(20):4223-30. doi:10.1182/blood-2010-05-284505.

81. Purroy N, Abrisqueta P, Carabia J, et al. Co-culture of primary CLL cells with bone marrow mesenchymal cells, CD40 ligand and CpG ODN promotes proliferation of chemoresistant CLL cells phenotypically comparable to those proliferating in vivo. *Oncotarget*. 2014;6(10):7632-7643. doi:10.18632/ONCOTARGET.2939.

82. Jitschin R, Braun M, Qorraj M, et al. Stromal cell–mediated glycolytic switch in CLL cells involves Notch-c-Myc signaling. *Blood*. 2015;125(22):3432-3436. doi:10.1182/BLOOD-2014-10-607036.

83. Burger JA, Burger M, Kipps TJ. Chronic Lymphocytic Leukemia B Cells Express Functional CXCR4 Chemokine Receptors That Mediate Spontaneous Migration Beneath Bone Marrow Stromal Cells. *Blood*. 1999;94(11):3658-3667. doi:10.1182/BLOOD.V94.11.3658.

84. Paggetti J, Haderk F, Seiffert M, et al. Exosomes released by chronic lymphocytic leukemia cells induce the transition of stromal cells into cancer-associated fibroblasts. *Blood*. 2015;126(9):1106-1117. doi:10.1182/BLOOD-2014-12-618025.

85. Bagnara D, Kaufman MS, Calissano C, et al. A novel adoptive transfer model of chronic lymphocytic leukemia suggests a key role for T lymphocytes in the disease. *Blood*. 2011;117(20):5463-5472. doi:10.1182/BLOOD-2010-12-324210.

86. Riches JC, Davies JK, McClanahan F, et al. T cells from CLL patients exhibit features of T-cell exhaustion but retain capacity for cytokine production. *Blood*. 2013;121(9):1612-1621. doi:10.1182/BLOOD-2012-09-457531.

87. McClanahan F, Hanna B, Miller S, et al. PD-L1 checkpoint blockade prevents immune dysfunction and leukemia development in a mouse model of chronic lymphocytic leukemia. *Blood*. 2015;126(2):203-211. doi:10.1182/blood-2015-01-622936.

88. Kay NE, Zarling J. Restoration of Impaired Natural Killer Cell Activity of B-Chronic Lymphocytic Leukemia Patients by Recombinant Interleu kin-2. *Am J Hematol*. 1987;24(2):161-167. doi:10.1002/ajh.2830240207.

89. Jitschin R, Braun M, Büttner M, et al. CLL-cells induce IDOhi CD14+HLA-DRlo myeloid-derived suppressor cells that inhibit T-cell responses and promote T Regs. *Blood*. 2014;124(5):750-760. doi:10.1182/blood-2013-12-546416.

90. Fu TB, Virgilio L, Narducci MG, et al. Characterization and localization of the TCL-1 oncogene product. *Cancer Res*. 1994;54(24):6297-301. PMID: 7987816.

91. du Bois GC, Song SP, Kulikovskaya I, et al. Purification and characterization of recombinant forms of TCL-1 and MTCP-1 proteins. *Protein Expr Purif*. 1998;12(2):215-225. doi:10.1006/prep.1997.0822.

92. Fu ZQ, Du Bois GC, Song SP, et al. Crystal structure of MTCP-1: implications for role of TCL-1 and MTCP-1 in T cell malignancies. *Proc Natl Acad Sci U S A*. 1998;95(7):3413-3418. doi:10.1073/pnas.95.7.3413.

93. Petock JM, Torshin IY, Wang YF, et al. Crystal structures of Tcl1 family oncoproteins and their conserved surface features. *ScientificWorldJournal*. 2002;2:1876-1884. doi:10.1100/tsw.2002.826.

94. Pekarsky Y, Hallas C, Russo G,et al. Abnormalities at 14q32.1 in T Cell Malignancies Involve Two Oncogenes. *Proc Natl Acad Sci U S A.* 1999;96(6):2949-2951. doi:10.1100/tsw.2002.826.

95. Stern MH, Soulier J, Rosenzwajg M, et al. MTCP-1: A novel gene on the human chromosome Xq28 translocated to the T cell receptor α/δ locus in mature T cell proliferations. *Oncogene*. 1993;8(9):2475-2483.

96. Virgilio L, Narducci MG, Isobe M, Billips LG, et al. Identification of the TCL1 Gene Involved in T-Cell Malignancies. *Proc Natl Acad Sci U S A*. 1994;91(26):12530–12534.

97. Noguchi M, Ropars V, Roumestand C, et al. Proto-oncogene TCL1: more than just a coactivator for Akt. *FASEB J*. 2007;21:2273-2284. doi:10.1096/fj.06-7684rev.

98. Auguin D, Barthe P, Royer C, et al. Structural basis for the co-activation of protein kinase B by T-cell leukemia-1 (TCL1) family proto-oncoproteins. *J Biol Chem*. 2004;279(34):35890-902. doi:10.1074/jbc.M400364200.

99. Künstle G, Laine J, Pierron G, et al. Identification of Akt Association and Oligomerization Domains of the Akt Kinase Coactivator TCL1. *Mol Cell Biol*. 2002;22(5):1513-1525. doi:10.1128/MCB.22.5.1513-1525.2002.

100. Pekarsky Y, Hallas C, Croce CM. The Role of TCL1 in Human T-Cell Leukemia. *Oncogene*. 2001;20:5638–5643. doi:https://doi.org/10.1038/sj.onc.1204596.

101. Miyazaki T, Miyazaki S, Ashida M, et al. Functional Analysis of Tcl1 Using Tcl1-Deficient Mouse Embryonic Stem Cells. *PLoS ONE*. 2013;8(8):71645. doi:10.1371/journal.pone.0071645.

102. Stachelscheid J, Jiang Q, Herling M. The Modes of Dysregulation of the Proto-Oncogene T-Cell Leukemia/Lymphoma 1A. *Cancers*. 2021;13(21):5455. doi:10.3390/CANCERS13215455.

103. Narducci MG, Fiorenza MT, Kang SM, et al. TCL1 Participates in Early Embryonic Development and Is Overexpressed in Human Seminomas. *Proc Natl Acad Sci U S A*. 2002;99(18):11712-11717. doi:https://doi.org/10.1073/pnas.182412399 2002.

104. Said JW, Hoyer KK, French SW, et al. TCL1 Oncogene Expression in B Cell Subsets from Lymphoid Hyperplasia and Distinct Classes of B Cell Lymphoma. *Lab Invest*. 2001;81(4):555-64. doi:10.1038/labinvest.3780264.

105. Herling M, Patel KA, Hsi ED, et al. TCL1 in B-cell tumors retains its normal B-cell pattern of regulation and is a marker of differentiation stage. *Am J Surg Pathol*. 2007;31(7):1123-1129. doi:10.1097/PAS.0b013e31802e2201.

106. Narducci MG, Pescarmona E, Lazzeri C, et al. Regulation of TCL1 Expression in B-and T-Cell Lymphomas and Reactive Lymphoid Tissues*. Cancer Res*. 2000;60:2095-2100. PMID:10786666.

107. Hoyer KK, Herling M, Bagrintseva K, et al. T Cell Leukemia-1 Modulates TCR Signal Strength and IFN-γ Levels through Phosphatidylinositol 3-Kinase and Protein Kinase C Pathway Activation. *J Immunol*. 2005;175(2):864-873. doi:10.4049/jimmunol.175.2.864.

108. Herling M, Patel KA, Teitell MA, et al. High TCL1 expression and intact T-cell receptor signaling define a hyperproliferative subset of T-cell prolymphocytic leukemia. *Blood*. 2008;111(1):328-37. doi:10.1182/blood-2007-07-101519.

109. Patil P, Cieslak A, Bernhart SH, et al. Reconstruction of rearranged T-cell receptor loci by whole genome and transcriptome sequencing gives insights into the initial steps of T-cell prolymphocytic leukemia. *Genes Chromosomes and Cancer*. 2020;59(4):261-267. doi:10.1002/gcc.22821.

110. Aggarwal M, Villuendas R, Gomez G, et al. TCL1A expression delineates biological and clinical variability in B-cell lymphoma. *Mod Pathol*. 2009;22:206-215. doi:10.1038/modpathol.2008.148.

111. Herling M, Patel KA, Weit N, et al. High TCL1 levels are a marker of B-cell receptor pathway responsiveness and adverse outcome in chronic lymphocytic leukemia. *Blood*. 2009;114(21):4675-4686. doi:10.1182/blood-2009-03-208256.

112. Bichi R, Shinton SA, Martin ES, et al. Human Chronic Lymphocytic Leukemia Modeled in Mouse by Targeted TCL1 Expression. *Proc Natl Acad Sci U S A*. 2002;99(10):6955-60. doi:10.1073/pnas.102181599.

113. Virgilio L, Lazzeri C, Bichi R, et al. Deregulated Expression of TCL1 Causes T Cell Leukemia in Mice. *Proc Natl Acad Sci U S A*. 1998;95(7):3885-9. doi:10.1073/pnas.95.7.3885.

114. Hoyer KK, French SW, Turner DE, et al. Dysregulated TCL1 promotes multiple classes of mature B cell lymphoma. *Proc Natl Acad Sci U S A*. 2002;99(22):14392-14397. doi:10.1073/pnas.212410199.

115. Simonetti G, Teresa M, Bertilaccio S, et al. Perspectives Mouse models in the study of chronic lymphocytic leukemia pathogenesis and therapy. *Blood*. 2014;124(7):1010-9. doi:10.1182/blood-2014-05-577122.

116. Amini S, Fathi F, Mobalegi J, Sofimajidpour H, Ghadimi T. The expressions of stem cell markers: Oct4, Nanog, Sox2, nucleostemin, Bmi, Zfx, Tcl1, Tbx3, Dppa4, and Esrrb in bladder, colon, and prostate cancer, and certain cancer cell lines. *Anat Cell Biol*. 2014;47(1):1-11. doi:10.5115/acb.2014.47.1.1.

117. Laine J, Künstle G, Obata T, Sha M, Noguchi M. The protooncogene TCL1 is an Akt kinase coactivator. *Mol Cell*. 2000;6(2):395-407. doi:10.1016/S1097-2765(00)00039-3.

118. Gaudio E, Spizzo R, Paduano F, et al. Tcl1 interacts with Atm and enhances NF- kB activation in hematologic malignancies. *Blood*. 2012;119(1):180-188. doi:10.1182/blood-2011-08-374561.

119. Pekarsky Y, Palamarchuk A, Maximov V, et al. Tcl1 Functions as a Transcriptional Regulator and Is Directly Involved in the Pathogenesis of CLL. *Proc Natl Acad Sci U S A*. 2008;105(50):19643-8. doi:10.1073/pnas.0810965105.

120. Ameyar M, Wisniewska M, Weitzman JB. A role for AP-1 in apoptosis: The case for and against. *Biochimie*. 2003;85(8):747-752. doi:10.1016/j.biochi.2003.09.006.

121. Matoba R, Niwa H, Masui S, et al. Dissecting Oct3/4-Regulated Gene Networks in Embryonic Stem Cells by Expression Profiling. *PLoS ONE*. 2006;1(1):26. doi:10.1371/journal.pone.0000026.

122. Ivanova N, Dobrin R, Lu R, et al. Dissecting self-renewal in stem cells with RNA interference. *Nature*. 2006;442(7102):533-8. doi:10.1038/nature04915.

123. Jiang J, Chan YS, Loh YH, et al. A core Klf circuitry regulates self-renewal of embryonic stem cells. *Nat Cell Biol*. 2008;10(3):353-60. doi:10.1038/ncb1698.

124. Hiromura M, Suizu F, Narita M, et al. Identification of nerve growth factor-responsive element of the TCL1 promoter as a novel negative regulatory element. *J Biol Chem*. 2006;281(38):27753-64. doi:10.1074/jbc.M602420200.

125. Pekarsky Y, Santanam U, Cimmino A, et al. Tcl1 Expression in Chronic Lymphocytic Leukemia Is Regulated by miR-29 and miR-181. *Cancer Res*. 2006;66(24):11590-3. doi:10.1158/0008-5472.CAN-06-3613.

126. Efanov A, Zanesi N, Nazaryan N, et al. CD5+CD23+ leukemic cell populations in TCL1 transgenic mice show significantly increased proliferation and Akt phosphorylation. *Leukemia*. 2010;24(5):970-975. doi:10.1038/leu.2010.46.

127. Cardinaud B, Moreilhon C, Marcet B, et al. miR-34b/miR-34c: a regulator of TCL1 expression in 11q- chronic lymphocytic leukaemia? *Leukemia*. 2009;23(11):2174-7. doi:10.1038/leu.2009.125.

128. Balatti V, Rizzotto L, Miller C, et al. TCL1 targeting miR-3676 is codeleted with tumor protein p53 in chronic lymphocytic leukemia. *Proc Natl Acad Sci U S A*. 2015;112(7):2169-74. doi:10.1073/pnas.1500010112.

129. Sivina M, Hartmann E, Vasyutina E, et al. Stromal cells modulate TCL1 expression, interacting AP-1 components and TCL1-targeting micro-RNAs in chronic lymphocytic leukemia. *Leukemia*. 2012;26:1812-1820. doi:10.1038/leu.2012.63.

130. Russo G, Isobe M, Gatti R, et al. Molecular analysis of a t(14;14) translocation in leukemic T-cells of an ataxia telangiectasia patient. *Proc Natl Acad Sci U S A*. 1989;86(2):602-6. doi:10.1073/pnas.86.2.602.

131. Virgilio L, ISOBEt M, Grazia Narducci M, et al. Chromosome Walking on the TCLI Locus Involved in T-Cell Neoplasia. *Proc Natl Acad Sci U S A*. 1993;90(20):9275-9279.

132. Pekarsky Y, Koval A, Hallas C, et al. Tcl1 Enhances Akt Kinase Activity and Mediates Its Nuclear Translocation. *Proc Natl Acad Sci U S A*. 2000;97(7):3028-33. doi:10.1073/pnas.040557697.

133. Palamarchuk A, Yan PS, Zanesi N, et al. Tcl1 protein functions as an inhibitor of de novo DNA methylation in B-cell chronic lymphocytic leukemia (CLL). *Proc Natl Acad Sci U S A*. 2012;109(7):2555-60. doi:10.1073/pnas.1200003109.

134. Yuille MR, Condie A, Stone EM, et al. TCL1 is activated by chromosomal rearrangement or by hypomethylation. *Genes Chromosomes Cancer*. 2001;30(4):336-341. doi:10.1002/gcc.1099.

135. Loh YH, Zhang W, Chen X, et al. Jmjd1a and Jmjd2c histone H3 Lys 9 demethylases regulate self-renewal in embryonic stem cells. *Genes Dev*. 2007;21(20):2545-57. doi:10.1101/gad.1588207.

136. Yi F, Pereira L, Merrill BJ. Tcf3 Functions as a Steady State Limiter of Transcriptional Programs of Mouse Embryonic Stem Cell Self Renewal. *Stem Cells*. 2008;26(8):1951-60. doi:10.1634/stemcells.2008-0229.

137. Dawson MA, Kouzarides T. Cancer Epigenetics: From Mechanism to Therapy. *Cell*. 2012;150(1):12-27. doi:10.1016/J.CELL.2012.06.013.

138. STANCHEVA, I. Epigenetics. Eds. C. D. Allis, T. Jenuwein, D. Reinberg & M.-L. Caparros. Cold Spring Harbor Laboratory Press. *Genetical Research*. 2007;89(2):124-125. doi:10.1017/S0016672307008750.

139. Klutstein M, Nejman D, Greenfield R, Cedar H. DNA Methylation in Cancer and Aging. *Cancer Research*. 2016;76(12):3446-3450. doi:10.1158/0008-5472.CAN-15-3278.

140. Quagliano A, Gopalakrishnapillai A, Barwe SP. Understanding the Mechanisms by Which Epigenetic Modifiers Avert Therapy Resistance in Cancer. *Front Oncol*. 2020;10:992. doi:10.3389/fonc.2020.00992.

141. Baylin SB, Jones PA. A decade of exploring the cancer epigenome - biological and translational implications. *Nature reviews Cancer*. 2011;11(10):726-734. doi:10.1038/NRC3130.

142. Schones DE, Zhao K. Genome-wide approaches to studying chromatin modifications. *Nature Reviews Genetics*. 2008;9(3):179-191. doi:10.1038/nrg2270.

143. Creyghton MP, Cheng AW, Welstead GG, et al. Histone H3K27ac separates active from poised enhancers and predicts developmental state. *Proc Natl Acad Sci U S A*. 2010;107(50):21931-21936. doi:10.1073/PNAS.1016071107/-/DCSUPPLEMENTAL.

144. Skvortsova K, Stirzaker C, Taberlay P. The DNA methylation landscape in cancer. *Essays in Biochemistry*. 2019;63(6):797. doi:10.1042/EBC20190037.

145. Allfrey VG, Faulkner R, Mirsky AE. Acetylation And Methylation Of Histones And Their Possible Role In The Regulation Of Rna Synthesis. *Proc Natl Acad Sci U S A*. 1964;51(5):786-94. doi:10.1073/pnas.51.5.786.

146. Audia JE, Campbell RM. Histone modifications and cancer. Cold Spring Harbor Perspectives in Biology. 2016;8(4). doi:10.1101/cshperspect.a019521.

147. Cerbo V di, Schneider R. Cancers with wrong HATs: the impact of acetylation. *Briefings in Functional Genomics*. 2013;12(3):231-243. doi:10.1093/bfgp/els065.

148. Fraga MF, Ballestar E, Villar-Garea A, et al. Loss of acetylation at Lys16 and trimethylation at Lys20 of histone H4 is a common hallmark of human cancer. *Nature Genetics.* 2005;37(4):391-400. doi:10.1038/ng1531.

149. Seligson DB, Horvath S, Shi T, et al. Global histone modification patterns predict risk of prostate cancer recurrence. *Nature*. 2005;435(7046):1262-1266. doi:10.1038/nature03672.

150. Bannister AJ, Kouzarides T. Regulation of chromatin by histone modifications. *Cell Res.* 2011;21(3):381-95. doi:10.1038/cr.2011.22.

151. Blum R. Stepping inside the realm of epigenetic modifiers. *Biomolecular Concepts*. 2015;6(2):119-136. doi:10.1515/bmc-2015-0008.

152. Zhao Z, Shilatifard A. Epigenetic modifications of histones in cancer. *Genome Biology*. 2019;20(1). doi:10.1186/s13059-019-1870-5.

153. Bannister AJ, Schneider R, Kouzarides T. Histone methylation: Dynamic or static? Cell. 2002;109(7):801-806. doi:10.1016/S0092-8674(02)00798-5.

154. Chen SS, Raval A, Johnson AJ, et al. Epigenetic changes during disease progression in a murine model of human chronic lymphocytic leukemia. *Proc Natl Acad Sci U S A*. 2009;106(32):13433-13438. doi:10.1073/pnas.0906455106.

155. Kulis M, Heath S, Bibikova M, et al. Epigenomic analysis detects widespread gene-body DNA hypomethylation in chronic lymphocytic leukemia. *Nature Genetics*. 2012;44(11):1236-42. doi:10.1038/ng.2443.

156. Landau DA, Clement K, Ziller MJ, et al. Locally Disordered Methylation Forms the Basis of Intratumor Methylome Variation in Chronic Lymphocytic Leukemia. *Cancer Cell*. 2014;26(6):813-825. doi:10.1016/j.ccell.2014.10.012.

157. Oakes CC, Seifert M, Assenov Y, et al. DNA methylation dynamics during B cell maturation underlie a continuum of disease phenotypes in chronic lymphocytic leukemia. *Nature Genetics.* 2016;48(3):253-264. doi:10.1038/ng.3488.

158. Cahill N, Bergh AC, Kanduri M, et al. 450K-array analysis of chronic lymphocytic leukemia cells reveals global DNA methylation to be relatively stable over time and similar in resting and proliferative compartments. *Leukemia*. 2013;27:150-158. doi:10.1038/leu.2012.245.

159. Raval A, Tanner SM, Byrd JC, et al. Downregulation of Death-Associated Protein Kinase 1 (DAPK1) in Chronic Lymphocytic Leukemia. *Cell*. 2007;129(5):879-890. doi:10.1016/j.cell.2007.03.043.

160. Claus R, Lucas DM, Ruppert AS, et al. Validation of ZAP-70 methylation and its relative significance in predicting outcome in chronic lymphocytic leukemia. *Blood.* 2014;124(1):42-48. doi:10.1182/blood-2014-02-555722.

161. Zhang L. Differential expression of histone post-translational modifications in acute myeloid and chronic lymphocytic leukemia determined by high-pressure liquid chromatography and mass spectrometry. *Journal of the American Society for Mass Spectrometry.* 2004;(15):77-86. doi:10.1067/j.jams.2003.10.001.

162. Singh R, Harshman SW, Ruppert AS, et al. Proteomic profiling identifies specific histone species associated with leukemic and cancer cells. *Clin Proteom*. 2014;12:22. doi:10.1186/s12014-015-9095-4.

163. Rendeiro AF, Schmidl C, Strefford JC, et al. Chromatin accessibility maps of chronic lymphocytic leukaemia identify subtype-specific epigenome signatures and transcription regulatory networks. *Nat. Commun*. 2016;7:11938. doi:10.1038/ncomms11938.

164. Beekman R, Chapaprieta V, Russiñol N, et al. The reference epigenome and regulatory chromatin landscape of chronic lymphocytic leukemia. *Nature Medicine*. 2018;24(6):868-880. doi:10.1038/s41591-018-0028-4.

165. Mallm J, Iskar M, Ishaque N, et al. Linking aberrant chromatin features in chronic lymphocytic leukemia to transcription factor networks. *Molecular Systems Biology*. 2019;15(5):1-20. doi:10.15252/msb.20188339.

166. van Damme M, Crompot E, Meuleman N, et al. Global histone deacetylase enzymatic activity is an independent prognostic marker associated with a shorter overall survival in chronic lymphocytic leukemia patients. *Epigenetics*. 2014;9(10):1374-1381. doi:10.4161/15592294.2014.969628.

167. Xanthopoulos C, Kostareli E. Advances in Epigenetics and Epigenomics in Chronic Lymphocytic Leukemia. *Current Genetic Medicine Reports*. 2019;7(4):214-226. doi:10.1007/s40142-019-00178-3.

168. Zhou K, Zhang Q, Liu Y, et al. Aberrant histone modification in CDI9 + B cells of patients with chronic lymphocytic leukemia. *OncoTargets and Therapy*. 2017;10:1173-1179. doi:10.2147/OTT.S121301.

169. Parker H, Rose-Zerilli MJJ, Larrayoz M, et al. Genomic disruption of the histone methyltransferase SETD2 in chronic lymphocytic leukaemia. *Leukemia*. 2016;30(11):2179-2186. doi:10.1038/LEU.2016.134.

170. Scialdone A, Hasni MS, Damm JK, Lennartsson A, Gullberg U, Drott K. The HDAC inhibitor valproate induces a bivalent status of the CD20 promoter in CLL patients suggesting distinct epigenetic regulation of CD20 expression in CLL in vivo. *Oncotarget*. 2017;8(23):37409-37422. doi:10.18632/ONCOTARGET.16964.

171. Maharaj K, Powers JJ, Achille A, et al. Silencing of HDAC6 as a therapeutic target in chronic lymphocytic leukemia. *Blood Adv*. 2018;2(21):3012-3024. doi:10.1182/bloodadvances.2018020065.

172. Papakonstantinou N, Ntoufa S, Chartomatsidou E, et al. The histone methyltransferase EZH2 as a novel prosurvival factor in clinically aggressive chronic lymphocytic leukemia. *Oncotarget*. 2016;7(24):35946-35959. doi:10.18632/ONCOTARGET.9371.

173. Chartomatsidou E, Ntoufa S, Kotta K, et al. Inhibition of EZH2 and immune signaling exerts synergistic antitumor effects in chronic lymphocytic leukemia. *Blood Adv*. 2019;3(12):1891-1896. doi:10.1182/BLOODADVANCES.2018030262.

174. Cuthbert GL, Daujat S, Snowden AW, et al. Histone deimination antagonizes arginine methylation. *Cell.* 2004;118(5):545-553. doi:10.1016/j.cell.2004.08.020.

175. Wang Y, Wysocka J, Sayegh J, et al. Human PAD4 Regulates Histone Arginine Methylation Levels via Demethylimination. *Science*. 2004;306(5694):279-83. doi:10.1126/science.1101400.

176. Chang B, Chen Y, Zhao Y, Bruick RK. JMJD6 is a histone arginine demethylase. *Science*. 2007;318(5849):444-7. doi:10.1126/science.1145801.

177. Shi Y, Lan F, Matson C, et al. Histone Demethylation Mediated by the Nuclear Amine Oxidase Homolog LSD1. *Cell*. 2004;119(7):941-953. doi:10.1016/J.CELL.2004.12.012.

178. Perillo B, Tramontano A, Pezone A, et al. LSD1: more than demethylation of histone lysine residues. *Experimental & Molecular Medicine*. 2020;52(12):1936-1947. doi:10.1038/s12276-020-00542-2.

179. Aravind L, Iyer LM. The SWIRM domain: a conserved module found in chromosomal proteins points to novel chromatin-modifying activities. *Genome Biol*. 2002;3(8):research0039.1. doi:10.1186/GB-2002-3-8-RESEARCH0039.

180. Chen Y, Yang Y, Wang F, et al. Crystal structure of human histone lysine-specific demethylase 1 (LSD1). *Proc Natl Acad Sci U S A*. 2006;103(38):13956-13961. doi:10.1073/PNAS.0606381103.

181. Gu F, Lin Y, Wang Z, et al. Biological roles of LSD1 beyond its demethylase activity. *Cell Mol Life Sci*. 2020;77(17):3341-3350. doi:10.1007/S00018-020-03489-9.

182. Stavropoulos P, Blobel G, Hoelz A. Crystal structure and mechanism of human lysine-specific demethylase-1. *Nature Structural & Molecular Biology.* 2006;13(7):626-632. doi:10.1038/nsmb1113.

183. Peng B, Wang J, Hu Y, et al. Modulation of LSD1 phosphorylation by CK2/WIP1 regulates RNF168-dependent 53BP1 recruitment in response to DNA damage. *Nucleic Acids Research*. 2015;43(12):5936. doi:10.1093/NAR/GKV528.

184. Metzger E, Willmann D, McMillan J, et al. Assembly of methylated KDM1A and CHD1 drives androgen receptor–dependent transcription and translocation. *Nature Structural & Molecular Biology 2016 23:2*. 2016;23(2):132-139. doi:10.1038/nsmb.3153.

185. Saleque S, Kim J, Rooke HM, Orkin SH. Epigenetic Regulation of Hematopoietic Differentiation by Gfi-1 and Gfi-1b Is Mediated by the Cofactors CoREST and LSD1. *Mol Cell*. 2007;27(4):562-572. doi:10.1016/J.MOLCEL.2007.06.039.

186. Shi YJ, Matson C, Lan F, Iwase S, Baba T, Shi Y. Regulation of LSD1 Histone Demethylase Activity by Its Associated Factors. *Mol Cell*. 2005;19(6):857-864. doi:10.1016/J.MOL-CEL.2005.08.027.

187. Majello B, Gorini F, Saccà CD, Amente S. Expanding the Role of the Histone Lysine-Specific Demethylase LSD1 in Cancer. *Cancers*. 2019;11(3):324. doi:10.3390/CANCERS11030324.

188. Forneris F, Binda C, Battaglioli E, et al. LSD1: oxidative chemistry for multifaceted functions in chromatin regulation. *Trends Biochem Sci*. 2008;33(4):181-189. doi:10.1016/j.tibs.2008.01.003.

189. Lan F, Nottke AC, Shi Y. Mechanisms involved in the regulation of histone lysine demethylases. *Curr Opin Cell Biol*. 2008;20(3):316. doi:10.1016/J.CEB.2008.03.004.

190. Metzger E, Wissmann M, Yin N, et al. LSD1 demethylates repressive histone marks to promote androgen-receptor-dependent transcription. *Nature*. 2005;437(7057):436-9. doi:10.1038/nature04020.

191. Perillo B, Ombra MN, Bertoni A, et al. DNA oxidation as triggered by H3K9me2 demethylation drives estrogen-induced gene expression. *Science*. 2008;319(5860):202-206. doi:10.1126/SCI-ENCE.1147674.

192. Wang J, Telese F, Tan Y, et al. LSD1n is an H4K20 demethylase regulating memory formation via transcriptional elongation control. *Nat Neurosci*. 2015;18(9):1256-1264. doi:10.1038/nn.4069.

193. Hosseini A. A comprehensive review of lysine-specific demethylase 1 and its roles in cancer. *Epigenomics*. 2017;9(8):1123-1142. doi:10.2217/epi-2017-0022.

194. Han X, Gui B, Xiong C, et al. Destabilizing LSD1 by Jade-2 Promotes Neurogenesis: An Antibraking System in Neural Development. *Mol Cell*. 2014;55(3):482-494. doi:10.1016/J.MOL-CEL.2014.06.006.

195. Peng B, Shi R, Jiang W, et al. Phosphorylation of LSD1 by PLK1 promotes its chromatin release during mitosis. *Cell & Bioscience*. 2017;7:15. doi:10.1186/s13578-017-0142-x.

196. Feng J, Xu G, Liu J, et al. Phosphorylation of LSD1 at Ser112 is crucial for its function in induction of EMT and metastasis in breast cancer. *Breast Cancer Res and Treatment*. 2016;159(3):443-456. doi:10.1007/S10549-016-3959-9.

197. Luo H, Shenoy AK, Li X, et al. MOF Acetylates the Histone Demethylase LSD1 to Suppress Epithelial-to-Mesenchymal Transition. *Cell Reports*. 2016;15(12):2665-2678. doi:10.1016/J.CELREP.2016.05.050.

198. Lan H, Tan M, Zhang Q, et al. LSD1 destabilizes FBXW7 and abrogates FBXW7 functions independent of its demethylase activity. *Proc Natl Acad Sci U S A*. 2019;116(25):12311-12320. doi:10.1073/PNAS.1902012116.

199. Chao A, Lin CY, Chao AN, et al. Lysine-specific demethylase 1 (LSD1) destabilizes p62 and inhibits autophagy in gynecologic malignancies. *Oncotarget*. 2017;8(43):74434-74450. doi:10.18632/ONCOTARGET.20158.

200. Wu Y, Zhou BP. Epigenetic regulation of LSD1 during mammary carcinogenesis. *Mol Cell Oncol*. 2014;1(3):e963426. doi:10.4161/21624011.2014.963426.

201. Balaguer F, Link A, Lozano JJ, et al. Epigenetic silencing of miR-137 is an early event in colorectal carcinogenesis. *Cancer Research*. 2010;70(16):6609-6618. doi:10.1158/0008-5472.CAN-10-0622/656299/P/EPIGENETIC-SILENCING-OF-MIR-137-IS-AN-EARLY-EVENT.

202. Althoff K, Beckers A, Odersky A, et al. MiR-137 functions as a tumor suppressor in neuroblastoma by downregulating KDM1A. *International Journal of Cancer*. 2013;133(5):1064-1073. doi:10.1002/IJC.28091.

203. Sun G, Ye P, Murai K, et al. miR-137 forms a regulatory loop with nuclear receptor TLX and LSD1 in neural stem cells. *Nat Commu.* 2011;2(1):1-10. doi:10.1038/ncomms1532.

204. Nam HJ, Boo K, Kim D, et al. Phosphorylation of LSD1 by PKCα Is Crucial for Circadian Rhythmicity and Phase Resetting. *Molecular Cell*. 2014;53(5):791-805. doi:10.1016/J.MOLCEL.2014.01.028.

205. Lv S, Bu W, Jiao H, et al. LSD1 is required for chromosome segregation during mitosis. *European Journal of Cell Biology*. 2010;89(7):557-563. doi:10.1016/J.EJCB.2010.01.004.

206. Nair VD, Ge Y, Balasubramaniyan N, et al. Involvement of Histone Demethylase LSD1 in Short-Time-Scale Gene Expression Changes during Cell Cycle Progression in Embryonic Stem Cells. *Molecular and Cellular Biology*. 2012;32(23):4861-4876. doi:10.1128/MCB.00816-12/SUPPL_FILE/ZMB023129755SO2.XLS.

207. Lin Y, Wu Y, Li J, et al. The SNAG domain of snail1 functions as a molecular hook for recruiting lysine-specific demethylase 1. *EMBO Journal*. 2010;29(11):1803-1816. doi:10.1038/emboj.2010.63.

208. Wu Y, Wang Y, Yang XH, et al. The Deubiquitinase USP28 Stabilizes LSD1 and Confers Stem-Cell-like Traits to Breast Cancer Cells. *Cell Reports*. 2013;5(1):224-236. doi:10.1016/J.CELREP.2013.08.030.

209. Hino S, Kohrogi K, Nakao M. Histone demethylase LSD1 controls the phenotypic plasticity of cancer cells. *Cancer Science*. 2016;107(9):1187-1192. doi:10.1111/cas.13004.

210. Maiques-Diaz A, Somervaille TC. LSD1: biologic roles and therapeutic targeting. *Epigenomics*. 2016;8(8):1103. doi:10.2217/EPI-2016-0009.

211. Harris WJ, Huang X, Lynch JT, et al. The Histone Demethylase KDM1A Sustains the Oncogenic Potential of MLL-AF9 Leukemia Stem Cells. *Cancer Cell.* 2012;21(4):473-487. doi:10.1016/j.ccr.2012.03.014

212. Sakamoto A, Hino S, Nagaoka K, et al. Lysine demethylase LSD1 coordinates glycolytic and mitochondrial metabolism in hepatocellular carcinoma cells. *Cancer Research*. 2015;75(7):1445-1456. doi:10.1158/0008-5472.CAN-14-1560/651671/AM/LYSINE-DEMETHYLASE-LSD1-COORDINATES-GLYCOLYTIC-AND.

213. Lin T, Ponn A, Hu X, Law BK, Lu J. Requirement of the histone demethylase LSD1 in Snai1-mediated transcriptional repression during epithelial-mesenchymal transition. *Oncogene*. 2010;29(35):4896-4904. doi:10.1038/onc.2010.234.

214. Sehrawat A, Gao L, Wang Y, et al. LSD1 activates a lethal prostate cancer gene network independently of its demethylase function. *Proc Natl Acad Sci U S A*. 2018;115(18):E4179-E4188. doi:10.1073/pnas.1719168115doi:10.1073/pnas.1719168115.

215. Bloehdorn J, Braun A, Taylor-Weiner A, et al. Multi-platform profiling characterizes molecular subgroups and resistance networks in chronic lymphocytic leukemia. *Nat Commu.* 2021;12(1). doi:10.1038/s41467-021-25403-y.

216. Landau DA, Carter SL, Stojanov P, et al. Evolution and impact of subclonal mutations in chronic lymphocytic leukemia. *Cell.* 2013;152(4):714-726.

217. Quesada V, Conde L, Villamor N, et al. Exome sequencing identifies recurrent mutations of the splicing factor SF3B1 gene in chronic lymphocytic leukemia. *Nature Genetics*. 2012;44(1):47-52. doi:10.1038/ng.1032.

218. Puente X, Beà S, Valdés-Mas R, et al. Non-coding recurrent mutations in chronic lymphocytic leukaemia. *Nature*. 2015;526:519–524. doi:https://doi.org/10.1038/nature14666.

219. Haferlach T, Kohlmann A, Wieczorek L, et al. Clinical utility of microarray-based gene expression profiling in the diagnosis and subclassification of leukemia: report from the International Microarray Innovations in Leukemia Study Group. *J Clin Oncol*. 2010;28(15):2529-2537. doi:10.1200/JCO.2009.23.4732.

220. Vermes I, Haanen C, Steffens-Nakken H, et al. A novel assay for apoptosis Flow cytometric detection of phosphatidylserine expression on early apoptotic cells using fluorescein labelled Annexin V. *Journal of Immunological Methods*. 1995;184(1):39-51. doi:10.1016/0022-1759(95)00072-I.

221. Op den Kamp JA. Lipid Asymmetry in Membranes. *Annu Rev Biochem*. 1979;48:47-71. doi:10.1146/annurev.bi.48.070179.000403.

222. Scholzen T, Gerdes J. The Ki-67 protein: from the known and the unknown. *J Cell Physiol*. 2000;182(3):311-22. doi:10.1002/(SICI)1097-4652(200003)182:3<311::AID-JCP1>3.0.CO;2-9.

223. Wagner J, Damaschke N, Yang B, et al. Overexpression of the Novel Senescence Marker β-Galactosidase (GLB1) in Prostate Cancer Predicts Reduced PSA Recurrence. *PLoS ONE*. 2015;10(4). doi:10.1371/JOURNAL.PONE.0124366.

224. Bradford MM. A rapid and sensitive method for the quantitation of microgram quantities of protein utilizing the principle of protein-dye binding. *Analytical Biochemistry*. 1976;72(1-2):248-254. doi:10.1016/0003-2697(76)90527-3.

225. Litovchick L. Immunoblotting. Cold Spring Harbor protocols. 2020(6):179-188. doi:10.1101/PDB.TOP098392.

226. Karch KR, Sidoli S, Garcia BA. Identification and Quantification of Histone PTMs Using High-Resolution Mass Spectrometry. *Methods in Enzymology*. 2016;574:3-29. doi:10.1016/bs.mie.2015.12.007.

227. Zipper H, Brunner H, Bernhagen J, et al. Investigations on DNA intercalation and surface binding by SYBR Green I, its structure determination and methodological implications. *Nucleic Acids Research*. 2004;32(12). doi:10.1093/nar/gnh101.

228. Vasyutina E, Boucas JM, Bloehdorn J, et al. The regulatory interaction of EVI1 with the TCL1A oncogene impacts cell survival and clinical outcome in CLL. *Leukemia*. 2015;29(10):2003-2014. doi:10.1038/leu.2015.114.

229. Hallek M, Fischer K, Fingerle-Rowson G, et al. Addition of rituximab to fludarabine and cyclophosphamide in patients with chronic lymphocytic leukaemia: A randomised, open-label, phase 3 trial. *The Lancet*. 2010;376(9747):1164-1174. doi:10.1016/S0140-6736(10)61381-5.

230. Sprüssel A, Schulte JH, Weber S, et al. Lysine-specific demethylase 1 restricts hematopoietic progenitor proliferation and is essential for terminal differentiation. *Leukemia*. 2012;26(9):2039-2051. doi:10.1038/leu.2012.157.

231. Fischer AH, Jacobson KA, Rose J, et al. Hematoxylin and eosin staining of tissue and cell sections. *CSH protocols*, 2008, pdb.prot4986.

232. Yuan ZF, Sidoli S, Marchione DM, et al. EpiProfile 2.0: A Computational Platform for Processing Epi-Proteomics Mass Spectrometry Data Graphical Abstract HHS Public Access. *J Proteome Res*. 2018;17(7):2533-2541. doi:10.1021/acs.jproteome.8b00133.

233. Wagle P, Nikolić M, Frommolt P. QuickNGS elevates Next-Generation Sequencing data analysis to a new level of automation. *BMC Genomics*. 2015;16(487):1-8. doi:10.1186/s12864-015-1695-x.

234. Li H, Durbin R. Fast and accurate short read alignment with Burrows-Wheeler transform. *Bioinformatics*. 2009;25(14):1754-1760. doi:10.1093/bioinformatics/btp324.

235. Trapnell C, Pachter L, Salzberg SL. TopHat: discovering splice junctions with RNA-Seq. *Bioinformatics*. 2009;25(9):1105-1111. doi:10.1093/bioinformatics/btp120.

236. Trapnell C, Williams BA, Pertea G, et al. Transcript assembly and abundance estimation from RNA-Seq reveals thousands of new transcripts and switching among isoforms HHS Public Access Author manuscript. *Nat Biotechnol*. 2010;28(5):511-515. doi:10.1038/nbt.1621.

237. Anders S, Huber W. Differential expression analysis for sequence count data. *Genome Biology*. 2010;11(R106):1-12. doi:10.1186/gb-2010-11-10-r106.

238. Durinck S, Moreau Y, Kasprzyk A, et al. BioMart and Bioconductor: a powerful link between biological databases and microarray data analysis. *Bioinformatics Applications Note*. 2005;21(16):3439-3440. doi:10.1093/bioinformatics/bti525.

239. Langmead B, Salzberg SL. Fast gapped-read alignment with Bowtie 2. *Nature Methods*. 2012;9(4):357-359. doi:10.1038/nmeth.1923.

240. Zhang Y, Liu T, Meyer CA, et al. Model-based analysis of ChIP-Seq (MACS). *Genome biology*. 2008;9(9):R137. doi:10.1186/gb-2008-9-9-r137.

241. Ramírez F, Ryan DP, Grüning B, et al. deepTools2: a next generation web server for deep-sequencing data analysis. *Nucleic acids research*. 2016;44(W1):W160-5. doi:10.1093/nar/gkw257.

242. Heinz S, Benner C, Spann N, et al. Simple Combinations of Lineage-Determining Transcription Factors Prime cis-Regulatory Elements Required for Macrophage and B Cell Identities. *Mol Cell*. 2010;38(4):576-89. doi:10.1016/j.molcel.2010.05.004.

243. Schrader A, Crispatzu G, Oberbeck S, et al. Actionable perturbations of damage responses by TCL1/ATM and epigenetic lesions form the basis of T-PLL. *Nat Commun*. 2018;9(1):697. doi:10.1038/s41467-017-02688-6.

244. Mosammaparast N, Kim H, Laurent B, et al. The histone demethylase LSD1/KDM1A promotes the DNA damage response. *Journal of Cell Biology*. 2013;203(3):457-470. doi:10.1083/jcb.201302092.

245. Fang Y, Liao G, Yu B. LSD1/KDM1A inhibitors in clinical trials: advances and prospects. *J Hematol Oncol*. 2019;12(1):129. doi:10.1186/s13045-019-0811-9.

246. Yigit B, Wang N, Hacken E ten, et al. SLAMF6 as a regulator of exhausted CD8+ T cells in cancer. *Cancer Immunology Research*. 2019;7(9):1485-1496. doi:10.1158/2326-6066.CIR-18-0664.

247. Yigit B, Halibozek PJ, Chen SS, et al. A combination of an anti-SLAMF6 antibody and ibrutinib efficiently abrogates expansion of chronic lymphocytic leukemia cells. *Oncotarget*. 2016;7(18):26346-26360. doi:10.18632/oncotarget.8378.

248. Oakes CC, Claus R, Schmidt C, et al. Reduced c-FOS Is Associated with Poor Prognosis and Clinical Course in Chronic Lymphocytic Leukemia. *Blood*. 2011;118(21):2433-2433. doi:10.1182/BLOOD.V118.21.2433.2433.

249. Marquez ME, Hernández-Uzcátegui O, Cornejo A, et al. Bone marrow stromal mesenchymal cells induce down regulation of CD20 expression on B-CLL: Implications for rituximab resistance in CLL. *Br J Haematol*. 2015;169(2):211-218. doi:10.1111/BJH.13286.

250. Burger JA, Ghia P, Rosenwald A, Caligaris-Cappio F. The microenvironment in mature B-cell malignancies: A target for new treatment strategies. *Blood*. 2009;114(16):3367-3375. doi:10.1182/blood-2009-06-225326.

251. Tsukada N, Burger JA, Zvaifler NJ, Kipps TJ. Distinctive features of "nurselike" cells that differentiate in the context of chronic lymphocytic leukemia. *Blood*. 2002;99:1030-1037. doi:10.1182/blood.v99.3.1030.

252. Qin Y, Vasilatos SN, Chen L, et al. Inhibition of histone lysine-specific demethylase 1 elicits breast tumor immunity and enhances antitumor efficacy of immune checkpoint blockade. *Oncogene*. 2018;38(3):390-405. doi:10.1038/s41388-018-0451-5.

253. Tu WJ, McCuaig RD, Tan AHY, et al. Targeting Nuclear LSD1 to Reprogram Cancer Cells and Reinvigorate Exhausted T Cells via a Novel LSD1-EOMES Switch. *Frontiers in Immunology*. 2020;11(1228):1-23. doi:10.3389/FIMMU.2020.01228.

254. Fang J, Ying H, Mao T, et al. Upregulation of CD11b and CD86 through LSD1 Inhibition Promotes Myeloid Differentiation and Suppresses Cell Proliferation in Human Monocytic Leukemia Cells. *Oncotarget*. 2017;8(49):85085-85101. doi:10.18632/oncotarget.18564.

255. Liang G, Lin JCY, Wei V, et al. Distinct localization of histone H3 acetylation and H3-K4 methylation to the transcription start sites in the human genome. *Proc Natl Acad Sci U S A*. 2004;101(19):7357. doi:10.1073/PNAS.0401866101.

256. Pearson RCM, Funnell APW, Crossley M. The mammalian zinc finger transcription factor Krüppel-like factor 3 (KLF3/BKLF). *IUBMB Life*. 2011;63(2):86-93. doi:10.1002/IUB.422.

257. Vu TT, Gatto D, Turner V, et al. Impaired B Cell Development in the Absence of Krüppel-like Factor 3. *J Immunol*. 2011;187(10):5032-5042. doi:10.4049/JIMMUNOL.1101450.

258. Turchinovich G, Thanh VT, Frommer F, et al. Programming of marginal zone B-cell fate by basic Krüppel-like factor(BKLF/KLF3). *Blood*. 2011;117(14):3780-3792. doi:10.1182/blood-2010-09-308742.

259. Neelamegam R, Ricq EL, Malvaez M, et al. Brain-penetrant LSD1 inhibitors can block memory consolidation. *ACS Chemical Neuroscience*. 2012;3(2):120-128. doi:10.1021/cn200104y.

260. Fiskus W, Sharma S, Shah B, et al. Highly effective combination of LSD1 (KDM1A) antagonist and pan-histone deacetylase inhibitor against human AML cells HHS Public Access. *Leukemia*. 2014;28(11):2155-2164. doi:10.1038/leu.2014.119.

261. Feng S, Jin Y, Cui M, Zheng J. Lysine-Specific Demethylase 1 (LSD1) Inhibitor S2101 Induces Autophagy via the AKT/mTOR Pathway in SKOV3 Ovarian Cancer Cells. *Med Sci Monit*. 2016;22:4742-4748. doi:10.12659/msm.898825.

262. Cusan M, Cai SF, Mohammad HP, et al. LSD1 Inhibition Exerts Its Antileukemic Effect by Re-commissioning PU.1-and C/EBPa-Dependent Enhancers in AML. *Blood*. 2018;131(15):1730-1742. doi:10.1182/blood-2017-09-807024.

263. Wang D, Liu Y, Zhang R, et al. Apoptotic transition of senescent cells accompanied with mito-chondrial hyper-function. *Oncotarget*. 2016;7(19):28286-28300. doi:10.18632/oncotar-get.8536.

264. Ohshima S. Apoptosis and necrosis in senescent human fibroblasts. *Ann N Y Acad Sci*. 2006;1067:228-34. doi: 10.1196/annals.1354.029.

265. Maes T, Mascaró C, Tirapu I, et al. ORY-1001, a Potent and Selective Covalent KDM1A Inhibitor, for the Treatment of Acute Leukemia. *Cancer Cell*. 2018;33(3):495-511.e12. doi:10.1016/j.ccell.2018.02.002.

266. McGrath JP, Williamson KE, Balasubramanian S, et al. Pharmacological Inhibition of the His-tone Lysine Demethylase KDM1A Suppresses the Growth of Multiple Acute Myeloid Leukemia Subtypes. *Cancer Res*. 2016;76(7):1975-88. doi:10.1158/0008-5472.CAN-15-2333.

267. Cui S, Lim KC, Shi L, et al. The LSD1 inhibitor RN-1 induces fetal hemoglobin synthesis and reduces disease pathology in sickle cell mice. *Blood*. 2015;126(3):386-396. doi:10.1182/blood-2015-02-626259.

268. Sankar S, Theisen ER, Bearss J, et al. Reversible LSD1 inhibition interferes with global EWS/ETS transcriptional activity and impedes Ewing sarcoma tumor growth. *Clin Cancer Res*. 2014;20(17):4584-4597. doi:10.1158/1078-0432.CCR-14-0072.

269. Macheleidt IF, Dalvi PS, Lim SY, et al. Preclinical studies reveal that LSD1 inhibition results in tumor growth arrest in lung adenocarcinoma independently of driver mutations. *Molecular On-cology*. 2018;12(11):1965-1979. doi:10.1002/1878-0261.12382.

270. Dalvi PS, Macheleidt IF, Lim SY, et al. LSD1 inhibition attenuates tumor growth by disrupting PLK1 mitotic pathway. *Mol Cancer Res.* 2019;17(6):1326-1337. doi:10.1158/1541-7786.mcr-18-0971.

271. Mohammad HP, Smitheman KN, Kamat CD, et al. A DNA Hypomethylation Signature Predicts Antitumor Activity of LSD1 Inhibitors in SCLC. *Cancer Cell*. 2015;28(1):57-69. doi:10.1016/j.ccell.2015.06.002.

272. Fürstenau M, Eichhorst B. Novel agents in chronic lymphocytic leukemia: New combination therapies and strategies to overcome resistance. *Cancers (Basel)*. 2021;13(6):1-18. doi:10.3390/cancers13061336.

273. Maharaj K, Powers JJ, Achille A, et al. Silencing of HDAC6 as a therapeutic target in chronic lymphocytic leukemia. *Blood Advances*. 2018;2(21):3012-3024. doi:10.1182/BLOODAD-VANCES.2018020065.

274. Ciardullo C, Aptullahoglu E, Woodhouse L, et al. Non-genotoxic MDM2 inhibition selectively induces a pro-apoptotic p53 gene signature in chronic lymphocytic leukemia cells. *Haematolog-ica*. 2019;104(12):2429-2442. doi:10.3324/haematol.2018.206631.

275. Ianevski A, Giri AK, Aittokallio T. SynergyFinder 2.0: visual analytics of multi-drug combination synergies. *Nucleic Acids Research*. 2020;48(W1):W488-W493. doi:10.1093/NAR/GKAA216.

276. Wang J, Wu Z, Zhu X, et al. Lysine-specific demethylase 1 (LSD1) serves as an potential epigenetic determinant to regulate inflammatory responses in mastitis. *International Immunopharmacology*. 2021;91:1-7. doi:10.1016/j.intimp.2020.107324.

277. Yu Z, Liu H, Fan J, et al. MicroRNA-155 Participates in the Expression of LSD1 and Proinflammatory Cytokines in Rheumatoid Synovial Cells. *Mediators Inflamm.* 2020;2020:4092762. doi:10.1155/2020/4092762.

278. Hong KS, Ahn JH, Jang JG, et al. GSK-LSD1, an LSD1 inhibitor, quashes SARS-CoV-2-triggered cytokine release syndrome in-vitro. *Signal Transduction and Targeted Therapy*. 2020;5(1). doi:10.1038/s41392-020-00391-5.

279. Gaidano G, Foà R, Dalla-Favera R. Molecular pathogenesis of chronic lymphocytic leukemia. *J Clin Invest*. 2012;122(10):3432-3438. doi:10.1172/JCI64101.

280. Ott CJ, Federation AJ, Schwartz LS, Freedman ML, Brown JR, Correspondence JEB. Enhancer Architecture and Essential Core Regulatory Circuitry of Chronic Lymphocytic Leukemia. *Cancer Cell*. 2018;34:982-995.e7. doi:10.1016/j.ccell.2018.11.001.

281. Pastore A, Gaiti F, Lu SX, et al. Corrupted coordination of epigenetic modifications leads to diverging chromatin states and transcriptional heterogeneity in CLL. *Nature Communications.* 2019;10(1):1-11. doi:10.1038/s41467-019-09645-5.

282. Holmes KB, Sadreev II, Rawstron AC, et al. Ibrutinib induces chromatin reorganisation of chronic lymphocytic leukaemia cells. *Oncogenesis*. 2019;8(5):1-11. doi:10.1038/s41389-019-0142-2.

283. Schmidl C, Vladimer GI, Rendeiro AF, et al. Combined chemosensitivity and chromatin profiling prioritizes drug combinations in CLL. *Nature Chemical Biology*. 2019;15(3):232-240. doi:10.1038/s41589-018-0205-2.

284. Mansouri L, Wierzbinska JA, Plass C, Rosenquist R. Epigenetic deregulation in chronic lymphocytic leukemia: Clinical and biological impact. *Seminars in Cancer Biology*. 2018;51:1-11. doi:10.1016/j.semcancer.2018.02.001.

285. Schulte JH, Lim S, Schramm A, et al. Lysine-Specific Demethylase 1 Is Strongly Expressed in Poorly Differentiated Neuroblastoma: Implications for Therapy. *Cancer Res*. 2009;69(5):2065-2071. doi:10.1158/0008-5472.CAN-08-1735.

286. Hayami S, Kelly JD, Cho HS, et al. Overexpression of LSD1 contributes to human carcinogenesis through chromatin regulation in various cancers. *International Journal of Cancer*. 2011;128(3):574-586. doi:10.1002/IJC.25349.

287. Theisen ER, Gajiwala S, Bearss J, et al. Reversible inhibition of lysine specific demethylase 1 is a novel anti-tumor strategy for poorly differentiated endometrial carcinoma. *BMC Cancer*. 2014;14:752. doi:10.1186/1471-2407-14-752.

288. Wu J, Du Y, Kong F, et al. Prognostic role of LSD1 in various cancers: evidence from a meta-analysis. *Onco Targets Ther*. 2015;8:2565-70. doi:10.2147/OTT.S89597.

289. Kim D, Kim K il, Baek SH. Roles of lysine-specific demethylase 1 (LSD1) in homeostasis and diseases. *Journal of Biomedical Science*. 2021;28(1):1-14. doi:10.1186/s12929-021-00737-3.

290. Michnick SW, Ear PH, Landry C, et al. Protein-Fragment Complementation Assays for Large-Scale Analysis, Functional Dissection and Dynamic Studies of Protein–Protein Interactions in Living Cells. *Methods in Molecular Biology*. 2011;756:395-425. doi:10.1007/978-1-61779-160-4_25.

291. Knittel G, Liedgens P, Reinhardt HC. Targeting ATM-deficient CLL through interference with DNA repair pathways. *Front Genet*. 2015;6:207. doi:10.3389/fgene.2015.00207.

292. Stankovic T, Nicholas D, Kwok M, et al. Synthetic Lethality In CLL With DNA Damage Response Defect By Targeting ATR Pathway. *Blood*. 2013;122(21):120-120. doi:10.1182/BLOOD.V122.21.120.120.

293. Davids MS, Brown JR. Targeting the B Cell Receptor Pathway in Chronic Lymphocytic Leukemia. *Leuk Lymphoma*. 2012;53(12):2362-2370. doi:10.3109/10428194.2012.695781.

294. Smeenk G, Wiegant WW, Vrolijk H, et al. The NuRD chromatin-remodeling complex regulates signaling and repair of DNA damage. *J Cell Biol*. 2010;190(5):741-749. doi:10.1083/jcb.201001048.

295. Yang GJ, Lei PM, Wong SY, et al. Pharmacological Inhibition of LSD1 for Cancer Treatment. *Molecules.* 2018;23(12):3194. doi:10.3390/MOLECULES23123194.

296. Steinbrecher D, Michael B, Jebaraj C, et al. Telomere length in poor-risk chronic lymphocytic leukemia: associations with disease characteristics and outcome Telomere length in poor-risk chronic lymphocytic leukemia: associations with disease characteristics and outcome. *Leuk Lymphoma.* 2018;59(7):1614-1623. doi:10.1080/10428194.2017.1390236.

297. Jebaraj BMC, Stilgenbauer S. Telomere Dysfunction in Chronic Lymphocytic Leukemia. *Front Oncol.* 2021;10:612665. doi:10.3389/fonc.2020.612665.

298. Norris K, Hillmen P, Rawstron A, et al. Telomere length predicts for outcome to FCR chemotherapy in CLL. *Leukemia*. 2019;33(8):1953-1963. doi:10.1038/s41375-019-0389-9.

299. Song DY, Kim JA, Jeong D, et al. Telomere length and its correlation with gene mutations in chronic lymphocytic leukemia in a Korean population. *PLoS One.* 2019;14(7):e0220177. doi:10.1371/journal.pone.0220177.

300. Scoumanne A, Chen X. The lysine-specific demethylase 1 is required for cell proliferation in both p53-dependent and -independent manners. *J Biol Chem.* 2007;282(21):15471-5. doi:10.1074/jbc.M701023200.

301. Hofbauer JP, Heyder C, Denk U, et al. Development of CLL in the TCL1 transgenic mouse model is associated with severe skewing of the T-cell compartment homologous to human CLL. *Leukemia.* 2011;25(9):1452-8. doi:10.1038/leu.2011.111.

302. Tinhofer I, Weiss L, Gassner F, et al. Difference in the relative distribution of CD4+ T-cell subsets in B-CLL with mutated and unmutated immunoglobulin (Ig) VH genes: Implication for the course of disease. *Journal of Immunotherapy.* 2009;32(3):302-309. doi:10.1097/CJI.0B013E318197B5E4.

303. Ji X, Guo D, Ma J, et al. Epigenetic Remodeling Hydrogel Patches for Multidrug-Resistant Triple-Negative Breast Cancer. *Advanced Materials*. 2021;33(18). doi:10.1002/ADMA.202100949.

304. Boulding T, McCuaig RD, Tan A, et al. LSD1 activation promotes inducible EMT programs and modulates the tumour microenvironment in breast cancer. *Scientific Reports*. 2018;8(1). doi:10.1038/S41598-017-17913-X.

305. Singer DS, Hosogane E, Rao S, et al. Lysine-Specific Histone Demethylase 1A Regulates Macrophage Polarization and Checkpoint Molecules in the Tumor Microenvironment of Triple-Negative Breast Cancer. *Frontiers in Immunology.* 2019;1:1351. doi:10.3389/fimmu.2019.01351.

306. Nicosia L, Boffo FL, Ceccacci E, et al. Pharmacological inhibition of LSD1 triggers myeloid differentiation by targeting GSE1 oncogenic functions in AML. *Oncogene.* 2021;41(6):878-894. doi:10.1038/s41388-021-02123-7.

307. Zhao J, Jin W, Yi K, et al. Combination LSD1 and HOTAIR-EZH2 inhibition disrupts cell cycle processes and induces apoptosis in glioblastoma cells. *Pharmacol Res.* 2021;171:105764*.* doi:10.1016/j.phrs.2021.105764.

308. Burger JA, Gribben JG. The microenvironment in chronic lymphocytic leukemia (CLL) and other B cell malignancies: Insight into disease biology and new targeted therapies. *Seminars in Cancer Biology*. 2014;24:71-81. doi:10.1016/j.semcancer.2013.08.011.

309. Ganghammer S, Gutjahr J, Hutterer E, et al. Combined CXCR3/CXCR4 measurements are of high prognostic value in chronic lymphocytic leukemia due to negative co-operativity of the receptors. *Haematologica*. 2016;101(3):e99-e102. doi:10.3324/haematol.2015.133470.

310. Lee MG, Wynder C, Schmidt DM, et al. Brief Communication Histone H3 Lysine 4 Demethylation Is a Target of Nonselective Antidepressive Medications. *Chemistry & Biology*. 2006;13:563-567. doi:10.1016/j.chembiol.2006.05.004.

311. Zheng YC, Ma J, Wang Z, et al. A Systematic Review of Histone Lysine-Specific Demethylase 1 and Its Inhibitors. *Medicinal Research Reviews*. 2015;35(5):1032-1071. doi:10.1002/MED.21350.

312. Salamero O, Montesinos P, Willekens C, et al. First-in-Human Phase I Study of Iadademstat (ORY-1001): A First-in-Class Lysine-Specific Histone Demethylase 1A Inhibitor, in Relapsed or Refractory Acute Myeloid Leukemia. *J Clin Oncol*. 2020;38(36):4260-4273. doi:10.1200/JCO.19.03250.

313. Konovalov S, Garcia-Bassets I. Analysis of the levels of lysine-specific demethylase 1 (LSD1) mRNA in human ovarian tumors and the effects of chemical LSD1 inhibitors in ovarian cancer cell lines. *J Ovarian Res*. 2013;6(1):75. doi:10.1186/1757-2215-6-75.

314. Castex J, Willmann D, Kanouni T, et al. Inactivation of Lsd1 triggers senescence in trophoblast stem cells by induction of Sirt4. *Cell Death Dis*. 2017;8(2):e2631. doi:10.1038/cddis.2017.48.

315. He Y, Zhao Y, Wang L, et al. LSD1 promotes S-phase entry and tumorigenesis via chromatin co-occupation with E2F1 and selective H3K9 demethylation. *Oncogene*. 2018;37:534-543. doi:10.1038/onc.2017.353.

316. Sonnemann J, Zimmermann M, Marx C, et al. LSD1 (KDM1A)-independent effects of the LSD1 inhibitor SP2509 in cancer cells. *Br J Haematol.* 2018;183(3):494-497. doi:10.1111/bjh.14983.

317. Burger JA, Keating MJ, Wierda WG, et al. Safety and activity of ibrutinib plus rituximab for patients with high-risk chronic lymphocytic leukaemia: A single-arm, phase 2 study. *Lancet Oncol.* 2014;15(10):1090-9. doi:10.1016/S1470-2045(14)70335-3.

318. Chanan-Khan A, Cramer P, Demirkan F, et al. Ibrutinib combined with bendamustine and rituximab compared with placebo, bendamustine, and rituximab for previously treated chronic lymphocytic leukaemia or small lymphocytic lymphoma (HELIOS): A randomised, double-blind, phase 3 study. *Lancet Oncol*. 2016;17(2):200-211. doi:10.1016/S1470-2045(15)00465-9.

319. Seymour JF, Ma S, Brander DM, et al. Venetoclax plus rituximab in relapsed or refractory chronic lymphocytic leukaemia: a phase 1b study. *Lancet Oncol*. 2017;18(2):230-240. doi:10.1016/S1470-2045(17)30012-8.

320. Seymour JF, Kipps TJ, Eichhorst B, et al. Venetoclax–Rituximab in Relapsed or Refractory Chronic Lymphocytic Leukemia. *N Engl J Med*. 2018;378(12):1107-1120. doi:10.1056/nejmoa1713976.

321. Wen S, Wang J, Liu P, et al. Novel combination of histone methylation modulators with therapeutic synergy against acute myeloid leukemia in vitro and in vivo. *Cancer Lett*. 2018;413:35-45. doi:10.1016/j.canlet.2017.10.015.

322. Meng F, Sun G, Zhong M, et al, Brewer MA. Inhibition of DNA methyltransferases, histone deacetylases and lysine-specific demethylase-1 suppresses the tumorigenicity of the ovarian cancer ascites cell line SKOV3. *International Journal of Oncology*. 2013;43(2):495-502. doi:10.3892/IJO.2013.1960.

323. Duan YC, Ma YC, Qin WP, et al. Design and synthesis of tranylcypromine derivatives as novel LSD1/HDACs dual inhibitors for cancer treatment. *Eur J Med Chem*. 2017;140:392-402. doi:10.1016/j.ejmech.2017.09.038.

324. Huang Y, Vasilatos SN, Boric L, et al. Inhibitors of histone demethylation and histone deacetylation cooperate in regulating gene expression and inhibiting growth in human breast cancer cells. *Breast Cancer Res Treat*. 2012;131(3):777-789. doi:10.1007/s10549-011-1480-8.

325. Woyach JA, Johnson AJ, Byrd JC. The B-cell receptor signaling pathway as a therapeutic target in CLL. *Blood*. 2012;120(6):1175-1184. doi:10.1182/BLOOD-2012-02-362624.

326. Byrd JC, Furman RR, Coutre SE, et al. Targeting BTK with Ibrutinib in Relapsed Chronic Lymphocytic Leukemia. *N Engl J Med*. 2013;369(1):32-42. doi:10.1056/NEJMoa1215637.

327. Byrd JC, Brown JR, O'Brien S, et al. Ibrutinib versus ofatumumab in previously treated chronic lymphoid leukemia. *N Engl J Med*. 2014;371(3):213-223. doi:10.1056/NEJMOA1400376.

328. Burger JA, Tedeschi A, Barr PM, et al. Ibrutinib as Initial Therapy for Patients with Chronic Lymphocytic Leukemia. *N Engl J Med*. 2015;373(25):2425-2437. doi:10.1056/NEJMOA1509388.

329. Kondo K, Shaim H, Thompson PA, et al. Ibrutinib modulates the immunosuppressive CLL microenvironment through STAT3-mediated suppression of regulatory B cell function and inhibition of the PD-1/PD-L1 pathway. *Leukemia*. 2018;32(4):960-970. doi:10.1038/leu.2017.304.

330. Kim D, Nam HJ, Lee W, et al. PKCα-LSD1-NF-κB-Signaling Cascade Is Crucial for Epigenetic Control of the Inflammatory Response. *Mol Cell*. 2018;69(3):398-411.e6. doi:10.1016/j.molcel.2018.01.002.

Appendix

KDM1A in T-prolymphocytic leukemia (T-PLL)

We have demonstrated that TCL1A interacts with KDM1A and enhances its demethylase activity in B cells. And we found a relevant pathogenetic role of KDM1A as a pro-oncogenic marker in CLL cells and their microenvironment. Given that TCL1A is overexpressed in T-prolymphocytic leukemia (T-PLL) which is a rare and aggressive mature (post-thymic) T-cell neoplasm that had been recognized as distinct from CLL in 1973 (*Staber PB et al., Leukemia.; 2019*), and the aberrant TCL1A expression is also associated with aggressive disease in T-PLL. It is of interest to identify the role of KDM1A in T-PLL.

Interestingly, we observed a less abundant interaction of TCL1A with KDM1A in T-PLL T cells than that in CLL B cells demonstrated by co-IPs immunoblotting (**Figure A1**). Although we could show that the protein levels of KDM1A are higher in T-PLL samples compared to healthy T cells (**Figure A2**). When analyzing RNA-seq data of T-PLL patient samples (*Till Braun et al., Haematologica. 2020)*, different *KDM1A* expression levels do not correlate with overall survival in T-PLL (**Figure A3**). Taking advantage of the Dox-inducible *Kdm1a* knockdown mouse model (**Figure A4**), we analyzed the effect of *Kdm1a* knockdown in a T-PLL mouse model (*Lck-TCL1A* mice). These mice develop a T-PLL-like disease with a CD4-/CD8+ phenotype at the age of around 10-15 months. Therefore, we started Dox treatment for non-leukemic mice at the age of 11 months, thereby analyzing the leukemia incidence and overall survival. However, no differences were observed between *Lck-TCL1A* and *iKdm1a^{KD};Lck-TCL1A* mice under Dox application (**Figure A5**).

Taken together, the expression of KDM1A in T-PLL might not have a significant impact on its pathogenesis. This suggests that the stronger interaction of TCL1A with KDM1A in B cells might be specific in CLL pathogenesis. However, more comprehensive functional studies are needed to characterize the network around the TCL1A-KDM1A complex in cell-specific contexts.
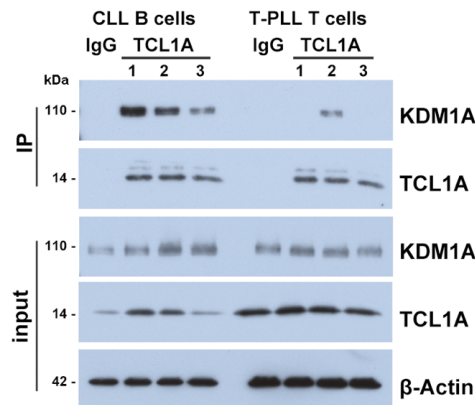
Figure A1. TCL1A interacts with KDM1A in CLL cells and T-PLL cells. Immunoblots of co-IPs using IgG or TCL1A antibodies illustrating higher abundance of TCL1A-KDM1A interaction in primary CLL cells vs. T-PLL cells. Each lane represents an individual B-CLL or T-PLL sample.
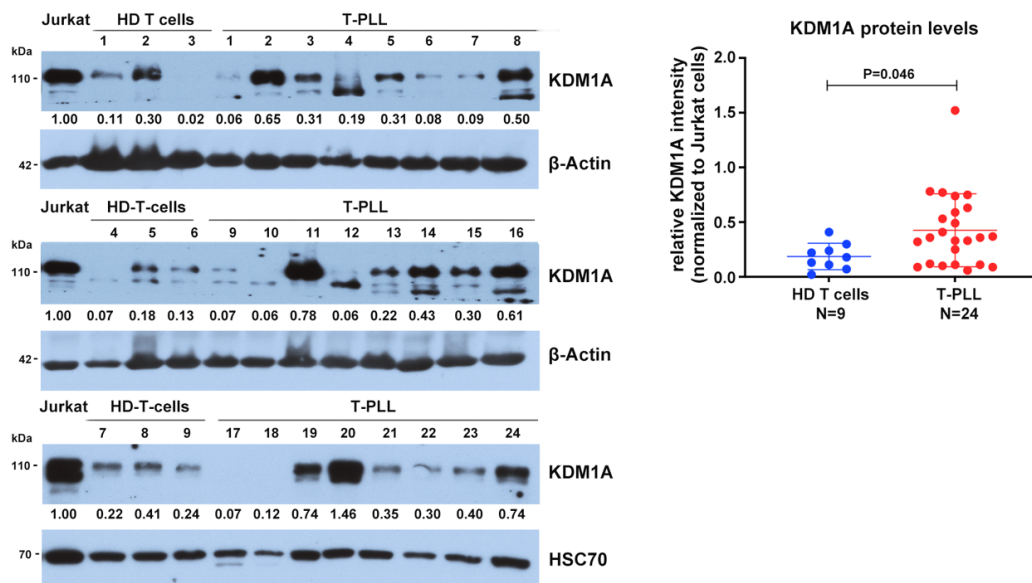

Figure A2. The protein levels of KDM1A in T-PLL and healthy T cells. Immunoblots (left) and densitometry (right) analysis demonstrate that the protein levels of KDM1A are higher in T-PLL samples compared to healthy donor (HD) T cells. Mann Whitney test.
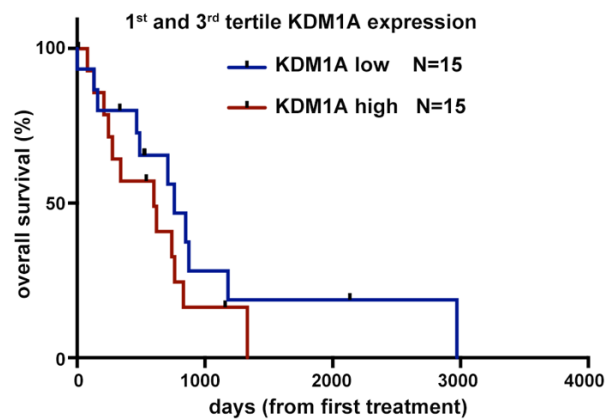
Figure A3. The Kaplan-Meier curve shows no significant difference of overall survival in T-PLL patients with different *KDM1A* expression levels. Patients were divided into three tertiles according to the mRNA levels of *KDM1A* analyzed using RNA-seq (*Till Braun et al., Haematologica. 2020*).
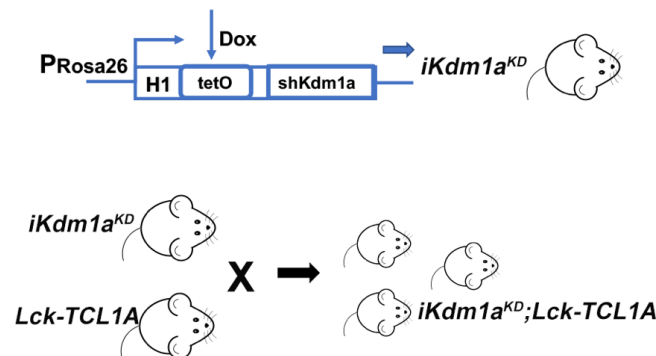

Figure A4. Establishment of the inducible *Kdm1a* knockdown T-PLL mouse model. Inducible *Kdm1a* knockdown mice (*iKdm1a*[KD]) were crossbred with *Lck-TCL1A* mice to achieve *Kdm1a* knockdown in *Lck-TCL1A* mice in a Dox inducible manner (*iKdm1a*[KD]*;Lck-TCL1A*).
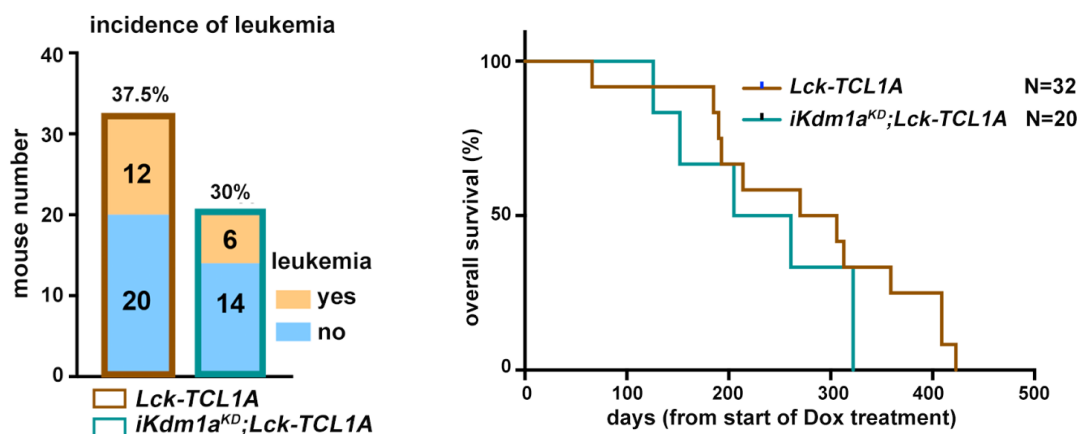

Figure A5. The effect of *Kdm1a* knockdown in *Lck-TCL1A* mice. Left: Bar chart showing the incidence of leukemia in *Lck-TCL1A* and *iKdm1a*[KD]*;Lck-TCL1A* animals exposed to Dox. Right: the Kaplan-Meier curve shows no significant difference of overall survival between *Lck-TCL1A* and *iKdm1a*[KD]*;Lck-TCL1A*.

Curriculum Vitae

PERSONAL INFORMATION

Name:	Qu Jiang
Address:	Kyffhäuserstr. 52, 50674 Cologne
Date of Birth:	12 Nov.1990
Nationality:	Chinese
Marital Status:	married
Email:	qu.jiang@uk-koeln.de
	qu.jiang@outlook.com

EDUCATION

01/2017 – 08/2022	Ph.D. student, University Clinic Cologne
	Research group of PD Dr. med. Marco Herling
	Thesis: "The oncogenic role of lysine-specific demethylase KDM1A in chronic lymphocytic leukemia"
07/2015 – 06/2016	Master of Medicine in Hematology, Chongqing Medical University, Chongqing, China
09/2009 – 06/2014	Bachelor of Medicine in Clinical Medicine Science, Chongqing Medical University, Chongqing, China
09/2006 – 06/2009	High school diploma, Chongqing Fudan High School, Chongqing, China
09/2003 – 06/2006	Junior high school diploma, Chongqing Fudan Middle School, Chongqing, China

PROFESSIONAL EXPERIENCE

03/2014 – 09/2014	Internship in the First Affiliated Hospital of Chongqing Medical University, Chongqing, China
10/2014 – 12/2014	Internship in the CHRU of Brest, Hospital of Morvan, Brest, France
01/2015 – 03/2015	Internship in the First Affiliated Hospital of Chongqing Medical University, Chongqing, China
04/2015 – 09/2015	Internship in the CHRU of Strasbourg, Strasbourg, France
10/2015 – 06/2016	Internship in the First Affiliated Hospital of Chongqing Medical University, Chongqing, China

LANGUAGE SKILLS

Chinese:	native language
English:	first language during studies
French:	second language during studies
German:	beginner

AWARDS

2010 – 2014	Award of Excellent Student Cadre, Chongqing Medical University
2012 – 2013	National Encouragement scholarship, Chongqing, China
2016	Award of Excellent graduate, Chongqing Medical University

PUBLICATIONS

1. **Jiang Q**, Stachelscheid J, Bloehdorn J, et al. Oncogenic role and target properties of the lysine-specific demethylase KDM1A in chronic lymphocytic leukemia. (In revision)

2. Stachelscheid J, **Jiang Q**, Christoph Aszyk, et al. The proto-oncogene TCL1A deregulates mitotic checkpoint transition and genomic stability in CLL. *Blood*. 2022. doi:10.1182/blood.2022015494.

3. Stachelscheid J, **Jiang Q**, Herling M. The Modes of Dysregulation of the Proto-Oncogene T-Cell Leukemia/Lymphoma 1A. *Cancers*. 2021;13(21):5455.

4. **Jiang Q**, Zhang HB. Paraneoplastic pemphigus associated with chronic lymphocytic leukemia: A case report. *Medicine*. 2017;96(8):e6184.

5. **Jiang Q**, Zhang HB. Rhabdomyolysis after allogeneic hematopoietic stem cell transplantation. *Indian J Hematol Blood Transfus*. 2016;32(3).

6. Zhang L, **Jiang Q**, Wang J, Zhang HB. Adult Hemophagocytic Lymphohistiocytosis with PRF1, LYST and RAG1 Gene Mutations and Epstein-Barr Virus Infection. *Journal of international medical research*. 2022. Accepted

7. Miao Q, Wang J, **Jiang Q**, et al. The clinical analysis of allogeneic hematopoietic stem cell transplantation treatment in 25 patients with acute lymphoblastic leukemia. *Laboratory Medicine and Clinic*. 2017;14(09):1262-1265. (In Chinese)

8. Wang J, Sun JY, **Jiang Q**, et al. Clinical study of autologous peripheral blood stem cell transplantation for 15 patients with Hodgkin's lymphoma. *Journal of Modern Medicine & Health*. 2017;33(11):1644-1646. (In Chinese)

9. **Jiang Q**, Zhang HB, Yang L, Luo H, Miao Q, Deng XM. A clinical observation of HLA haploidentical hematopoietic stem cell transplantation for 23 patients with leukemia[J]. *Chinese Journal of Tissue Engineering Research*. 2016;20(28):4218-4225. (In Chinese)

10. **Jiang Q**, Zhang HB. The role of mesenchymal stem cells in the hemapoietic stem cell transplantation[J]. *Chongqing Medicine*. 2015;44(36):5164-5167. (In Chinese)

Eidesstattliche Erklärung

Ich versichere, dass ich die von mir vorgelegte Dissertation selbständig angefertigt, die benutzten Quellen und Hilfsmittel vollständig angegeben und die Stellen der Arbeit − einschließlich Tabellen, Karten und Abbildungen −, die anderen Werken im Wortlaut oder dem Sinn nach entnommen sind, in jedem Einzelfall als Entlehnung kenntlich gemacht habe; dass diese Dissertation noch keiner anderen Fakultät oder Universität zur Prüfung vorgelegen hat; dass sie − abgesehen von unten angegebenen Teilpublikationen − noch nicht veröffentlicht worden ist, sowie, dass ich eine solche Veröffentlichung vor Abschluss des Promotionsverfahrens nicht vornehmen werde. Die Bestimmungen der Promotionsordnung sind mir bekannt. Die von mir vorgelegte Dissertation ist von PD Dr. med. Marco Herling betreut worden.

Übersicht der Publikationen

Oncogenic role and target properties of the lysine-specific demethylase KDM1A in chronic lymphocytic leukemia

Qu Jiang, Johanna Stachelscheid, Johannes Bloehdorn, Francien Grotenhuijs, Christoph Aszyk, Tony Müller, Alicja Pacholewska, Ozlem Onder, Zhefang Wang, Prerana Wagle, Sandra Robrecht, Priya S. Dalvi, Bianca Plosnita, Petra Mayer, Janine Altmüller, Birgit Gathof, Thorsten Persigehl, Kirsten Fischer, Billy Jebaraj, Rupert Ecker, Yue Zhao, Christiane J. Bruns, Stephan Stilgenbauer, Kojo Elenitoba-Johnson, Michal R. Schweiger, Michael Hallek, Margarete Odenthal, Elena Vasyutina[#], and Marco Herling[#]. (In revision)

The contribution of the authors is listed on the next page.

The proto-oncogene TCL1A deregulates cell cycle and genomic stability in CLL

Johanna Stachelscheid, Qu Jiang, Christoph Aszyk, Kathrin Warner, Nadine Bley, Tony Müller, Olga Vydzhak, Konstantinos Symeonidis, Giuliano Crispatzu, Petra Mayer, Stuart James Blakemore, Gudrun Goehring, Sebastian Newrzela, Stephanie Hippler, Sandra Robrecht, Karl-Anton Kreuzer, Christian Pal-lasch, Marcus Krueger, Axel Lechner, Kirsten Fischer, Stephan Stilgenbauer, Dirk Beutner, Michael Hallek, Daniel Auguin, Stefan Hüttelmaier, Johannes Bloehdorn[#], Elena Vasyutina[#], and Marco Herling[#]. *Blood.* 2022. Accepted.

The Modes of Dysregulation of the Proto-Oncogene T-Cell Leukemia/Lymphoma 1A

Johanna Stachelscheid, Qu Jiang, Marco Herling. *Cancers*. 2021;13(21):5455.

[#] Authors contributed equally

Ich versichere, dass ich alle Angaben wahrheitsgemäß nach bestem Wissen und Gewissen gemacht habe und verpflichte mich, jedmögliche, die obigen Angaben betreffende Veränderungen, dem Dekanat unverzüglich mitzuteilen.

Köln, den 27.10.2022   Qu Jiang

_____

Unterschrift

Oncogenic role and target properties of the lysine-specific demethylase KDM1A in chronic lymphocytic leukemia

Author contributions:

Experimental design:

Qu Jiang, Johanna Stachelscheid, Johannes Blohdorn, Eleva Vasyutina, and Marco Herling

Manuscript preparation:

Qu Jiang, Johanna Stachelscheid, Tony Müller, and Marco Herling

In vivo and in vitro experiments and data analyses: Qu Jiang

The following parts were done in collaboration with others (Figures in the dissertation):

1. TCL1A Co-IP MS in primary cells:
   - TCL1A Co-IP experiments were done by Christoph Aszyk in CLL and tonsilar B cells (**Figure 6**).
   - Data analyses were done by Johanna Stachelscheid and Qu Jiang (**Figure 6 and Figure 15**).

2. Histone PTM MS:
   - Ozlem Onder and Kojo Elenitoba-Johnson performed experiments and data analyses (**Figure 25**).

3. CLL8 trial data:
   - Johannes Bloehdorn, Sandra Robrecht, Kirsten Fischer, Stephan Stilgenbauer, and Michael Hallek were responsible for the CLL8 trial data. Billy Jebaraj analyzed the telomere length.
   - Johannes Bloehdorn performed the clustering analyses and GSEA (**Figure 28A, Figure 29B**).
   - Qu Jiang performed the comparison analyses (**Figure 28B, Figure 29A, Figure 30**).
   - Sandra Robrecht analyzed the survival data (**Figure 31**).

4. Tissue cytometry data process:
   - Qu Jiang, Bianca Plosnita, and Rupert Ecker analyzed the tissue cytometry data.

5. RNA-seq:
   - Raw RNA-seq data were processed by Prerana Wagle.
   - Qu Jiang (**Figure 48-50**) and Priya S. Dalvi (**Figure 48**) analyzed the processed data.

6. ChIP-seq:
   - Raw ChIP-seq data were processed by Alicja Pacholewska.
   - Qu Jiang and Alicja Pacholewska analyzed the processed data.
   - Heatmaps were created by Alicja Pacholewska (**Figure 54**, **Figure 59**).

7. Drug screen:
   - Qu Jiang and Francien Grotenhuijs tested the substances in co-cultured CLL cells (**Figure 63-64**).

8. shCtrl. and shKDM1A constructs were generated by Zhefang Wang.